Evapotranspiração e *stress* hídrico em cobertos lenhosos mediterrânicos: estimativa *versus* medição em olival e vinha

Nuno Miguel Santos da Conceição

Orientadores:

Doutora Maria Isabel Freire Ribeiro Ferreira
Professora Catedrática, Instituto Superior de Agronomia, Universidade de Lisboa

Doutor Manuel Lameiras de Figueiredo Campagnolo
Professor Associado, Instituto Superior de Agronomia, Universidade de Lisboa

Doutor Mário Manuel de Miranda Furtado Campos Cunha
Professor Auxiliar, Faculdade de Ciências, Universidade do Porto

TESE ELABORADA PARA OBTENÇÃO DO GRAU DE DOUTOR EM ENGENHARIA DOS BIOSSISTEMAS

2017

Evapotranspiração e *stress* hídrico em cobertos lenhosos mediterrânicos: estimativa *versus* medição em olival e vinha

Nuno Miguel Santos da Conceição

Orientadores:

Doutora Maria Isabel Freire Ribeiro Ferreira

Doutor Manuel Lameiras de Figueiredo Campagnolo

Professor Associado, Instituto Superior de Agronomia, Universidade de Lisboa

Doutor Mário Manuel de Miranda Furtado Campos Cunha

Professor Auxiliar, Faculdade de Ciências, Universidade do Porto

TESE ELABORADA PARA OBTENÇÃO DO GRAU DE DOUTOR EM ENGENHARIA DOS BIOSSISTEMAS

Júri

Presidente:

Doutora Maria Helena Mendes da Costa Ferreira Correia de Oliveira

Professora Associada, Instituto Superior de Agronomia, Universidade de Lisboa.

Vogais:

Doutora Maria Isabel Freire Ribeiro Ferreira

Professora Catedrática, Instituto Superior de Agronomia, Universidade de Lisboa

Doutor Aureliano Natálio Coelho Malheiro

Professor Auxiliar, Escola de Ciências Agrárias e Veterinárias, Universidade de Trás-os-Montes e Alto Douro

Doutora Fernanda Maria dos Reis Torroaes Valente

Professora Auxiliar, Instituto Superior de Agronomia, Universidade de Lisboa

Doutora Maria Teresa Gomes Afonso do Paço

Professora Auxiliar, Instituto Superior de Agronomia, Universidade de Lisboa

Doutora Teresa Maria Santana Barreto Soares David

Investigadora Auxiliar, Instituto Nacional de Investigação Agrária e Veterinária

Doutora Isabel Maria Valgôde Alves Pôças

Bolseira Pós-Doutoramento, Instituto Superior de Agronomia, Universidade de Lisboa

Instituições financiadoras e âmbito:
Fundação para a Ciência e Tecnologia, bolsa SFRH/BD/66967/2009

2017

Agradecimentos

Quero agradecer a todos quantos de forma directa ou indirecta contribuíram para a minha formação social e académica. Neste momento menciono as pessoas que mais de perto estiveram envolvidas na concepção e execução do trabalho agora apresentado, sem uma ordem especial.

Um muito obrigado à minha orientadora Profa. Maria Isabel Ribeiro Ferreira por ter tornado possível a realização de mais esta etapa, pelo seu contributo e pela sua amizade. Aos professores meus co-orientadores Prof. Manuel Lameiras Campagnolo e Prof. Mário Furtado Campos Cunha por terem aceite o desafio do trabalho a que nos propusemos.

Um agradecimento e muito obrigado para o Prof. Carlos Arruda Pacheco pelos seus ensinamentos, nomeadamente na área da pedologia e amizade.

Uma palavra de amizade para o Prof. Pedro Leão de Sousa cujo incentivo me permitiu melhorar os conhecimentos sobre automação dos sistemas de rega sobre pressão. Reconheço e agradeço a confiança depositada pela Profa. Graça Abrantes e Profa. Cristina Oliveira.

Uma palavra especial de agradecimento para a Dra. Teresa do Paço, Dr. José Silvestre e Dr. Aureliano Malheiro pela confiança e ajuda.

À Dra. Nadezhda Nadezhdina, ao Dr. José Enrique Fernández e Dr. Steve Green pela disponibilidade para as tarefas de campo, pelos ensinamentos e reconhecimento da minha pequena contribuição no trabalho desenvolvido.

Ao Eng. Pedro Oliveira da empresa Mezão Telecomunicações pela ajuda sincera.

Agradeço também ao Eng. Miguel Boteta e Enga. Marta Fabião a colaboração prestada, bem como as facilidades concedidas pelo Centro Operativo e de Tecnologia do Regadio (COTR).

Para a minha mãe, o meu pai, e os meus irmãos Valdemar e Ondina um sorriso pela ajuda. Ao meu tio António e primo Daniel e Sr. José Ferreira Carlos pela fácil disponibilidade e pelo transporte de equipamentos usados em Beja. Aos meus primos Rodrigo e Leonardo, muito obrigado pela ajuda.

Muito obrigado aos meus colegas e amigos que colaboraram no trabalho experimental: Berta Cumbane, Jorge Cunha, José Miguel Gama, Luca Tezza, Melanie Häusler, Soroor Amindezfooli, Sónia Lourenço e Sónia Surgy. Um agradecimento também para o Bruno Correia cuja ajuda com os pequenos circuitos electrónicos foi decisiva.

Uma palavra de agradecimento (póstuma) ao comendador Leonel Cameirinha pela sua sensibilidade e por ter disponibilizado as infraestruturas do Monte Novo e Figueirinha onde se realizaram as experiências em vinha (Beja). Para os funcionários do Monte Novo e Figueirinha nomeadamente o Sr. Aníbal pela preciosa disponibilidade e ajuda, o meu obrigado.

Agradeço também ao Sr. Manuel Duarte a disponibilidade para o uso do olival de sequeiro do Monte Outeirinho e facilidades concedidas.

Agradeço à empresa Agrícola Alentejo, SA. pelas facilidades concedidas no acesso às infraestruturas da exploração agrícola do Monte do Pardieiro, nomeadamente o olival de regadio onde foram realizadas as experiências. Para os funcionários do Monte do Pardieiro, na pessoa do Sr. Pereira, um muito obrigado.

Sei que não mencionei todos quantos devia e gostaria, mas fica o meu obrigado sincero, com votos de que o trabalho apresentado seja útil.

Citação

Enquanto o poço não seca, não sabemos dar valor à água.
Thomas Fuller (clérigo e historiador, 1608 – 1661)

O pessimista reclama do vento. O optimista espera que ele mude. O sábio ajusta as velas.
William Arthur Ward (escritor, 1921 – 1994)

Companies pay too much attention to the cost of doing something. They should worry more about the cost of not doing it.
Philip Kotler (economista e professor de marketing, 1931)

Dedicatória

Para os meus pais, irmãos, padrinhos, tios, à minha família e amigos.

Com o desejo de que a realidade se mantenha fiel ao Mundo.
Com a saudade dos cuja vida não permitiu o sorriso deste momento.
Um muito obrigado pela doce ternura.

Termino com um sorriso para a minha mãe, madrinha e irmã.

Resumo

Pretendeu-se melhorar o conhecimento sobre o uso da água e relações hídricas de ecossistemas agrícolas lenhosos, numa região de elevada escassez hídrica estival (Alentejo, Portugal), obtendo parâmetros para a gestão da água em agricultura e dados de referência (*ground–truth*) para avaliar e melhorar as estimativas do uso da água partindo de detecção remota. Foram estudados três ecossistemas: uma vinha em rega deficitária (*Vitis vinifera* 'Aragonez'), um olival intensivo em rega deficitária (*Olea europaea* 'Arbequina') e um olival tradicional de sequeiro ('Cobrançosa'). Estudaram-se os efeitos da carência hídrica na dinâmica de utilização da água, quantificando a evapotranspiração, transpiração, evaporação do solo e estado hídrico do solo e plantas. Contribuiu-se para o esclarecimento da estrutura e funcionamento do sistema radicular das oliveiras na gestão da água pela planta e sua importância nas estratégias de sobrevivência. Identificou-se redistribuição hidráulica nas direcções vertical e horizontal, respectivamente no olival de sequeiro e de regadio. Em sequeiro a água do solo extraída pelas raízes finas de camadas profundas (abaixo de 1.2 m) aparece como indispensável para a sobrevivência das plantas. A água armazenada no solo do olival de regadio, abaixo da zona onde se detectam visualmente raízes, pode também ser uma fracção importante da transpiração durante o período estival. As cultivares estudadas de videira e oliveira mostraram comportamento isohídrico mas com estratégias de uso da água contrastantes. Para potencial de base (Ψ_{base}) de -1 MPa, as videiras encontravam-se em stress hídrico intenso, com elevada redução da transpiração, enquanto as oliveiras regadas, para igual Ψ_{base} apresentavam uma redução de transpiração inferior a 20 %. Investigou-se ainda a viabilidade do uso de dados de detecção remota na estimativa do uso da água, através de modelos empíricos baseados em índice de vegetação e de modelos semi–empíricos de dois compartimentos, tendo-se obtido numa amostra selecionada estimativas próximas dos fluxos medidos.

Palavras chave: uso da água, Alentejo, rega deficitária, sistema radicular, detecção remota

Abstract

The main goal of this study was to improve the knowledge on water use and water relations of woody agricultural ecosystems in a region of high water scarcity (Alentejo, Portugal), obtaining parameters for agriculture water management and ground-truth data to assess and improve water use estimates from remote sensing. Three agricultural ecosystems were studied: a deficit irrigated vineyard (*Vitis vinifera* 'Aragonez'), an intensive deficit irrigated olive orchard (*Olea europaea* 'Arbequina') and a traditional rainfed olive orchard ('Cobrançosa'). Water stress effects on water use dynamics were studied, quantifying evapotranspiration, transpiration, soil evaporation and water status of the soil and plants. A contribution was made to the clarification of the functioning of the root system of the olive trees in regard to water uptake and its importance in the survival strategies. Hydraulic redistribution was identified in the vertical and horizontal directions, respectively in the rainfed and irrigated olive orchards. In rainfed conditions, soil water uptake by fine roots from deep layers (below 1.2 m) appears as indispensable for the trees survival. At the irrigated orchard, soil water in layers where roots are not visually detected, can also be an important fraction of the transpiration during the summer period. The studied vine and olive cultivars showed near-isohydric behavior but with contrasting water use strategies. For predawn leaf water potential (Ψ_{predawn}) of -1 MPa, the vines had important transpiration reduction, while the irrigated olive trees for the same value of Ψ_{predawn} only suffered 20 % of transpiration reduction. The reliability of the use of remote sensing data in water use estimation was investigated through empirical models based on vegetation index and semi-empirical two-compartment models. The obtained estimates were in good agreement with the measured values for the sample considered.

Keywords: water use, Alentejo, deficit irrigation, root system, remote sensing

Notas

No presente trabalho foi usado como separador decimal o símbolo ponto ".".

O texto desta tese não foi escrito ao abrigo do Novo Acordo Ortográfico.

As secções Lista de referências e Lista de símbolos, siglas e abreviaturas não se aplicam ao capítulo Publicações, uma vez que cada um dos artigos constituintes é autónomo, nomeadamente quanto à lista de referências e nomenclatura, e está de acordo com as regras editoriais da respectiva entidade editora. A secção Lista de símbolos, siglas e abreviaturas também não se aplica ao Anexo I.

O texto desta tese foi processado usando *software* gratuito e de código livre. Foi usada a distribuição LaTeX `MiKTeX` (`https://miktex.org/`), no ambiente de desenvolvimento `TeXstudio` (https://www.texstudio.org/), tendo as referências bibliográficas sido processadas usando a biblioteca `BibLaTeX` (com *backend=biber*).

Lista de símbolos, siglas e abreviaturas

Λ (adim.) – fracção de evaporação;

λ_w ($J\,kg^{-1}$) – calor latente de vaporização da água;

ρ_w ($kg\,m^{-3}$) – massa volúmica da água;

Ψ_{base} (MPa) – potencial hídrico foliar medido antes do nascer do sol ou potencial de base;

Ψ_{ramo} (MPa) – potencial hídrico do ramo;

$\Psi_{ramo\ min}$ (MPa) – potencial hídrico do ramo mínimo;

ETr ($kg\,m^{-2}\,s^{-1}$ ou $mm\,dia^{-1}$) – densidade de fluxo de evapotranspiração;

ET_o ($kg\,m^{-2}\,s^{-1}$ ou $mm\,dia^{-1}$) – densidade de fluxo de evapotranspiração da cultura de referência (relva);

G ($W\,m^{-2}$) – densidade de fluxo de calor sensível por condução para o solo;

gs ($m\,s^{-1}$) – condutância estomática;

H ($W\,m^{-2}$) – densidade de fluxo de calor sensível para a atmosfera;

$TeorAgua_{SondaNeutrões}$ ($m^3\,m^{-3}$) – teor de água do solo medido com o método neutrónico (*i.e.* com sonda de neutrões);

LAI (adim.) – índice de área foliar;

Ks (adim.) – coeficiente de *stress* (carência hídrica);

Kc (adim.) – coeficiente cultural;

Kcb (adim.) – coeficiente cultural basal;

Ke (adim.) – coeficiente de evaporação do solo;

RH (%) – humidade relativa do ar;

R_n ($W\,m^{-2}$) – densidade de fluxo correspondente ao balanço de radiação;

$T_{ref.humida}$ (K) – $T_{ref.seca}$ (K) – temperatura de uma superfície idêntica à folha, do ponto de vista óptico e aerodinâmico, mas com resistência de superfície nula ou máxima, respectivamente;

T_{ar} (K) – temperatura do ar;

T_{folha} (K) – temperatura da folha;

$Tr_{relativa}$ (adim.) – transpiração relativa;

Tr ($kg\,m^{-2}\,s^{-1}$) – densidade de fluxo de transpiração;

Tr_{max} ($kg\,m^{-2}\,s^{-1}$) – densidade de fluxo de transpiração máxima;

T_{solo} (K) – temperatura do solo;

$V_{DiâmetroTronco}$ (m) – variação do diâmetro do tronco;

$T_{RadConj}$, *ensemble directional radiometric surface temperature* (Norman e Becker, 1995);

CAG – método de medição de fluxo de seiva *Calibrated Average Gradient*;

DR – detecção remota;

ETM_+ – sensor *Enhanced Thematic Mapper Plus* a bordo do satélite Landsat-7;

FAO – *Food and Agriculture Organization of the United Nations*;

FS – fluxo de seiva;

HFD – método de medição de fluxo de seiva *Heat Field Deformation*;

IRGA – *infrared gas analyser*;

I_{veg}– índice de vegetação;

METRIC^{TM} – modelo *Mapping EvapoTranspiration at High Resolution using Internalised Calibration*;

NDVI – índice de vegetação *Normalized Difference Vegetation Index*;

SAVI – índice de vegetação *Soil-Adjusted Vegetation Index*;

SEBAL – modelo *Surface Energy Balance Algorithm for Land*;

SLSTR – sensor *Sea and Land Surface Temperature Radiometer* a bordo dos satélites da constelação Sentinel-3;

SVAT – *Soil-Vegetation-Atmosphere Transfer models*;

TM – sensor *Thematic Mapper* a bordo do satélite Landsat-5;

cdo – comprimento de onda;

Copernicus – programa Europeu Copernicus;

ddfluxo – densidade de fluxo;

Landsat – programa Norte Americano Landsat;

Sentinel-2 – constelação de satélites Sentinel-2 do programa Copernicus;

Sentinel-2A – satélite Sentinel-2A;

Sentinel-2B – satélite Sentinel-2B;

ZcCl – zona conservativa da camada limite turbulenta;

e.g. – abreviatura do latim *exempli gratia*, com significado de "por exemplo "(Dicionário-Priberam, 2017);

et al. – abreviatura do latim *et alii*, com significado de "e outros "(Dicionário-Priberam, 2017);

i.e. – redução do latim *id est*, com significado de "isto é "(Dicionário-Priberam, 2017);

lato sensu – expressão latina *lato sensu* com significado de "em sentido lato, em sentido muito geral "(Dicionário-Priberam, 2017);

vide – palavra latina *vide* usada para remeter para outro local do texto ou para outro texto (Dicionário-Priberam, 2017).

Índice

Introdução

O conhecimento do uso da água pelos ecossistemas é importante não só para a gestão da rega, em que a apropriada determinação da quantidade e oportunidade da rega, não só permite reduzir o consumo de água e energia, para idênticas produções, como, por exemplo, previne ou minimiza a lixiviação de nutrientes e resíduos de produtos fitofarmacêuticos, mas também para a gestão dos ecossistemas, naturais ou agrícolas, em regime de sequeiro. Em regime de sequeiro, a problemática consiste em projectar e decidir no sentido de aumentar a disponibilidade de água no solo e optimizar o seu uso pelas plantas.

Nas plantas lenhosas, nomeadamente porque são perenes, a manutenção de um equilíbrio fisiológico é deveras importante, porque os desequilíbrios desenvolvidos num ciclo vegetativo podem adicionalmente comprometer a planta e/ou a produção durante vários ciclos vegetativos seguintes. Este equilíbrio, embora desejável, é difícil de manter sobretudo em zonas de clima mediterrânico onde, na época estival, as consequências da escassez natural de água podem comprometer a produção adequada de fotoassimilados, conduzindo por exemplo ao desequilíbrio entre os processos vegetativos e reprodutivos nos ciclos vegetativos actual e futuros. Contudo é aceite que, nas culturas lenhosas, uma carência hídrica moderada e controlada (nomeadamente em períodos seleccionados do ciclo reprodutivo e/ou vegetativo) pode favorecer o equilíbrio fisiológico da planta e/ou a qualidade da produção e/ou produtividade da água (Girona et al., 2002; Silvestre, 2003). Sempre que exista uma carência hídrica natural acentuada (inter-anual e intra-anual), nomeadamente nas zonas mediterrânicas, a prática da rega é indispensável para se obter um volume e qualidade de produção regular ao longo dos sucessivos ciclos vegetativos.

Com o aumento da probabilidade da ocorrência de acontecimentos extremos, aumento da temperatura e redução da precipitação (IPCC, 2013, 2014), nomeadamente nas zonas mediterrânicas (IPMA, 2014; Loizidou et al., 2016), em consequência das alterações climáticas em grande parte relacionadas com as alterações antrópicas da concentração de gases com efeito de estufa (IPCC, 2015; Cook et al., 2016; Büntgen et al., 2017), é de esperar que a variabilidade inter-anual e intra-anual da disponibilidade natural de recursos hídricos seja acentuada, com consequências a nível ecológico (Melo-Abreu et al., 2004; Campoy et al., 2011) e social (Riera et al., 2007; Fiorentino et al., 2008; Büntgen et al., 2011; Teixeira e Rolim, 2014), nomeadamente pela desertificação[1](Min-Agricultura, 2013; ICNF, 2014b; Ponti et al., 2014).

O conhecimento das dinâmicas dos fluxos de massa e energia das superfícies vegetadas para a atmosfera (*e.g.* evapotranspiração), a compreensão das estratégias de sobrevivência e a possibilidade de construção de mapas com informação sobre o uso da água constituem

[1]Os autores ICNF (2014a) salientam que a expressão " desertificação humana " tem sido utilizada como sinónimo de despovoamento, mas não se deve confundir com o termo " desertificação " no sentido da Convenção das Nações Unidas para o Combate à Desertificação (United-Nations, 1994), isto é, a degradação do solo em climas com um certo grau de secura, resultante de fatores naturais ou das atividades humanas. Contudo, nas condições de Portugal, correm a par os dois conceitos.

ferramentas de elevado valor na gestão dos ecossistemas da Terra e das culturas agrícolas em particular.

As técnicas clássicas para medição da evapotranspiração (métodos hidrológicos e micrometeorológicos) e para quantificação da carência hídrica (indicadores do estado hídrico do solo e da planta), em condições naturais (*vide* Jarvis e McNaughton, 1986), têm grandes limitações, em termos operacionais, nomeadamente devido à instalação física dos sensores, para poderem ser usadas pelo utilizador comum. Também não são adequadas para construção de mapas de uso da água.

Os cobertos agrícolas lenhosos que são descontínuos, devido essencialmente ao povoamento radicular do solo não homogéneo e profundo e à estrutura descontínua e esparsa do copado, conduzem a dificuldades adicionais na aplicação dos métodos clássicos de medição da evapotranspiração (ETr). A rega localizada é um contributo de origem antrópica a juntar à heterogeneidade "natural" destes cobertos que dificulta o uso destas abordagens pela localização das zonas de solo humedecido pela rega.

As técnicas de detecção remota (DR), ao permitirem obter informação sobre os ecossistemas abrangendo áreas vastas, têm sido utilizadas em tentativas de mapeamento de uso da água (ou indicadores qualitativos relacionados) e por vezes também no mapeamento da intensidade da carência hídrica (Anderson e Kustas, 2008).

Dada a resolução espacial relativamente grosseira dos dados de detecção remota por satélite, coloca-se naturalmente a questão de esta fonte de informação poder não ser suficiente para responder às necessidades práticas. Em particular, coloca-se a hipótese de os dados de satélite deverem ser complementados por informação de elevada resolução espacial (a necessária para permitir individualizar os compartimentos relevantes, para os fluxos de massa e energia) por forma a ser possível obter resultados satisfatórios para a estimativa de ETr (e suas componentes) e da intensidade da carência hídrica (*e.g.* Bellvert et al., 2013). Os escassos resultados publicados para cobertos anisotrópicos não nos levam a rejeitar essa hipótese.

Esta tese enquadra-se num contexto da elevada importância dos cobertos anisotrópicos, a nível socioeconómico e ecológico, em climas mediterrâneos, e no facto de estes constituírem o elemento principal na paisagem (em mosaicos heterogéneos). A necessidade de analisar a evolução temporal em áreas vastas, heterogéneas e a perspectiva da continuação da democratização da utilização dos sensores e/ou informação de DR, contribui para o interesse crescente no uso destas técnicas. Neste sentido, este trabalho pretende não só contribuir para aumentar o conhecimento sobre o uso da água e as relações hídricas dos ecossistemas agrícolas, obtendo ainda parâmetros para a gestão da água em agricultura, como fornecer uma referência (*ground-truth*) para avaliar e melhorar as estimativas por DR.

Objectivo e enquadramento

Com este trabalho pretendia-se obter novos conhecimentos sobre os efeitos da carência hídrica na dinâmica de utilização da água pelos cobertos agrícolas anisotrópicos (vinha e olival) numa região mediterrânica de elevada escassez natural de água e para o esclarecimento do funcionamento do sistema radicular na gestão da água pela planta e a sua importância nas estratégias de sobrevivência. Investigamos também sobre as possibilidades do uso de dados de DR na estimativa do uso da água e detecção da carência hídrica.

Para atingir estes objectivos, estudou-se o uso da água, em condições de carência hídrica, e a gestão da rega deficitária aplicando os métodos clássicos de medição de ETr e suas componentes, e de quantificação do estado hídrico da planta e do solo, que se consideraram como referência. Estes dados foram combinados com outros obtidos por DR, nomeadamente dos sensores *Thematic Mapper* (TM) e *Enhanced Thematic Mapper Plus* (ETM^+) a bordo dos satélites Landsat-5 e Landsat-7, respectivamente.

As culturas estudadas foram: vinha (regada) e olival (regado e não regado) respectivamente em Beja e Ferreira do Alentejo, zonas de elevada escassez natural de recursos hídricos e onde o regadio está em desenvolvimento. A componente experimental do plano de trabalhos incluiu os seguintes grupos de tarefas:

– medições utilizando o método micrometeorológico das flutuações instantâneas (ETr), um método gravimétrico (microlisímetros, evaporação do solo) e um método de medição do fluxo de seiva nos troncos (método da dissipação térmica, Granier, 1985), combinados de forma a obter séries temporais contínuas de valores da transpiração;

– medições utilizando métodos de fluxo de seiva em raízes, com vista a complementar a informação sobre a relação entre a dinâmica do uso da água e as estratégias de sobrevivência;

– medições do estado hídrico do solo e da planta;

– medições em relação a parâmetros do solo e coberto, necessários à caracterização da situação experimental e modelação;

– recolha de dados de detecção remota usando sensores portáteis;

– para as estimativas por detecção remota (*e.g.* ETr) foi feita a compilação, processamento e análise de dados de reflectância à superfície (bandas do visível, infravermelho próximo e infravermelho médio) e de temperatura derivada da banda térmica dos sensores TM e ETM^+, previamente processados (*i.e.* com correcções) pelo *software* especializado LEDAPS (*Landsat Ecosystem Disturbance Adaptive Processing System,* Masek et al., 2006; Vermote e Saleous, 2007; Schmidt et al., 2013) e disponíveis no arquivo (de domínio público) USGS[1] Landsat *Climate Data Record Surface Reflectance* (GeologicalSurvey, 2015).

[1] *United States of America Geological Survey.*

As principais tarefas experimentais foram desenvolvidas no âmbito dos projectos de investigação PTDC/AGR-AAM/69848/2006, TELERIEG [2] e WUSSIAAME [3] sob a responsabilidade da investigadora, Professora Maria Isabel Ferreira, do ora Departamento de Engenharia Rural, agora Departamento de Ciências e Engenharia de Biossistemas, do Instituto Superior de Agronomia e enquadrados no Centro de Estudos de Engenharia Rural (CEER), posteriormente designado por *Linking Landscape, Environment, Agriculture and Food* (LEAF).

[2] *Uso de la teledetección para la recomendación y seguimiento de las prácticas de riego en el espacio SUDOE.*

[3] *Water Use, Survival Strategies and Impact of Agrochemicals in Agricultural Mediterranean Ecosystems*, PTDC/AACAMB/100635/2008.

Estado da arte

Os cobertos vegetais podem classificar-se em contínuos ou descontínuos (anisotrópicos). Coberto descontínuo é aquele em que a disposição espacial das plantas leva à existência de uma cobertura do solo incompleta ou heterogénea, dando origem a descontinuidades entre a massa vegetal lenhosa e o solo ou a vegetação em sobcoberto (são exemplos os pomares, vinhas e montados).

Já as culturas arvenses (*e.g.* os cereais para produção de grão, as oleaginosas e as proteaginosas), as culturas forrageiras e as pastagens, quando dispostas de forma a cobrir totalmente o solo, constituem um coberto mais ou menos uniforme e contínuo, designando-se então por cobertos vegetais contínuos. Consequências destas arquitecturas espaciais são discutidas em Ferreira (1996) e Ferreira et al. (2008). Seleccionaram-se as culturas de vinha e oliveira porque são exemplos de cobertos agrícolas anisotrópicos cultivados na zona mediterrânica desde a antiguidade e para os quais ainda não estão completamente esclarecidos os mecanismos de uso da água em condições de carência hídrica, tanto a nível da transpiração como do funcionamento e importância relativa das raízes nos vários compartimentos abaixo da superfície.

A notável adaptação da oliveira[1] a condições de carência hídrica confere-lhe a capacidade de crescer e obter produções comerciais aceitáveis em condições de sequeiro em áreas onde a precipitação anual é cerca de 500 mm ou inferior, e onde a estação seca pode durar cinco ou seis meses (Fernández e Moreno, 1999). Também a vinha é capaz de sobreviver e produzir, apesar de pouco, em condições de carência hídrica intensa, sabendo-se que a partir da floração ou do vingamento a carência hídrica intensa afecta o desenvolvimento vegetativo, as capacidades fotossintéticas do coberto e as componentes da produção. Por outro lado, como salientado por Silvestre (2003), situações de conforto hídrico são susceptíveis de aumentar o vigor e provocar uma diminuição da qualidade da vindima, situação que se pretende evitar, sendo uma das culturas onde o controlo do estado hídrico mais benefícios económicos pode trazer.

Os artigos que constituem esta tese não detalham em particular os aspectos metodológicos mas incluem revisão direccionada para os processos em análise. Em consequência, optou-se por dar neste capítulo algum destaque às metodologias de forma a evitar redundância com os artigos publicados.

[1] A oliveira (*Olea europaea* L.) constitui um elemento característico da paisagem Mediterrânica sendo considerada, tal como a videira (*Vitis vinifera* L.), a figueira (*Ficus carica* L.) e a tamareira (*Phoenix dactylifera* L.), das plantas lenhosas cultivadas mais antigas (Zohary e Spiegel-Roy, 1975; Weiss, 2015).

3.1 Medição da evapotranspiração e suas componentes

Rana e Katerji (2000) defendem a classificação proposta por Rose e Sharma (1984) que agrupa os diferentes métodos de medição da evaporação (*lato sensu*) nos cobertos vegetais, em função dos principais conceitos subjacentes à sua formulação. Definem-se assim três grupos de métodos (tabela 3.1): hidrológicos, micrometeorológicos e outros. Os métodos hidrológicos baseiam-se na resolução da equação do balanço hídrico no solo (conservação da massa) em condições naturais ou em lisímetros. Os métodos micrometeorológicos baseiam-se em medições de grandezas relacionadas com os fluxos, em um ou vários níveis, na zona conservativa da camada limite turbulenta (ZcCl), ou seja, onde a densidade de fluxo (ddfluxo) da entidade i é constante em função da altura na camada limite (cerca dos primeiros 15 % da altura total da camada limite) de preferência na sub-camada inercial (*inertial sublayer*, Monteith e Unsworth, 1990). Estes métodos permitem apenas medir a ddfluxo média da entidade i (*bulk rates of exchange*) entre a superfície evaporante j e a altura z na ZcCl. Os métodos micrometeorológicos só são aplicáveis a cobertos extensos e de altura uniforme, de forma a respeitar a validade das equações e a evitar efeitos de advecção. Os outros métodos baseiam-se em medições em plantas individuais ou partes da planta.

Apenas os métodos hidrológicos e micrometeorológicos têm aplicabilidade para medir a evapotranspiração em condições naturais (Ferreira, 1996), uma vez que os outros métodos, necessitam de modelos de extrapolação da amostra para a população (*up-scaling* ou *aggregation*, Jarvis e McNaughton, 1986) ou os dispositivos experimentais perturbam demasiado as condições naturais. A ETr também pode ser medida usando as técnicas baseadas na cintilometria da atmosfera, que medem a variação do índice de refracção do ar (Ward et al., 2013; Brunsell et al., 2011), podendo ser preferidas na medição dos fluxos de água para a atmosfera em zonas muito heterogéneas (Brunsell et al., 2011; Ward, 2017).

Para medir a evaporação do solo têm sido usados métodos hidrológicos, nomeadamente microlisímetros (*e.g.* Daamen et al., 1993) e medições em câmaras de trocas gasosas. Por exemplo Raz-Yaseef et al. (2010) adaptaram, para medir a evaporação do solo, um sensor IRGA (*Infra Red Gas Analyzer*).

Tabela 3.1: Principais métodos para medição da evaporação (*lato sensu*) em cobertos vegetais.

Classe	Designação	Variável	Tipo medição
Hidrológicos	Lisímetro de pesagem	ETr, Tr	Directa
	Microlisímetros	Es	Directa
	Lisímetro de drenagem	ETr, Tr	Indirecta
	Balanço hídrico do solo	ETr	Indirecta
Micrometeorológicos	Método aerodinâmico	ETr	Indirecta
	Método da razão de *Bowen*	ETr	Indirecta
	Método das flutuações instantâneas	ETr	Directa
	Métodos baseados em combinações dos anteriores (*e.g.* método aerodinâmico simplificado)	ETr	Indirecta
Outros métodos	Métodos de medição do fluxo de seiva	Tr	Indirecta
	Câmaras de trocas gasosas	Tr, Es	Indirecta

Os métodos hidrológicos apresentam grandes limitações de aplicação em cobertos anisotrópicos lenhosos e esparsos principalmente devido à heterogeneidade de povoamento do solo pelas raízes na direcção horizontal e vertical (raízes profundantes). Por outro lado a utilização de lisímetros pode criar condições artificiais para o desenvolvimento radicular. Por exemplo, Girona et al. (2002) concluiram que dois grupos de árvores com 8 anos de idade (*Prunus persica* L. Bastch) sujeitas a rega deficitária, um grupo dentro de um lisímetro ($4 \times 2 \times 2$ m^3) e outro grupo, em condições naturais no pomar, apresentaram respostas distintas nomeadamente quanto ao padrão de extracção de água do solo. Considera-se em geral ainda necessário entrar em conta com o padrão de humedecimento, profundidade do solo e volume explorado pelas raízes em condições de rega de elevada frequência, para definir o volume de solo efectivamente explorado pelas raízes em termos de absorção de água.

Nos cobertos descontínuos existem mais restrições na aplicação dos métodos micrometeorológicos para a medição de ETr, sobretudo os que usam relações fluxo-gradiente (método aerodinâmico e da razão de Bowen), uma vez que os pressupostos nas equações das trocas de massa e energia são mais questionáveis nestes casos (Denmead, 1984; Monteith e Unsworth, 1990). O método das flutuações instantâneas (EC) é normalmente considerado o método de referência para a medição de ETr (Kustas, 1990; Baldocchi et al., 2001; Baldocchi, 2014b). Uma discussão mais detalhada sobre os métodos micrometeorológicos pode ser encontrada, por exemplo, em Monteith e Unsworth (1990) e sobre a aplicabilidade dos diferentes métodos em cobertos anisotrópicos lenhosos esparsos na zona mediterrânica em Rana e Katerji (2000) e em Ferreira et al. (2008).

3.2 Combinação de métodos para medição da evapotranspiração e suas componentes

Tendo em conta os métodos disponíveis para medir a evaporação nos cobertos vegetais e as restrições na sua utilização em geral e nos cobertos anisotrópicos lenhosos e esparsos em particular, tem sido usado no grupo de trabalho, desde 1994 (Ferreira, 1996) uma combinação de métodos de forma a medir a evapotranspiração (ETr), a transpiração (Tr) e a evaporação do solo (Es, *vide* Paço, 2003; Silvestre, 2003; Ferreira et al., 2008; Silva, 2009). A intercepção não é explicitada nas situações em que é possível admitir que tenha reduzida expressão (*e.g.* durante o período estival nas condições de clima mediterrâneo). A metodologia consiste em primeiro lugar aplicar o método EC como referência para medição dos fluxos de calor latente (LE) e sensível (H), convertendo o primeiro no correspondente fluxo de massa (ETr), verificando-se a qualidade das medições analisando o erro de fecho da equação do balanço de energia (equação 3.1) entre outras abordagens.

$$R_n = LE + G + H \tag{3.1}$$

onde:

R_n (W m^{-2}) – densidade de fluxo de radiação líquida;
G (W m^{-2}) – densidade de fluxo de calor sensível para o solo;
H (W m^{-2}) – densidade de fluxo de calor sensível para a atmosfera;
LE (W m^{-2}) – densidade de fluxo de calor latente.

O método EC baseia-se na técnica de cálculo designada por decomposição de *Reynolds* (Reynolds, 1895; Aubinet et al., 2012; Launder, 2015) e necessita da medição, apenas num nível na ZcCl (ao contrário dos restantes métodos micrometeorológicos baseados nas relações fluxo-gradiente, que necessitam de medições em dois ou mais níveis) da componente vertical da velocidade do vento (normalmente usando anemómetros sónicos) e da concentração de outra entidade relacionada com a densidade de fluxo que se pretende medir. No caso de ETr é medida a humidade absoluta, usando sensores que permitam frequências de medição tipicamente de 10 Hz–20 Hz (*e.g.* higrómetros de Crípton e *Lyman-alpha*, e sensores IRGA).

Segundo Baldocchi (2003) as primeiras aplicações do método das flutuações instantâneas terão ocorrido em 1926 (estudo das transferências de quantidade de movimento), por Scrase (1930), mas com tecnologia rudimentar. De acordo com Baldocchi (2014a) durante as décadas de 1940 e 1950 ocorreram avanços teóricos (*e.g.* teoria da similaridade de Monin-Obukhov, Foken, 2006), e tecnológicos (*e.g.* anemómetro de fio quente) tendo sido desenvolvidos trabalhos inovadores como *e.g.* Swinbank (1951). Em Baldocchi (2003), Foken (2006), Aubinet et al. (2012) e Burba (2013) podem ser consultados mais detalhes sobre a história, bases teóricas e aplicação práctica do método micrometeorológico das flutuações instantâneas.

Em geral os investigadores medem as outras componentes do balanço energético para a verificação do erro de fecho da equação do balanço de energia. O valor de H pode ser medido recorrendo ao método micrometeorológico EC, como acima referido. O balanço de radiação (R_n) pode ser medido usando pirradiómetros ou conjuntos de dois piranómetros (balanço de radiação de pequeno comprimento de onda, cdo) associados a dois pirgeómetros (balanço de radiação de longo cdo).

O fluxo de calor por condução para o solo (G) é obtido pela medição do fluxo de calor sensível a uma dada profundidade p (normalmente 5 cm) usando placas de fluxo de calor, ao qual se adiciona a variação de energia acumulada na camada de solo entre a superfície e a profundidade p. Para o cálculo da variação de armazenamento de energia é necessário conhecer a capacidade térmica mássica do solo e a variação de temperatura do solo ocorrida no intervalo de tempo de integração. Mais detalhes poderão ser consultados em Paço (2003) e Silva (2009).

A evaporação do solo pode medir-se usando microlisímetros. Contudo devido a dificuldades experimentais no uso desta abordagem[2] e às diferentes resoluções espaciais e temporais dos diferentes métodos[3] é necessário recorrer à utilização de modelos para Es (*vide* Paço et al., 2014), fazendo-se a respectiva calibração local.

O fluxo de seiva pode ser medido com o método de Granier (Granier, 1985; Granier e Gross, 1987) constituindo uma alternativa relativamente simples e económica e que tem sido explorada pela equipa, ao nível da precisão e desempenho (*e.g.* Ferreira et al., 2012b) mas que, por poder fornecer valores subestimados, requer calibração caso a caso (Ferreira et al., 2004; Ferreira et al., 2008). Assim, combinando os resultados de medição de ETr (método EC) e Es é possível obter valores para Tr_{EC} (equação 3.2) que, depois de relacionados com os obtidos pelos métodos de fluxo de seiva, permitem obter séries

[2] O processo de medição da evaporação do solo é muito moroso e por exemplo nem sempre a textura e/ou estrutura do solo permitem a amostragem necessária. Este aspecto assume especial relevância em solos de textura argilosa e/ou com baixo teor em água.

[3] Regra geral as séries temporais de LE provenientes das medições (automáticas) com o método EC têm uma resolução temporal de 30 min. Para se conseguir a mesma resolução temporal com microlisímetros é necessário um elevado investimento em mão-de-obra, sendo que não é possível antecipar se as condições de *fecth* são adequadas.

temporais à escala sazonal para Tr (*vide* o diagrama de fluxo apresentado no Anexo I).

$$Tr_{\mathrm{EC}} = ETr - Es \tag{3.2}$$

onde:

$\mathrm{Tr_{EC}}$ ($\mathrm{kg\,m^{-2}\,s^{-1}}$ ou $\mathrm{mm\,dia^{-1}}$) – densidade de fluxo de transpiração calculada subtraindo a evaporação do solo à evapoptranspiração medida com o método das flutuações instantâneas;

ETr ($\mathrm{kg\,m^{-2}\,s^{-1}}$ ou $\mathrm{mm\,dia^{-1}}$) – densidade de fluxo de evapotranspiração;

Es ($\mathrm{kg\,m^{-2}\,s^{-1}}$ ou $\mathrm{mm\,dia^{-1}}$) – densidade de fluxo de evaporação do solo.

Para quantificar o fluxo de seiva nas raízes podem usar-se métodos que permitam medir fluxos nos dois sentidos: o método da deformação do campo de calor (HFD, *Heat Field Deformation*, Nadezhdina et al., 1998) e o método *Calibrated Average Gradient* (CAG, Testi e Villalobos, 2009; Green et al., 2009).

3.3 Quantificação do estado hídrico da planta

Em geral, procura-se quantificar o estado hídrico das plantas para compreender os mecanismos relacionados com o uso da água e para utilização na gestão da rega. A definição de carência hídrica (*vide* Hsiao, 1973; Hinckley e Ceulemans, 1989; Lichtenthaler, 1996; Chaves et al., 2003; De Leonardis et al., 2012) é controversa; de acordo com Hsiao et al. (1976), a intensidade da carência hídrica é função da redução do potencial hídrico em relação a valores considerados óptimos. A avaliação do estado hídrico da planta pode ser feita realizando medições directamente na planta (Kramer, 1963), no solo, e ainda através das implicações da carência hídrica na intensidade relativa dos fluxos ou gradientes atmosféricos (como por exemplo a transpiração relativa, $\mathrm{Tr_{relativa}}$, equação 3.3). Indicadores do estado hídrico do solo são por exemplo o teor de água no solo e o potencial de água do solo.

$$Tr_{relativa} = \frac{Tr}{Tr_{max}} \tag{3.3}$$

onde:

$\mathrm{Tr_{relativa}}$ (adim.) – transpiração relativa;

Tr ($\mathrm{kg\,m^{-2}\,s^{-1}}$ ou $\mathrm{mm\,dia^{-1}}$) – densidade de fluxo de transpiração;

$\mathrm{Tr_{max}}$ ($\mathrm{kg\,m^{-2}\,s^{-1}}$ ou $\mathrm{mm\,dia^{-1}}$) – densidade de fluxo de transpiração máxima.

Na planta as variáveis mais frequentemente utilizadas são o potencial hídrico, a variação de diâmetro de um órgão seleccionado (frequentemente o tronco ou ramos) e variáveis daí derivadas, a condutância estomática (gs) e a temperatura da folha ($\mathrm{T_{folha}}$). Para o potencial hídrico, as grandezas mais usadas são o potencial hídrico foliar medido antes do nascer do sol (potencial de base, Ψ_{base}) e o potencial hídrico do xilema mínimo ($\Psi_{\mathrm{ramo\ min}}$).

A utilização de $\mathrm{T_{folha}}$ baseia-se no efeito da redução de Tr (menor quantidade de energia usada na vaporização da água, o que implica maior H), consequência da redução de gs devido à carência hídrica (mantendo os restantes factores constantes). Nos cobertos

anisotrópicos de elevada extensão vertical, regra geral, a resistência aerodinâmica é reduzida (factor de desacoplamento baixo) pelo que gs tem papel preponderante no controlo de Tr em igualdade de condições de procura atmosférica (Jarvis, 1985; Ferreira-Gama, 1987; Ferreira et al., 2008).

Poderíamos admitir que variáveis que utilizem a T_{folha} serão um bom indicador de gs. Contudo, o valor instantâneo de T_{folha} depende da radiação, da velocidade do vento, temperatura e humidade do ar (Fuchs, 1990) tendo o valor absoluto de T_{folha} pouco interesse prático (no sentido da quantificação da carência hídrica). Em termos práticos têm-se utilizado a distribuição da T_{folha} no copado e/ou na planta (Jones et al., 2002; Gonzalez-Dugo et al., 2012) e índices construídos normalizando T_{folha} com outras variáveis nomeadamente a temperatura do ar e de superfícies tomadas como referência.

Jones (1999) propõe versões melhoradas do índice CWSI (*crop water stress index*), inicialmente proposto por Idso (1982) e Jackson et al. (1981), que usam superfícies de referência idênticas à superfície evaporante do ponto de vista óptico e aerodinâmico, diferindo apenas na resistência de superfície, nomeadamente a equação 3.4.

$$CWSI_{Jones} = \frac{T_{folha} - T_{ref.humida}}{T_{ref.seca} - T_{ref.humida}} \tag{3.4}$$

onde:

$CWSI_{Jones}$ (adim.) – *crop water stress index* (Jones, 1999);

T_{folha} (K) – temperatura da folha;

$T_{ref.humida}$ (K), $T_{ref.seca}$ (K) – temperatura de uma superfície idêntica à folha, do ponto de vista óptico e aerodinâmico, mas com resistência de superfície nula ou máxima, respectivamente.

3.4 Modelos conceptuais para as trocas de massa e energia nos copados

Para modelar as trocas de massa e energia (fluxos radiativos e não radiativos) entre os cobertos vegetais (solo e vegetação) e a atmosfera envolvente têm sido desenvolvidos diferentes modelos, que diferem na forma como conceptualizam a estrutura do copado (mono-camada e um único compartimento ou multi-compartimentos, normalmente mono-dimensionais) e no tipo de funções usadas para descrever os processos físicos e biológicos (existem desde modelos empíricos até modelos com diferentes equilíbrios entre funções empíricas e de base física).

Os modelos mono-camada (*big leaf*) admitem que é possível identificar uma superfície fictícia onde se encontra a fonte ou o sumidouro de todos os fluxos (radiativos e não radiativos). Este tipo de modelo tem sido aplicado com relativo sucesso nos cobertos homogéneos (*e.g.* equação de Penman-Monteith, Monteith, 1965).

Os modelos multi-compartimentos mais simples modelam o copado distinguindo apenas dois compartimentos, um para a vegetação e outro para o solo exposto. Os modelos mais complexos dividem estes dois compartimentos em sub-compartimentos (camadas). Estes modelos são usados essencialmente para obviar às limitações dos modelos mono-camada quando aplicados nos cobertos anisotrópicos, onde é importante a partição da ETr em Tr e Es (Shuttleworth e Wallace, 1985; Jones e Vaughan, 2010) ou conhecer os fluxos provenientes de diferentes estratos de vegetação.

O modelo dos coeficientes culturais (van-Wijk e de-Vries, 1954; Jensen, 1968; Wright, 1982) sistematizado e divulgado pela FAO (*Food and Agriculture Organization of the United Nations*, Doorenbos e Pruitt, 1977; Allen et al., 1998) conjuga módulos de base essencialmente física (*e.g.* estimativa da ET_o) com módulos empíricos e pode ser aplicado usando uma estrutura mono-camada ou de dois compartimentos. A equação de Penman-Monteith com os parâmetros para a relva (Allen et al., 1998) é usada geralmente para estimar ET_o segundo um modelo mono-camada. Contudo pode ser usada para estimar a evaporação em geral, normalmente associada a modelos mono-camada. Na aplicação deste modelo a uma cultura seguem-se três fases (na versão de dois compartimentos): na primeira fase estima-se ET_o, numa segunda fase é feito o ajustamento do coeficiente cultural basal (Kcb) que pressupõe conforto hídrico e do coeficiente de evaporação (Ke) e por último estima-se o valor do coeficiente de carência hídrica (Ks).

3.5 Estimativa da evapotranspiração com base em informação de detecção remota

O termo detecção remota (DR) terá surgido apenas no início da década de 1960 com o significado de observação e medição de grandezas de um objecto sem contacto físico com o sensor ou observador (Jones e Vaughan, 2010). Ao nível do conhecimento e tecnologia actual as técnicas de DR não permitem medir os fluxos não radiativos de massa e energia de um copado sendo necessário calibrar as estimativas com medidas resultantes da aplicação de técnicas convencionais de medição (Gentine et al., 2007; Jones e Vaughan, 2010).

Courault et al. (2005) propõem uma classificação dos diferentes modelos, que têm sido desenvolvidos para usar informação de DR na estimativa dos fluxos de massa e energia, em função da sua complexidade que depende principalmente da relação entre os módulos empíricos e de base física. Considera assim quatro grandes grupos:

i) métodos empíricos directos, quando a informação de DR é usada directamente em modelos semi-empíricos para estimar ETr;

ii) métodos baseados em índices de vegetação (I_{veg}), que usam um valor de ET como referência (a partir de medições no solo, por exemplo ET_o) e estimam um factor de ajustamento para estimar ETr.

iii) métodos baseados no balanço de energia (BE), que calculam ETr como resíduo da equação do balanço de energia e combinam módulos de base empírica e de base física. Alguns modelos operacionais de um compartimento, como o SEBAL (*Surface Energy Balance Algorithm for Land*, Bastiaanssen et al., 1998a) no qual se baseia o modelo METRIC^{TM} (*Mapping EvapoTranspiration at High Resolution using Internalised Calibration*, Allen et al., 2007) e de dois compartimentos, como o STSEB (*Simplified Two-Source Energy Balance Model*, Sánchez et al., 2008) pertencem a este grupo;

iv) métodos determinísticos, baseiam-se em modelos mais complexos tais como *Soil-Vegetation-Atmosphere Transfer models* (SVAT).

A revisão de Calera et al. (2017) trata sobre os diferentes modelos e métodos integrando dados de detecção remota para estimativa de ETr, suas vantagens e desvantagens, nomeadamente, no sentido da sua utilização na condução e gestão da rega na exploração agrícola. Também a revisão feita por Alvino e Marino (2017) trata da aplicação das

técnicas de detecção remota na estimativa de ETr e para monitorizar o estado hídrico da planta e do solo.

Descrevem-se seguidamente alguns aspectos mais detalhados sobre esses modelos, colocando em evidência as potencialidades e as limitações do uso de dados de DR para estimar ETr e suas componentes. Importa referir que a maioria dos modelos desenvolvidos têm sido optimizados para usar informação de detecção remota proveniente de sensores a bordo de satélites. Uma das limitações do uso desta informação reside na baixa resolução temporal associada à informação de maior resolução espacial. Ainda no início da década de 2010 existiam investigadores que realçavam a importância e necessidade da construção de constelações de satélites com sensores compatíveis (dependente de disponibilidade financeira) para aumentar a resolução temporal dos dados permitindo a adequada monitorização dos cobertos vegetais relativamente ao estado hídrico. Por exemplo os investigadores Campos et al. (2010) para aumentar o volume de dados do sensor TM disponíveis para o seu trabalho localizaram o campo experimental numa zona de sobreposição de duas faixas de passagem do satélite Landsat-5 (*Path-Row* 199–33 e 200–33) aumentando assim a resolução temporal[4] de 16 para 7–9 dias.

Neste sentido e no âmbito do programa Copernicus[5], a família de satélites Sentinel-2 foi projectada para recolher dados multiespectrais[6] tendo os satélites Sentinel-2A e Sentinel-2B da constelação sido lançados em 22 de Junho de 2015 e 7 de Março de 2017 respectivamente (Programa Copernicus, 2017). Contudo nos satélites Sentinel as bandas no infravermelho térmico têm uma resolução espacial de 1000 m (sensor *Sea and Land Surface Temperature Radiometer*, SLSTR) o que torna os dados inadequados para o uso em modelos de estimativa de ETr que usem dados no infravermelho térmico. A resolução espacial dos sensores com banda no infravermelho térmico a bordo dos satélites Landsat-7 (60 m) e Landsat-8 (100 m) permite a utilização dos dados para estimativa de ETr ao nível da parcela agrícola. Os dados provenientes dos satélites em funcionamento pertencente ao programa Landsat (Landsat-7 e Landsat-8) podem ser usados como provenientes de uma constelação de satélites.

[4] A resolução temporal dos dados de qualidade, provenientes de sensores (desde o visível até ao infravermelho térmico) a bordo de satélites, depende da frequência de passagem do satélite e do estado da atmosfera, nomeadamente da existência de nuvens.

[5] Copernicus é o novo nome para o antigo programa *Global Monitoring for Environment and Security programme* (GMES) e consiste num sistema de serviços Europeu para monitorização da Terra. Este sistema de serviços engloba um conjunto de sub-sistemas que recolhem dados provenientes de várias fontes (satélites de observação da Terra e sensores *in situ*, tais como estações no solo, na atmosfera e no mar).

O sistema de satélites é constituído por vários conjuntos de satélites especializados, designados de famílias Sentinel. Sentinel-1, -2, -3, -5P e -6 são satélites dedicados, enquanto que Sentinel-4 e -5 são sensores a bordo de satélites meteorológicos EUMETSAT (*European Organisation for the Exploitation of Meteorological Satellites*). O primeiro satélite (Sentinel-1A) foi lançado em 2014.

[6] Sensor com resolução espectral de 13 bandas no intervalo 443.9 nm–2202.4 nm e resolução espacial entre 10 m e 60 m. A resolução temporal de cada satélite permite uma frequência de visita de 5 dias, sendo de 10 dias para cada satélite individual. Os dados são utilizáveis, nomeadamente, para monitorizar a superfície da Terra.

Os métodos baseados nos índices de vegetação usam-nos para estimar Kcb por meio de funções empíricas e seguem modelos baseados no conceito de coeficiente cultural para estimar ETr (equações 3.5 e 3.6). Estes modelos regra geral, associam módulos independentes da informação de DR para estimativa de ET_o, de Ks e de Ke. Por exemplo Campos et al. (2010) estimaram ETr numa vinha regada (sem sobcoberto) à escala de tempo diária usando um modelo com base em I_{veg} (modelo de dois compartimentos) que compararam com valores de ETr obtidos com o método EC. Usaram dados do sensor TM (Landsat-5) para estimar Kcb (equações 3.7 e 3.8) e o balanço hídrico na zona explorada pelas raízes para estimar Ks e Ke.

$$ETr = Ks_{medio} \times Kc \times ET_o \tag{3.5}$$

$$ETr = (Ks \times Kcb + Ke)\, ET_o \tag{3.6}$$

$$Kcb = 1.44 \times NDVI - 0.10 \qquad r^2 = 0.96 \tag{3.7}$$

$$Kcb = 1.79 \times SAVI - 0.08 \qquad r^2 = 0.93 \tag{3.8}$$

onde:

ETr ($kg\,m^{-2}\,s^{-1}$ ou $mm\,dia^{-1}$) – densidade de fluxo de evapotranspiração;

ET_o ($kg\,m^{-2}\,s^{-1}$ ou $mm\,dia^{-1}$) – densidade de fluxo de evapotranspiração da cultura de referência (relva);

Kc (adim.) – coeficiente cultural;

Ks (adim.) – coeficiente de carência hídrica;

Kcb (adim.) – coeficiente cultural basal;

Ke (adim.) – coeficiente de evaporação do solo;

NDVI (adim.) – *Normalized Difference Vegetation Index* (Rouse et al., 1973);

SAVI (adim.) – *Soil-Adjusted Vegetation Index* (Huete, 1988).

Os métodos baseados no balanço de energia caracterizam as condições actuais da superfície evaporante usando a $T_{RadConj}$[7] e I_{veg}. A $T_{RadConj}$ é usada para medir H (usando uma função fluxo-grafiente), sendo a ETr calculada como termo residual da equação do balanço de energia mono-dimensional (equação 3.9). No modelo SEBAL o NDVI (*Normalized Difference Vegetation Index*, Rouse et al., 1973) é usado com a $T_{RadConj}$ na estimativa de G. Os modelos que usam a $T_{RadConj}$ terão de ter em conta as diferenças entre $T_{RadConj}$ e a temperatura aerodinâmica da superfície (*vide* Chehbouni et al., 1996) na medição de H, especialmente em cobertos heterogéneos (*vide* Norman et al., 1995;

[7]Para uma superfície heterogénea e não isotérmica (por exemplo um copado agrícola) não é possível em termos teóricos a igualdade entre a temperatura termodinâmica e a temperatura radiativa pelo que Norman e Becker (1995) definem, para superfícies heterogéneas e não isotérmicas, o conceito de temperatura radiométrica direccional conjunta da superfície ($T_{RadConj}$, *ensemble directional radiometric surface temperature*) e de emissividade conjunta (*ensemble emissivity*).

Chehbouni et al., 1997), pelo que têm sido desenvolvidos modelos com diferentes graus de complexidade de forma a trabalhar com esta diferença.

$$LE = R_n - G - H \tag{3.9}$$

onde:

G ($\mathrm{W\,m^{-2}}$) – densidade de fluxo de calor sensível para o solo;

H ($\mathrm{W\,m^{-2}}$) – densidade de fluxo de calor sensível para a atmosfera;

LE ($\mathrm{W\,m^{-2}}$) – densidade de fluxo de calor latente, que corresponde a ETr quando expressa em densidade de fluxo de massa de água evaporada ($\mathrm{kg\,m^{-2}\,s^{-1}}$ ou $\mathrm{mm\,dia^{-1}}$);

$\mathrm{R_n}$ ($\mathrm{W\,m^{-2}}$) – densidade de fluxo de radiação líquida ou balanço de radiação.

No modelo SEBAL (Bastiaanssen et al., 1998a; Bastiaanssen et al., 1998b; Bastiaanssen et al., 2005) um dos principais pressupostos é de que a fracção de evaporação (Λ, equações 3.10 e 3.11) é constante durante o período diurno permitindo assim a estimativa da ETr média diária (equação 3.12, Bastiaanssen et al., 2005) usando dados de DR de uma única observação diária. Segundo 2005, esta condição tem sido verificada experimentalmente em ecossistemas onde o teor de água no solo não varia muito e não existe advecção.

$$LE = \Lambda\,(R_n - G) \tag{3.10}$$

$$\Lambda_t = \frac{LE_t}{R_{nt} - G_t} = \frac{LE_t}{LE_t + H_t} = \frac{R_{nt} - G_t - H_t}{R_{nt} - G_t} \tag{3.11}$$

$$ETr_{24h} = \frac{8.64 \times 10^6}{\lambda_w \times \rho_w} \times \Lambda \times R_{n24h} \tag{3.12}$$

onde:

ETr ($\mathrm{mm\,dia^{-1}}$) – densidade de fluxo de evapotranspiração;

LE ($\mathrm{W\,m^{-2}}$) – densidade de fluxo de calor latente;

Λ (adim.) – fracção de evaporação;

G ($\mathrm{W\,m^{-2}}$) – densidade de fluxo de calor para o solo;

H ($\mathrm{W\,m^{-2}}$) – densidade de fluxo de calor sensível;

$\mathrm{R_n}$ ($\mathrm{W\,m^{-2}}$) – densidade de fluxo de radiação líquida;

λ_w ($\mathrm{J\,kg^{-1}}$) – calor latente de vaporização da água;

ρ_w ($\mathrm{kg^3\,m^{-1}}$) – massa volúmica da água.

As variáveis com o índice t, representam valores instantâneos no tempo t, as variáveis com índice $24h$ representam os totais para períodos de 24 horas.

Contudo Gentine et al. (2011) referem que os estudos que conduziram à conclusão de que a Λ é constante ao longo do dia se basearam em períodos de medições de curta duração. Tendo feito um estudo mais detalhado concluíram que a preservação da Λ só se verifica em condições especiais (dias de céu limpo, com radiação solar intensa e

em climas húmidos). Nas outras situações em que Λ não é constante isso deve-se à diferença de fase e amplitude entre a ETr e H, induzidas pela sua diferente resposta ao fluxo de radiação solar. Gonzalez-Dugo et al. (2009) compararam medições de ETr (culturas de milho e soja em condições de sequeiro) com estimativas de ET provenientes de modelos baseados na resolução do BE (modelos mono-camada e de dois compartimentos) e modelos baseados em I_{veg}. Embora considerem haver boas estimativas referem que o modelo baseado nos I_{veg} sobrestimou a ETr durante um período de carência hídrica na cultura de milho. Consideram ainda que modelos baseados apenas em I_{veg} não serão sensíveis à carência hídrica enquanto não ocorrer redução de biomassa e/ou alterações na geometria do copado. Os resultados obtidos por (Conceição et al., 2011) em vinha com rega deficitária estão de acordo com estas conclusões.

Do ponto de vista operacional Pôças et al. (2014) ao usarem o modelo METRIC^{TM} para estimar ETr de um olival super-intensivo melhoraram as entradas padrão do modelo relativamente ao índice de área foliar (LAI), altura de rugosidade para as transferência de momento e $T_{RadConj}$ do copado. Para isso estimaram $T_{RadConj}$ das oliveiras com base na $T_{RadConj}$ do copado (proveniente do sensor TM) definindo três compartimentos: oliveiras, solo exposto e não exposto à radiação solar directa.

Materiais e Métodos

A metodologia seguida baseou-se na medição de variáveis relacionadas com o uso da água e quantificação do estado hídrico com métodos de medição no solo (usualmente designadas por *ground-truth data*), cujas medidas se consideram como referência para análise dos dados de detecção remota e calibração/validação de modelos. A caracterização das condições experimentais e os métodos usados são descritos nas publicações que constituem o corpo deste documento, bem como noutros a que não se deu tanto destaque. Uma vez que há abordagens transversais aos vários locais usados, neste ponto procura-se destacar as metodologias principais para um posterior enquadramento em relação aos aspectos abordados nos artigos publicados ou em publicação.

Foram selecionadas como parcelas experimentais três parcelas agrícolas comerciais e uniformes relativamente à cultura, solo e práticas culturais:

– ensaios de 2008 a 2010: vinha regada (distâncias de plantação 1.1 m por 2.8 m, figura 4.1);

– ensaios de 2010 a 2012: olival intensivo regado (figura 4.2, distâncias de plantação 4.7 m por 7.0 m) e olival tradicional de sequeiro (figura 4.3, distâncias de plantação 7.0 m por 7.0 m).

Para as medições com as técnicas clássicas foram usados dois tipos de delineamento relativamente ao controlo do estado hídrico, em qualquer das culturas regadas (vinha e olival intensivo):

– parcela de grandes dimensões (condução da rega pelo agricultor, no mínimo 150 m na direcção dos ventos dominantes, parcela-agricultor), onde o estado hídrico da cultura resulta das práticas culturais executadas pelo agricultor (rega ou sequeiro);

– ciclos de *stress* (ou ciclos de carência hídrica), foram definidas duas parcelas de pequena dimensão (sub-parcela A e sub-parcela B) sendo que no tempo inicial ($t_{inicial} = 0s$) as plantas das sub-parcelas A e B têm estado hídrico idêntico e em conforto hídrico. Para $t > t_{inicial}$ a sub-parcela A é mantida em conforto hídrico e a na sub-parcela B é suprimida a rega, indo o estado hídrico, da sub-parcela B, evoluindo no sentido da maior intensidade de carência hídrica.

Na parcela-agricultor (figuras 4.4, 4.5, 4.6, 4.7 e 4.8) foi medida a evapotranspiração pelo método EC, a evaporação do solo e o fluxo de seiva numa amostra (6 ou mais plantas), usando-se a combinação de métodos descrita na secção 3.2 para medir a transpiração. O estado hídrico das plantas foi quantificado medindo o valor do Ψ_{base} com periodicidade de cerca de 10 a 15 dias.

Nas sub-parcelas A e B foi medido o fluxo de seiva e outras variáveis não automatizáveis para caracterizar o estado hídrico das plantas e do solo, mas com uma periodicidade muito mais elevada (durante os ciclos de carência hídrica) do que na parcela-agricultor, incluindo algumas medições ao longo do dia com intervalos de uma a duas horas (cinética diária).

O fluxo de seiva nas raízes das oliveiras foi abordado de forma autónoma, com dois métodos diferenciados capazes de quantificar fluxos em direcções opostas, com o objectivo de identificar e quantificar fluxos negativos, por redistribuição hidráulica ao nível do solo.

Foram recolhidos dados de detecção remota (na vinha em 2010 e nos olivais em 2011 e 2012) usando sensores portáteis: uma câmara térmica, uma câmara multiespectral e um espectroradiómetro (325 µm–1075 µm). A câmara térmica usada foi: FLIR ThermaCam E300 (7.5 µm–13 µm), com resolução de 320 por 240 *pixel*. A câmara multiespectral usada foi: JAI AD-080 GE 2 CCD, com resolução de 1024 por 768 *pixel*, com uma banda no infravermelho próximo (760 µm–970 µm, máximo em 800 µm) e com três bandas na zona do espectro visível (azul (400 µm–520 µm), com máximo em 450 µm; verde (460 µm–620 µm), com máximo em 540 µm; vermelho (560 µm–690 µm), com máximo em 610 µm). Estes equipamentos foram cedidos pela Universidade do Porto (Professor Mário Cunha).

Figura 4.1: Vinha onde decorreram os trabalhos experimentais. Monte Novo e Figueirinha, Beja, Portugal, início de Abril de 2009.

Em suma, foram feitas medições automatizadas em registo contínuo da evapotranspiração (ETr), da transpiração (Tr), do fluxo turbulento de calor sensível para a atmosfera (H), do balanço de radiação (R_n), do fluxo de calor sensível para o solo (G), da temperatura do solo (T_{solo}), da variação de diâmetro do tronco ($V_{DiâmetroTronco}$), e de variáveis meteorológicas (humidade relativa (RH), temperatura do ar (T_{ar}), direcção do vento e precipitação). Também foram feitas medições não automatizadas de evaporação do solo (Es) e indicadores do estado hídrico da planta (potencial hídrico foliar medido antes do nascer do sol, Ψ_{base}). O teor de água no solo (indicador do estado hídrico do solo, $TeorAgua_{SondaNeutrões}$) foi medido apenas nos olivais. Admitiu-se que estas medidas são representativas da zona de influência das medições com o método das flutuações instantâneas *i.e.* a montante da torre metálica na direcção do vento dominante.

Nas sub-parcelas A e B foram feitas medições de Tr, variação do diâmetro do tronco e de indicadores do estado hídrico do solo ($TeorAgua_{SondaNeutrões}$) e da planta (Ψ_{base}). Durante os ciclos de *stress* , foram ainda medidas as grandezas Ψ_{ramo} e gs para melhor caracterizar o estado hídrico das plantas.

Os dados de reflectância à superfície (com correção atmosférica Ledaps, Masek et al., 2006; Vermote e Saleous, 2007; Schmidt et al., 2013) das bandas do visível, infravermelho próximo, infravermelho médio e de temperatura derivada da banda térmica dos

Figura 4.2: Olival de regadio onde decorreram os trabalhos experimentais, vista do topo da torre metálica de observações. Monte do Pardieiro, Ferreira do Alentejo, Portugal, Julho de 2013.

sensores TM e ETM$^+$ foram obtidos do arquivo USGS *Climate Data Record* (Geological-Survey, 2015), processados e analisados. Para o processamento dos dados foi necessário desenvolver algoritmos e ferramentas informáticas tendo-se recorrido a *software* gratuito e de código livre nomeadamente o programa R e sua linguagem (R-Core-Team, 2017) integrado no ambiente de desenvolvimento Rstudio (Rstudio-Team, 2016). A análise envolveu técnicas estatísticas para correlacionar as variáveis medidas com técnicas de DR (reflectâncias e temperaturas) com as variáveis medidas usando as técnicas clássicas.

Figura 4.3: Olival de sequeiro onde decorreram os trabalhos experimentais, vista do cimo da torre metálica de observações. Monte do Outeirinho, Ferreira do Alentejo, Portugal, Julho de 2013.

Figura 4.4: Vinha, vista da parcela-agricultor. Torre metálica de observações com os sensores para medição dos fluxos de calor sensível e latente pelo método das flutuações instantâneas e sensores para a medição de variáveis meteorológicas. Monte Novo e Figueirinha, Beja, Portugal, final de Maio de 2009.

Figura 4.5: Vinha, vista da parcela-agricultor. Videiras equipadas com sensores de fluxo de seiva (método de Granier, Granier, 1985), sendo visível a protecção contra a radiação solar directa nos troncos. Monte Novo e Figueirinha, Beja, Portugal, início de Outubro de 2009.

Figura 4.6: Olival de regadio, vista da parcela-agricultor com equipamentos instalados. Ao fundo a torre metálica de observações onde se encontravam instalados os sensores para aplicação do método das flutuações instantâneas (medição dos fluxos de calor sensível e calor latente). Também são visíveis árvores equipadas com sensores de fluxo de seiva no tronco e nas raízes. Monte do Pardieiro, Ferreira do Alentejo, Portugal, final de Julho de 2013.

Figura 4.7: Olival de sequeiro, vista da parcela-agricultor com árvores equipadas com sensores de fluxo de seiva no tronco e nas raízes. A posição da torre metálica de observações (método das flutuações instantâneas) é visível junto da segunda oliveira, da segunda fila de árvores (da esquerda para a direita) mostrada na fotografia. Também é possível observar o fendilhamento largo e profundo do solo (*vide* Conceição et al., 2017c). Monte do Outeirinho, Ferreira do Alentejo, Portugal, meados de Setembro de 2012.

Figura 4.8: Olival de sequeiro, aspecto do sistema de captação de energia solar para alimentação dos equipamentos e sensores. Monte do Outeirinho, Ferreira do Alentejo, Portugal, final de Novembro de 2012.

Estrutura da tese

A tese inclui a compilação de sete artigos sujeitos ao processo de revisão pelos pares, cinco publicados, um já revisto (aguardando publicação) e um em fase de revisão, aqui apresentados por ordem cronológica de submissão. No seu enquadramento poderão ser referidas outras publicações resultantes do trabalho de equipa mas a que não se deu o mesmo destaque, por não reunirem os requisitos legais[1] (*e.g.* não indexadas por *Institute for Scientific Information* (ISI) ou *Scopus*), por não se focarem no tema central da tese, por a contribuição própria não ter sido tão relevante ou por um equilíbrio dos temas visados em relação com os objectivos. Os artigos seleccionados foram os seguintes:

1. **Conceição et al. (2011)**

Conceição N., Ferreira M.I., Pacheco C.A., Fabião M., Boteta L., Silvestre J. 2011. Transpiration from a vineyard in South Portugal – stress coefficients, NDVI and leaf water potential. Acta Horticulturae 922:277–284.

2. **Ferreira et al. (2012b)**

Ferreira M.I., Silvestre J., Conceição N., Malheiro A.C. 2012. Crop and stress coefficients in rainfed and deficit irrigation vineyards using sap flow techniques. Irrigation Science 30(5):433–447.

Em 2012: factor de impacto[2]de 2.289 e no primeiro quartil[3] em *Agronomy and Crop Science* e *Water Science and Technology*.

Participação do candidato: instalação e recolha de dados numa das vinhas consideradas (Beja), participação na análise de dados, contribuindo para a redacção com comentários críticos.

3. **Nadezhdina et al. (2014)**

Nadezhdina N., Ferreira M.I., Conceição N., Pacheco C.A., Häusler M., David T.S. 2014. Water uptake and hydraulic redistribution under a seasonal climate: long–term study in a rainfed olive orchard. Ecohydrology 8:387–397.

Em 2014: factor de impacto de 1.234 e no primeiro quartil em *Ecology*.

Participação do candidato: participação na instalação, recolha de dados de fluxo de seiva e variáveis meteorológicas, participação na recolha de dados do estado hídrico do solo e participação na análise preliminar dos dados.

[1]Regulamento Geral dos ciclos de estudos conducentes ao grau de doutor no Instituto Superior de Agronomia.

[2]`https://jcr.incites.thomsonreuters.com/`

[3]`http://www.scimagojr.com/`

4. **Conceição et al. (2017a)**

Conceição N., Häusler M., Lourenço S., Pacheco C.A., Tezza L., Ferreira M.I. 2017. Evapotranspiration measured in a traditional rainfed and an irrigated intensive olive orchard during a year of hydrological drought. Acta Horticulturae 1150:281–288.

5. **Conceição et al. (2017c)**

Conceição N., Tezza L., Lourenço S., Häusler M., Boteta L., Pacheco C.A., Ferreira M.I. Importance of very fine roots in deep soil layers for the survival of rainfed olive trees. Acta Horticulturae. Versão revista aceite em 2017. No prelo.

6. **Conceição et al. (2017b)**

Conceição N., Tezza L., Häusler M., Lourenço S., Pacheco C.A., Ferreira M.I. 2017. Three years of monitoring evapotranspiration components and crop and stress coefficients in a deficit irrigated intensive olive orchard. Agricultural Water Management 191:138—152.

Em 2016: factor de impacto de 2.848 e no primeiro quartil em *Water Science and Technology*.

7. **Häusler et al. (2018)**

Häusler M., Conceição N., Tezza L., Sánchez J.M., Campagnolo M., Häusler A.J., Silva J.M.N., Warneke T., Heygster G., Ferreira M.I. 2018. Estimation and partitioning of actual daily evapotranspiration at an intensive olive grove using the STSEB model based on remote sensing. Agricultural Water Management 201:188–198.

Em 2016: factor de impacto de 2.848 e no primeiro quartil em *Water Science and Technology*.

Participação do candidato: instalação e recolha de dados da evapotranspiração e transpiração, participação na análise de dados respectiva, bem como no processamento de imagens correspondentes a um dos itens do artigo, contribuindo para a redacção com comentários críticos.

Os artigos Ferreira et al. (2012b), Conceição et al. (2017b) e Conceição et al. (2017a) apresentam e discutem, respectivamente, os resultados obtidos sobre o uso da água na vinha (Beja), no olival de regadio e no olival de sequeiro (Ferreira do Alentejo), por aplicação das técnicas clássicas de medição nomeadamente da evapotranspiração e suas componentes. Estes dados constituem a informação de referência usada na definição e validação dos modelos usados em Conceição et al. (2011) e Häusler et al. (2018) onde se usam respectivamente o conceito de NDVI e modelação com um modelo de dois compartimentos (*Simplified Two-Source Energy Balance Model*, STSEB, Sánchez et al., 2008).

Em Conceição et al. (2011) analisou-se a sensibilidade do índice de vegetação NDVI para traduzir ou não os efeitos do *stress* hídrico de curto prazo (*vide* Myers, 1988), tendo sido usados os dados de detecção remota provenientes do sensor TM. Partindo dos dados resultantes das medições com técnicas clássicas, explora-se a possibilidade de usar modelos de estimativa de Kcb integrando dados de detecção remota (NDVI), combinando com Ks para obter Tr. Estes modelos pela sua relativa simplicidade têm aplicabilidade prática na condução da rega das culturas lenhosas sujeitas a carência hídrica.

Em Ferreira et al. (2012b) apresenta-se e discute-se o uso da água pela vinha do ensaio desenvolvido nesta tese (Beja), com rega deficitária, em comparação com outros quatro estudos anteriores também em vinha, partindo das medições de ETr e suas componentes com as técnicas clássicas e usando a combinação de métodos descrita em 3.2. Apresenta-se também uma metodologia para a decomposição das componentes Kcb e Ks, tendo-se

relacionado um indicador do estado hídrico (Ψ_{base}) com Ks.

Em Häusler et al. (2018) foi usado o modelo STSEB (Sánchez et al., 2008) para estimar ETr e suas componentes em cinco datas do ano de 2011 partindo de dados de detecção remota (sensor TM). Adicionalmente, comparam-se os valores medidos de evapotranspiração com uma série temporal com mais observações das variáveis de detecção remota constituída juntando dados dos sensores TM e ETM$^+$ por forma a verificar se as cinco imagens seleccionadas, como entrada do modelo, são representativas.

Em Conceição et al. (2017b) analisam-se os resultados das experiências feitas no olival de regadio gerido em rega deficitária (Ferreira do Alentejo). Apresenta-se e discute-se o uso da água pelo olival nos anos de 2010 a 2012 nomeadamente a evolução sazonal da transpiração diária para os três anos considerados, bem como de Kcb e Ks. É ainda discutida a repartição da energia entre os fluxos convectivos H e LE. Pela análise dos dados obtidos no ciclo de *stress* realizado em 2011 foi obtida uma função matemática que relaciona o indicador do estado hídrico (Ψ_{base}) com o indicador de *stress* (Tr/ET_o). Esta função foi utilizada para estimar a evolução sazonal de Ks do olival.

Nos restantes três artigos aborda-se a extracção radicular e analisa-se a distribuição espacial de água no solo para relacionar com a redistribuição hidráulica e o seu papel enquanto estratégia de sobrevivência nestes cobertos. Em Conceição et al. (2017a) analisa-se comparativamente o uso da água no olival de regadio e de sequeiro durante o ano de seca hidrológica de 2012 e discute-se a evolução sazonal da evaporação do solo e do armazenamento de água no solo no caso especial deste ano. É dada alguma enfase à distribuição radicular e à extracção radicular.

Os artigos Conceição et al. (2017c) e Nadezhdina et al. (2014) tratam da distribuição espacial da água no solo e das raízes, do uso da água do solo pelas raízes e da redistribuição hidráulica pelo sistema radicular. Discute-se também a importância da distribuição das raízes finas no solo e da redistribuição hidráulica para a sobrevivência dos indivíduos.

Em Nadezhdina et al. (2014) apresentam-se e discutem-se as evidências da ocorrência de redistribuição hidráulica na direcção vertical (*hidraulic lift*) no olival de sequeiro em consequência da dessecação diferencial das camadas de solo ao longo do perfil vertical. Também em Nadezhdina et al. (2012) (não seleccionado) se apresentam resultados, ainda preliminares, sobre redistribuição hidráulica, quer no olival de regadio quer no de sequeiro. Em Ferreira et al. (2013) (não seleccionado) é dado relevo às possíveis funções e importância da toiça da oliveira adulta no processo de redistribuição hidráulica, nomeadamente como orgão de armazenamento e redistribuição de água proveniente das raízes com acesso às camadas de solo em profundidade (durante o Verão) e das raízes com acesso às camadas superficiais (primeiras chuvas de Outono).

Para esta análise usaram-se os dados de fluxo de seiva (método da deformação do campo de calor Nadezhdina et al., 1998) medido nas raízes, no tronco e na toiça durante os anos de 2010 a 2012. Outros dois artigos não seleccionados (Malheiro et al., 2016; Ferreira et al., 2018) alargam o âmbito desta análise, pelo uso de outra técnica inovadora (Testi e Villalobos, 2009; Green et al., 2009), na quantificação das quantidades envolvidas na redistribuição hidráulica, quer numa parcela de vinha (Favaios), quer no olival de sequeiro (Ferreira do Alentejo).

Publicações

6.1 Conceição et al. (2011)

Conceição N., Ferreira M.I., Pacheco C.A., Fabião M., Boteta L., Silvestre J. 2011. Transpiration from a vineyard in South Portugal – stress coefficients, NDVI and leaf water potential. Acta Horticulturae 922:277–284.

Transpiration from a Vineyard in South Portugal – Stress Coefficients, NDVI and Leaf Water Potential

N.S. Conceição[1], M.I. Ferreira[1], C.A. Pacheco[1], M. Fabião[2], L. Boteta[2] and J.C. Silvestre[3]
[1]Instituto Superior de Agronomia, Technical University of Lisbon (TULisbon), Tapada da Ajuda, 1349-017 Lisboa, Portugal
[2]COTR - Tecnologia de Regadio, Quinta da Saúde, Apartado 354, 7801-904 Beja, Portugal
[3]INRB-INIA – Dois Portos, Quinta da Almoínha, 2565-191, Dois Portos, Portugal

Keywords: remote sensing, crop coefficient, normalized difference vegetation index, deficit irrigation, *Vitis vinifera* L., water stress, eddy covariance

Abstract

Transpiration (T) of a disease-free crop, well-fertilized and well watered can be estimated using reference evapotranspiration (ETo) and basal crop coefficients (Kcb) When plants are under water stress it is necessary to consider a stress coefficient (Ks, defined as $T_{actual}/T_{maximum}$), T being estimated from Kcb×Ks×ETo. Remote sensing has recently been used for Kcb estimations, namely using normalized difference vegetation index (NDVI). Due to the controversy on how NDVI reflects short or long term stress conditions, we compare ground truth observations for T (combination of sap flow and eddy covariance techniques) and estimated T for the crop (using NDVI, T_{NDVI}). Our aim is to analyze the ratio $T_{measured}/T_{NDVI}$, and its relationship with a water stress indicator, predawn leaf water potential (ψ_p), in order to contribute to the discussion on the meaning of T_{NDVI}. To study this, we used data from experimental work on a vineyard during summer 2008 and 2009, in the South of Portugal (38.050 N, 7.921 W). Average ETo during summer was 7 mm/day. T during summer ranged between 0.5 and 3.0 mm/day. NDVI was calculated from LANDSAT 5 TM imagery and Kcb, estimated using a methodology developed on DEMETER project, ranged from 0.62 to 0.75 for the 7 days of observation. Assuming NDVI equation provides Kcb, therefore not reflecting a component of Ks, this coefficient would be calculated as $T_{measured}/(ETo \times Kcb_{NDVI})$. In fact, a good agreement was found between calculated Ks and ψ_p ($Ks = 1.3 \times e^{(3.1 \times \psi p)}$). Using this last equation or equivalent, it would be possible to map actual T from ψ_p and Kcb (estimated from NDVI). The equation suggests that, for this range of ψ_p ($-0.2 > \psi_p > -0.7$ MPa), NDVI does not incorporate the effect of water stress on T.

INTRODUCTION

Transpiration (T) of a disease-free crop, well-fertilized and well watered can be estimated using reference evapotranspiration (ETo) and basal crop coefficients (Kcb) obtained from algorithms such as the one proposed in FAO Irrigation and Drainage Paper 56. This requires meteorological data and crop parameters at the plot scale. Remote sensing can be used for Kcb estimations. For instance, NDVI (normalized difference vegetation index) is a vegetation index that has been proposed to estimate Kcb, either using a linear relationship or not (Calera et al., 2005; Hunsaker et al., 2005; Er-Raki et al., 2007, 2010; Campos et al., 2010) mainly for low crops. The main reason for the relationship NDVI-Kcb is the fact that NDVI is related to leaf area index and the fractional ground cover, that partially explain variations on Kcb, as reviewed in Allen et al. (1998). When crops are under water stress, there is a decrease on ET and T and a stress coefficient (Ks) can be considered (Itier et al., 1990). Allen et al. (1998) proposed T=Kcb×Ks×ETo. In some cases, water stress induces changes in plant biomass (Gonzalez-Dugo et al., 2009) and color of leaves, modifying NDVI. The hypothesis that NDVI could provide a combined coefficient Kcb.Ks, therefore being used for irrigation scheduling in such stress conditions, has been considered. It is expected that the possible importance of water stress effect on NDVI depends on the intensity and duration of stress and also on the crop behavior. Our questions are:

1. to which extent is NDVI affected by water stress, in the case-study here shown?
2. can the ratio between $T_{measured}$ and ETo×Kcb (being Kcb estimated from NDVI, providing T_{NDVI}) be identified with Ks?

We will answer these two aspects using the analysis of the relationship between a selected water stress indicator and $T_{measured}$ /T_{NDVI} calculated as above.

In the following, ground truth observations for T ($T_{measured}$, which results from a combination of sap flow and eddy covariance techniques) and estimated T for the crop, using NDVI to estimate Kcb (T_{NDVI}) were compared and its ratio ($T_{measured}$ /T_{NDVI}) related with predawn leaf water potential (ψ_p) as the selected water stress indicator.

MATERIALS AND METHODS

Experimental Site

The experiment was conducted in a commercial irrigated vineyard (*Vitis vinifera* L. 'Aragonez', grafted on cv. '1103P'), with 6.0 ha situated within a continuous area of 30 ha vineyard. The site is located 6 km from *Beja*, *Portugal* (38.050 N, 7.921W, *Monte Novo e Figueirinha*, *Beja*).

The vineyard was planted in 2002 with a planting distance of 1.1×2.8 m; the training system was vertical soot positioning. The grapevines were spur pruned on a bilateral Royat cordon with 16 buds per vine. The mean grapevines height and canopy width were about 1.8 m and 1.0 m, respectively. The row orientation was approximately north-south.

The soil was bare, between the rows with tillage and beneath the canopy without (Fig. 1). The vineyard was drip irrigated, with emitters for each 1.0 m (flow 2.4 L/h), suspended above the ground in the vine row. The soil is a shallow clay vertisol with abundant gravels and few stones, profile type: Ap-Bw-C-R derived from basic rocks. Depth of root zone is about 0.6 m, and some fine roots may explore rock fissures up to 1.5 m depth.

Experimental work took place between May and October in 2008 and 2009.

Measurement of Energy Balance Components

The eddy covariance technique (EC) was used to measure sensible heat flux (H) and latent heat flux (LE) or evapotranspiration (ETec). The sensors, a CSAT 3-D sonic anemometer and a KH20 krypton hygrometer (both Campbell Scientific, Inc. Logan, UT, USA), were placed on a metallic tower at a height of 3.2 m, oriented into the dominant wind direction (NW, N). The data were stored (30 minute's averages) in a CR23X data logger (Campbell Scientific, Inc. Logan, UT, USA). LE was corrected using WPL correction (Webb et al., 1980) and for oxygen absorption (Tanner et al., 1993).

A footprint analysis, according to the methodology described in Schuepp et al. (1990), allowed the evaluation of the relative contribution of fluxes coming from different areas within the plot to the total measured flux (more than 90% of the measured LE came from an upwind area less then 200 m away from the measurement point). In the eddy covariance area the vines were subjected to the same agricultural practices and were assumed to be homogeneous.

The metallic tower at the vineyard was also used to install a wind vane (model W200P, Vector Instruments, Rhyl, United Kingdom), as well as a capacitive sensor (air temperature and humidity). The in-situ measurements of meteorological variables were used for EC corrections and the footprint analysis.

Net radiation (Rn) was measured with a net radiometer (model NR2, Kipp & Zonen, Delft, Netherlands), which was placed 3.2 m above the ground. In order to determine the soil heat flux (G), seven soil heat flux plates (HFT-3.1, REBS, Seattle, USA) were placed at a depth of 0.05 m along a perpendicular line between vine rows. Soil heat storage above the heat flux plates was quantified with temperature measurements using copper-constantan thermocouples placed 0.025 m above each plate. Data were stored in a CR10X data logger (Campbell Scientific, Inc. Logan, UT, USA). G,

H and Rn were measured with the aim of verifying the closure of the energy balance equation ($Rn - G = H + LE$) and were used to evaluate the quality of the EC data.

Reference Evapotranspiration Calculation

Meteorological data from a nearby station belonging to COTR – Centro Operativo e de Tecnologia de Regadio (www.cotr.pt), located at *Beja* (38°02'15" N, 07°53'06" W, ca. 206 m height a.s.l.) were used to calculate ETo, with the Penman-Monteith equation, using reference crop parameters (grass with a height of 0.12 m, a surface resistance of 70 s m^{-1} and an albedo of 0.23 according to Allen et al., 1998).

Sap Flow Measurement and Transpiration Calculation

Sap flow was monitored with 1.0 and 0.5 cm long radial sap flow meters (heat dissipation method, Granier 1985) from Umweltanalytische Produkte GmbH (Germany).

The heated probe was installed on the stems in the range of 0.30 to 0.45 m above the ground. The temperature difference between the probes was measured every 60 s with a copper-constantan thermocouple connected to a CR10X with an AM416 relay multiplexer (Campbell Scientific, Inc. Logan, UT, USA) and averaged every 30 min.

Calibration of sap flow sensors was obtained using ET data from eddy covariance method (Ferreira et al., 2004) in the period with negligible soil evaporation. Using this calibration a complete data-series for T, for the entire vegetative cycle was obtained from sap flow data. Therefore, the transpiration data are representative of the eddy covariance area.

Stress Coefficient Calculation

When the soil water potential drops below a threshold value, depending on root density and ET rates (Denmead and Shaw, 1962), the crop is water stressed.

The effects of soil water stress were considered by Allen et al. (1998), for practical uses, by using a water stress coefficient (Ks) so that ETc is obtained by (Ks×Kcb+Ke) ETo, where ETc is crop ET without stress, Ke is the soil evaporation coefficient and Kcb is the basal crop coefficient, being ETo.Kcb the maximal T for the crop considered. Assuming T= Ks×Kcb×ETo, Ks can be calculated (Fig. 2) as Ks=T/(Kcb×ETo).

Leaf Water Potential Measurement

Leaf water potential was measured (Fig. 3a) at pre-dawn (ψ_p) with a pressure chamber (PMS Instruments, Corvallis, Oregon, USA), using 6 leaves per day, on average. When not measured, ψ_p was estimated by using interpolation from the trend observed, whenever this seamed reliable.

Normalized Difference Vegetation Index and Basal Crop Coefficient Calculations

NDVI maps were obtained from LANDSAT 5 TM images (geometrical and atmospheric corrected, SPIDER (2009)) and NDVI was calculated (Rouse et al., 1973) as: NDVI=(IRC - R)/(IRC + R), where R is the reflectance value in the red region ([0.63, 0.69 μm], band 3 of LANDSAT 5 TM) and IRC is on the reflectance value in the near infrared region ([0.76, 0.90 μm], band 4 of LANDSAT 5 TM). NDVI values used were a mean of the 8 central pixel (30×30 m) with an area of 0.72 ha corresponding to the area in the centre of the larger one influencing eddy covariance data, as determined by the foot-print analysis (1.6 ha). Basal crop coefficient (Kcb) was derived from NDVI (Campos et al., 2010) as Kcb=a×NDVI+b, where a=1.36 and b=-0.066 (SPIDER, 2009).

RESULTS AND DISCUSSION

The seasonal evolution of measured ψ_p is presented on Figure 3a for the years 2008 and 2009. The irrigation days and depths for 2009 are presented on Figure 3b.

EC measurements provided a very small closure error (4 and 12%, in 2008 and 2009, Fig. 4), concerning the surface energy balance (LE+H = Rn-G) (Fig. 5), is within the limits usually found for measurements performed with the EC method (10 to 30%)

(e.g. Wilson et al., 2002). As a conclusion, it was possible to obtain final absolute values of T quite reliable. After calibration using EC data, T ranged from 0.5 to 3.0 mm per day, during summer.

Average ETo during summer was 7 mm/day. Kcb estimated from NDVI (Eq. [1]) ranged from 0.66 to 0.80 (June 16 to August 18) and from 0.62 to 0.75 (May 16 to August 21) during 2008 and 2009, respectively.

Ks calculated as $T_{measured}$ /(Kcb × ETo), where Kcb was estimated from NDVI, and ψ_p were related as $Ks = 1.3 \times e^{(3.1 \times \psi p)}$ (Fig. 6). The seven days were all those that met the following simultaneous conditions: available LANDSAT 5 images (with no clouds) and good data for T and ψ_p. The line in Fig. 6 is in agreement, in its shape and values, to the ones presented by Denmead and Shaw (1962), and other previous experiments on vineyards (not published) which suggests that the Ks, calculated as explained, is close to the actual decrease in T (Ks function). In other words, this means that the ratio between $T_{measured}$ and T_{NDVI} (ETo ×Kcb estimated from NDVI) can be identified with Ks, for this range of ψ_p ($-0.2 > \psi_p > -0.7$ MPa). In conclusion, from the relationship shown, it could be suggested that NDVI was not much affected by water stress. This is the answer to the questions formulated in the introduction. Independent work done by the TELERIEG project partners reached the same conclusions that if NDVI gives a good idea of the coefficient needed to estimate maximum water needs from ETo, was not a good indicator of water stress for the situations studied, as it reflects almost only long-term water stress effects, being useless to give a warning to the farmer (TELERIEG, 2010).

Furthermore, using this type of relationship, it would be possible to estimate actual T under water stress conditions using ETo, calculated Kcb (from NDVI) and measured ψ_p. This could be applied to variations of T in space and in time, both of interest for precision irrigation.

ACKNOWLEDGEMENTS

Research was supported by the projects: 1) PTDC/AGR-AAM/69848/2006 "*Estratégias de rega deficitária em vinha - indicadores de carência hídrica e qualidade*" financed by *Fundação para a Ciência e a Tecnologia* (*FCT*); 2) TELERIEG **(**SOE1/P2/E082) "*Uso de la teledetección para la recomendación y seguimiento de las prácticas de riego en el espacio SUDOE*"**.** We also thank *Sociedade Agrícola do Monte Novo e Figueirinha* for the vineyard's facilities.

Literature Cited

Allen, R.G., Pereira, L.S., Raes, D. and Smith, M. 1998. Crop Evapotranspiration Guidelines for Computing Crop Water Requirements: FAO Irrigation and Drainage Paper 56. FAO, Rome, Italy.

Calera, A., Jochum, A., Cuesta, A., Montoro, A. and López Fuster, P. 2005. Irrigation management from space: Towards user-friendly products. Irrigation and Drainage Systems 19:337-355.

Campos, I., Neale, C., Calera, A., Balbontín, C. and González-Piqueras, J. 2010. Assessing satellite-based basal crop coefficients for irrigated grapes (*Vitis vinifera* L.), Agricultural Water Management 98:45-54.

Denmead, T. and Shaw, H. 1962. Availability of soil water to plants as affected by soil moisture content and meteorological conditions. Agronomy Journal 54:385-90.

Er-Raki, S., Chehbouni, A. and Duchemin, B. 2010. Combining satellite remote sensing data with the FAO-56 dual approach for water use mapping in irrigated wheat fields of a semi-arid region. Remote Sensing 2(1):375-387.

Er-Raki, S., Chehbouni, A., Guemouria, N., Duchemin, B., Ezzahar, J. and Hadria, R. 2007. Combining FAO-56 model and ground-based remote sensing to estimate water consumptions of wheat crops in a semi-arid region. Agricultural Water Management 87:41-54.

Ferreira, M.I., Paço, T.A. and Silvestre, J. 2004. Combining techniques to study evapo-transpiration in woody crops: application to small areas – two case studies. Acta Hort.

664:225-232.
Gonzalez-Dugo, M., Neale, C., Mateos, L., Kustas, W., Prueger, J., Anderson, M. and Li, F. 2009. A comparison of operational remote sensing-based models for estimating crop evapotranspiration, Agricultural and Forest Meteorology, 149:1843-1853.
Granier, A. 1985. Une nouvelle méthode pour la mesure du flux de sève brute dans le tronc des arbres. Annales des Sciences Forestières 42 :193-200.
Hunsaker, D., Pinter, P. and Kimball, B. 2005. Wheat basal crop coefficients determined by normalized difference vegetation index. Irrigation Science 24:1-14.
Itier, B., Katerji, N., Flura, D. and Ferreira, I. 1990. Relative evapotranspiration in relation to soil water deficit and predawn leaf water potential – application to tomato crop. Acta Hort. 278:101-112.
Rouse, J., Hass, R., Schell, J. and Deering, D. 1973. Monitoring Vegetation Systems in the Great Plains with ETRS. p.309-317. In: Proceedings of the Third ERTS Symposium.
Schuepp, P.H., Leclerc, M.Y., MacPherson, J.I. and Desjardins, R.L. 1990. Footprint prediction of scalar fluxes from analytical solutions of the diffusion equation. Boundary-Layer Meteorology 50:355-373.
Tanner, B.D., Swiatek, E. and Greene, J.P. 1993. Density fluctuations and use of the krypton hygrometer in surface flux measurements. In: Proceeding of the 1993 National Conference on Irrigation and Drainage Engineering, Park City, Utah, 21-23 July 1993, Irrigation and Drainage Division, American Society of Civil Engineers.
Webb, E.K., Pearman, G.I. and Leuning, R. 1980. Correction of flux measurements for density effects due to heat and water vapour trasfer. Quarterly Journal of Royal Meteorological Society 106:85-100.
Wilson, K., Goldstein, A., Falge, E., Aubinet, M., Baldocchi, D., Berbigier, P., Bernhofer, C., Ceulemans, R., Dolman, H., Field, C., Grelle, A., Ibrom, A., Law, B.E., Kowalski, A., Meyers, T., Moncrieff, J., Monson, R., Oechel, Tenhunen, Valentini and Verma, S. 2002. Energy balance closure at FLUXNET sites. Agricultural and Forest Meteorology 113:223-243.
SPIDER. 2009. http://zeus.idr-ab.uclm.es/publico/index_cotr.html?zone=385.
TELERIEG**,** Uso de la teledetección para la recomendación y seguimiento de las prácticas de riego en el espacio SUDOE**.** 2010. http://sigma.imida.es/webFS/fs.

Figures

Fig. 1. Vineyard where the field experiment was developed (Beja, Portugal, 2009/07/10).

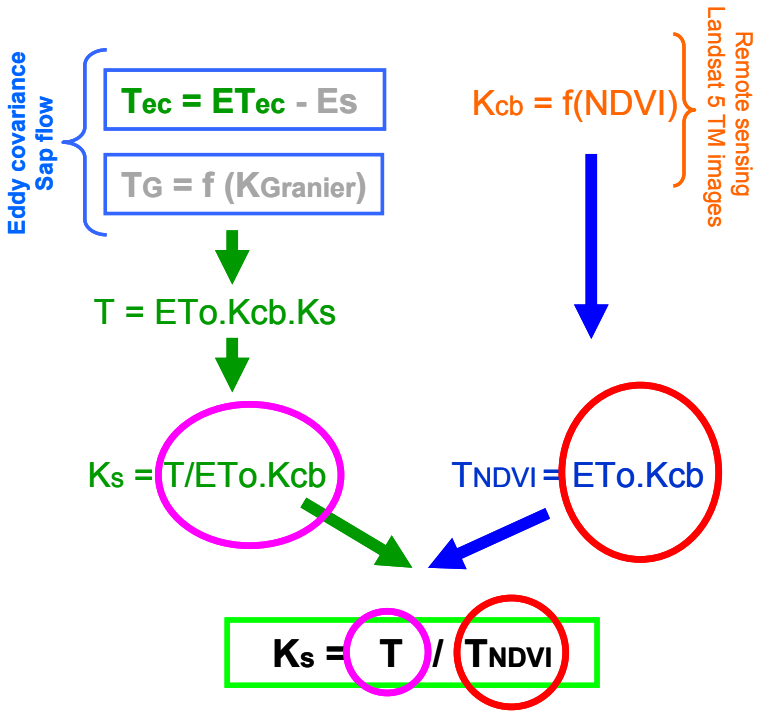

Fig. 2. Stress coefficient calculation with ground truth observations and remote sensing data. Tec, transpiration (T) calculated by difference between measured evapotranspiration using eddy covariance method (ETec) and measured soil evaporation (Es) (or using periods with negligible Es); T_G, T calculated from sap flow data (Granier method) with local calibration of sap flow method; T_{NDVI}, transpiration calculated from remote sensing data; ETo, Kcb and Ks, reference evapotranspiration, basal crop coefficient and water stress coefficient respectively (Allen et al., 1998).

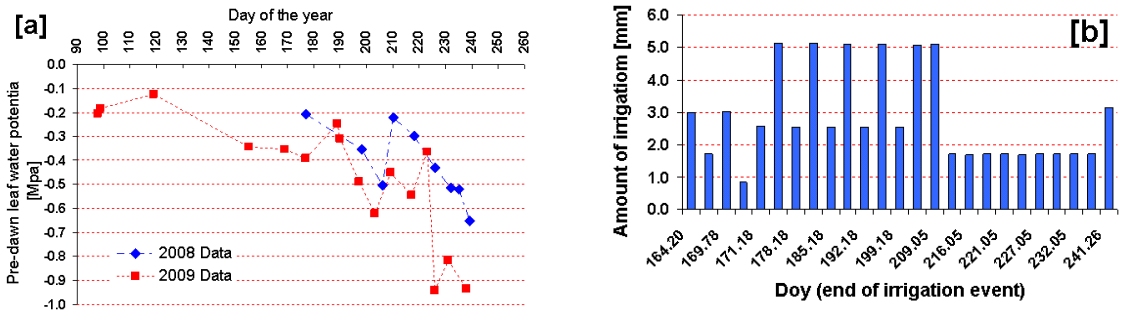

Fig. 3. [a] Leaf water potential measured in a vineyard (data for the years 2008 and 2009); [b] Irrigation events (data for the year 2009). Beja, Portugal.

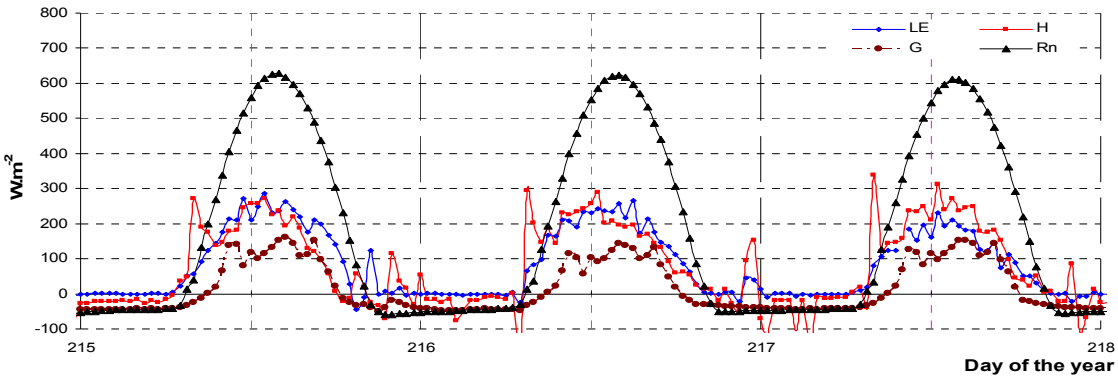

Fig. 4. Energy partition (time = solar time + 0:40) as obtained with the EC technique. LE – latent heat flux; H – sensible heat flux; Rn - net radiation; G - soil heat flux, for a vineyard (*Beja*, *Portugal*, 2008). LE was corrected with WPL correction (Webb et al., 1980) and for oxygen absorption (Tanner et al., 1993).

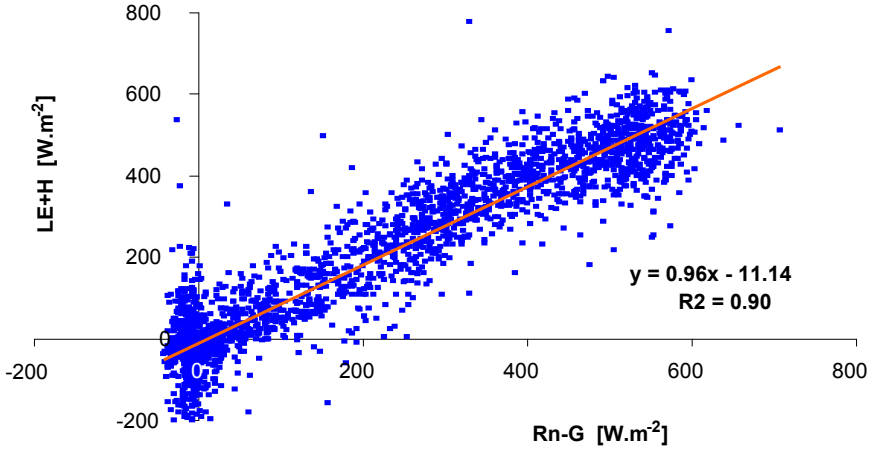

Fig. 5. Closure error of surface energy balance equation for a vineyard (Beja, Portugal, 2008). For the year 2009 the closure error was 12%.

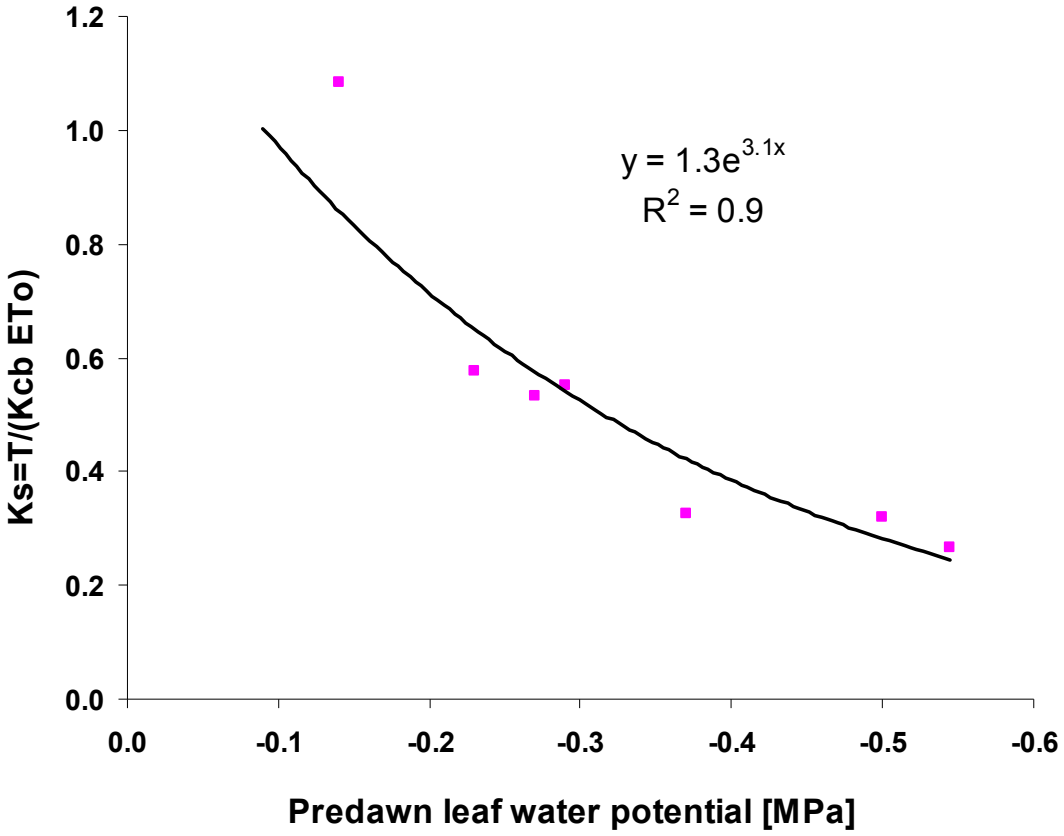

Fig. 6. Predawn leaf water potential as function of Ks (Allen et al., 1998). Ks as calculated assuming valid the function Ks= $T_{measured}$/(ETo×Kcb). Kcb was estimated from NDVI. T was calculated using a combination of techniques: eddy covariance and sap flow (Ferreira et al., 2004). Data for the years 2008 and 2009, Beja, Portugal.

6.2 Ferreira et al. (2012b)

Ferreira M.I., Silvestre J., Conceição N., Malheiro A.C. 2012. Crop and stress coefficients in rainfed and deficit irrigation vineyards using sap flow techniques. Irrigation Science 30(5):433–447.

Irrig Sci (2012) 30:433–447
DOI 10.1007/s00271-012-0352-2

REVIEW

Crop and stress coefficients in rainfed and deficit irrigation vineyards using sap flow techniques

Maria Isabel Ferreira · José Silvestre · Nuno Conceição · Aureliano C. Malheiro

Received: 6 August 2011 / Accepted: 22 March 2012 / Published online: 15 June 2012

Abstract Projected climate changes and expansion of viticulture to drier regions justify the installation and management of deficit irrigation (DI) strategies. Contradictory results on the effect of DI on crops may be ascribed to the incorrect application of these techniques. The lack of discrimination between basal crop (K_{cb}) and stress coefficients (K_s) can be an obstacle to proper irrigation management. A sap flow (SF) technique associated with microlysimeters and eddy covariance (EC) methods was applied to five commercial vineyards, aiming to discriminate those coefficients, during the driest period of the vegetative cycle. A comparative analysis of the coefficients, in relation to measured vegetation parameters (for K_{cb}) and plant water status (for K_s) is presented. K_{cb}, ranging from about 0.35 to 0.75, was highly correlated with leaf area index at stand level. K_s, which decreased till 0.2 in the most stressed vineyard, was well correlated to plant water status (K_s function), represented by predawn leaf water potential. K_s functions for the different experiments exhibited falling slopes with decreasing water status, with variable trends depending on the rates of maximal crop transpiration (T_m). These experimental results show that specific parameters for K_s functions, necessary to estimate water use and irrigation depths, in order to control the stress levels in DI scheduling, are also dependent on T_m.

Communicated by S. Ortega-Farias.

M. I. Ferreira (✉) · N. Conceição
Departamento de Ciências e Engenharia de Biossistemas (DCEB/CEER), Instituto Superior de Agronomia, Technical University of Lisbon (TULisbon), Tapada de Ajuda, 1349-017 Lisbon, Portugal
e-mail: isabelferreira@isa.utl.pt

J. Silvestre
INIA-Dois Portos, Instituto Nacional de Investigação Agrária e Veterinária, IP, Quinta da Almoínha, 2565-191 Dois Portos, Portugal

A. C. Malheiro
Centre for Research and Technology of Agro-Environmental and Biological Sciences (CITAB), University of Trás-os-Montes e Alto Douro, P. O. Box 1013, 5001-801 Vila Real, Portugal

Introduction

In well irrigated crops (vegetables and most orchards), as in traditionally non-irrigated stands, such as vineyards, deficit irrigation (DI) strategies—regulated deficit irrigation (RDI) (Dry and Loveys 1999; Romero et al. 2010), sustained deficit irrigation (SDI) (Chalmers et al. 2010) or partial root-drying (PRD) (Sadras 2009)—are increasingly used to improve water use efficiency (Kassam et al. 2007; Geerts and Raes 2009). Furthermore, in countries where vineyards are traditionally rainfed, projected climate changes and the spread to drier areas (Malheiro et al. 2010) also justify the installation and management of DI. Nevertheless, research results on water use concerning the application of DI techniques under field conditions and the long-term impacts on production have been found to be contradictory (Chaves et al. 2010). In some studies (Dry et al. 2001; Du et al. 2008), PRD is reported to have improved yield per unit of applied water, whereas in others (Bravdo et al. 2004; Gu et al. 2004; Intrigliolo and Castel 2009) no significant differences were observed. In a meta-analysis of field-grown horticultural crops, including grapevines, Sadras (2009) observed no improvement in water use efficiency under PRD, in relation to conventional irrigation. Apparent discrepancies may be due to differences in local conditions, namely soil texture, genotypic variety (Chaves et al. 2010), data analysis and incorrect application

of these techniques which efficiency, according to Sadras (2009), could be improved if closely monitored.

The estimation of the value of evapotranspiration (ET) for irrigation scheduling applications using practical models, such as one largely spread by FAO irrigation paper 56 (Allen et al. 1998), concerns the use of the maximal value of ET for the crop (ET_m, also called ET_c), or maximal transpiration for the crop (T_m), under the climate and cultural practices considered. ET_m or T_m can be calculated from reference evapotranspiration (grass, ET_o) and, respectively, the so-called crop coefficient (K_c) or the basal crop coefficient ($K_{cb} = T_m/ET_o$) using the nomenclature of the dual coefficient approach, as in Allen et al. 1998). Calculating ET as ET_m assumes continuous adequate available soil water for optimum plant growth. When applying DI strategies, a stress coefficient ($K_s = T/T_m$, i.e. the ratio between actual and maximum crop transpiration) is necessary for estimating ET. Therefore, K_c or K_{cb} and K_s are much needed for a proper application of DI.

Even if some authors (e.g. Allen et al. 1998) present a general proposal for estimating K_s, specific K_s functions for vineyards, from field experiments, are not generally available. A common practice for DI management consists on the use of a selected percentage of the estimated ET from a well-watered control (=ET_m), for instance irrigating at 50 % of ET_m, often not considering irrigation efficiency (e.g. Patakas et al. 2005). This approach is difficult to interpret in terms of the use of K_s.

If irrigation depth is not combined with a soil water balance follow-up (or other water status indicator), the use of a constant percentage of ET_m to calculate irrigation depth can lead to a continuous decrease in root-zone water content and not to a defined threshold level of water stress. In order to analyse this aspect, the concept of K_s function, which relates T reduction to the stress level applied, can be used.

The main objectives of this research were the following: (1) to analyse the relationship between K_{cb} and simple canopy parameters in the different vineyards, (2) to discriminate K_{cb} and K_s coefficients in several, mostly rainfed, vineyards (3) to relate K_s with water stress, in order to obtain K_s functions and (4) to compare these functions for the different analysed situations. Consequently, besides the comparative analysis of K_{cb} and K_s coefficients, this work aims to contribute to the discussion on the consequences of the differences observed in K_s functions in controlling the stress levels in DI.

Materials and methods

In order to fulfil the objectives, the following main intermediate steps were considered for data collection: (1) measurement of ET in several commercial vineyards using EC method (2) measurement of T in the same plots where ET is measured, using always the same approach of combining methods, (3) measurement of T in some specific aside experiments, with different water status levels, in order to get a reference for T (T_m) and (4) assessment of plant water status. Before describing the experimental conditions and the application of the methods used, the justification for the general strategy applied to obtain long-term T data (Ferreira et al. 2004) is presented.

ET can be obtained with a micrometeorological method if large homogeneous plots can be used and meteorological conditions are adequate. When those two conditions are not fulfilled, a strategy to obtain continuous (seasonal time scale) and reliable values for plant water use is required. The main general advantage of sap flow methods is the ability to provide continuous measurements, in the long term, independently of plot size and weather conditions.

However, underestimations of sap flow values (SF) have been reported (Ferreira et al. 2008). Tarara and Ferguson (2001) found a strong underestimation for high flows in vines, when using a sap flow heat balance method. For ring porous species, as grapevines, Bush et al. (2010) reported a difference of two to three orders of magnitude between SF estimates using the *Granier* method and a calibration procedure conducted on excised stems. Clearwater et al. (1999) in tropical species found a 45 % underestimation of SF with the same method used in this study (Granier 1985, 1987). The use of this method with the original calibration equation was shown to strongly underestimate SF in vineyards (Ferreira et al. 2008) due to uncertainty in the corrections accounting for variability in radial profile, natural gradients, wood parameters or even limited sampling (Ferreira et al. 2004, 2008). The reliability of SF estimates can be analysed by comparing SF with data from gravimetric method, in a lysimeter (e.g. Yunusa et al. 2000), using a cross-section of the stem cut from the plant (e.g. Goodwin et al. 2006), with T chambers (e.g. Intrigliolo et al. 2009) or even using eddy covariance (EC) measurements to obtain ET, which requires simultaneous measurements of ET, SF and soil evaporation (E_s) except when negligible, during the periods of comparison. This last methodology was used here, with the advantage of using non-disturbed plants and determining a range of fluxes in its natural environment.

Experimental sites

This comparative study was based on data gathered at five commercial vineyards (*Vitis vinifera* L.) in well renowned Portuguese wine regions (Fig. 1), with different climatic and edaphic conditions. Table 1 summarizes main site characteristics (soil type, basic canopy and climatic

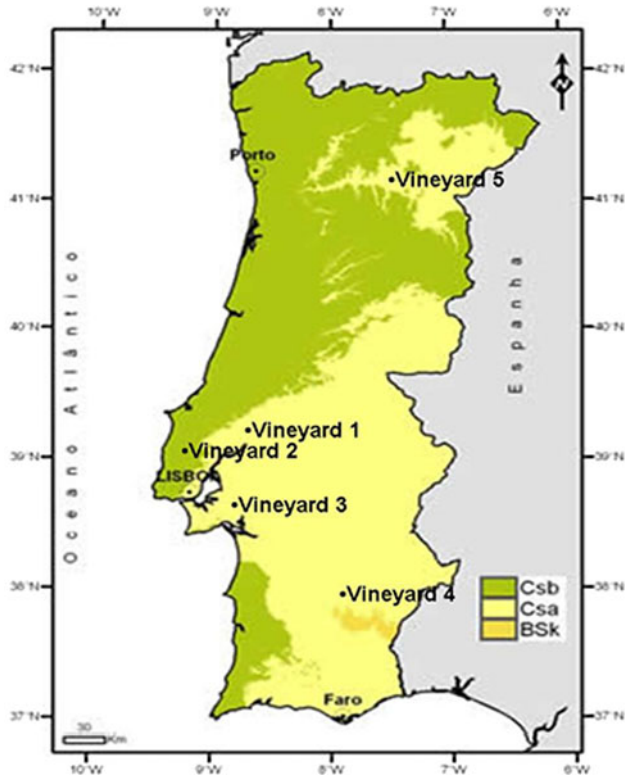

Fig. 1 Location of the five experimental vineyards (Portugal) associated to the Köppen-Geiger climate types. Adapted from IM (2008, www.meteo.pt)

parameters). The climate is temperate, of the Mediterranean type, characterized by a sinusoidal pattern of precipitation, dry summer and wet autumn/winter/early spring. According to Reis and Gonçalves (1981) and IM (2008, www.meteo.pt) in vineyards 1, 3, 4 and 5, the climate is humid mesothermic with dry hot summer (*C*sa, Köppen classification) and in vineyard 2, it is a cool-summer Mediterranean climate (*C*sb) with Atlantic influence. At vineyard 4, there is a transition to a cold semi-arid climate, with hot and dry summer and cold winters (BSk), also called steppe climate (Kottek et al. 2006).

1. Vineyard 1—SANTARÉM-TEJO located at Tagus Valley (Central Portugal), near Santarém (latitude 39° 10′ N, longitude 8° 44′ W, 5 m above sea level). The training system was vertical shoot positioning. The grapevines were spur pruned on a bilateral Royat cordon with 16 buds per vine. The area was 24 ha. The fetch in the ET measurement point was around 600 m. The measurements were taken between flowering and maturity, during 1996 and 1997. There was no irrigation. Leaf area index on a total area basis (LAI), at veraison, measured according to Carbonneau (1976) was 2.39 and 1.96, in 1996 and 1997,

Table 1 Characteristics of experimental sites

Plot	Year of results	Location/ wine region	Yearly average rainfall (mm)	Yearly average ET_o[a] (mm)	Soil	Cultivar/plantation date/rootstock	Plant density (vines ha^{-1})	Canopy height and width (m)	Stem diameter (m)	Leaf area index (–)	Ground cover (%)	Irrigation
1	1996 and 1997	Santarém/Tejo	707	1,436	Clay	Trincadeira/1984/SO_4	3,030	1.7 and 0.9 (1996)	0.049	2.39 (1996)	33 (1996)	NA
					Sandy Loam (Flm)			1.7 and 0.8 (1997)		1.96 (1997)	28 (1997)	
2	1998/1999	Alenquer/Lisboa	624	1,264	Loam	Castelão/1993/1103P	3,333	1.6 and 0.6	0.025	1.66	16	NA
3	2002	Palmela/Setúbal	746	1,407	Sandy (ARh)	Syrah/1990/1103P	2,975	1.5 and 0.5	0.033	1.32	18	NA
4	2008 and 2009	Beja/Alentejo	606	1,775	Clay Vertisol	Aragonez syn. Tempranillo/2002/1103P	2,350	1.75 and 1.0	0.035	2.15	42	Drip
5	2009	Favaios/Douro	630	1,100	Loam (anthrosol)	Moscatel Galego syn. Muscat à Petits Grains/1998/196-17Cl	4,545	1.5 and 0.6	0.026	1.4	25	NA

NA non applicable (rainfed)

[a] Obtained from PM equation (Allen et al. 1998)

respectively. The ground cover (GC), obtained from shaded area close to solar noon, was 28 % (1997).

2. Vineyard 2—ALENQUER-LISBOA located near Alenquer (39° 04′N, 9° 06′W, 155 m asl, *Oeste* region). Training system: Espalier—double Guyot, total area: 2 ha. The measurement period occurred between August and early December 1998 and from the beginning of the vegetative cycle (April) to the veraison (August) 1999. Measurements were taken in three small sub-plots (about 1 ha each) with slopes of 3, 10 and 17 %, facing SW. There were no conditions for micrometeorological measurements of ET. There was no irrigation. Average LAI, measured in 1998 (late summer) was 1.66; GC was 16 %.
3. Vineyard 3—PALMELA-SETÚBAL located near Palmela (Setúbal Peninsula) (38° 35′N, 8° 49′W, 25 m asl). The training system was vertical shoot positioning. The area was 216 ha and the fetch above 1000 m. The measurement period occurred between flowering and the end of the vegetative cycle. In spite of an impermeable layer at 1 m, below the sandy soil, some roots (>3 m deep) explored groundwater. Data are from a rainfed plot. LAI was measured according to Lopes and Pinto (2000) on 15 plants (all shoots). The reduced LAI (1.32 in 2002), can be attributed to the sandy soil. The corresponding GC was 18 %.
4. Vineyard 4—BEJA-ALENTEJO, located at 6 km from Beja (38° 03′N, 7° 55′, 200 m asl), in the warmest and driest region of Portugal. The training system was vertical shoot positioning. The grapevines were spur pruned on a bilateral Royat cordon with 16 buds per vine. The row orientation was approximately N-S. The soil is shallow with abundant gravels and few stones. Depth of root zone was about 0.6 m; some fine roots explored rock fissures up to 1.5 m depth. There was tillage between the rows and no tillage beneath the canopy. Experimental work took place in an area of 6.0 ha with a fetch above 300 m (within a continuous vineyard area of 30 ha), between flowering and the end of the vegetative cycle (May–October) from 2008 to 2010. Seasonal T was measured during 2009 vegetative cycle. The vineyard was drip irrigated, with emitters 1.0 m apart (flow 2.4 L/h), suspended above the ground in the vine row. Apart from main large plot where ET and T were measured, several small sub-plots of 162 m^2 with 3 replicates (486 m^2 in total for each treatment), placed downwind in relation to the tower for the EC measurements, were temporarily irrigated keeping the values of predawn leaf water potential (PLWP) at different levels: above −0.4, between −0.4 and −0.6 and between −0.6 and −0.9 MPa, being a well irrigated sub-plot used as a reference (T_m). This work, performed in 2010, contributed to the K_s functions (K_s vs. PLWP). LAI in the main plot was measured in 2009 as 2.15. GC was 42 %.
5. Vineyard 5—FAVAIOS-DOURO located at the Demarcated Region of Douro, planted on a plateau. The commercial rainfed vineyard (41° 15′N, 7° 28′W, 600 m asl) was trained as a bilateral cordon with 12 buds per vine. The distance to the plot border in the upwind direction (fetch) was 180 m. The measurement period occurred between flowering and the end of the vegetative cycle. LAI was 1.4 (berry maturation), estimated by the non-destructive method of Carbonneau (1976). GC was 25 %.

Flux measurements and sap flow estimates

EC method was used in four of the five experimental sites during the limited periods necessary for the comparison with sap flow data, in order to correct SF estimates and obtain reliable T values. Combining ET measured by EC (ET or ET_{EC}) and E_s (when above zero) estimated from the model based on local measurements, T_{EC} (mm/day) was obtained as:

$$T_{EC} = ET - E_s \quad (1)$$

T_{EC} was compared to SF_{stand} from Eq. (4b) in order to obtain a relationship for the correction of sap flow raw data and to get reliable values of T.

The need for this approach (sap flow methods to get a continuous data set and EC during short periods or with interruptions) to calibrate/correct SF is related to operational limitations of EC (Ferreira et al. 2004, 2008) mainly ascribed to dew and limited fetch, when wind turns from the dominant direction, causing frequent interruptions in data sets.

EC data for selected periods were collected using a krypton hygrometer (KH20) and a 1-D sonic anemometer with a fine wire thermocouple (model CA27 and 127, *Campbell Scientific*, *Inc*., Logan, UT, USA) in 1996 and 1997 (vineyard 1), and with a 3-D sonic anemometer (CSAT3, *Campbell Scientific*, *Inc*., Logan, UT, USA) in 2001, 2002 (vineyard 3), 2008 and 2009 (vineyard 4 and 5). EC sensors were placed in the main plot, rainfed (vineyards 1, 3 and 5) or irrigated (vineyard 4) at a height of, respectively, 3.5, 3.0, 3.2 and 3.0 m, for plots 1, 3, 4 and 5, with a path separation of 0.1 m.

Raw data were collected at a frequency of 10 Hz and occasionally stored for foot-print analysis. The raw data were processed with a 21X data logger in vineyard 1, CR23X in vineyard 3 and 4 and CR3000 in vineyard 5 (*Campbell Scientific*, *Inc*., Logan, UT, USA). Latent (LE) and sensible (H) heat flux densities were calculated over

30 min averaging intervals (except for vineyard 1 where a 20 min interval was used). In vineyard 5 (Favaios, Douro), all raw data were stored and further processed with the EdiRe processing package, which comprises a set of modulated programs (R. Clement, University of Edinburgh, UK). A 2-D coordinate rotation of wind velocity components by the run rotation method (McMillen 1988) was carried out, accounting for the effect of slope (3 %) in the flux (Paço et al. 2011). Corrections for air density variation (Webb et al. 1980) and for UV radiation absorption by oxygen (Tanner et al. 1993) were performed in all cases. EC data were selected according to fetch and footprint analysis and validated through spectral analysis and energy balance (EB) equation closure.

For verification of EB closure, net radiation flux density (R_n) and soil heat flux density (G) were measured: R_n, with a net radiometer (Swissteco, S1 or Kipp and Zonen NR2), at same high as EC sensors, placed from the vineyard alleyway at one-fourth of the distance between lines, G at the soil surface, with heat flux plates (REBS HFT 3.1 and/or Hukseflux HFP01) plus soil thermocouples, placed at regular distances in a transept (perpendicular to lines), in the vineyards were EC method was used. For the estimation of G, 5–7 heat flux plates and soil thermocouples were placed at 5 and 2.5 cm deep, respectively. For the estimation of soil heat storage, soil heat capacity was calculated from measured or estimated soil water content. Further details are given in Ferreira et al. (2008) for vineyards 1 and 3, Conceição et al. (2011) for vineyard 4 and Malheiro et al. (2011) for vineyard 5.

SF was measured in all (five) vineyards plots with the *Granier* method (Granier 1985, 1987). SF sensors (UP GmbH, Landshut, Germany) were installed in representative plants in upwind direction of the same plot where EC was used: 7 vines in 1996, 1997 (vineyard 1), 9 in 1998/99 (vineyard 2), 6 vines in 2001 and 2002 (vineyard 3), 12 (vineyard 4) and 6 (vineyard 5) in 2009. The two probes of each sensor (0.002 m diameter, 0.01 m in length) were inserted 0.1 m apart. SF was calculated assuming that sapwood conductive area equalled cross-sectional area (verified by destructive measurements using colourants or sap flow radial profile using the heat pulse and the heat field deformation methods (unpublished data). Corrections for natural thermal gradients were performed. The up-scaling, from SF measured at the different points of the sample (individual plants) to the value correspondent to average SF in the vineyard, often performed on the basis of stem diameters could be improved thanks to the good relationship obtained between plant leaf area (LA) measured or estimated and daily SF for the corresponding plant, applied to the average vineyard LA. For instance, for vineyard 1, SF = 1.27 LA − 4.2 ($r^2 = 0.99$, $n = 4$), with SF ranging from 4 to 14 L day^{-1} plant^{-1} and LA from 6 to 14 m^2 plant^{-1}, approximately; for vineyard 3, SF = 0.89 LA + 0.11 ($r^2 = 0.87$, $n = 9$) with SF approximately from 1.5 to 6 L day^{-1} plant^{-1} and LA from 2 to 8 m^2 plant^{-1}). These results implicitly suggest that, in these cases, the measurements in each point were representative of the whole plant. Such good relationships between SF and LA are not always found elsewhere. For instance, when azimuthal variability is high (e.g. in forest trees, David et al. 2004; Nadezhda et al. 2007), the sap flow density measured at one single point may not be representative of the whole plant. Since consistently strong relationships between LA and SF for individual plants were found (also in Hatton et al. 1995), vineyard SF (up-scaling to SF_{stand}) was estimated using the following three step procedure:

(a) calculating SF of individual vines (SF_i, m^3 plant^{-1} s^{-1}), based on measured SF density (SFD_i, m^3 s^{-1} per m^{-2} of functional xylem) and functional xylem area per plant (X_i, m^2/plant) where i denotes plant number (1 to n):

$$SF_i = SFD_i \times X_i \quad (2)$$

(b) measuring leaf area of the sampled vines (LA_i, m^2 of active leaves/plant) and calculating for each plant SF per unit of leaf area (SFI_i, m^3 s^{-1} m^{-2} of active leaves):

$$SFI_i = SF_i/LA_i \quad (3)$$

(c) calculating stand SF density in a total soil area basis (SF_{stand} m^3 m^{-2} s^{-1}) using Eq. (4a), by multiplying stand leaf area index on a total area basis (LAI_{stand}, m^2 of active leaves/m^2 of soil) and average SF per unit of leaf area of the sample ($\sum SFI_i/n$) :

$$SF_{stand} = LAI_{stand} \sum SFI_i/n \quad (4a)$$

or, if converting this SF density to another time scale (e.g. L m^{-2} day^{-1} or mm day^{-1}), as:

$$SF_{stand} = 86.4 \times 10^6\ LAI_{stand} \sum SFI_i/n \quad (4b)$$

In rainfed vineyards, E_s was assumed to be negligible during the periods when EC and SF data were compared (dry summer). In the irrigated vineyard 4 (Beja), E_s was measured during short periods, using a set of microlysimeters with a diameter of 16 cm and double wall, built and used according to Daamen et al. (1993). Soil evaporation was calculated by an average weighted in relation to the area represented by each microlysimeter (with varying distance to plant row and to dripper as well as in relation to sunlight/shadow). The microlysimeters were refilled each day with new undisturbed soil from any equivalent position. For refilling, the inner wall was inserted vertically into the soil, the material aside

excavated in order to slide its bottom plate, immediately fixed with tape. The microlysimeter was cleaned, weighed and placed inside its own outer wall, which has a fixed position. It was weighted at intervals of 30 min. Microlysimeters located under a dripper have a closed chamber below, for drainage (total lysimeter height: 25 cm). In order to estimate E_s for all days of EC measurements, values of E_s measured during another set of a few days (30-min and daily values) were compared with model estimations. As referred later, the values of E_s/ET were low enough to justify this approach. The best adequacy was found with this model:

$$E_s = f_w \mathrm{ET_o}\ e^{0.267\ \Sigma \mathrm{ET_o}/\overline{\mathrm{ET_o}}} \quad (5)$$

where E_s comes in mm day^{-1}, f_w is the average fraction of soil surface wetted by irrigation event (adimensional), $\Sigma \mathrm{ET_o}$ is the cumulated value of $\mathrm{ET_o}$ since last irrigation event (mm) and $\overline{\mathrm{ET_o}}$ is the running average of daily $\mathrm{ET_o}$ for the last days (mm). If days are similar, the ratio $\left(\Sigma \mathrm{ET_o}/\overline{\mathrm{ET_o}}\right)$ can be replaced by the number of days since last irrigation event (n), as in Ferreira et al. (1997).

Use of predawn leaf water potential as a plant water status indicator for K_s analysis

The selection of a water stress indicator took into consideration this specific objective of comparing K_s functions for diverse environmental conditions. Plant water status was characterized by the values of predawn leaf water potential (PLWP). In all experiments, the monitoring of plant water status was preferred to soil water status (soil water potential or soil water content) due to operational reasons or limitations linked to the crop (woody) and soil types. In fact, soil measurements are difficult to perform in stony soils and may fail from lack of spatial representativeness. Furthermore, in most experimental situations, a representative value for average soil water content in the root zone was difficult to obtain when most roots explore deep soil layers.

Stem water potential is considered a very convenient water status indicator for cultivars/species with anisohydric behaviour (Schultz 2003). However, this variable can be inadequate to characterize water stress in plants with isohydric behaviour (Tardieu and Simonneau 1998; Ferreira et al. 2008). In vineyards 1 and 5, where both measurements (stem and predawn leaf water potential) were performed, the cultivars displayed isohydric behaviour (Silvestre and Ferreira 2000; Malheiro et al. unpublished data). As a consequence of the variable behaviour observed in vines (Tardieu and Simonneau 1998; Schultz 2003), the values of PLWP were selected for the purpose of this study and measured in at least 9 leaves fully expanded leaves, with a Scholander pressure chamber (Scholander et al. 1965).

Reference evapotranspiration, crop and stress coefficients

Reference evapotranspiration (grass, $\mathrm{ET_o}$) was calculated according to Allen et al. (1998), using data from nearby standard meteorological stations or experimental plots. When a moderate or intense water stress is imposed, the so-called actual ET ($\mathrm{ET_a}$ or $\mathrm{ET_{adjust}}$, cf Allen et al. 1998) is estimated as $\mathrm{ET_o} \times K_{cb} \times K_s + E_s$, and T as $\mathrm{ET_o} \times K_{cb} \times K_s$ (see "Introduction"). In the following sections, the discrimination between K_{cb} and K_s ($=T/T_m$) is explained and these coefficients analysed.

Results and discussion

Evapotranspiration from eddy covariance method and soil evaporation from microlysimeters

EC method provided convective fluxes of sensible and latent energy (H and LE), which were summed up and compared with the available energy (Rn-G) to assess the error in the energy balance closure. Figure 2a–c show the closure error for experiments 1, 3 and 4. The EC data from Douro vineyard (5) were discussed in Paço et al. (2011). The sum of measured convective fluxes (30 min) accounted for more than 91, 95, 87 and 93 % of the available energy in the experiments 1, 3, 4 and 5, respectively. These values correspond to a closure error relatively low compared to the range usually considered acceptable (Twine et al. 2000; Wilson et al. 2002; Oncley et al. 2007; Foken 2008). Therefore, the data gathered with the EC method were considered valid for the purpose of the study, without the need to distribute the residual according to the Bowen ratio, that would impact on K_c daily values by about 10 %. In fact, that procedure, suggested for instance by Twine et al. (2000) and Foken (2008), is not a definitive solution as the reason for lack of closure is still controversial (Warland et al. 2001; Foken 2008). Foken (2008) suggests the lack of closure is a scale problem related to landscape heterogeneity and considers that the closure is not a test for quality measurements by itself. The implications of the 5–10 % possible underestimation due to lack of closure will be considered when discussing K_{cb} results.

The high scatter observed in closure (30 min values) could be partially attributed to the hysteresis explained by heat stored in vegetation and possible horizontal advection (Oncley et al. 2007). In fact, even in a vineyard with high vLAI (therefore vegetation mass), as in vineyard 4 (Beja), heat stored in vegetation could account only for a few tens of W m^{-2} (about 3 % of available energy).

The relationship between E_s measured in the irrigated vineyard with microlysimeters, during a few summer days,

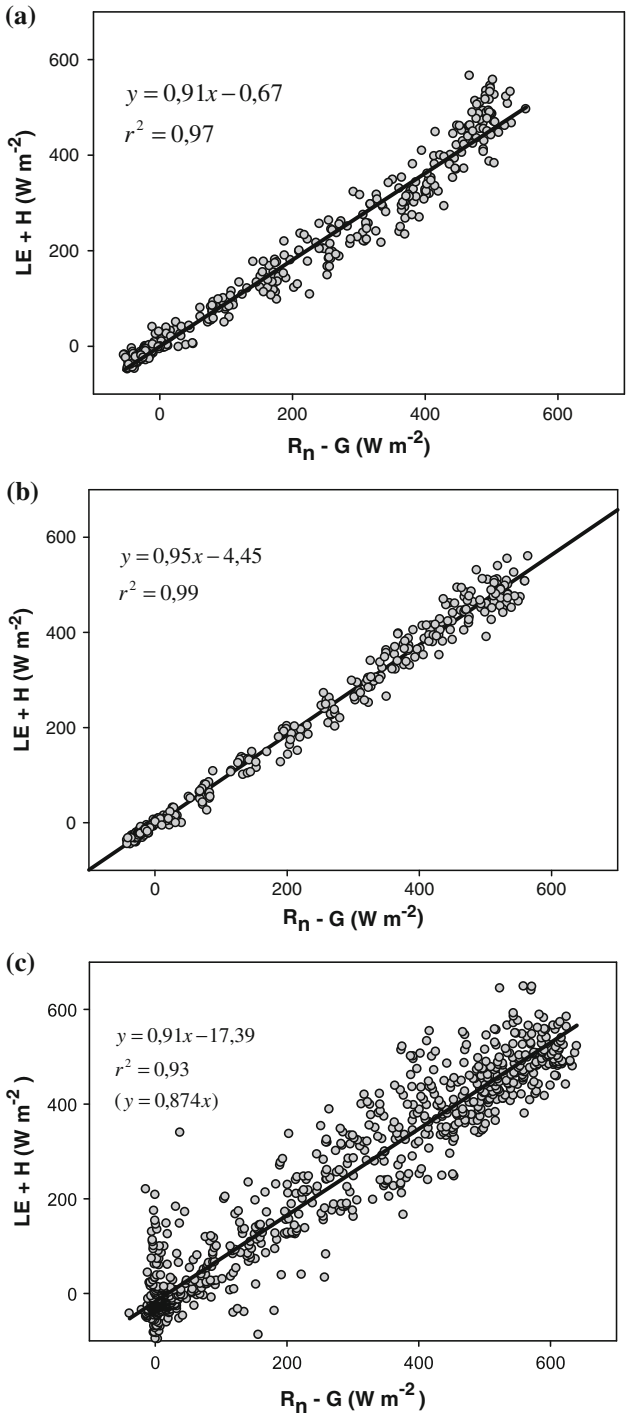

Fig. 2 Energy balance closure at **a** vineyard 1 (Santarém 1996), **b** vineyard 3 (Palmela 2001) and **c** vineyard 4 (Beja 2009), Portugal—over a 10-day period and in July–August: sensible (H), latent (LE), soil heat (G) and net radiation (R_n) density fluxes

and estimated was 1:1 ($r^2 = 0.87$). The model did not provide such good estimates for the days after rain. E_s was usually below 0.5 mm day^{-1} during summer, which represents about 15 % of T. Therefore, the errors in estimating E_s have little impact in the correction of SF.

Comparing sap flow estimates and transpiration at hourly scale

The comparison of results obtained at half-hour intervals is shown as an example, for vineyard 1 (Fig. 3), to justify the need for correction of SF estimates and explain why this is done using daily values. The relationships shown is between SF and T obtained from EC data during periods of negligible soil evaporation, that is, when $E_s \approx 0$ and ET $\approx T$. In this case, as in others (data not shown), there is experimental evidence of an underestimation of SF calculated from the original equation (Granier 1985, 1987), except for low flow rates. Braun and Schmid (1999) also did not find underestimation for very low flows (up to 4 L day^{-1} vine^{-1}). In this very low range, a linear relationship 1:1 for daily values was obtained in vineyards 1 and 3. However, the flows measured at our field conditions reach more than 12 L day^{-1} vine^{-1}. Daily underestimations in high flow conditions were also observed in other ring porous species, such us kiwi (Ferreira et al. 2008; Silva et al. 2008).

The hysteresis in Fig. 3 specially suggests an effect of capacitance. The separation between morning and afternoon data considers that the mass of water stored in plant organs decreases during the morning (apparent SF underestimation even higher) and increases during afternoon and night (attenuating apparent SF underestimation) as also shown from sap flow measurements in David et al. (1997) and Loustau et al. (1996). This hysteresis effect makes it difficult to correct half-hourly values, in order to obtain T. As a consequence, for the correction of SF data, the relationships between T and SF was analysed at a daily scale. This correction is of local interest as it accommodates, in

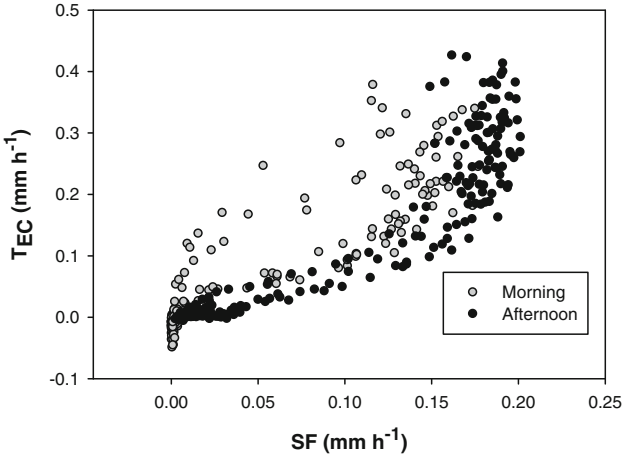

Fig. 3 Relationships between sap flow (SF) estimated by the *Granier* method (original equation) and transpiration (T) measured by eddy covariance (EC) method (half-hour fluxes in L/h) for periods of negligible soil evaporation ($T \approx$ ET) at vineyard 1 (Santarém)

one step, several aspects including those specific of the experimental set-up.

Correction of transpiration from sap flow measurements, at a daily scale

For periods of negligible soil evaporation, the relationship between SF_{stand} [from Eq. (4b)] and ET_{EC} (=T_{EC} as $E_s \approx 0$ [Eq. (1)]) was the same for the 2 cultivars and the 4 years of observations in vineyard 1 and 3 (Santarém and Palmela vineyards, Eq. (6) and Fig. 4), for T_{EC} between 1 and 3 mm day^{-1} ($r^2 = 0.84$, Ferreira et al. 2008).

$$T = 1.1 \times SF_{stand}^{1.5} \quad (6)$$

This line (points on right side of Fig. 4) should not be linear because of its physical meaning (considering possible causes of underestimation) and of general experimental evidence of higher underestimation for higher flux densities. Equation (6) was used for correction of daily SF_{stand} to obtain T not only in vineyards 1 and 3 but also in vineyard 2, as described in Ferreira et al. (2004) as, due to the relief and the small plot size of each plot, it was impossible to apply the EC method and only the SF could be measured. Even if this relationship was shown later not to be as general as initially thought, this should not affect K_s but only K_c that, consequently, will be analysed separately, during the discussion for this vineyard 2. Later for vineyards 4 and 5, the relationships obtained for T_{EC} (from EC) and SF_{stand} were different (Fig. 4, left points).

As a consequence, a relationship between T_{EC} and SF_{stand} was considered valid only for each particular experiment. We emphasize that this approach has the advantage of accommodating in one single step several reasons for unreliable SF estimates, such as xylem area uncertainty, high flows, natural gradients, uneven radial profiles, etc. Furthermore, in an analysis case by case, the problem of SF sampling or up-scaling is less critical, as this is incorporated in the general correction equation.

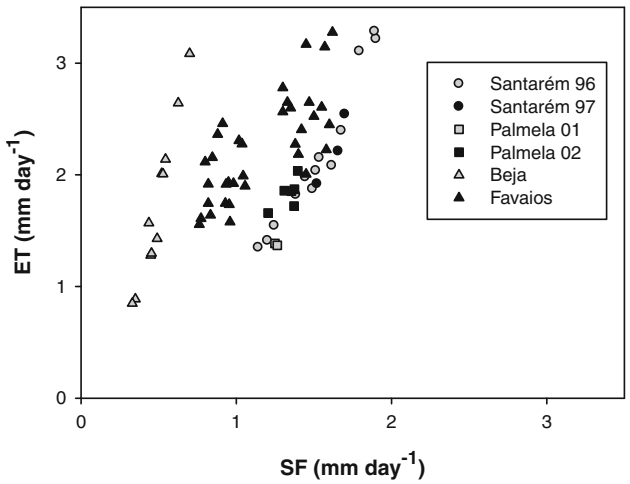

Fig. 4 Relationships between daily fluxes from sap flow, SF (original *Granier* equation) and eddy covariance (EC) methods, for negligible soil evaporation ($ET_{EC} = T_{EC}$) at vineyard 1 (Santarém 1996, 1997), vineyard 3 (Palmela 2001, 2002), vineyard 4 (Beja 2009) and vineyard 5 (Favaios-Douro 2009)

Seasonal courses of transpiration

Sap flow data were corrected based on the relationships shown in Fig. 4. Transpiration (T) was estimated for long periods of the vegetative cycle (Fig. 5a–c). T from late May/June till harvest, in the plots controlled by the farmer, ranged from 4 to less than 2 mm day^{-1}, at the peak and from 2 to 0.3 mm day^{-1}, at the end of the vegetative cycle, under intense or moderate summer water stress. As expected, T varies considerably between the five locations (in maximum flow rate, a difference above 100 % was observed across sites). The time lag between dates of maximum values reached 2 months. It should be highlighted that, during Summer, the lower T values were found in the only irrigated vineyard (4, Beja-Alentejo), in spite of the higher ET_o. It is worth to emphasize that, although the 5 studied experiments were located in the same geographical area (Western Iberia), it is not possible to generalize absolute values of extreme or even seasonal T.

The most likely hypothesis to explain the differences for T are (1) climatic conditions (expressed by ET_o, considering $T = ET_o \times K_{cb} \times K_s$), (2) LAI (influencing K_{cb}) and (3) water stress (influencing K_s). Therefore, differences between years and vineyards are mainly related to meteorological conditions (ET_o, precipitation), crop parameters and irrigation strategy when it occurred (frequency and depths, inducing different stress levels). In the following, the relative importance of these three aspects on T variations will be analysed, in order to discriminate between K_{cb} and K_s effects.

Transpiration in relation to ET_o

Figure 6a–c displays local ET_o for the different situations and Fig. 7, the relationship T/ET_o. T/ET_o peaks (up to about 0.7) at the end of rainy spring (when K_s is at its maximum, 1) and decreases to less than 0.4, by the end of dry summer. It should be noted that, in general, the more severe (and earlier) is the atmospheric stress imposed to the crop (higher ET_o, e.g. Palmela and Beja, vineyards 3 and 4) the earlier maximum transpiration rates occur (Fig. 5).

The large range of ET_o rates partially explain the differences in T: the scatter observed in T/ET_o (Fig. 7) was expected to be considerably less than in Fig. 4 (T). However, the scatter is still quite high, even in late spring (when $K_s = 1$ in almost all vineyards), suggesting that, further to

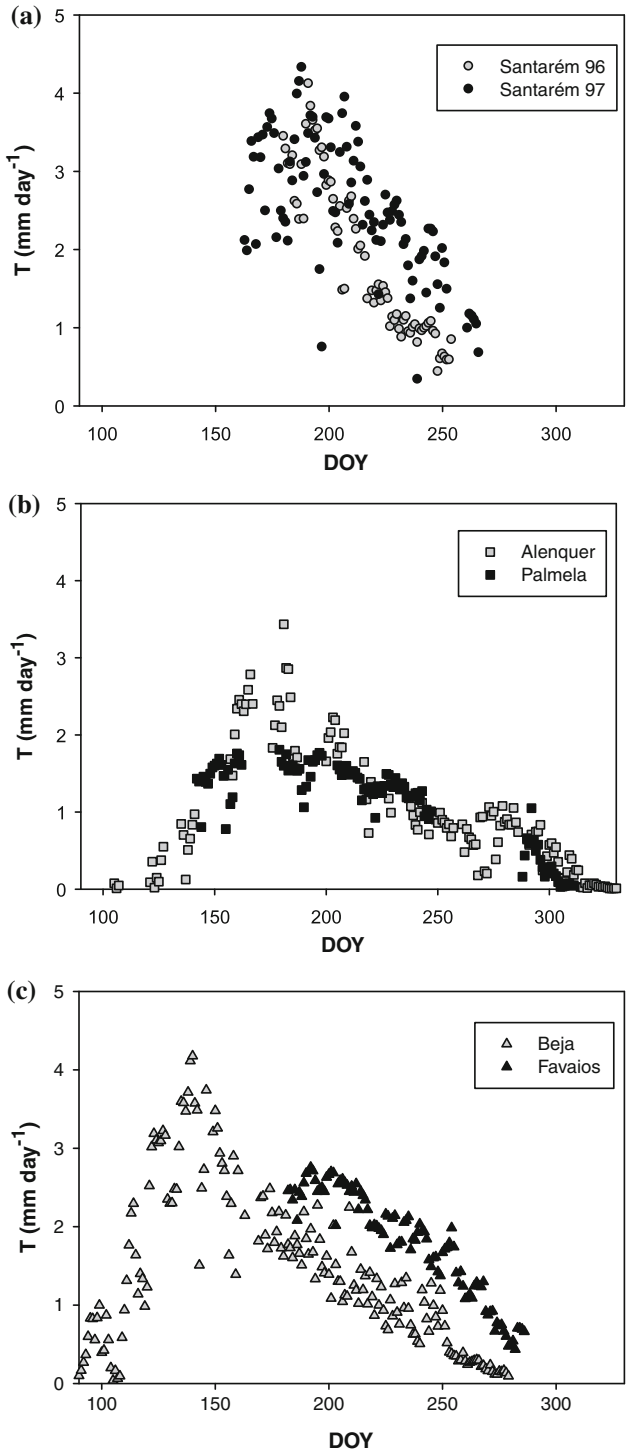

Fig. 5 Seasonal evolution of transpiration (T) in all 5 vineyards: **a** Santarém 1996 and 1997, **b** Alenquer 2008/2009 and Palmela 2002, and **c** Beja 2009 and Favaios-Douro 2009. *DOY* day of the year

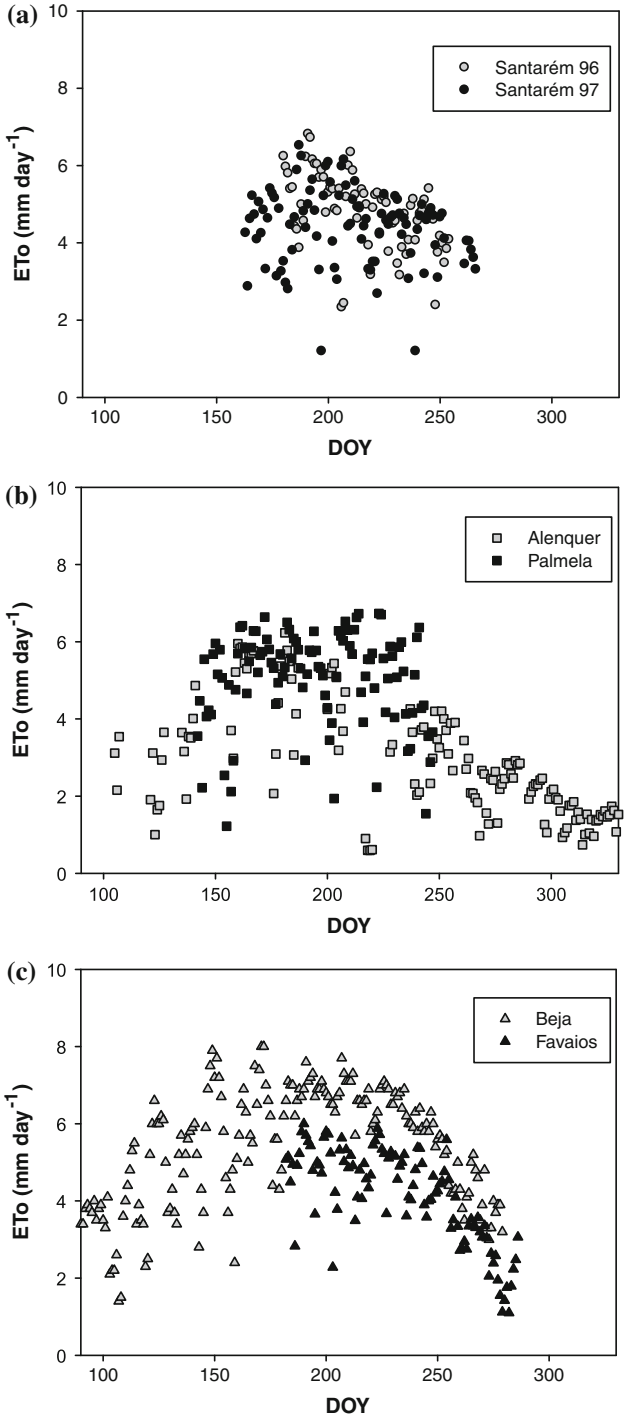

Fig. 6 Reference evapotranspiration (ET_o) for the 5 vineyards during transpiration measurements: **a** Santarém 1996 and 1997, **b** Alenquer 2008/2009 and Palmela 2002, and **c** Beja 2009 and Favaios-Douro 2009. *DOY* day of the year

ET_o, K_{cb}—and later, both coefficients—have a major role in explaining the differences in T.

T/ET_o equals K_{cb} in rainy spring ($K_s = 1$) and is clearly different between the vineyards. The values of K_s seem to decrease sharply, as soon as soil dries out and water stress occurs, with an important time lag (up to 2 months) at the different vineyards. For example, in vineyard 4, T/ET_o starts to decrease before flowering.

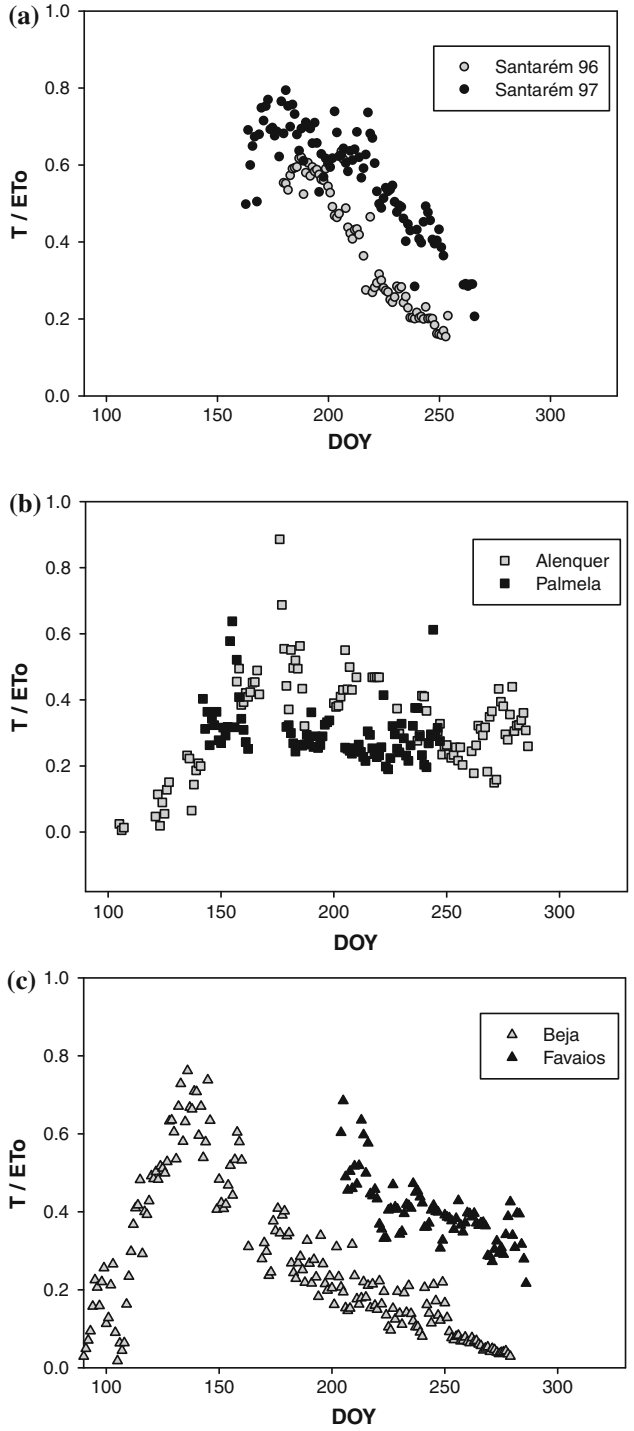

Fig. 7 Ratio of transpiration with reference evapotranspiration (T/ET_o) for the 5 vineyards during transpiration measurements: **a** Santarém 1996 and 1997, **b** Alenquer 2008/2009 and Palmela 2002 and c Beja 2009 and Favaios-Douro 2009. *DOY* day of the year

The inverse relationship between T/ET_o and ET_o (very sharp as observed in several experiments, unpublished data) confirms the importance of the limitations imposed by the low hydraulic conductivity in the roots vicinity, when ET_o increases. Conversely, when ET_o decreases, there is a higher capacity of the system to respond to atmospheric demand: some points that are out of the normal range, in Figs. 6 and 7, were explained by an atmospheric demand (expressed by ET_o) lower than normal for the season, with T/ET_o above the average for the period. This is consistent with the interpretation of K_s functions, discussed later.

Basal crop coefficients and how to separate it from short-term stress effects on transpiration

Under field conditions, particularly non-irrigated, T is modified as a consequence of the simultaneous variation in the coefficients K_{cb} and K_s and it is not always obvious to separate these two effects, as it is difficult to have a well irrigated plot in one wine grape commercial vineyard, providing the reference to obtain relative transpiration $= T/T_m$, a good approximation of K_s (Ferreira et al. 1997; Valancogne et al. 1997; Malheiro et al. 2011). However, some experiments can be designed so that some plants are well irrigated (non-limiting soil moisture) and are used as reference, providing an approximation of T_m.

The temporal variation of T/ET_o ($=K_{cb} \times K_s$) and the plant water status were analysed in parallel. K_{cb} was determined when the water status prevented water stress, evaluated PLWP. The threshold value selected was −0.2 MPa, as suggested from our previous studies (e.g. Silvestre et al. 1999) using the relationship with stomatal conductance and other water stress indicators and also from other studies (e.g. Deloire et al. 2004). Maximal K_{cb} values (before PLWP decreased from −0.2 MPa) were 0.75 and 0.60 for vineyard 1 (Santarém, respectively 1996 and 1997, late June-July), 0.35 for vineyard 3 (Palmela, late May–June), 0.70 for vineyard 4 (Beja, early May) and 0.51 for vineyard 5 (Douro, late July). For the special case of vineyard 2 (Alenquer, Oeste) where ET_{EC} was not measured, the value estimated from the use of the 'calibration' Eq. (6) provided 0.55 for K_{cb}, observed in late June-July.

The K_{cb} values could increase by 5–13 % if the energy balance was forced to closure.

Soon after a period of maximal K_{cb} for each vineyard and year (K_{cb} max) extracted using a running average of about 1 week, T decreased due to water stress and the two coefficients (K_s and K_{cb}) apply. K_{cb} during subsequent weeks was obtained (interpolation) taking into account data from (1) possible periods of appreciable rain and (2) T measured in a few plants well irrigated (for T_m) during more or less limited periods. The values of K_{cb} could be obtained from Fig. 7 ($=T/ET_o$, before T starts to decrease due to water stress). The maximal values of K_{cb} are later related to LAI (Fig. 8).

It is worth to emphasize that long-term stress affects both coefficients. When stress reduces T, not only K_s decreases from 1, but also K_{cb} slightly decreases in all

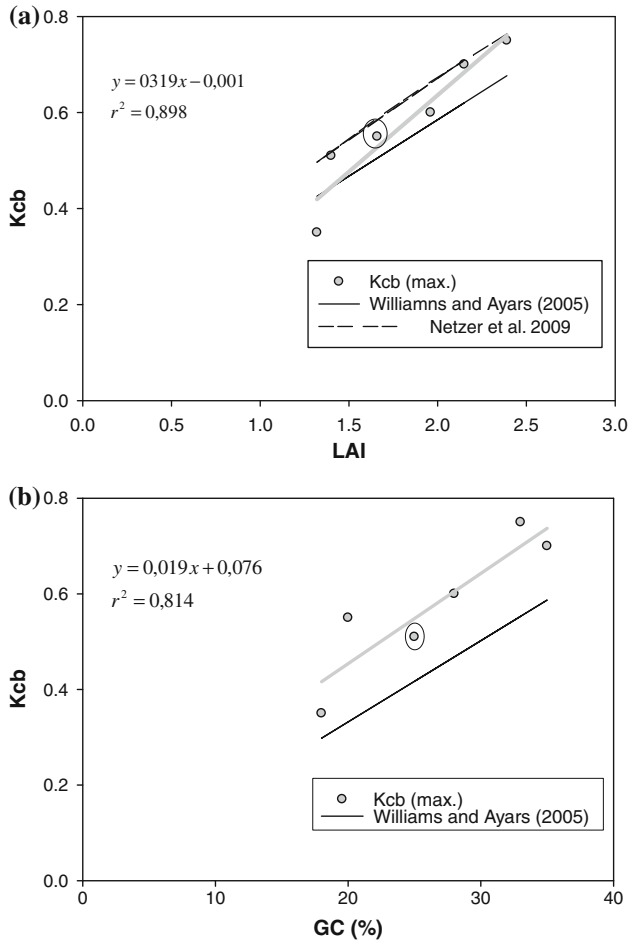

Fig. 8 Relationship between basal crop coefficient (K_{cb}) and **a** leaf area index (LAI) and **b** ground cover (GC) for the 5 vineyards (Santarém 1996, 1997, Alenquer 2008/2009, Palmela 2002, Beja 2009 and Favaios-Douro 2009), compared to the results presented by Williams and Ayars (2005) and Netzer et al. (2009). The values from vineyard 2 are marked with a *circle*

vineyards (except in vineyard 3—Palmela). This general trend is partially related to the decrease in LA due to long-term stress imposed to the vines. In fact, the loss of basal leaves was confirmed by observation, documented by photos, even in the irrigated vineyard (DI) of Beja (vineyard 4). The different behaviour observed at the Palmela vineyard 3 (under moderate stress, as shown in Fig. 10 by $K_s < 1$, apparently not affecting LA and K_{cb}) can be ascribed to possible access to underground water, and to the different cultivar used (Syrah) well adapted to water stress (originated from Iran) which is not as much isohydric as the other cultivars studied (Schultz 2003).

Long-term stress affects LA (more than affects GC or canopy height); therefore, it reduces K_{cb}. After long-term stress and a consequent decrease in LA, even if those plants are irrigated for T_m (and K_s equals 1) it is not possible to obtain K_{cb} values as high as the ones observed in the plants that were not submitted to long-term stress. In natural conditions, at the end of a long dry period, as rainfed plants adjust LA, the reduction of T is simultaneously caused by their water status condition (reflected in K_s) and the reduction in LA (affecting K_{cb}). The interpretation of T will require the discrimination of these two effects.

Transpiration in relation to canopy parameters: relationship between basal crop coefficient and leaf area index

Several authors have related K_{cb} with crop parameters related to foliage density, for different crops. Allen and Pereira (2009) using data from literature, proposed to estimate K_{cb} from fraction of GC, height and other data; Campos et al. (2010) associated remote sensing vegetation indices (for vineyards) with K_{cb}, for instance. The values of K_{cb} used in the previous paragraphs are now related to LAI and GC, for the 5 vineyards. These results (Fig. 8) showed that K_{cb} variations were mostly explained by LAI and, to a less extent, by GC.

The fact that the value of K_{cb} for vineyard 2 (values are average for the three slopes) appears in line with the others (Fig. 8a) suggests that the Eq. (6) was adequate for those vines and the values estimated for T are correct. Consequently, it seems possible to rely on T_m data series for this special case.

For the range of LAI here found (1.3–2.4), our results are remarkably consistent (Fig. 8a) with those obtained from a simple model presented by Williams and Ayars (2005) and with the relationship obtained by Netzer et al. (2009), both from work in vines with lysimeters, though in the last case the relationship was between LAI and K_c (not K_{cb}). Considering the values of E_s observed by Netzer et al. (2009), K_{cb} would be 5 % lower than the values of K_c presented (Fig. 8a).

K_{cb} is also related to GC but the GC values measured in these experiments are lower than the correspondent calculated shaded area from Williams and Ayars (2005) model (assuming that shaded area at noon for their lines N–S, is about the same as GC).

Our results for K_{cb} were also compared with those calculated using the approach suggested by Allen and Pereira (2009), either using their equation based on LAI or the so-called fraction of GC adjusted by plant height. These authors consider table or raisin grapes, on one side, and winegrapes on the other side (where an average $K_s = 0.7$ is assumed for K_{cb} calculation). For a coherent approach, we considered the case of table grapes (because K_s is not constant) and calculated K_{cb} with their equation 5a. Using our LAI data, there was an important model overestimation for K_{cb} (K_{cb} measured $= 0.56$ K_{cb} estimated $+ 0.535$, $r^2 = 0.91$). Using the effective fraction of GC, there was a

better estimation but with high scattering (K_{cb} measured = 0.95 K_{cb} estimated, $r^2 = 0.58$). The K_{cb} shown in their Table 3 (Allen and Pereira 2009) for the parameters of our vineyards (using the 'low/young table grapes', due to the GC observed) was about 0.6, which is within the range found in the present study for K_{cb} (from 0.35 to 0.75).

GC is easier to measure than LAI. However, we can argue that under the atmospheric conditions of our experiments, and for the geometry of this crop, LAI is probably a better parameter then GC to be used for K_{cb} estimations, because of the high canopy roughness with efficient penetration of light and wind in the canopy, promoting T from lower leaves. Data from our experiments provided LAI = 0.054 GC + 0.378 ($r^2 = 0.756$).

Transpiration and water status: stress coefficient functions

The values of T/ET_o (=$K_{cb} \times K_s$) divided by K_{cb} (obtained by interpolation, when appropriate) provided K_s, the third aspect impacting T, in this analysis. The K_s values observed in these commercial vineyards decreased down to 0.2, being this lower value found precisely in the only irrigated vineyard (Beja-Alentejo), where the lower values of T and T/ET_o during summer were found, as mentioned above (Figs. 5, 7, respectively).

These K_s values were related to PLWP (Fig. 10). There is a relatively similar trend with a decreasing slope as stress develops. However, there are some variations. For a commonly used threshold of PLWP = −0.45 MPa, K_s varies approximately between 0.3 and 0.6. After PLWP reaches a certain threshold, K_s decreases with a higher rate for higher PLWP which is explained by the expected decrease in soil hydraulic conductivity, limiting root water uptake, and is in agreement with the work developed by Denmead and Shaw (1962).

These authors (using soil water potential instead of PLWP) also discussed the importance of maximal ET rates for the crop (ET_m), in the behaviour of the relationship presented in Fig. 10, showing that the slope of the trend lines is more dramatic for higher T_m ($T_m = T$ with soil at field capacity). In order to verify if the results in Fig. 10 are consistent with their work, confirming this interpretation of the scattering observed, T_m was calculated as T/K_s (Fig. 9). The higher T_m are for Beja (vineyard 4) and the lower for Palmela (vineyard 3) (Fig. 9, indirectly also from Fig. 5).

In fact (Fig. 10), for a certain value of PLWP the lower values of K_s were obtained for Beja (vineyard 4), where the higher values of T_m (and also of ET_o) were found. Conversely, for a given PLWP, the higher K_s were found (vineyard 3, Palmela) where the lower T_m were reported. All other results are generally consistent with this interpretation, suggesting that the different trends observed in Fig. 10 are not only scattering around single lines. Instead they are partially related to the different T_m rates, requiring the distinction of lines with different parameters (different K_s functions).

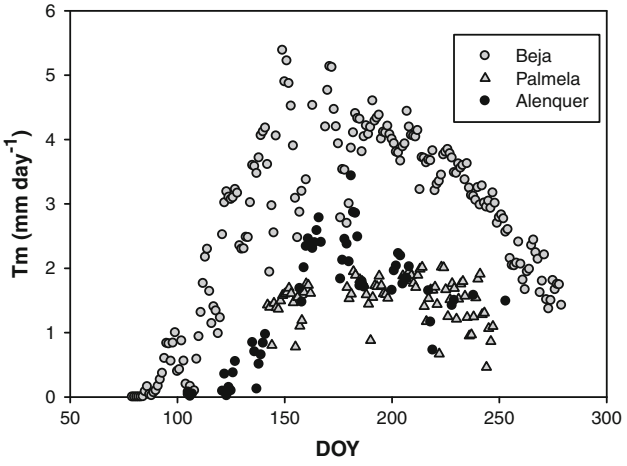

Fig. 9 Maximum crop transpiration (T_m) for the vineyard 4 (Beja, 2009), vineyard 3 (Palmela, 2002) and vineyard 2 (Alenquer, 1998/1999). *DOY* day of the year

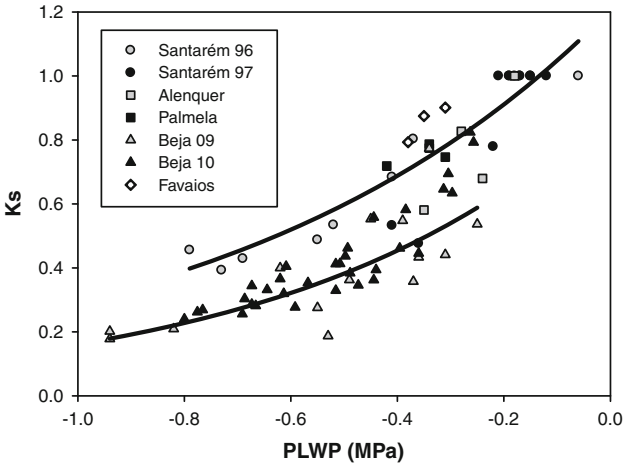

Fig. 10 Relationship between stress coefficient (K_s) and predawn leaf water potential (PLWP) for the 5 vineyards (Santarém 1996, 1997, Alenquer 2008/2009, Palmela 2002, Beja 2009 and 2010, including sub-plots of deficit irrigation, and Favaios-Douro 2009). The *lines* show the regression observed for the vineyards in Santarém 1996 ($K_s = 1.217\ e^{1.444\ PLWP}$, $R^2 = 0.941$) and Beja 2009 ($K_s = 0.839\ e^{1.642\ PLWP}$, $R^2 = 0.646$), with the lower and higher T_m values (in relation to other sites and years)

Conclusions

Seasonal values of T, K_{cb} and K_s in five commercial vineyards located in Western Iberia (Portugal) were obtained. Furthermore, the relations of K_s to a plant water

status indicator were analysed in order to discuss and compare K_s functions. Transpiration rates (T) varied considerably between sites and were mostly explained by the relatively large variations of K_{cb} and K_s, rather than ET_o, for the ranges found, an interesting fact to keep in mind when comparing vineyards in different contexts.

The maximal values of T/ET_o ($K_s = 1$) correspondent to K_{cb}, ranged from 0.75 to 0.35, depending on vineyards and years. The analysis of the variation in K_{cb} between sites (1st objective) showed that this variation was mostly explained by LAI ($r^2 = 0.90$); K_{cb} was also correlated with ground cover (GC, $r^2 = 0.81$). When there is water stress, the discrimination between coefficients (2nd objective) provided K_s, obtained from T/ET_o divided by K_{cb}. K_s decreased from 1 to 0.2 (irrigated vineyard in dry area) and in several rainfed remained above 0.5 by the end of summer. These low K_s values emphasize the importance of the consideration of K_s when estimating T.

K_s and PLWP were related (K_s functions, 3rd objective) showing a decreasing slope but a large apparent scattering (25–30 % variation around average). The results provide evidence that the driving force, expressed as T for non-stress conditions (T_m), had a role to explain the different trends. This important experimental result is in agreement with theory related to water uptake from soil to roots, suggesting the need to consider T_m as an input to obtain the parameters of K_s functions and therefore providing an answer to the last formulated question (4th).

K_s functions support an adequate calculation of the irrigation depths. If T_m rates differ significantly, there is an increased uncertainty associated with K_s calculation. Unknown parameters of K_s functions, with consequent errors in water use estimation, when simulating the soil water balance, bring an uncertain degree of the estimated soil water status.

The knowledge of water status improves the understanding of DI impacts. As a consequence of the variable parameters for K_s functions, the use of a percentage of ET_m to schedule DI leads to uncertainty in controlling water stress. For a better precision in controlling the stress levels applied in DI, adequate K_s functions—where K_s is related with any available water status indicator measured or estimated—could be used to the advantage of DI. Practical and reliable models to obtain K_s functions are a challenge for future work.

Acknowledgments The researches were supported by several projects financed by *Fundação para a Ciência e a Tecnologia* (FCT, Portugal) referred in previous publications (vineyards 1, 2 and 3). As to vineyards 4 and 5, the projects "Estratégias de rega deficitária em vinha—indicadores de carência hídrica e qualidade" PTDC/AGR-AAM/69848/2006 (FCT, Portugal) and "Uso da teledetección para a recomendaccion e seguimiento de las practicas de riego en el espacio SUDOE" (SOE1/P2/E082) provided financial support. We thank private owners for the vineyard's facilities (*Real Companhia Velha* and *Herdade de Monte Novo e Figueirinha*, respectively, at Douro Valley and Alentejo experimental fields).

References

Allen RG, Pereira LS (2009) Estimating crop coefficients from fraction of ground cover and height. Irrig Sci 28:17–34

Allen RG, Pereira LS, Raes D, Smith M (1998) Crop evapotranspiration: guidelines for computing crop water requirements. FAO Irrigation and Drainage Paper 56. FAO, Rome

Braun P, Schmid J (1999) Sap flow measurements in grapevines (*Vitis vinifera* L.) 2. Granier measurements. Plant Soil 215:47–55

Bravdo B, Naor A, Zahavi T, Gal Y (2004) The effects of water stress applied alternatively to part of the wetting zone along the season (PRD-partial rootzone drying) on wine quality, yield, and water relations of reed wine grapes. Acta Hortic 664:101–109

Bush SE, Hultine KR, Sperry JS, Ehleringer JR (2010) Calibration of thermal dissipation sap flow probes for ring- and diffuse-porous trees. Tree Physiol 30:1545–1554

Campos I, Neale CMU, Calera A, Balbontín C, González-Piqueras J (2010) Assessing satellite-based basal crop coefficients for irrigated grapes (*Vitis vinifera* L.). Agric Water Manag 98:45–54

Carbonneau A (1976) Principes et méthodes de mesure de la surface foliaire. Essai de caractérisation des types de feuilles dans le genre Vitis. Ann Amélior Plantes 26:327–343

Chalmers YM, Downey MO, Krstic MP, Loveys BR, Dry PR (2010) Influence of sustained deficit irrigation on colour parameters of Cabernet Sauvignon and Shiraz microscale wine fermentations. Aust J Grape Wine Res 16(2):301–313

Chaves MM, Zarrouk O, Francisco R, Costa JM, Santos T, Regalado AP, Rodrigues ML, Lopes CM (2010) Grapevine under deficit irrigation: hints from physiological and molecular data. Ann Bot 105:661–676

Clearwater MJ, Meinzer FC, Andrade JL, Goldstein G, Holbrook NM (1999) Potential errors in measurement of nonuniform sap flow using heat dissipation probes. Tree Physiol 19:681–687

Conceição N, Ferreira MI, Pacheco CA, Fabião M, Boteta L, Silvestre J (2011) Transpiration from a vineyard in South Portugal—stress coefficients, NDVI and leaf water potential. Acta Hort 922:277–284

Daamen CC, Simmonds LP, Wallace JS, Laryea KB, Sivakumar MVK (1993) Use of microlysimeters to measure evaporation from sandy soils. Agric For Meteorol 65:159–173

David T, Ferreira MI, David JS, Pereira JS (1997) Transpiration on an adult *Eucalyptus globulus* plantation during a spring-summer period, in central Portugal. Oecologia 110:153–159

David TS, Ferreira MI, Cohen S, Pereira JS, David JS (2004) Constraints on transpiration from an evergreen oak tree in southern Portugal. Agric For Meteorol 122:193–205

Deloire A, Carbonneau A, Wang ZP, Ojeda H (2004) Vine and water a short review. J Int Sci Vigne Vin 38:1–13

Denmead OT, Shaw RH (1962) Availability of soil water to plants as affected by soil moisture content and meteorological conditions. Agron J 54:385–390

Dry PR, Loveys BR (1999) Grapevine shoot growth and stomatal conductance are reduced when part of the root system is dried. Vitis 38(4):151–156

Dry PR, Loveys BR, McCarthy MG, Stoll M (2001) Strategic irrigation management in Australian vineyards. J Int Sci Vigne Vin 35:129–139

Du T, Kang S, Zhang J, Li F, Yan B (2008) Water use efficiency and fruit quality of table grape under alternate partial root-zone drip irrigation. Agric Water Manag 95:659–668

Ferreira MI, Valancogne C, Michaelsen J, Pacheco CA, Ameglio T, Daudet F-A (1997) Evapotranspiration, water stress indicators and soil water balance in a Prunus persica orchard, in central Portugal. Acta Hortic 449:379–384

Ferreira MI, Paço TA, Silvestre J (2004) Combining techniques to study evapotranspiration in woody crops: application to small areas—two case studies. Acta Hortic 664:225–232

Ferreira MI, Paço TA, Silvestre J, Silva RM (2008) Evapotranspiration estimates and water stress indicators for irrigation scheduling in woody plants. In: Sorensen ML (ed) Agricultural water management research trends. Nova Science Publishers, Inc., New York, pp 129–170

Foken T (2008) The energy balance closure problem: an overview. Ecol Appl 18(6):1351–1367

Geerts S, Raes D (2009) Deficit irrigation as an on-farm strategy to maximize crop water productivity in dry areas. Agric Water Manag 96:1275–1284

Goodwin I, Whitefield DM, Connor DJ (2006) Effects of tree size on water use of Peach (*Prunus persica* L. Batsch). Irrig Sci 24:59–68

Granier A (1985) Une nouvelle méthode pour la mesure du flux de sève brute dans le tronc des arbres. Ann Sci For 42:193–200

Granier A (1987) Mesure du flux de sève brute dans le tronc du Douglas par une nouvelle méthode thermique. Ann Sci For 44:1–44

Gu S, Du G, Zoldoske D, Hakim A, Cochran R, Fugelsang K, Jorgensen G (2004) Effects of irrigation amount on water relations, vegetative growth, yield and fruit composition of Sauvignon blanc grapevines under partial rootzone drying and conventional irrigation in the San Joaquin Valley of California, USA. J Hortic Sci Biotechnol 79(1):26–33

Hatton TJ, Greenslade D, Reece PH (1995) Estimation of stand transpiration in Eucalyptus populnea woodland with the heat pulse method: measurement errors and sampling strategies. Tree Physiol 15:219–227

IM (Instituto de Meteorologia) (2008) Classificação climática de Köppen, Normais Climatológicas 71-00). www.meteo.pt(pt/oclima/normais.clima/). Accessed 18 July 2011

Intrigliolo DS, Castel JR (2009) Response of *Vitis vinifera* cv. 'Tempranillo' to partial rootzone drying in the field: water relations, growth, yield and fruit and wine quality. Agric Water Manag 96:282–292

Intrigliolo DS, Lasko AN, Piccioni RM (2009) Grapevine cv. "Riesling" water use in the northeastern United States. Irrig Sci 27:253–262

Kassam AH, Molden D, Fereres E, Doorembos J (2007) Water productivity: science and practice—introduction. Irrig Sci 25:185–188

Kottek M, Grieser J, Beck C, Rudolf B, Rubel F (2006) World Map of the Köppen-Geiger climate classification updated. Meteorol Z (Berl) 15:259–263

Lopes CM, Pinto P (2000) Estimation de la surface foliaire principale et secondaire d'un rameau de vigne. Prog Agric Vitic 117(7): 160–166

Loustau D, Berbigier P, Roumagnac P, Pacheco CA, David JS, Ferreira MI, Pereira JS, Tavares R (1996) Transpiration of a 64 year-old Maritime Pine stand in Portugal: 1-Seasonal course of water flux. Oecologia 107:33–42

Malheiro AC, Santos JA, Fraga H, Pinto JG (2010) Climate change scenarios applied to viticultural zoning in Europe. Clim Res 43:163–177

Malheiro AC, Gonçalves IN, Fernandes-Silva AA, Silvestre JC, Conceição NS, Paço TA, Ferreira MI (2011) Relationships between relative transpiration of grapevines and plant and soil water status in Portugal's Douro Wine Region. Acta Hortic 922:261–267

McMillen RT (1988) An eddy correlation technique with extended applicability to nonsimple terrain. Bound Layer Meteorol 43:231–245

Nadezhda N, Nadezhdin V, Ferreira MI, Pitacco A (2007) Variability with xylem depth in sap flow in trunks and branches of mature olive trees. Tree Physiol 27:105–113

Netzer Y, Yao C, Shenker M, Bravdo B-A, Schwartz A (2009) Water use and the development of seasonal crop coefficients or Superior Seedless grapevines trained to an open-gable trellis system. Irrig Sci 27:109–120

Oncley SP et al (2007) The energy balance experiment EBEX-2000. Part I: overview and energy balance. Bound Layer Meteorol 123(1):1–28

Paço TA, Conceição NS, Ferreira MI, Malheiro AC, Fernandes-Silva AA, Silvestre JC (2011) Vineyard evapotranspiration measurement in non-flat terrain conditions by the eddy covariance technique—Douro Wine Region, Portugal. Acta Hortic 922:295–302

Patakas A, Noitsakis B, Chouzouri A (2005) Optimization of irrigation water use in grapevines using the relationship between transpiration and plant water status. Agric Ecosyst Environ 106:253–259

Reis R, Gonçalves M (1981) O clima de Portugal, Fascículo XXXII. Caracterização climática da região agrícola do Ribatejo e Oeste. INMG (Instituto Nacional de Meteorologia e Geofísica), Lisboa

Romero P, Fernández-Fernández JI, Martinez-Cutillas A (2010) Physiological thresholds for efficient regulated deficit-irrigation management in winegrapes grown under semiarid conditions. Am J Enol Vitic 61:300–312

Sadras VO (2009) Does partial root-zone drying improve irrigation water productivity in the field? A meta-analysis. Irrig Sci 27:183–190

Scholander PF, Bradstreet ED, Hemmingsen EA, Hammel HT (1965) Sap pressure in vascular plants: negative hydrostatic pressure can be measured in plants. Science 148:339–346

Schultz HR (2003) Differences in hydraulic architecture account for near isohydric behaviour of two field grown *Vitis vinfer*a L. cultivars during drought. Plant, Cell Environ 26:1393–1405

Silva R, Paço TA, Ferreira MI (2008) Transpiration of kiwifruit orchard using Granier sap flow method calibrated in field conditions. Acta Hortic 792:593–600

Silvestre J, Ferreira MI (2000) Effects of irrigation on transpiration and water relations of vineyards, in the Tejo valley (central Portugal). Acta Hortic 537:305–309

Silvestre J, Ferreira MI, Valancogne C (1999) Evapotranspiration and water relations from a vineyard in Central Portugal during spring-summer periods. Acta Hortic 493:213–218

Tanner BD, Swiatek E, Greene JP (1993) Density fluctuations and use of the krypton hygrometer in surface flux measurements. In: Proceeding of the 1993 National Conference on Irrigation and Drainage Engineering, Park City, UT, 21–23 July 1993. Irrigation and Drainage Division, American Society of Civil Engineers, 8 pp

Tarara JM, Ferguson JC (2001) Device for simulating high rates of sap flow in grapevines. Am J Enol Vitic 52:260–265

Tardieu FE, Simonneau T (1998) Variability among species of stomatal control under fluctuating soil water status and evaporative demand: modeling isohydric and anisohydric behaviours. J Exp Bot 49:419–432

Twine TE, Kustas WP, Cook DR, Houser PR, Meyers TP, Prueger JH, Starks PJ, Wesely ML (2000) Correcting eddy-covariance flux underestimates over a grassland. Agric For Meteorol 103: 279–300

Valancogne C, Ameglio T, Ferreira MI, Cohen M, Archer P, Dayau S, Daudet F-A (1997) Relations between relative transpiration and predawn leaf water potential in different fruit trees species. Acta Hortic 449:423–429

Warland JS, Dias GM, Thurtell GW (2001) A tunable diode laser system for ammonia flux measurements over multiple plots. Environ Pollut 114:215–221

Webb EK, Pearman GI, Leuning R (1980) Correction of flux measurements for density effects due to heat and water vapour trasfer. Q J R Meteorol Soc 106:85–100

Williams LE, Ayars JE (2005) Grapevine water use and crop coefficient are linear functions of the shaded area measured beneath the canopy. Agric For Meteorol 132:201–211

Wilson K et al (2002) Energy balance closure at FLUXNET sites. Agric For Meteorol 113:223–243

Yunusa IAM, Walker RR, Loveys BR, Blackmore DH (2000) Determination of transpiration in irrigated grapevines: comparison of the heat-pulse technique with gravimetric and meteorological methods. Irrig Sci 20:1–8

6.3 Nadezhdina et al. (2014)

Nadezhdina N., Ferreira M.I., Conceição N., Pacheco C.A., Häusler M., David T.S. 2014. Water uptake and hydraulic redistribution under a seasonal climate: long–term study in a rainfed olive orchard. Ecohydrology 8:387–397.

ECOHYDROLOGY
Ecohydrol. **8**, 387–397 (2015)
Published online 26 August 2014 in Wiley Online Library
(wileyonlinelibrary.com) DOI: 10.1002/eco.1545

Water uptake and hydraulic redistribution under a seasonal climate: long-term study in a rainfed olive orchard

Nadezhda Nadezhdina,[1]* Maria Isabel Ferreira,[2] Nuno Conceição,[2] Carlos Arruda Pacheco,[2] Melanie Häusler[2] and Teresa Soares David[3]

[1] *Institute of Forest Botany, Dendrology and Geobiocenology, Mendel University, Zemedelska 3, 613 00 Brno, Czech Republic*
[2] *Instituto Superior de Agronomia, University of Lisbon, Tapada da Ajuda, 1349-017 Lisboa*
[3] *Instituto Nacional de Investigação Agrária e Veterinária, Av. da República, Quinta do Marquês, 2780-159 Oeiras, Portugal*

ABSTRACT

Hydraulic redistribution plays a relevant role in the water relations of trees in climates with alternation between warm/dry and cold/wet periods. We aim to illustrate the ability of Mediterranean deep-rooted rainfed olive trees to maintain transpiration during the hot dry season and to redistribute soil water through roots, tending to temporarily homogenize soil moisture vertically. Sap flow was monitored by the heat field deformation method for 2·5 years in the stem, lignotuber, medium and shallow roots of an olive tree tracing the long-term variations in the patterns of transpiration, water uptake and hydraulic redistribution. During the same period, soil water content and meteorological data were measured and related to sap flow. Results show that hydraulic redistribution within the rhizosphere buffers the seasonal and long-term water deficits. Under high evaporative demand during the dry summer, the deeper roots connected to stem through the lignotuber uptake water supporting transpiration needs and reducing the intensive drying of the upper soil layers. Copyright © 2014 John Wiley & Sons, Ltd.

KEY WORDS sap flow; heat field deformation technique; soil moisture; water uptake; hydraulic redistribution; lignotuber; rainfed agriculture; Olea europaea

Received 13 November 2013; Revised 2 July 2014; Accepted 29 July 2014

INTRODUCTION

Dimorphic or multi-layered root architecture is common in trees from Mediterranean-type ecosystems (Kurz-Besson *et al*., 2006; David *et al*., 2013; Gabarron-Galeote *et al*., 2013), allowing the water uptake from different soil horizons (Richards and Caldwell, 1987; Caldwell and Richards, 1989; Ryel, 2004). Although root volume usually decreases in depth (Schenk and Jackson, 2002), deep roots have an important role in water-limited environments (McElrone *et al*., 2007; Bleby *et al*., 2010; Maeght *et al*., 2013) often poor in nutrients, namely regions with Mediterranean climate.

When roots occupy layers with different soil moisture, water may be redistributed within the soil profile in response to water potential gradients. Under these circumstances, trees may act as equalizers (Breazeale and Crider, 1934 referred by Caldwell *et al*., 1998) or homogenizers (Ivanov *et al*., 2010; Burgess, 2011; Guswa, 2012) of soil moisture within the volume occupied by roots. Homogenization of soil moisture is a dynamic process, which may occur in response to the processes of transpiration (Tr), i.e. water movement from wet soil to the atmosphere, and hydraulic redistribution (HR), i.e. root water transport from wetter to dryer soil layers (Richards and Caldwell, 1987). When the soil in the rhizosphere is homogeneously wet, transpiration promotes soil moisture heterogeneity due to the faster and energetically easier drying of the superficial soil, where most roots concentrate (Canadell *et al*., 1996; Schenk and Jackson, 2002). Heterogeneity is reached faster in the soil colonized by tree roots than in bare soil (see Figure 2 in Prieto *et al*., 2012). By performing HR during the night, tree roots promote fast homogenization of soil moisture through their pipe network (Dawson, 1993; Prieto *et al*., 2012). When the soil in the rhizosphere is heterogeneously wet, transpiration also contributes to soil moisture homogenization (Nadezhdina *et al*., 2009; Guswa, 2012).

Sap flow methods that measure bidirectional flows are an important tool to disclose the functioning of the below-ground part of trees (Burgess *et al*., 1998, 2001; Nadezhdina *et al*., 2010). When the whole bulk of the soil is wet, sap flow in all tree organs is always acropetal (moving to foliage) during the day and sometimes during the night (transpiration and storage refilling), depending on the evaporative demand of the atmosphere and available

*Correspondence to: Nadezhda Nadezhdina, Institute of Forest Botany, Dendrology and Geobiocenology, Mendel University, Zemedelska 3, 613 00 Brno, Czech Republic. E-mail: nadezdan@mendelu.cz

energy. However, when the soil dries, reverse (negative) flows may occur in roots at night indicating water transfer from wet to dry soil through them (HR). Root sap flow may be used as a tracer of the long-term variation in the patterns of tree water uptake (WU) and HR. Long-term records of root sap flow coupled with meteorological data may also give insight into the soil water status of the rhizosphere, even in the absence of soil moisture measurements (Nadezhdina *et al*., 2010). This is especially important in stony soils where deep soil layers are difficult to access (Bleby *et al*., 2010).

In a previous study, Nadezhdina *et al*. (2009) showed that roots can act as temporary horizontal homogenizers of soil moisture, based on the monitoring of root sap flow. The application of localized irrigation on a Douglas-fir root in a very dry superficial soil created heterogeneous soil moisture conditions, immediately reflected in root sap flow. Sharp differences in root WU and HR were observed. However, the differences in WU declined gradually in time because of the homogenizing processes.

Roots can also homogenize soil moisture vertically. This process is more often documented because of the usually larger vertical soil water potential gradients. The mechanism of water redistribution by roots has been reported in different climates and species (Brooks *et al*., 2002; Hultine *et al*., 2003; Oliveira *et al*., 2005; Nadezhdina *et al*., 2006, 2008; Wang *et al*., 2011; Miller *et al*., 2012; David *et al*., 2013). It is particularly relevant in seasonal climates, such as the Mediterranean climates, with alternation between dry and hot summers and wet and cold winters. Under these conditions, trees often tap groundwater, an additional source of water for root uptake and HR during summers (Lubczynski and Gurwin, 2005; David *et al*., 2007, 2013; Miller *et al*., 2010). In some olive cultivars, stomatal control is another important mechanism to cope with summer drought (Perez-Martin *et al*., 2014). The lignotuber, a woody swelling structure at stem base in olive trees, was also found to redistribute and store soil water in a circadian basis, especially in very dry periods (Ferreira *et al*., 2013).

In this work, we monitored tree WU and HR during 2·5 years using continuous automated measurements of sap flow in shallow and medium roots and in the lignotuber. Stem sap flow was also measured because the stem is the organ where the WU is integrated (Figure 1a) and because, on a daily basis, it may correspond to actual tree transpiration (water storage in plant organs in consecutive days is usually negligible compared with daily water use, as observed by Ferreira *et al.* (1997), Moriana *et al*. (2003) and Fernandez and Cuevas (2010)).

We hypothesized that the lignotuber might contribute to soil moisture dynamics and although root WU might vary considerably across seasons in different root types (Figure 1b, dry and wet periods), the average water uptake (AWU) of roots and lignotuber would remain proportional to tree transpiration. The confirmation of this hypothesis would support the findings that in dry soil conditions, trees temporarily tend to homogenize soil moisture by adjusting their flow patterns through different root types. This prevents

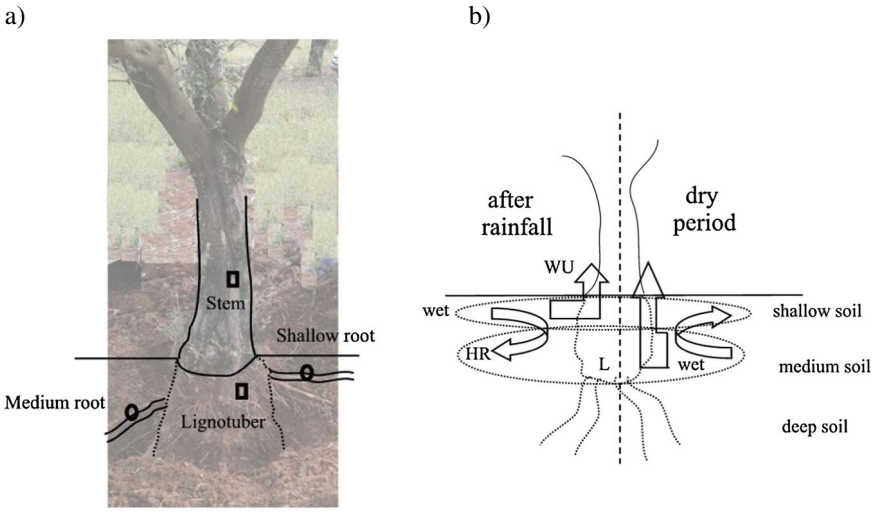

Figure 1. (a) scheme of the installation of sap flow sensors in the stem, lignotuber and roots of an olive tree. Roots were equipped with single-point Heat Field Deformation sensors (circles), and stem and lignotuber (L) (extending from stem basis belowground) were equipped with multi-point (three measuring points) sensors (rectangles). Horizontally directed roots were considered as shallow and roots directed from lignotuber to deeper soil layers as medium; (b) hypothetical functioning of roots in the soil profile where soil moisture was measured from surface to 120 cm depth. Because of soil traits deeper soil layers were not accessible. The behaviour of deep roots was inferred from that of L (to which all roots were assumed to be connected), hence possibly behaving as a 'buffering mixer'. The vertical dashed line separates wet (left) and dry (right) periods, i.e. when the upper soil is wet after rainfall and when the wettest soil layers are the medium or deep ones. Right-angled arrows indicate root water uptake (WU) and curve arrows hydraulic redistribution (HR).

the drop in soil moisture below a certain threshold, enabling the trees to maintain the activity of upper roots.

METHODS

The experimental work took place at a rainfed olive orchard (38° 03′ N, 7° 55′, 200 m asl) close to Ferreira do Alentejo, Portugal. The climate is humid mesothermal with dry hot summers. Long-term precipitation is 572 mm year^{-1}, 5% of which falls during summer (http://www.ipma.pt/pt/oclima/normais.clima/1971-2000/002/). The soil is a calcic vertisol with ApBtC profile. The clay (Bt) and the loam-clay (Ap) horizons have 6% and 16% of coarse elements, respectively. From our observations, the minimum observed soil water content was around 20% $m^3\,m^{-3}$, depending on soil layers and horizontal location. It can be roughly assumed as value of the permanent wilting point. Site reference evapotranspiration (ETo) was assessed using the Penman–Monteith equation with usual grass parameters (height 0·12 m, surface resistance 70 s m^{-1}, albedo 0·23, according to Allen *et al*., 1998) and meteorological data from a nearby station (www.cotr.pt, SAGRA network).

The olive orchard (cultivar Cobrançosa) was planted in 1990 (trees at 7 m × 7 m). A traditional training system was used. Tillage was practised in rows, not beneath the crowns. Average tree height, leaf area index (ground area basis) and canopy cover in 2010 were 4·2 m, 1·05 and 18%, respectively.

Sap flow data reported in this study were measured by the heat field deformation (HFD) method from June 2010 till the end of 2012. Sensors were installed in stem, roots and lignotuber, in the upper soil close to tree stem due to soil texture. The connection of the sensors to shallow or medium soil layers was inferred visually, during installation, from root positioning (inclination) towards shallow or deeper soil (Figure 1a), and confirmed later on the basis of the response of root sap flow to rain events following soil drought (Nadezhdina *et al*., 2010). Although 12 single-point sensors were installed in roots, only six functioned throughout the whole experimental period, four in shallow oriented roots and two in deeper oriented roots accessible without excessively disturbing the soil. Sensors in shallow roots were installed 5–10 cm below soil surface, whereas sensors in medium roots were installed 15–20 cm below soil surface (see also Figure 1 in Ferreira *et al*., 2013). Hereafter, these roots will be considered as shallow and medium roots, to distinguish from deeper roots possibly connected to the lowest level of the lignotuber (Figure 1a). One multi-point sensor (three measuring points) was installed in tree stem and another one in the lignotuber of the same tree between the insertion of shallow and medium roots (Figure 1a). After installation, root sensors were covered by silicon (to protect against water) and then by soil. The stem sensor was insulated against sun flecks and rain water.

The HFD method is based on the deformation of heat field generated by a linear heater around two pairs of differential thermocouples in the axial and tangential directions around it, being the ratio between temperatures proportional to sap flow (Nadezhdina *et al*., 1998). Sap flow was normalized by the maximum value observed during the experimental period to assess the long-term contribution of each root to tree transpiration, WU or HR (qualitative comparison). For the stem and lignotuber, the average sap flow (three xylem layers) was normalized by the average maximum to emphasize the seasonal dynamics. The same dataset was used in Ferreira *et al*. (2013), where sap flow daily dynamics in roots, stem and lignotuber was described in detail. In this paper, we analyse the relationships between sap flow data, soil moisture and ETo, as well as the dynamics of night sap flow.

For understanding the input of different root types to seasonal WU, the normalized maximum daily values of sap flow (average for each root type and lignotuber) were compared with ETo, also normalized by the maximum value observed during the experimental period. HR was characterized by night sap flow values, i.e. when competitive sinks of the atmosphere are minimum. Hereafter, tree transpiration (Tr), root WU and HR refer to normalized values derived either from midday (Tr, WU) or predawn (HR) sap flow records.

Sap flow was compared with direct soil moisture measurements. Soil water content ($m^3\,m^{-3}$) was measured with neutron probe model 4301 (Troxler Electronic Laboratories, Inc, Research Triangle Park, NC, USA) in 12 access tubes distributed horizontally in three positions from tree stems. Measurements were taken every 2 weeks from soil surface to 120-cm depth at 20-cm intervals. As mentioned before, deeper soil layers were not accessible. To be consistent, the soil profile was considered divided in shallow and medium layers, the shallow one occupied by roots extending from soil surface to 60 cm depth and the medium one occupied by roots extending from 80- to 120-cm depth (Figure 1b).

RESULTS

Figure 2 shows the seasonal variation in soil moisture and minimum (night) sap flow in roots (shallow and deep), lignotuber and stem. During the experimental period (June 2010 to December 2012), soil moisture reflected the inter- and intra-annual variability in rainfall: 2011 was the wettest year and 2012 the driest one. Differences were mainly due to winter-early spring rainfall (Ferreira *et al*., 2013). In the extremely dry 2012 winter, rainfall was about 10% of the long-term average for winter months in the region so that soil moisture was especially low even in medium layers

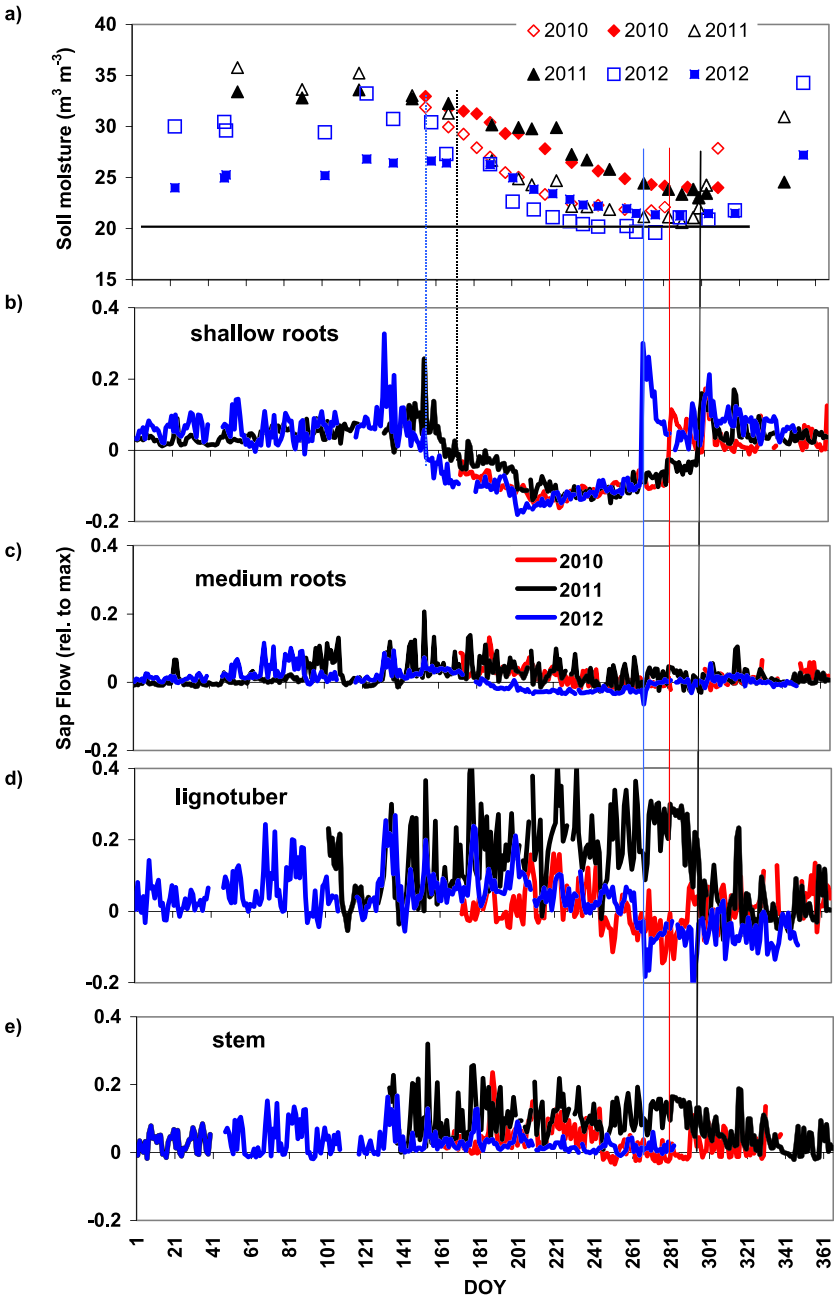

Figure 2. Seasonal dynamics of (a) soil moisture in shallow (0–60 cm, open symbols) and medium (80–120 cm, closed symbols) layers; normalized minimum sap flow in shallow (b) and medium roots (c), lignotuber (d) and stem (e). Dashed vertical lines indicate the onset and end, respectively, of hydraulic redistribution (HR); different years are indicated by different colours. The horizontal line in (a) corresponds to the lowest value of soil moisture, a threshold defined by direct measurements corresponding to the occurrence of HR.

(Figure 2a). From June onwards, soil moisture decreased progressively, faster in shallow than in medium soil, either in wet or dry years. The difference in soil moisture between layers increased and then declined from the middle to end of the dry season. The decrease in shallow layers stopped when soil moisture approached 0·20 $m^3 m^{-3}$ (Figure 2a).

Negative (reverse) night flows started to occur in shallow roots almost at the same time in 2010 and 2011, but more than 2 weeks earlier in 2012 (Figure 2b) when the shallow soil started to be relatively dry (Figure 2a). At the end of the dry period, abrupt changes in shallow root sap flow (from negative to positive) were observed in response to autumn rainfall. Soil moisture in the shallow soil (0–60 cm) responded with a certain delay, especially in 2012. At the time soil moisture in the shallow layer stopped declining (approx. DOY 225), reverse flows in shallow roots became similar in magnitude in all years, gradually decreasing till the end of the dry period.

Night flows in medium roots were often close to zero (Figure 2c) and less variable than in shallow roots or lignotuber. Reverse flows in these roots were much lower than in shallow roots. They were only recorded occasionally at the end of the dry period in 2011 and 2010 but started earlier and lasted for about 3 months in the very dry 2012.

In the lignotuber, night flows were higher than in roots and stem and quite variable, reaching maximum values in 2011 (Figure 2d). Reverse flows were occasionally observed at the end of the dry period and upon the autumn rains in all years, lasting longer in 2012. Low reverse flows in the stem were also recorded occasionally at the end of the dry period in 2010 and 2012.

The positive night flows observed in the stem may indicate night transpiration (NTr) and storage refilling (R). The recorded flows in the stem followed a pattern similar to the sap flow values observed in the lignotuber (Figure 2e) and were directly correlated to them: $NTr + R = 0{\cdot}62$ lignotuber sap flow (LSF) $+ 0{\cdot}03$, $r^2 = 0{\cdot}74$ for 2010; $NTr + R = 0{\cdot}58$ LSF, $r^2 = 0{\cdot}77$ for 2011; $NTr + R = 0{\cdot}42$ LSF $+ 0{\cdot}01$, $r^2 = 0{\cdot}6$ for 2012.

Figure 3a shows the variation of normalized night sap flow in different tree organs (stem, roots and lignotuber) with average soil moisture from surface to 120 cm. Shallow roots were more exposed to soil drying showing reverse flows when soil moisture dropped below 29 $m^3\,m^{-3}$. The occasional positive peaks of sap flow in shallow roots, when soil moisture was lower than 29 $m^3\,m^{-3}$, were caused by rainfall events of different intensity. Negative flows in medium roots and lignotuber were observed when positive flows occurred in shallow roots. However, night sap flows in medium roots, lignotuber and stem were mostly positive above soil moisture values of 22 $m^3\,m^{-3}$ (vertical dashed line in Figure 3a). Below this value, very small flows, close to zero or negative, were recorded in all tree organs. Figure 3b shows the variation of night sap flow in shallow and medium roots with soil moisture of the corresponding layers. Positive night flows highly varied in roots of both types when soil moisture was higher than 29 $m^3\,m^{-3}$ (area marked by rectangle). With the drying of shallow or medium soil, positive flows in both root types rapidly turned negative (arrows pointing down to ellipse). Although sap flow variability in shallow roots in the positive (rectangle) and negative (ellipse) areas was comparable, soil moisture variations in the wetter area (rectangle) were higher than in drier one (ellipse). Sap flow recovered fast from negative to positive in shallow roots because of rain (grey horizontal arrow), even without an apparent increase in soil moisture, which occurred with a certain delay. Reverse flows in medium roots occurred either because of gradual drying of the medium soil (dashed arrow pointing down) or to the abrupt increase of shallow root flow upon shallow soil rewetting (horizontal dashed arrow directed to negative flows). The negative

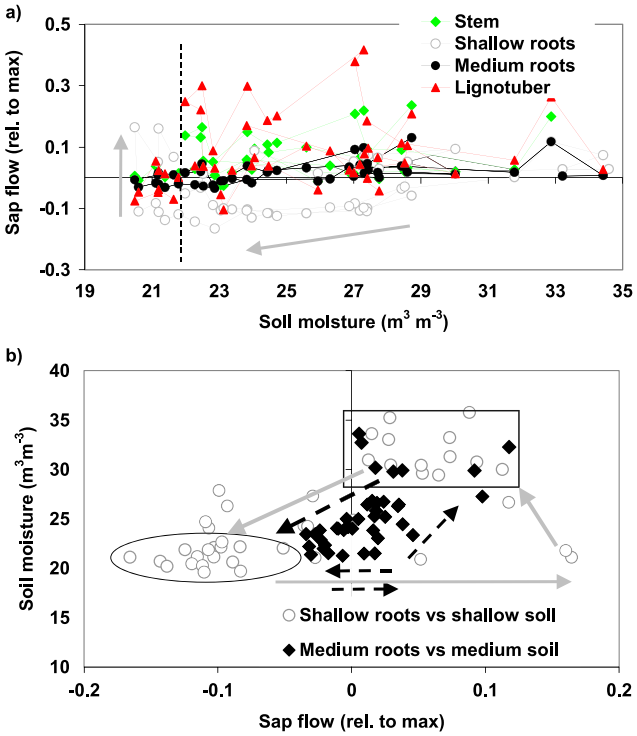

Figure 3. (a) Relationship between normalized minimum (night) sap flow in stem, roots, lignotuber and average soil moisture from surface till 120 cm. Vertical dashed line defines the 'critical' threshold for tree survival (soil moisture below 22 $m^3\,m^{-3}$). (b) Relationship between normalized minimum sap flow in shallow and medium roots and soil moisture in corresponding soil layers. Values inside the rectangle correspond to high soil moisture and positive flow; values inside the ellipse correspond to periods of very dry soil and reverse (negative) flow. The grey arrows show the variation in shallow root sap flow from gradual shallow soil drying to rewetting after rain. The dashed black arrows refer to medium root sap flow.

flows in medium roots changed to positive when rain recharged the medium soil (dashed arrow directed to positive flows and to higher soil moisture).

Three particular situations were selected from the seasonal sap flow dynamics (Figures 2 and 3) to try to characterize and conceptually model WU (maximum daily sap flow) and HR (minimum night sap flow) by roots and lignotuber in olive trees under high evaporative demand (Figure 4): (1) high soil moisture in the shallow soil, as usually occurs after the first rainfall events following summer drought (Figure 4a); (2) dry shallow soil but wetter medium and deep soils, as observed at the end of the dry period in 2011 (Figure 4b); and (3) dry shallow, medium and deep soils, as observed at the end of the dry period in 2012 (Figure 4c).

In order to analyse the seasonal variations in maximum tree WU due to inter-annual variations in soil water, maximum normalized values of daily sap flow in stem, lignotuber and different roots were compared with normalized values of ETo for each year (Figure 5). The relationship between daily sap flow in the stem (SSF, considered equal to Tr) and ETo (Figure 5a) was the

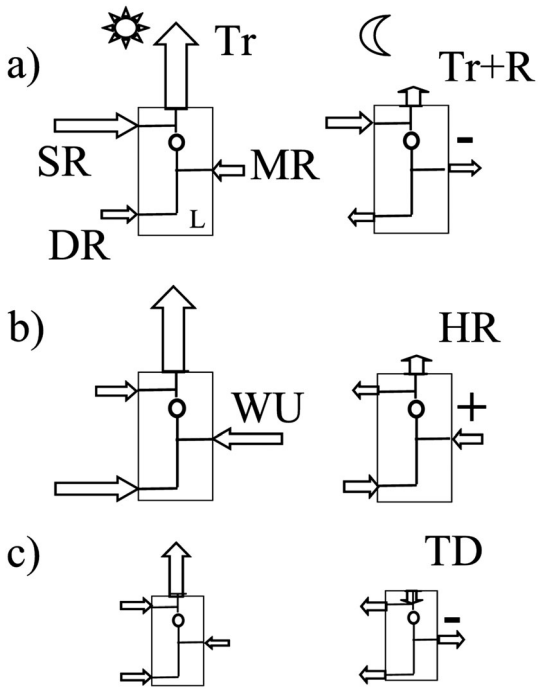

Figure 4. Conceptual model for the seasonal water uptake (WU) and hydraulic redistribution (HR) of the lignotuber (L, rectangle) of an olive tree during the day (midday, left) and night (right) for three periods with similarly high evaporative demand: (a) wet period after rainfall, when the shallow soil is wet but medium and deep layers are still dry; (b) dry period with dry shallow soil, moderately dry medium soil and wet deep soil; (c) very dry shallow and medium soil, characterized by low WU and low transpiration (Tr) during the day and by HR at night in all measured parts of the rhizosphere and the stem base. R is storage refilling at nights, TD is tissue dessication. Circles mark the position of the HFD multi-point sensor installed in L; + and − indicate the direction of sap flow during the night. Arrows directed into L indicate positive WU; arrows directed outwards indicate HR. Variations in the volume of L denote variable water storage capacity.

strongest in 2011 ($r^2 = 0{\cdot}72$) but declined in 2010. In the very dry 2012, no relation was observed. Figure 5a also shows the high correspondence between stem sap flow and AWU of roots. A close relationship was found between SSF and AWU, with the slope of the regressions close to 1 in 2010 (SSF = 1·05 AWU, $r^2 = 0{\cdot}73$) and 2011 (SSF = 0·96 AWU, $r^2 = 0{\cdot}94$), decreasing in 2012 (SSF = 0·87 AWU, $r^2 = 0{\cdot}94$). LSF represented more than 70% of AWU: LSF = 0·78 AWU, $r^2 = 0{\cdot}72$ in 2010; LSF = 0·8 AWU, $r^2 = 0{\cdot}93$ in 2011; LSF = 0·72 AWU, $r^2 = 0{\cdot}72$ in 2012. It was proportional to ETo ($r^2 = 0{\cdot}67$) in 2011 (Figure 5b), when rainfall was close to the long-term average. The highest values of LSF were recorded in the middle of 2011. In relation to normalized Eto, the lowest SF values were recorded in 2012. Figure 5c shows the seasonal variation in WU by different root types (shallow and medium). The highest seasonal variation in WU was observed in shallow roots. When the soil was homogeneously wet, flows were higher in shallow than in medium roots but became similar under high evaporative demand. When the shallow soil dried, sap flow was lower in shallow roots and the higher flow was recorded in medium roots under the same evaporative demand during the dry period. The highest sap flow values were recorded in 2010 in the shallow roots following a 36-mm rainy period (in 3 days) at the end of the dry period, and in the medium roots at the time of the seasonal peak in the atmospheric demand (July).

To characterize the seasonal differences in HR, the two most contrasting years in the amount and distribution of annual rainfall were selected: 2011 and 2012. Normalized daily maximum and minimum night sap flows in shallow roots and lignotuber (considered representative of deeper roots according to sap flow sensor insertion) were related to sap flows in stem from June to November of 2011 and 2012, including the dry period and the transition to the wet period (Figure 6a and b, respectively). Storage refilling and sap flow in the lignotuber were substantially higher in the wet 2011, where water was well available in the deeper soil (Figure 6a). Higher night reverse flows were recorded in shallow roots during 2012 and higher positive flows were recorded in them following rain events. In 2012, stem sap flow was close to zero during most of the nights, occasionally negative. The maximum sap flow values (Figure 6b) were much higher in 2011 than in 2012.

DISCUSSION

In this study, we analysed sap flow functioning in different organs of an olive tree – stem, shallow and medium roots and lignotuber, under varying climatic and edaphic conditions during a long period (2·5 years), which included three growing seasons. To our knowledge, this is the longest dataset where sap flow was continuously monitored in different bodies of an olive tree. Fernandez *et al.* (2001, 2006) examined sap flow responses to drought in roots and stems of olive trees during several months, whereas Santos *et al.* (2007) and Karray *et al.* (2008) only measured stem sap flow during 4 months and 2 years, respectively. In our study, we also followed soil moisture dynamics in the rhizosphere to assess sap flow restrictions upon drying of different soil layers and to disclose how and when water is up taken and redistributed. Particular attention has been given to the role of the lignotuber; a storage organ for starch and nutrients supporting the demands for regrowth (James, 1984) recently was found to be also relevant in the transport of water in olive trees (Ferreira *et al.*, 2013, based on the same dataset). The installation of a multi-point HFD sensor in the lignotuber between the connections of shallow and medium roots was relevant to achieve better insight into its hydraulic functioning. Its response to drought differs from that of stem because of the apparent HR between these roots via lignotuber. To support this, Figure 2 shows that the pattern of minimum (night) SSF mimics that of the lignotuber, although with lower relative

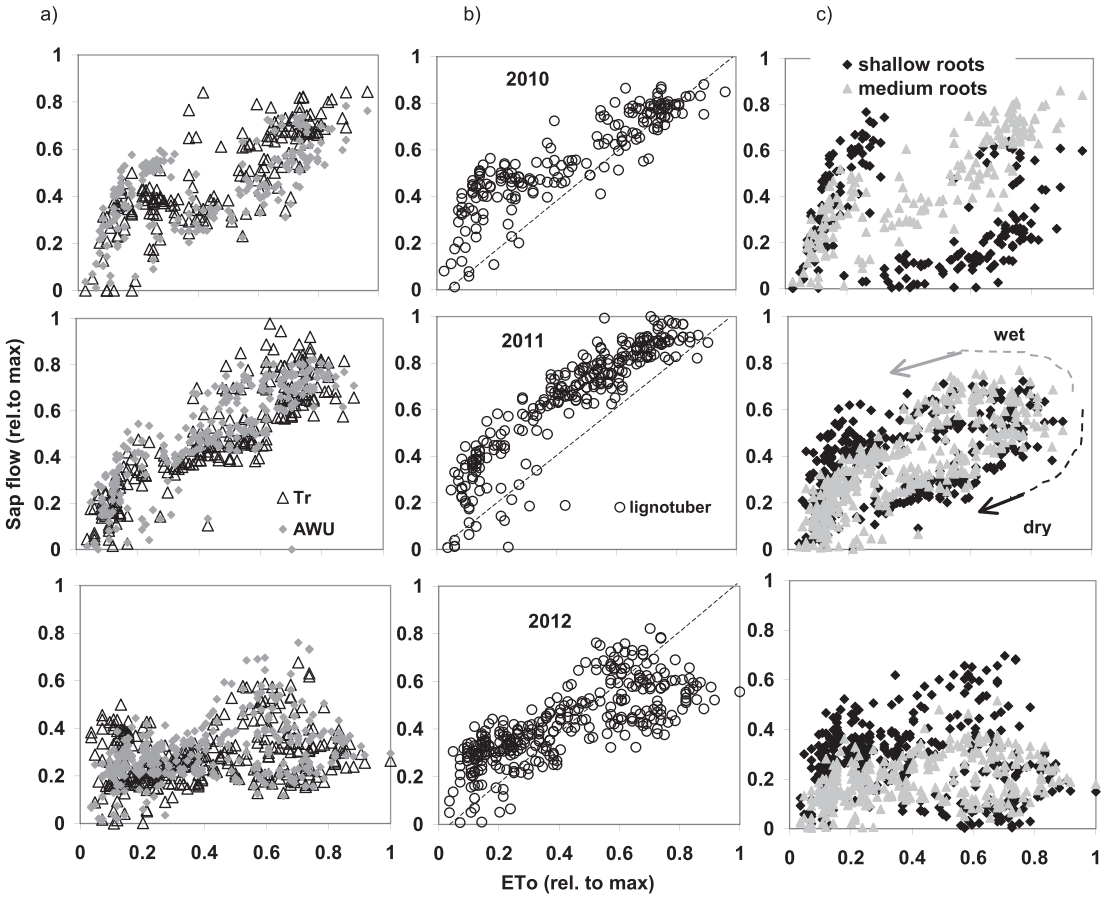

Figure 5. Normalized daily values for (a) reference evapotranspiration (ET0) versus actual transpiration (Tr, stem sap flow) and versus the average water uptake (AWU, average sap flow of roots and lignotuber); (b) ET0 versus lignotuber sap flow and (c) ET0 versus root water uptake (WU) occupying different parts of the rhizosphere – shallow and medium roots (2010 to 2012). Dashed curved lines in (c) show the directions of flow decrease in shallow roots (black) and of flow increase in medium roots as shallow soil dries. The opposite direction is observed when the shallow soil is wet.

flows in the stem (Figure 2d and e). However, periodical reverse flows were observed in the lignotuber, whereas in the stem flows decreased approaching zero but not being negative (except occasionally at the end of the dry periods in 2010 and 2012, Figures 2 and 6). This occasional reverse flow in stem may indicate redistribution of water stored in tree tissues to the dry soil, i.e. tissue desiccation (Nadezhdina *et al*., 2010) that can occur under critical tree water status (when no other source of water seems to be available for redistribution to the very dry soil besides that in plant tissues).

The seasonal dynamics of sap flow and soil moisture, and their relationships in the observation period, show that the largest amplitude of response to soil drying occurred in shallow roots and lignotuber (Figures 2 and 3). Relationship between night sap flow and soil moisture also allowed the definition of two phases with distinct sap flow behaviours: the 'available' phase, when soil moisture was above $22\,m^3\,m^{-3}$, and the 'critical' phase when it was below $22\,m^3\,m^{-3}$ (vertical dashed line in Figure 3a). In the first one, water was accessible to roots at least in one soil layer and sap flow rates highly varied: positive night flows prevailed in the stem and lignotuber, flows were close to zero in medium roots and reverse flows prevailed in shallow roots when soil moisture was between 29 and $22\,m^3\,m^{-3}$. In the last one, roots had no access to wet soil, and therefore, night sap flow rates were negative and similar in all organs. Reverse flows in shallow roots started to occur when soil moisture dropped below $29\,m^3\,m^{-3}$ in the observed soil profile (0–120 cm) (Figure 3a). The magnitude of reverse flow in shallow roots slightly decreased in the 'critical' area because of the lack of water to support hydraulic lift. When soil moisture decreased below $29\,m^3\,m^{-3}$, the occasional positive sap flow peaks in shallow roots were observed, corresponding to sporadic intense rainfall events. These positive peaks were accompanied by negative peaks (reverse flows) in medium roots and lignotuber, which promptly used shallow soil moisture provided by rain to refill their depleted storages through hydraulic descent. Small rains decreased the magnitude of reverse flows in shallow roots, although not preventing hydraulic lift, as reported by Bleby *et al*. (2010). During

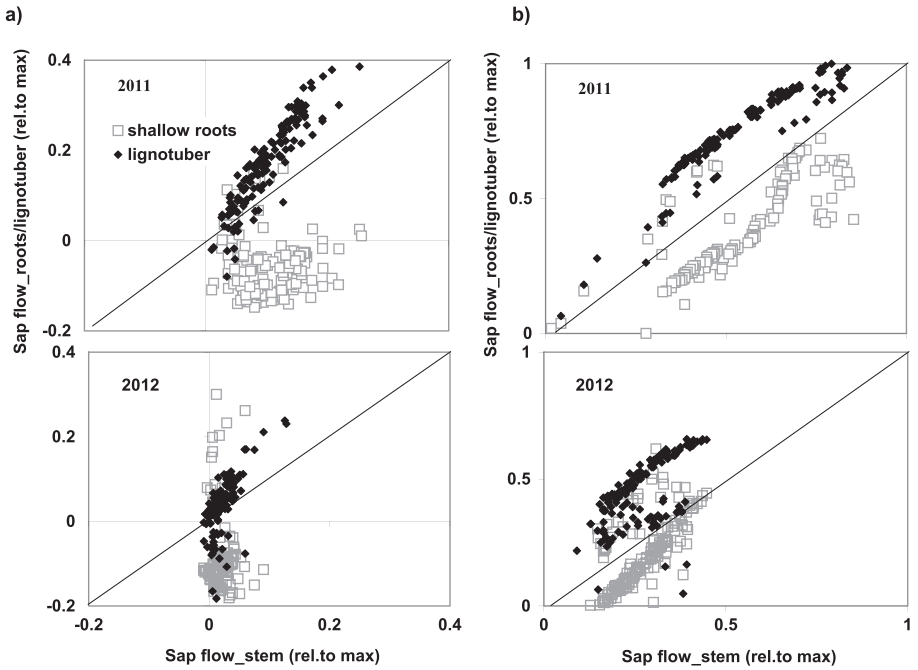

Figure 6. Relationships between normalized minimum (left) and maximum (right) sap flow in roots, lignotuber and stem of the studied olive tree. Sap flow in the lignotuber represents sap flow in deep roots. Data refer to June to November periods, i.e. mostly dry periods and subsequent rewetting.

the observation period, only 2012 was 'critical' in relation to soil water availability (from DOY 228 to DOY 302, *ca* 3 months, soil moisture in the whole profile was lower than 22 $m^3 m^{-3}$). During 2010 and 2011, soil moisture only approached the 'critical' value at the end of the dry season.

The relationships between root sap flow and soil moisture per soil layer and root type evidenced in Figure 3b corroborate those from Figure 3a: reverse flows occurred when the soil around the corresponding root dries. In shallow roots, reverse flows occurred gradually when shallow soil (0–60 cm) dried below about 29 $m^3 m^{-3}$ (grey arrow pointing down in Figure 3b), indicating the occurrence of hydraulic lift. In medium roots, reverse flows occurred gradually, when medium soil dried below about 25 $m^3 m^{-3}$ (dashed arrow pointing down in Figure 3b) indicating hydraulic lift from deeper soil, or abruptly (grey dashed horizontal arrow in Figure 3b) indicating hydraulic descent from shallow roots after rain. Thus, reverse flows in shallow roots indicate shallow soil drying, whereas in medium roots, they may also indicate soil watering. In any case, reverse flows can be used as indicators of stress in the soil layers occupied by observed roots. This is an important feature for irrigation control and arboriculture (particularly in large trees) identifying the root sectors that are subject to effective irrigation. The much lower magnitude of reverse flows in medium than in shallow roots may be ascribed to the smaller water potential gradients between deep and medium soil than between deep and shallow soil (during the dry period, soil moisture is the lowest in the shallow soil). After rain, reverse flows in shallow roots abruptly change to positive depending on rain intensity and importance of soil drying (horizontal grey arrow in Figure 3b indicates the fast reaction of root sap flow compared with soil moisture changes). The fast increase in root sap flow in the upper layers (0–60 cm) after rain in relation to soil moisture could be due to the role of soil cracks and fast uptake and redistribution of water by roots (Figures 2 and 3) and to the delayed change in soil moisture, till the entire root system and the tree aboveground become replenished. Further research is needed to confirm this finding (probably monitoring soil moisture at shorter intervals than 2 weeks as we did in our study). This behaviour was not observed in medium roots because of the process of re-watering in this particular soil: the medium soil was wetted more gradually; therefore, no abrupt changes in the water potential gradient driving sap flow were observed (dashed arrow pointing up in Figure 3b). These 'drying-watering' cycles observed in night sap flow from shallow and medium roots were repeated seasonally and were completely irreversible in shallow roots.

Transpiration closely followed the AWU suggesting a good representativeness of the selected root types (Figure 5a). Both AWU and Tr were directly correlated with ETo in 2010 and 2011, although Tr decreased with increasing ETo at the end of the dry periods (possibly meaning moderate water stress). The proportionality between Tr and ETo was not observed during the very dry 2012, as soil moisture was then the prevailing limiting factor (Leitgeb *et al.*, 2002). Because of the water stress, the maximum stem sap flow (a surrogate of maximum actual transpiration) never corresponded to the

maximum ETo, especially in 2012. On the other hand, rather high values of Tr and AWU were observed under lower evaporative demands (values up to 30% of maximum ETo) after rainy periods following dry periods. These high flows occurred in response to the evaporative demand and also because of the refilling of the aboveground part of the tree depleted by drought. Thus, the limitation of Tr under high ETo and the refilling of the tree storage under lower ETo are responsible for the deviation from direct linearity in the slope of the relationship between Tr and ETo. The change in proportionality between Tr and ETo also indirectly stresses the role of stomatal control for tree survival.

The relationship between normalized daily ETo and root WU shows two opposite branches (Figure 5c) indicating the periodical restriction of WU in different soil horizons. When the rhizosphere was homogeneously wet (wet branch), the WU was usually higher in shallow than in medium roots because of the lower resistance to uptake water from shallow soil, as observed by Bleby *et al*. (2010). In the dry period (dry, lower branch), shallow root sap flow was lower, indicating the prevailing WU from the wetter medium soil. In 2012, the WU by medium roots was the lowest in the majority of days or approached that by shallow roots in the dry period. In this year, soil water availability in medium soil was low and close to that of shallow soil (Figure 2a). In 2012, the lignotuber was mostly supported by the deepest roots and shallow roots receiving occasional small rains. On the basis of this finding, we can assume a stronger proportionality in the relationship between lignotuber and deep roots (not reachable in this study) because (1) deep roots are not subject to soil dryness as shallow roots and (2) water available for deep roots should also be available for lignotuber. However, the input of deep roots to average WU is often expected to be small because of their usually low root volume (Canadell *et al*., 1996), as observed in dimorphic root systems, and/or because of possible higher soil-to-root resistance in deep soil (Markewitz *et al*., 2010). Whatever the situation, the role of deep roots is crucial for tree survival (Bleby *et al*., 2010).

In the dry season in 2010 and 2011, the high positive flows in the lignotuber (Figures 2d and 3a) showed that only deep roots uptake water for night transpiration and stem refilling (Figure 2e) and for hydraulic lift to shallow roots (Figure 2b) as water lacks in shallow or medium soil (visible through reverse flows or flows close to zero in shallow and medium roots, respectively). However, in the critically dry year (2012), deep water was also limited as evidenced by the decrease of sap flow in the lignotuber and stem in the second part of the dry period in 2012. The lignotuber seems to behave as a buffering mixer. Because of its position in linking different root types, it controls soil moisture availability in the whole rhizosphere, up-taking water from the whole bulk of the soil through different root types, storing water temporarily (it could be a small fraction of daily use but ecologically important), and distributing it to the tree crown for transpiration or to soil layers (from wet to dry) during the night (Figure 3) provided that water is available at least in part of the rhizosphere. The lignotuber transports water almost equally in all xylem layers (as it measured till 1·5 cm below bark) in contrast to the stem, where sap flow is much higher in the outer xylem for the same depth below bark (Ferreira *et al*., 2013). The sap flow profiles in the lignotuber support the hypothesis that it acts as an important water storage organ although possibly representing a small fraction of daily water use.

The described processes generally confirm our simplified conceptual model of WU and HR by different root types connected to stem through the lignotuber (Figure 4), although the last case (Figure 4c, during the night) is based on few observations and should be confirmed by further research with larger sampling. This model based on long-term sap flow measurements expresses the ability to observe, via sap flow in roots, the redistribution of water according to its seasonal availability. Figure 5c confirms through shallow root behaviour that the dry soil provides less water during day time (see decrease of maximum WU by shallow roots during the dry period, whereas sap flow in medium roots is higher in deeper and wetter soil). Moreover, at nights, the roots in the dryer soil receive water (see negative night sap flows in shallow roots in Figures 2, 3, 6 during the dry period) whereas the wet soil provides more water during the day and also during the night. In this sense, there is a kind of homogenizing effect of soil moisture by roots. The magnitude of reverse flows gradually increased in the first part of the dry periods, when the water potentials between shallow and medium soil (driving forces for HR) increased, due to the prevailing process of increasing heterogeneity in the soil. The further decrease in the magnitude of reverse flows was due to the following gradual decrease in the gradient of water potentials between soil layers in the second part of the dry periods, indicating the gradual drying of deeper soil layers.

CONCLUSIONS

Our results show that HR within the rhizosphere has a relevant role in buffering the seasonal and long-term water deficits, influencing soil water dynamics during the growing season. Soil drying decreases the WU by roots and stops WU during the night from drier layers, which may even become receptors of soil moisture through HR. WU increases with soil wetting, with water being up taken even during the night by HR (soil moisture providers). Thus, after soil dryness is installed in the upper layers, the differences in soil moisture between wet and dry soil decrease fast because of tree roots.

Soil heterogeneity also occurred after autumn rains following drought when the dry shallow soil became

abruptly wet within hours and WU from wet shallow soil exceeded Tr. In such cases, root WU from wet shallow soil also contribute to refilling of aboveground organs (added to Tr). This contributes to faster soil moisture homogenizing (shallow soil dries faster because of that).

Sap flow in roots reflects the water availability in the whole soil. Local soil moisture conditions are integrated in root responses and show soil moisture availability in the rhizosphere and its influence in tree water status. Night flow rates are of special importance because of their opposite flow signal according to soil water availability. Reverse night flows in roots give simple and precise signals about soil water depletion and its location.

From a methodological perspective, it was shown that when sap flow sensors are installed below the insertion of shallow root in the lignotuber, the latter is a convenient place to analyse the availability of water from deeper soil sources for the tree. It is especially important for cases when deeper roots or soil layers are difficult to access for sap flow or soil moisture measurements. Care should be taken on extrapolation of results derived from only one tree, although the long period of observations provided a large repetition in time. Furthermore, the emphasis of this analysis was put in dynamics.

Finally, the extremely dry 2012 represented a unique possibility to foresee the impact of climate change on tree hydraulic functioning. It suggests that even in deep-rooted trees the lignotuber is an important organ for adaptation to seasonal drought, although its buffering capacity may be limited under high soil water depletion (intense and prolonged dry periods).

ACKNOWLEDGEMENTS

This research was funded by the Portuguese Foundation for Science and Technology – Project PTDC/AAC-AMB/100635/2008 (WUSSIAAME) and fellowship to Nuno Conceição (SFRH/BD/66967/2009). Thanks are due to Luca Tezza and Luís Miguel Boteta for participation in collection of soil water status. Thanks are also due to Manuel Duarte, for the facilities provided at his orchard (Monte do Outeirinho). The work of the first author was partially supported by the Czech projects OPVK-CZ.1.07/2.3.00/20.0267 and IGA-LDF-73/2013. The authors also thank Andrew j. Guswa and another anonymous reviewer for their constructive valuable comments and suggestions, which helped to improve this paper.

REFERENCES

Allen RG, Pereira LS, Raes D, Smith M. 1998. Crop evapotranspiration: guidelines for computing crop water requirements. *FAO Irrigation and Drainage* Paper 56. FAO, Rome.

Bleby TM, McElrone AJ, Jackson RB. 2010. Water uptake and hydraulic redistribution across large woody root systems to 20 m depth. *Plant, Cell and Environment* **33**: 2132–2148.

Breazeale JF, Crider FJ. 1934. Plant association and survival, and the build-up of moisture in semi-arid soils. *Arizona Agricultural Experimental Station Technical Bulletin* **53**: 95–123.

Brooks JR, Meinzer FC, Coulombe R, Gregg J. 2002. Hydraulic redistribution of soil water during summer drought in two contrasting Pacific Northwest coniferous forests. *Tree Phisiology* **22**: 1107–1117.

Burgess SSO. 2011. Can hydraulic redistribution put bread on our table? *Plant and Soil* **341**: 25–29.

Burgess SSO, Adams MA, Turner NC, Ong CK. 1998. The redistribution of soil water by tree root systems. *Oecologia* **115**: 306–311.

Burgess SSO, Adams MA, Turner NC, White DA, Ong CK. 2001. Tree roots: conduits for deep recharge of soil water. *Oecologia* **126**: 158–165.

Caldwell MM, Richards JH. 1989. Hydraulic lift: water efflux from upper roots improves effectiveness of water uptake by deep roots. *Oecologia* **79**: 1–5.

Caldwell MM, Dawson TE, Richards JH. 1998. Consequences of water efflux from the roots of plants. *Oecologia* **113**: 151–61.

Canadell J, Jackson RB, Ehleringer JR, Mooney HA, Sala OE, Schulze ED. 1996. Maximum rooting depth of vegetation types at the global scale. *Oecologia* **108**: 583–595.

David TS, Henriques MO, Besson CK, Nunes J, Valente F, Vaz M, Pereira JS, Siegwolf R, Chaves MM, Gazarini LC, David JS. 2007. Water use strategies in two co-occurring Mediterranean evergreen oaks: surviving the summer drought. *Tree Physiology* **27**: 793–803.

David TS, Pinto C, Nadezhdina N, Cermak J, David J. 2013. Root functioning, tree water use and hydraulic redistribution in Quercus suber trees: a modeling approach based on root sap flow. *Forest Ecology and Management* **307**: 136–146.

Dawson TE. 1993. Hydraulic lift and the water use by plants: implications for water balance, performance and plant–plant interactions. *Oecologia* **95**: 565–574.

James S. 1984. Lignotubers and burls-their structure, function and ecological significance in Mediterranean ecosystems. *Botanical Reviews* **50**: 225–266.

Ferreira MI, Pacheco CA, Valancogne C, Michaelsen J, Ameglio T, Daudet FA. 1997. Evapotranspiration, water stress indicators and soil water balance in a Prunus persica orchard, in central Portugal. *Acta Horticulturae* **449**: 379–384.

Ferreira MI, Conceição N, David TS, Nadezhdina N. 2013. Role of lignotuber versus roots in the water supply of rainfed olive. *Acta Horticulturae* **991**: 181–188.

Fernandez JE, Palomo MJ, Díaz-Espejo A, Clothier BE, Green SR, Giron IF, Moreno F. 2001. Heat-pulse measurements of sap flow in olives for automating irrigation: tests, root flow and diagnostics of water stress. *Agricultural Water Management* **51**: 99–123.

Fernandez JE, Diaz-Espejo A, Infante JM, Duran P, Palomo MJ, Chamorro V, Giron IF, Villagarcia L. 2006. Water relations and gas exchange in olive trees under regulated deficit irrigation and partial rootzone drying. *Plant and Soil* **284**: 273–291.

Fernandez JE, Cuevas MV. 2010. Irrigation scheduling from stem diameter variations:a review. *Agricultural and Forest Meteorology* **150**: 135–151.

Gabarron-Galeote MA, Ruiz-Sinoga JD, Quesada MA. 2013. Influence of aspect in soil and vegetation water dynamics in dry Mediterranean conditions: functional adjustment of evergreen and semi-deciduous growth forms. *Ecohydrology* **6**: 241–255.

Guswa AJ. 2012. Canopy vs. roots: production and destruction of variability in soil moisture and hydrologic fluxes. *Vadose Zone Journal* **11**. DOI: 10.2136/vzj2011.0159

Hultine KR, Williams DG, Burgess SSO, Keefer TO. 2003. Contrasting patterns of hydraulic redistribution in three desert phreatophytes. *Oecologia* **135**: 167–175.

Ivanov VY, Fatichi S, Jenerette GD, Espeleta JF, Troch PA, Huxman TE. 2010. Hysteresis of soil moisture spatial heterogeneity and the 'homogenizing' effect of vegetation. *Water Resources Research* **46**: W09521. DOI: 10.1029/2009WR008611

Karray JA, Lhomme JP, Masmoudi MM, Ben Mechlia N. 2008. Water balance of the olive tree–annual crop association: a modeling approach. *Agricultural Water Management* **95**: 575–586.

Kurz-Besson C, Otieno D, do Vale RL, Siegwolf R, Schmidt M, Herd A, Nogueira C, David TS, David JS, Tenhunen J, Pereira JS, Chaves M. 2006. Hydraulic lift in cork oak trees in a savannah-type Mediterranean

ecosystem and its contribution to the local water balance. *Plant and Soil* **282**: 361–378.

Leitgeb E, Gartner K, Nadezhdina N, Englisch M, Cermak J. 2002. Ecological effects of pioneer species on soil moisture regime in an early successional stage, following wind-throw in a Spruce stand. In *Proceedings of the IUFRO Conference on Restoration of Boreal and Temperate Forests*, Gardiner ES, Breland LJ (eds). Vejle: Denmark; 193–194.

Lubczynski MW, Gurwin J. 2005. Integration of various data sources for transient groundwater modeling with spatio-temporally variable fluxes – Sardon study case. Spain. *Journal of Hydrology* **306**: 71–96.

Maeght JL, Rewald B, Pierret A. 2013. How to study deep roots – and why it matters. *Frontiers in Plant Science* **4**: Article Number 299.

Markewitz D, Devine S, Davidson EA, Brando P, Nepstad DC. 2010. Soil moisture depletion under simulated drought in the Amazon: impacts on deep root uptake. *New Phytologist* **187**: 592–607.

McElrone AJ, Bichler J, Pockman WT, Addington RN, Linder CR, Jackson RB. 2007. Aquaporin-mediated changes in hydraulic conductivity of deep tree roots accessed via caves. *Plant, Cell and Environment* **30**: 1411–1421.

Miller GR, Chen X, Rubin Y, Ma S, Baldocchi DD. 2010. Groundwater uptake by woody vegetation in a semiarid oak savanna. *Water Resources Research* **46**: W10503.

Miller GR, Cable GM, McDonald AK, Bond B, Franz TE, Wang L, Gou S, Tyler AP, Zou CB, Scott RL. 2012. Understanding ecohydrological connectivity in savannas: a system dynamics modelling approach. *Ecohydrology* **5**: 200–220.

Moriana A, Orgaz F, Pastor M, Fereres E. 2003. Yield responses of a mature olive orchard to water deficit. *Journal of the American Society for Horticultural Science* **128**: 425–431.

Nadezhdina N, Cermak J, Nadezhdin V. 1998. Heat field deformation method for sap flow measurements. In *Measuring Sap Flow in Intact Plants*, Čermak J, Nadezhdina N (eds). Proc. 4th. Int. Workshop, Zidlochovice, Czech Republic, IUFRO Publications: Brno, 72–92.

Nadezhdina N, Čermak J, Gasparek J, Nadezhdin V, Prax A. 2006. Vertical and horizontal water redistribution within Norway spruce (*Picea abies*) roots in the Moravian Upland. *Tree Physiology* **26**: 1277–1288.

Nadezhdina N, Ferreira MI, Silva R, Pacheco CA. 2008. Seasonal variation of water uptake of a *Quercus suber* tree in Central Portugal. *Plant and Soil* **305**: 105–119.

Nadezhdina N, Steppe K, De Pauw DJW, Bequet R, Cermak J, Ceulemans R. 2009. Stem-mediated hydraulic redistribution in large roots on opposing sides of a Douglas-fir tree following localized irrigation. *New Phytologist* **184**: 932–943.

Nadezhdina N, David TS, David JS, Ferreira MI, Dohnal M, Tesar M, Gartner K, Leitgeb E, Nadezhdin V, Cermak J, Jimenez MS, Morales D. 2010. Trees never rest: the multiple facets of hydraulic redistribution. *Ecohydrology* **3**: 431–444.

Oliveira RS, Dawson TE, Burgess SSO, Nepstad DC. 2005. Hydraulic redistribution in three Amazonian trees. *Oecologia* **145**: 354–363.

Perez-Martin A, Michelazzo C, Torres-Ruiz JM, Flexas J, Fernández JE, Sebastiani L, Diaz-Espejo A. 2014. Regulation of photosynthesis and stomatal and mesophyll conductance under water stress and recovery in olive trees: correlation with gene expression of carbonic anhydrase and aquaporins. *Journal of Experimental Botany* **65**: 3143–56. DOI: 10.1093/jxb/eru160

Prieto I, Armas C, Pugnaire FI. 2012. Water release through plant roots: new insights into its consequences at the plant and ecosystem level. *New Phytologist* **193**: 830–841.

Richards JH, Caldwell MM. 1987. Hydraulic lift – substantial nocturnal water transport between soil layers by Artemisia tridentata roots. *Oecologia* **73**: 486–9.

Santos FL, Valverdea PC, Ramos AF, Reis JL, Castanheira NL. 2007. Water use and response of a dry-farmed olive orchard recently converted to irrigation. *Biosystems Engineering* **98**: 102–114.

Schenk HJ, Jackson RB. 2002. The global biogeography of roots. *Ecological Monographs* **72**: 311–328.

Ryel RJ. 2004. Hydraulic redistribution. In *Progress in Botany*, Esser K, Luttge U, Beyschlag W, Murata J (eds). Springer Verlag: New York, NY, USA, Berlin,Heidelberg; 413–435.

Wang G, Alo C, Mei R, Sun S. 2011. Droughts, hydraulic redistribution, and their impact on vegetation composition in the Amazon forest. *Plant Ecology* **212**: 663–673.

6.4 Conceição et al. (2017a)

Conceição N., Häusler M., Lourenço S., Pacheco C.A., Tezza L., Ferreira M.I. 2017. Evapotranspiration measured in a traditional rainfed and an irrigated intensive olive orchard during a year of hydrological drought. Acta Horticulturae 1150:281–288.

Evapotranspiration measured in a traditional rainfed and an irrigated intensive olive orchard during a year of hydrological drought

N. Conceição[1,a], M. Häusler[1], S. Lourenço[1], C. Pacheco[1], L. Tezza[2] and M.I. Ferreira[1]

[1]Department Biosystems Engineering and LEAF at Instituto Superior de Agronomia, University of Lisbon (ULisboa), Portugal; [2]Department of Agronomy, Food, Natural Resource, University of Padova, Padova, Italy.

Abstract

Quantifying water use in ecosystems is important for irrigation and for planning of related infrastructures but also for the management of rainfed ecosystems, either natural or agricultural. Understanding how plants cope with highly variable available water in soil, as a function of inter- and intra-annual precipitation variability provides an insight on how to manage deficit irrigation. An experiment was performed from 2011 to 2013 on two olive orchards, one rainfed and another drip irrigated (*Olea europaea* 'Cobrançosa' and 'Arbequina', respectively) few km away from each other, in South Portugal, with the aim of understanding survival strategies and providing parameters for irrigation planning and scheduling. In the frame of this general study, sap flow was measured in stems and roots. The hydrological year 2011/2012, classified as dry to extremely dry, in almost all regions of Portugal, being the driest winter since 1931, provided a special opportunity to observe water stress impacts in the rainfed orchard. Different biometric and water status variables, namely leaf water potential at pre-dawn (PLWP) and soil moisture (0 to 1.3 m, with a neutron probe) were monitored. Between May and July 2012, direct measurements of actual evapotranspiration (ETa) using the eddy covariance micrometeorological method, were performed at the rainfed orchard. The latent (LE) and sensible (H) heat fluxes data were selected according to the footprint analysis (Schuepp et al., 1990) and to the energy balance closure error. Between July 2 and 10, average ETa was 1.5 mm day^{-1}. For a period of two months of LE and H measurements (May 15-July 15), PLWP decreased from -0.4 to -1.1 MPa. During the same period, the ratio H/LE increased from near one to three, while the relationship between ETa and reference evapotranspiration decreased from around 0.5 to 0.2. The decrease in available water in the observed soil layers was strong until mid-July, and decreased slowly until the total depletion that occurred in mid-September (before the first rains). These values are compared with those found for the irrigated orchard, as a reference. On the other side, they are interpreted using the outcomes from the parallel study of sap flow in roots.

Keywords: *Olea europaea*, evapotranspiration, water use, drought, survival strategies

INTRODUCTION

Even though olive trees have been cultivated since the ancient world (Zohary and Spiegel-Roy, 1975; Terral et al., 2004), there are still unanswered questions concerning the mechanism of the soil water use under stress conditions, as well as the functioning and importance of the root system in relation to transpiration (Ferreira et al., 2012, 2013). The remarkable ability of olive trees to tolerate water stress effects (Gucci and Barone, 2003) enables the trees to grow and get acceptable commercial production under rainfed conditions in areas where the annual rainfall is as low as 500 mm, and where the dry season can last 5-6 months (Fernández and Moreno, 1999).

The values of soil water content for which olive trees are able to maintain

[a]E-mail: nuconceicao@isa.ulisboa.pt

transpiration (Tr) were found to be significantly below the ones found in many fruit crops (Xiloyannis et al., 1999). These researchers presented outdoor experimental data of 5 years with two-year-old olive trees in small containers (18 L), in the south of Italy. To quantify the water stress intensity they used predawn leaf water potential (PLWP). Data analysis of stomatal conductance, Tr, photosynthetic rate and leaf CO_2 internal concentration as a function of PLWP suggested that the stomata progressively reduced the stomatal opening when PLWP values decreased from -0.9 MPa and closed at values lower than -7.0 MPa.

Santos et al. (2007) measured Tr (heat pulse compensation method) in 80-year-old olive trees with an irrigation system recently installed, during a dry year (precipitation about one third of the 30 years average, which was 580 mm) and observed that, for a period (51 days) around summer solstice without irrigation, Tr was reduced reaching 50 L day^{-1} and $tree^{-1}$, which was about 4-7% of reference evapotranspiration (ETo), while the estimated soil water balance indicated that all soil available water had been exhausted for the layer 0-0.65 m. Nothing was mentioned about the ability of the roots to exploit the deeper soil layers, namely in soils derived from schist with fissures filled with soil material between rupture plans of the weathering rock.

The water redistribution by the root system in olive trees was firstly analysed in a 3-year field study, including the 2012 drought, using two independent methods to measure reversible sap flow in roots (Ferreira et al., 2012, 2013). The circadian dynamics of flow in the roots at the rainfed olive orchard, either positive or negative at superficial roots, was related with a possible pattern of ground water use in different layers and emphasized the role of lower soil layers in providing water to Tr. These results will be useful to analyse the consequences of extreme water stress and some of the survival mechanisms of this species.

The general objective of this study was to characterize and compare the water use at a rainfed and at a deficit irrigated olive orchard, in a region with high natural water scarcity during summer (Alentejo, Portugal), by quantifying water status, evapotranspiration (ET) and its components and root sap flow dynamics, over three consecutive years (May 2010 to early November 2013). We report the water use during the extreme water scarcity conditions which we found during a particular drought, by lack of rain not only in summer, as usually, but also in winter. The hydrological year 2011/12 was classified, from a meteorological point of view, as extremely dry, corresponding to the driest winter since 1931, over the entire territory of Portugal (IPMA, 2013). The data reported were collected between May and October 2012, with additional information from other time periods.

MATERIALS AND METHODS

The experimental work took place at two commercial olive orchards (about 7 km away from each other), one traditional rainfed and another drip (deficit) irrigated. Both farms are located in the Alentejo region of Portugal, close to the town of Ferreira do Alentejo (160 km southeast of Lisbon) and 30 km west of the city of Beja. The climate is Csa (Köppen classification), temperate of Mediterranean type, with very hot and dry summers and mild and wet winters. In Beja, the annual rainfall is 572 mm (1971-2000, www.ipma.pt) and for December, January, February and March to May, 101, 74, 62 and 152 mm, respectively. The highest ever observed values for maximum temperature were 36.6, 43.3 and 45.2°C for May, June and July, respectively.

ETo was calculated from meteorological variables using the Penman-Monteith equation with the reference crop parameters (grass with 0.12 m in height, surface resistance of 70 m s^{-1}, albedo of 0.23) as described in Allen et al. (1998). The data from the weather station Herdade do Outeiro (38°20.7'N; 08°15.08'W, 74 m a.s.l., Datum 73) operated by COTR (Centro Operativo e de Tecnologia do Regadio, www.cotr.pt) were used.

At the traditional rainfed olive orchard (10 ha, farm Monte do Outeirinho, 38°0.95'N; 8°6.58'W, 150 m a.s.l., Datum WGS84), the trees (*Olea europaea* 'Cobrançosa') were planted in 1990, in squares of 7.0 m (204 tree ha^{-1}). The ground cover (spontaneous herbaceous vegetation) management was done mechanically on the middle row and chemically on the tree rows. The slope is between 3 and 7%. In 2010, the height of the trees was 4.15 m, the canopy projection area was 18.0 m^2 and the leaf area index on a total area basis (LAI_T, 49.0

m^2 soil $tree^{-1}$) was 1.05 m^2 m^{-2}.

The soil is a calcic Vertisol (FAO-UNESCO, 2006) with a very deep profile (type ApBtCk), derived from volcanic gabbro-diorite rock. The Ck horizon is very rich in secondary calcium carbonate, has loam texture with some swelling clays and is very dense (bulk density is about 1.8-1.9 Mg m^{-3}). The *solum* (Ap and Bt horizons), reaching to 0.4-0.7 m, has a clayey texture with swelling clays (wide and deep cracking) and a water content for field capacity (FC) and permanent wilting point (PWP) of approximately 0.36 and 0.19 m^3 m^{-3}, respectively, from observations in situ during 2010 to 2012. To characterize the soil water status, the water content was determined using neutron probes (model 4301, Troxler Electronic, USA), from the soil surface to a depth of 1.30 m in steps of 0.20 m, every two weeks (during spring and summer). The results reported concern twelve tubes installed in the tree rows at a distance of 1.2, 2.4 and 3.6 m away from the trees (four tubes in each position).

PLWP was measured to characterize the water status of the trees, by using a Scholander type pressure chamber on a variable number of healthy and fully expanded leaves (20 on average).

In 2012, some rainfall during spring (104 mm), together with the favourable conditions of temperature and radiation, allowed the rapid growth and development of ground cover. The senescence of the herbaceous understory occurred relatively quickly at around the last half of May to early June, and was cut in mid-June. Therefore, the contribution of the transpiration from the herbaceous plants to ET was negligible after mid-June. The first autumn rains began on September 23, day of the year (DOY) 267.

To measure actual evapotranspiration (ETa or correspondent latent heat flux, LE) the eddy covariance micrometeorological (EC) method, considered the reference to measure ET (Kustas, 1990), was used. To measure LE and the sensible heat flux (H), a sonic anemometer and a krypton hygrometer (respectively CSAT 3-D and KH20, Campbell Scientific, USA) were mounted on a metallic tower at 5.75 m above soil and oriented into the dominant wind direction. The measurements and the raw data storage were done at 10 Hz by a data logger (CR1000, Campbell Scientific, USA). The raw data (convective fluxes) were processed using the TK3 software (Mauder and Foken, 2011), calculating the average fluxes for 30 min intervals. The corrections for the air density variation (Webb et al., 1980) and for the oxygen absorption (Tanner et al., 1993) were performed. In addition to LE and H, by the EC method, the soil heat flux (G) and the net radiation (Rn) were measured to verify the closure error of the surface energy balance (SEB) equation (LE+H=Rn-G): Rn with a net radiometer (NR2, Kipp & Zonen, The Netherlands) and to obtain G, three flux plates with known thermal conductivity were installed at 0.05 m depth, perpendicular to the flow direction, the heat stored in the soil layer 0-0.05 m, being calculated from soil temperature measured with copper-constantan thermocouples installed at 0.025 m depth. Measurements (1/30 Hz), were averaged (10 min), stored (CR10X, Campbell Scientific, USA) and combined to get G.

A footprint analysis, according to the methodology described in Schuepp et al. (1990), allowed the evaluation of the relative contribution of fluxes coming from different areas within the plot to the total measured flux: more than 85% of the measured LE came from an upwind area less than 160 m away from the measurements point. LE and H fluxes were selected according to the footprint analysis (besides other restrictions) and only the fluxes from wind directions with fetch above 160 m were considered.

ETa was measured from mid-May to mid-July 2012 at the rainfed orchard, as the equipment was then moved to the irrigated orchard, for subsequent measurements from mid-July until mid-October (at 4.5 m above the soil surface).

At the irrigated orchard (10 ha, on a continuous area of 434 ha, farm Monte do Pardieiro, 38°1.34'N; 8°10.84'W, 97 m a.s.l.), the trees were planted in 2004 ('Arbequina'), with distances of 4.8 by 7.0 m (298 tree ha^{-1}). In 2010, the height of the trees was 3.2 m, the canopy projection area was 5.7 m^2 and LAI_T was 1.01 m^2 m^{-2}. The soil was classified as Arenic Luvisol Ferric (FAO-UNESCO, 2006). The farmer daily irrigated, from late spring to late summer, using a line of drippers (nominal flow of 1.6 L h^{-1}), spaced 0.75 m. The experimental design and the ground cover management were similar to the one described

for the rainfed orchard.

RESULTS AND DISCUSSION

The 2011/2012 hydrological year had very low precipitation (350 mm), especially January and February with 21 mm and 1 mm (Figure 1).

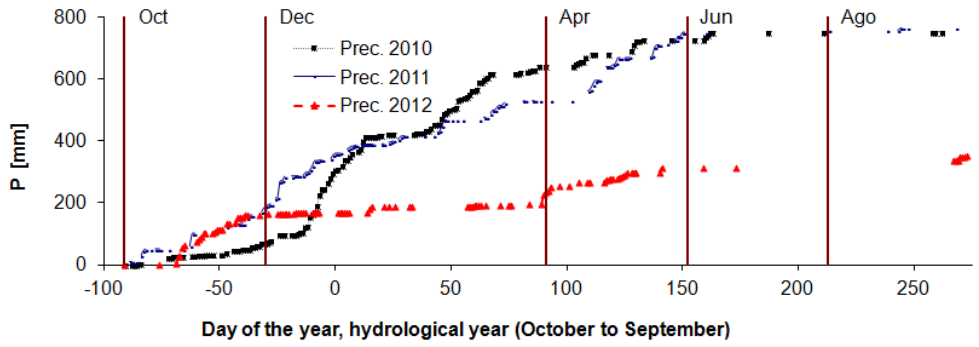

Figure 1. Cumulative rainfall over the hydrological years 2010 to 2012, at Ferreira do Alentejo.

For the rainfed orchard, contrary to the usual and expected situation, the precipitation until the end of spring was insufficient to bring the soil water to FC throughout the observed soil profile (0 to 1.3 m), where this condition was only roughly verified in the upper layers between 0 and 0.5 m (Figure 2); not autumn rains but only the spring rainfalls have increased the soil humidity in the layers between 0.7 m and 1.3 m, but without reaching the deeper soil layers. Since July 2012, the soil water content remained nearly constant down to 1.3 m (very close to the PWP) and with no conditions for significant capillary rise; it is possible to assume that the root system explores at depths below 1.3 m.

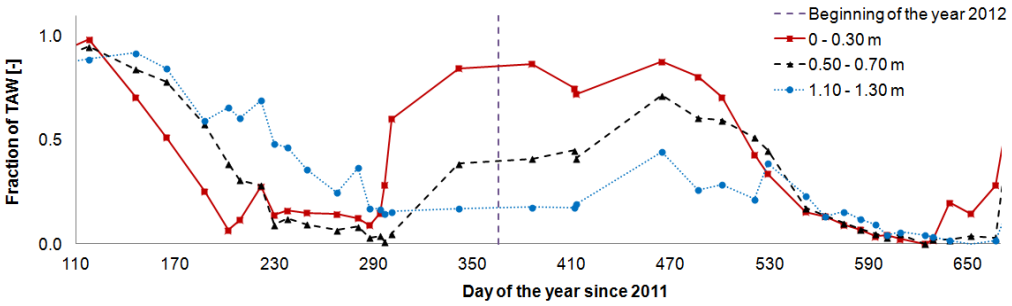

Figure 2. Seasonal evolution of TAW fraction, from late April 2011 to October 2012 based on soil humidity measurements at 1.2 m from the tree, at specified soil layers.

However, almost all the root biomass and the higher root concentration of all diameters were observed until 0.6 m, and only few medium, fine and very fine roots reached 2.5 m depth, using cracks and other discontinuities in the lithological material (unpublished data).

In order to understand the water use in relation with the water availability in upper soil layers, the seasonal course of the atmospheric fluxes (H and LE or ETa) and PLWP are discussed in the following.

For a normal hydrological year as 2011, at the rainfed orchard, PLWP in late May was -0.2 MPa (DOY 143), decreased to about -0.9 MPa until mid-July (DOY 195), reaching the minimum of -2.2 MPa in late October (before first autumn rains) while, at the irrigated orchard, PLWP was -0.1 MPa for late May (DOY 146), being more or less stable (-0.5 MPa) from DOY 210 to DOY 232 (mid July), reaching the minimum of -1.0 MPa for late October.

During 2012, for mid-May (DOY 135) PLWP was -0.4 MPa for both orchards (Figure 3) and decreased until mid-September, when the minimum were observed, -3.0 MPa and -1.0 MPa for rainfed and irrigated orchards, respectively (just before first autumn rains). On the irrigated orchard, the total irrigation for the season (2012) necessary to maintain such water status was 226 mm, distributed by 132 watering days (more 29 days than 2011), on average 1.7 mm day^{-1}.

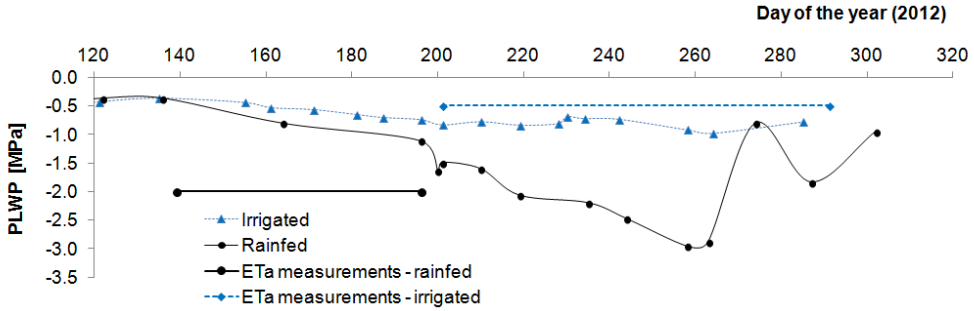

Figure 3. Predawn leaf water potential seasonal evolution from spring to autumn 2012 (rainfed and irrigated orchards).

This PLWP inter-annual variation at the rainfed orchard reflected the increased difficulties of water uptake by the trees during summer 2012. The results (Figure 3) also show a fast increase in PLWP, as a response to the first autumn rains (about 35 mm).

At the rainfed orchard, because Ap and Bt horizons are rich in swelling clays, with the first moderate to strong autumn rains, the water first fills the cracks and then slowly wets the surrounding soil volume. This mechanism favours a rapid response of the trees (which resulted in a rapid PLWP increase), once the trees had a large root concentration between 0.1 and 0.6 m depth.

The SEB equation closure error was better than 10% (for both orchards) which is within the limits frequently found (10 to 30%) with the EC method (Wilson et al., 2002). Considering the low closure error and recent recommendations (Foken et al., 2012), no adjustments were performed to LE and H, to force SEB equation closure.

An example of the available energy (Rn-G) partition between the convective terms LE and H, at the rainfed orchard, is given in Figure 4 (Rn also plotted). Five days after the last spring rain event (mid-May) the Bowen ratio (H/LE) had increased from 1 to 1.5, reaching 3.0 (average) during July. LE decreased consistently with the decrease of TAW and PLWP.

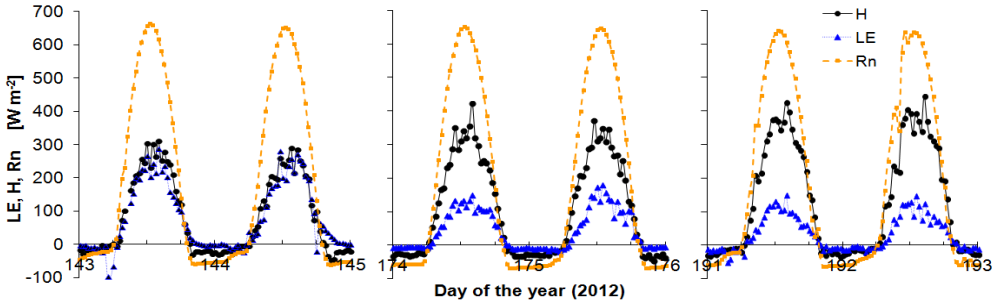

Figure 4. Measured fluxes (30 minutes data) for Rn, H and LE at the rainfed orchard (two selected days in May, June and July).

Considering the daily averages for two time periods, DOY 143 to 147 and DOY 191 to 195, ETo increased from 5.2 mm to 6.6 mm, ETa decreased from 2.8 mm to 1.4 mm (Figure 5) and the Bowen ratio increased from 1 to 3. For the irrigated orchard the daily averages for ETo, ETa and Bowen ratio, from DOY 201 to DOY 228, were 6.0 mm, 2.0 mm and 1.5,

respectively.

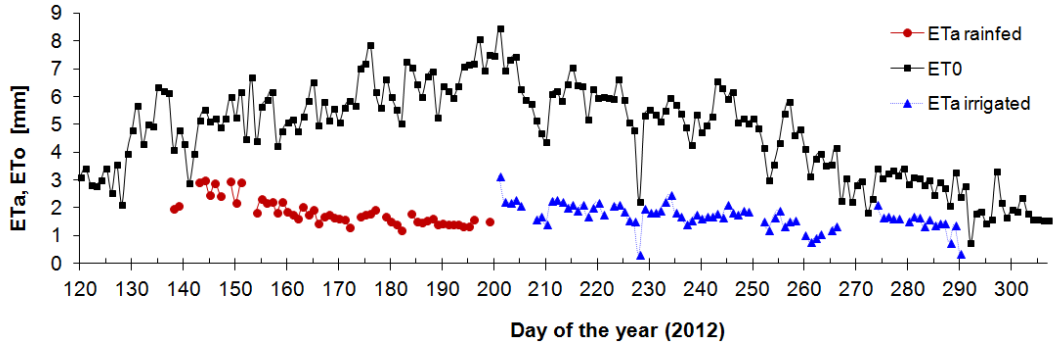

Figure 5. ETo and ETa seasonal evolution (2012) for rainfed and irrigated orchards. Time periods of EC measurements: May 15 to July 15 and July 20 to October 4, for rainfed and irrigated orchards, respectively.

At the rainfed orchard, ETa/ETo (Figure 6) between mid-May and mid-July decreased from 0.5 to 0.2 but it is possible to identify two periods. The first, ending about mid-June, showed a steeper slope, due to the decrease of the orchard Tr and especially the reduction of the ground cover vegetation Tr (senescence). During a second period (mid-June to mid-July), when Tr from the ground cover vegetation is already negligible and the difficulties of the trees to up-take water from the soil increased. At mid-June, the TAW fraction is more or less the same for all the observed soil layers until 1.3 m (about 20%, day 550, Figure 2) and further decreased, corresponding to soil water with high retention energy.

At the irrigated orchard, ETa/ETo (Figure 6) was relatively stable around 0.33 (mid-July to late September) while, for the same period in 2011, it was about 0.5 (data not shown), suggesting that irrigation was not enough to compensate the water lost by ET. In fact, from July 20 on, average ET is above average total irrigation depth. Overall, these results indicate that, during this drought, exploitation of soil layers deeper than those analysed, occurred in both orchards, but with different relative importance.

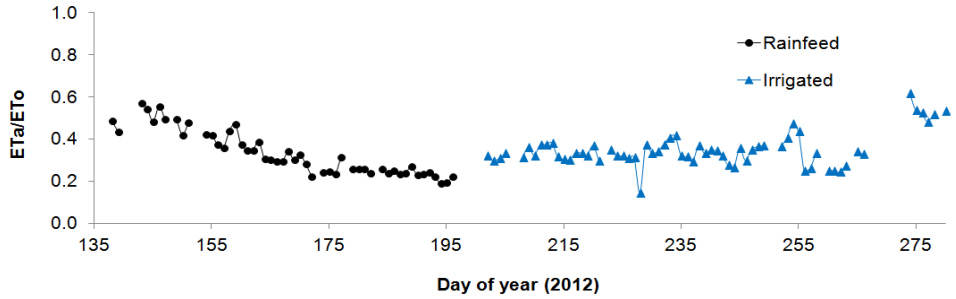

Figure 6. Seasonal evolution (2012) for ETa/ETo, for the rainfed and irrigated orchards.

CONCLUSIONS

The drought in the hydrological year 2011/2012 (driest winter since 1931, over the entire territory of Portugal) prevented TAW (on rainfed orchard) to recover in the observed soil profile (0 to 1.3 m), and of course, prevented the re-wetting of the deeper lithological layers. Only for the layer 0-0.5 m, the FC conditions were observed. The soil water balance method was not applied to depths greater than 1.3 m, but it was possible to observe the presence of fine and very fine roots in soil depths up to 2.5 m.

For the rainfed orchard during the two months of ET measurements (May 15 to July 15), ETa decreased from 3 to 1.5 mm day^{-1} corresponding to an increase in Bowen ratio (H/LE) from 1 to 3. ETa would certainly further decrease until late summer. During this

period, PLWP decreased from -0.4 to -1.1 MPa, and continued to decrease reaching later (mid-September) an extremely low value of -3.0 MPa, just before the first autumn rains. The TAW decrease (0 to 1.3 m) was very strong until mid-July, decreasing slowly afterwards, until total exploitation that occurred in mid-September.

At the irrigated orchard, PLWP decreased from -0.4 MPa (mid spring) to -1.0 MPa (late summer). ETa was relatively stable at about 2 mm, during the measurement time period. The Bowen ratio was 1.5 and ETa/ETo was 0.33, increasing after first autumn rains. The daily irrigation depth (in average 1.71 mm day^{-1}) was less than water consumption (but higher than in 2010 and 2011).

These results, obtained in a not representative hydrological year, gave us the opportunity to show how these olive trees use the soil water in adverse conditions, keeping up Tr and consequently photosynthesis. They are consistent with the ones shown by analysis of water redistribution in roots (Ferreira et al., 2012, 2013), suggesting that the main mechanism of survival is the use of water from deeper than observed soil layers, even at the irrigated plot.

ACKNOWLEDGEMENTS

The authors are very thankful to: the participating graduates and master students (non-automatic measurements) Soroor Amindezfooli, Berta Cumbane, José Miguel Gama, Sonia Surgy and Ondina Miguel; to COTR (www.cotr.pt) for providing meteorological daily statistics and for collaboration with the soil humidity measurements (2010 and 2011); to the owners of the farms Monte do Outeirinho (Mr. Manuel Duarte) and Monte do Pardieiro (Agricola Alentejo, SA.) and to the workers of the farm Monte do Pardieiro (Mr. Pereira and collaborators).

The experiments were co-financed by European Union through the project TELERIEG (SOE1/P2/E082) and by the Portuguese Agency for Science and Technology (FCT) through the project WUSSIAAME (PTDC/AACAMB/100635/2008). FCT also financed the fellowships SFRH/BD/66967/2009 and PD/BD/52698/2014.

Literature cited

Allen, R.G., Pereira, L.S., Raes, D., and Smith, M. (1998). Crop Evapotranspiration Guidelines for Computing Crop Water Requirements. FAO Irrigation and Drainage Paper 56 (Rome, Italy: FAO), pp.300.

FAO-UNESCO. (2006). IUSS Working Group WRB. World Reference Base for Soil Resources 2006. World Soil Resources Reports No. 103 (Rome, Italy: FAO).

Fernández, J.E., and Moreno, F. (1999). Water use by the olive tree. In Water Use in Crop Production, M.B. Kirkham, eds. (Binghamton, New York, USA: Haworth Press), p.101–162.

Ferreira, M.I., Conceição, N., Pacheco, C.A., and Green, S. (2012). O que fazem as oliveiras de noite ou redistribuição hidráulica num olival de sequeiro no Alentejo. Paper presented at: VI Simpósio Nacional de Olivicultura (Mirandela, Portugal).

Ferreira, M.I., Conceição, N., David, T.S., and Nadezhdina, N. (2013). Role of lignotuber versus roots in the water supply of rainfed olives. Acta Hortic. *991*, 181–188 http://dx.doi.org/10.17660/ActaHortic.2013.991.22.

Foken, T., Leuning, R., Oncley, S.R., Mauder, M., and Aubinet, M. (2012). Corrections and data quality control. In Eddy Covariance; a Practical Guide to Measurement and Data Analysis, M. Aubinet, T. Vesala, and D. Papale, eds. (The Netherlands: Springer Atmospheric Sciences, Springer), p.85–131.

Gucci, R., and Barone, E. (2003). Response of olive trees to drought. Paper presented at: La Gestion de la Sècheresse en Oléiculture et en Arboriculture Pluvial (Sousse, Tunisia).

IPMA. (2013). Relatório de Balanço da Seca 2012 (in Portuguese). http://www.portugal.gov.pt/media/916024/Relatorio_Balanco_GTSeca2012_v1.pdf (Accessed February 21, 2014).

Kustas, W.P. (1990). Estimates of evapotranspiration with a one- and two-layer model of heat transfer over partial canopy cover. J. Appl. Meteorol. *29* (*8*), 704–715 http://dx.doi.org/10.1175/1520-0450(1990)029<0704:EOEWAO>2.0.CO;2.

Mauder, M., and Foken, T. (2011). Documentation and Instruction Manual of the Eddy-Covariance Software Package TK3 (Bayreuth University).

Santos, F.L., Valverde, P.C., Ramos, A.F., Reis, J.L., and Castanheira, N.L. (2007). Water use and response of a dry-

farmed olive orchard recently converted to irrigation. Biosystems Eng. *98* (*1*), 102–114 http://dx.doi.org/10.1016/j.biosystemseng.2007.03.027.

Schuepp, P.H., Leclerc, M.Y., MacPherson, J.I., and Desjardins, R.L. (1990). Footprint prediction of scalar fluxes from analytical solutions of the diffusion equation. Boundary-Layer Meteorol. *50* (*1-4*), 355–373 http://dx.doi.org/10.1007/BF00120530.

Tanner, B.D., Swiatek, E., and Greene, J.P. (1993). Density fluctuations and use of the krypton hygrometer in surface flux measurements. Paper presented at: 1993 National Conference on Irrigation and Drainage Engineering (Park City, Utah, USA: Irrigation and Drainage Division, American Society of Civil Engineers).

Terral, J.F., Alonso, N., Buxo-i-Capdevila, R., Chatti, N., Fabre, L., Fiorentino, G., Marinval, P., Jordá, G.P., Pradat, B., Rovira, N., and Alibert, P. (2004). Historical biogeography of olive domestication (*Olea europaea* L.) as revealed by geometrical morphometry applied to biological and archaeological material. J. Biogeogr. *31* (*1*), 63–77 http://dx.doi.org/10.1046/j.0305-0270.2003.01019.x.

Webb, E.K., Pearman, G.I., and Leuning, R. (1980). Correction of flux measurements for density effects due to heat and water vapour transfer. Q. J. R. Meteorol. Soc. *106* (*447*), 85–100 http://dx.doi.org/10.1002/qj.49710644707.

Wilson, K., Goldstein, A., Falge, E., Aubinet, M., Baldocchi, D., Berbigier, P., Bernhofer, C., Ceulemans, R., Dolman, H., Field, C., et al. (2002). Energy balance closure at FLUXNET sites. Agric. For. Meteorol. *113* (*1-4*), 223–243 http://dx.doi.org/10.1016/S0168-1923(02)00109-0.

Xiloyannis, C., Dichio, B., Nuzzo, V., and Celano, G. (1999). Defence strategies of olive against water stress. Acta Hortic. *474*, 423–426 http://dx.doi.org/10.17660/ActaHortic.1999.474.86.

Zohary, D., and Spiegel-Roy, P. (1975). Beginnings of fruit growing in the old world. Science *187* (*4174*), 319–327 http://dx.doi.org/10.1126/science.187.4174.319. PubMed

6.5 Conceição et al. (2017c)

Conceição N., Tezza L., Lourenço S., Häusler M., Boteta L., Pacheco C.A., Ferreira M.I. Importance of very fine roots in deep soil layers for the survival of rainfed olive trees. Acta Horticulturae. Versão revista aceite em 2017. No prelo.

Importance of very fine roots in deep soil layers for the survival of rainfed olive trees

N. Conceição[1,a], L. Tezza[2], S. Lourenço[1], M. Häusler[1], L. Boteta[3], C. Pacheco[1] and M.I. Ferreira[1]

[1]Department Biosystems Engineering and LEAF at Instituto Superior de Agronomia, University of Lisbon (ULisboa), Portugal; [2]Department of Agronomy, Food, Natural Resource, University of Padova, Italy. [3]COTR, Centro Operativo e de Tecnologia do Regadio, Beja, Portugal

Abstract

In Portugal, traditional olive stands are usually rainfed, in spite of hot and dry summers. Aiming at quantifying water use versus water status and understanding survival strategies, in relation to summer water scarcity, an experiment was installed on a 20 year old rainfed olive orchard (Olea europaea 'Cobrançosa'), planted in a square grid of 7 m, in a calcic Vertisol soil (profile ApBtCk) in South Portugal (climate Csb, according to Köppen-Geiger classification). From mid- 2010 to 2013, the convection fluxes of heat and water vapour, sap flow in stem and roots, and water status in plants and soil, were measured. This period included the driest winter since 1931 (2012), followed by the usual dry summer, allowing the analysis of plants behaviour under such extreme conditions. Trenches were open down to 2.5 m, starting from below a tree, to analyse root distribution within the soil layers. We concluded that roots colonize the soil horizontally with a homogenous distribution in *solum* horizons (Ap and Bt horizons) with abundant large, medium and fine roots. Large roots were absent below the *solum*, Ck horizons (0.7 to 3 m), presenting only fine (< 1 mm) and very fine roots. We report here the measurements on volumetric water content in soil around 12 tubes (neutron scattering method), located in variable positions in relation to the trees. No water table existed down to 5 m deep; capillary rise could be considered null. In doing so, the temporal and spatial distribution of water uptake from the soil volume is analyzed, confirming the direct observations above and providing insights on the high importance of very fine roots, and in general the "hidden half", for plants survival.

Keywords: *Olea europaea*, water use, water balance, survival strategies, drought

INTRODUCTION

In order to estimate water balance from soil water measurements it is required to know roots distribution in the vertical and the two horizontal directions. Irrigated woody crops, especially when growing in Mediterranean climate are characterized by a highly anisotropic root system, which induces a difficulty in determining the soil volume to which measurements in each single position applies. This study took place in Portugal, one of the countries with the highest contrast between water availability in different seasons and also with a very high variability between years (www.ipma.pt), in a site near the driest and warmer region of the country. The general aim of this study was to quantify water use and understand survival strategies of woody rainfed plants namely the root water uptake dynamics of olive trees, using sap flow in roots and soil water content measurements. Experimental results (Ferreira et al., 2013, Nadezhdina et al, 2014) demonstrated that, by the end of summer, during night, some roots provide water to other roots which exhibit fluxes in opposite direction, towards soil (hydraulic redistribution, HR). The dynamics of this process demonstrates its importance for trees survival. Two questions remain concerning this dynamics: which is the main direction of this HR concerning the all soil volume and which roots play this role?

Even today the knowledge about the olive tree root system is scarce probably due to the difficulty in reaching it, as pointed by Fernández et al (1991). It is known since long time that the root system of rainfed plants obtained by vegetative propagation is different from

seed-grown plants (Natividade, 1940). Seed-grown plants root system is dominated by a central tap root that is short-lived (4-5 years). Natividade (1940) states that the growth of the original roots, from cuttings, from rootstocks and even the main root from seed-grown specimens, ceases after a certain age, being replaced by the roots arising from the base and higher levels of the trunk, where the new root system is established. Thus the root system of adult trees is made up solely of the roots arising from the cords (probably with function of aerial roots) and from the overgrowths at the base of the trunk. There is no difference in this shallow root system of the adult trees (concerning thick root architecture), whatever is the mean by which they have been propagated. Natividade (1941) studied some olive trees, upturned by the hurricane of February the 15th of 1941 and observed two features with significant uniformity, whatever the soil type where the trees vegetate: 1) the absence of main tap root; 2) the horizontal arrangement of the thick roots and the little depth they go. According to this study, these thick roots leave the periphery of the lignotuber and are oriented almost perpendicular to the stem axis without reaching very deep soil. This researcher doesn't make any reference to the fine roots distribution.

For a 12 years old rainfed olive orchard (2 m deep sandy loam soil) Fernández et al. (1991) from the observations using the trench method (0-0.6 m depth) concluded that the highest density of total roots was observed at depths below 0.5 m. Nevertheless at the surface there was a large quantity of roots and reaching distances greater than 2.5 m away from the trunk. From root density profiles by the auger method (0-1.8 m depth) the same tendency were observed i.e. higher root concentration in deeper than in top layers, except for distances less than l m from the tree. For the root density profile at 0.45 m away from the trunk they measured local maximums at 0.9 m and 1.6 m depth, the maximum being root density observed above 0.2 m. For the root profiles at 0.9 m and 1.4 m from the stem, the maximum root densities were measured at 1.4 m and 1.2 m depth, respectively.

Specifically here we use soil water content data and direct observations of the soil and roots profile to characterize root water uptake along the horizontal and vertical directions, in order to answer the questions above.

MATERIALS AND METHODS

The experimental work took place at a commercial rainfed olive orchard (Olea europaea 'Cobrançosa'), in the region of Alentejo, Portugal (38° 0.95' N, 8° 6.58' W, 150 m a.s.l., Datum WGS84). The climate is Csa, temperate of Mediterranean type, with very hot and dry summer and mild and wet winter, according to the climatic classification of Köppen. The 30-years average annual rainfall recorded 30 km away (Beja) is 572 mm (1971-2000). ETo was estimated with the Penman-Monteith equation with the grass reference crop parameters (0.12 m in height, surface resistance of 70 m s^{-1}, albedo of 0.23) using the meteorological data recorded at nearby newer weather station (Herdade do Outeiro, 38º 20.7' N, 08º 15.08' W, 74 m a.s.l., Datum 73, www.cotr.pt) at less than 10 km.

In 1990, plants (vegetative propagated) were installed with a spacing of 7 m to 7 m on a total area of 10 ha, the tree rows direction is about 61° with the north. In 2010, the trees high was 4.15 m, the canopy projected area was 18.0 m^2 (fraction ground cover by the canopy of 0.37), the trunk perimeter was 0.71 m, and the leaf area index on a total area basis (49 m^{-2}) was 1.05 m^2 m^{-2}. The ground cover (spontaneous herbaceous vegetation) was mowed mechanically on the middle row (NO to SE direction) and controlled chemically on the tree rows (NE to SO direction). There was no tillage.

The soil is a calcic Vertisol (FAO-UNESCO, 2006) with a very deep profile (type ApBtC1kC2kC3kC4k), derived from volcanic gabbro-diorite rock. The Ck horizons are very rich in secondary calcium carbonate, have loam texture with some swelling clays and are very dense. The *solum* (Ap and Bt horizons), reaching to 0.4-0.7 m, has a clayey texture with swelling clays developing wide and deep cracks from the surface downwards when soil dries out (visible down to 0.5 m on late summer). No water table was present down to 5 m deep; capillary rise could be considered null. The bulk density for Ap horizon (0-0.45 m) is 1.2 Mg m^{-3} and for Bt (0.45-0.9) is 1.6-1.7 Mg m^{-3}. Horizon C1k (0.9-1.35 m) has bulk density of 1.7-1.8 Mg m^{-3}. C2k (1.35-1.8 m) has more coarse texture than C1k, bulk density is 1.8 Mg

m^{-3}. Horizon C3k (1.8-2.5 m) has bulk density of 1.8-1.9 Mg m^{-3}. For depths below 2.5 m bulk density is 2.0-2.1 Mg m^{-3}. Until 2.8 m depth, it was not found solid rock.

Atmospheric convection fluxes of heat and water vapour, and water status in plants and soil, were followed in the general study (Conceição et al., 2016). Predawn leaf water potential (PLWP), sap flow in stem and roots (Ferreira et al. 2013, Nadezhdina et al. 2014) and soil water content were measured from middle 2010 to 2013. Such long period included the driest winter since 1931 (winter 2012), allowing the analysis of plants behaviour in extreme conditions.

On average, every two weeks, soil water content (SWC) measurements were taken from 0.2 to 1.20 m, in 0.20 m steps which, assuming each measurement concerns the surrounding 0.2 m, allows the soil water balance between 0.1 and 1.3 m to be estimated. Water content was measured using a neutron probe (model 4301, Troxler Electronic, USA), in twelve aluminium tubes (four tubes in each position) installed in the tree row (NE to SO direction), at three positions in relation to the trees: 1.2 m, 2.4 m (4.6 m from next tree) and 3.5 m (3.4 to 3.6, half distance between trees). PLWP was measured in healthy and fully expanded leaves (20 on average), by using a Scholander type pressure chamber from late spring to early autumn.

Soil trenches were open in two directions down to 2.8 m, starting from below one of the trees analysed, allowing analysis of roots distribution, twice during the study: at the beginning (2010), to study the profile, and after the end of the roots sap flow study.

RESULTS AND DISCUSSION

Precipitation and ETo during the study period (Fig. 1) illustrate the usual contrast concerning water scarcity between the wet/dry seasons (winter/summer), but also the special drought occurred in winter 2012. The total precipitation was 764 mm, 350 mm and 582 mm for the hydrological years 2010/2011, 2011/2012 and 2012/2013 respectively.

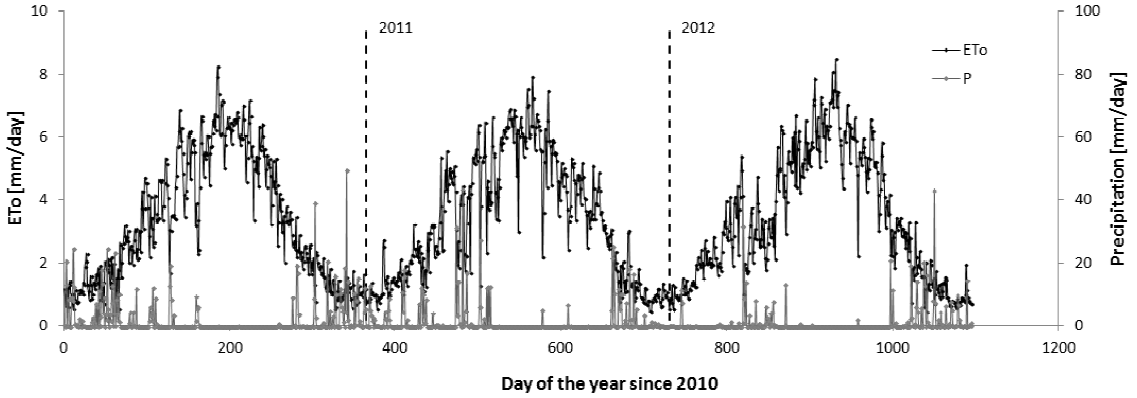

Figure 1. Daily reference evapotranspiration (ETo) and precipitation (P) during 2010, 2011 and 2012 at Ferreira do Alentejo (Herdade do Outeiro data). In January, respectively for 2010, 2011 and 2012, P was 115 mm, 57 mm and 21 mm; in February 141 mm, 53 mm and 1 mm and for December 177 mm, 9 mm and 52 mm. ETo for 2012 was 138 mm, 173 mm, 188 mm, 155 mm and 119 mm for each month from May to September (dry period) respectively.

PLWP decreased from values above - 0.5 MPa in spring to -1.4, -2.4 and -3.0 MPa in late summer, respectively for 2010, 2011 and 2012. These PLWP results are consistent with the ones observed for SWC (Fig. 2) where the values for 20 cm depth are slightly lower in 2012.

The soil data illustrate in general (Fig. 2, 4 and 5) an important aspect: SWC is very similar for the two extreme positions in relation to the trees (1.2 and 3.4 to 3.6 from tree). Besides, SWC decreases during the dry period, with a decreasing slope, tending to stabilize in what we can consider the in situ permanent wilting point (PWP).

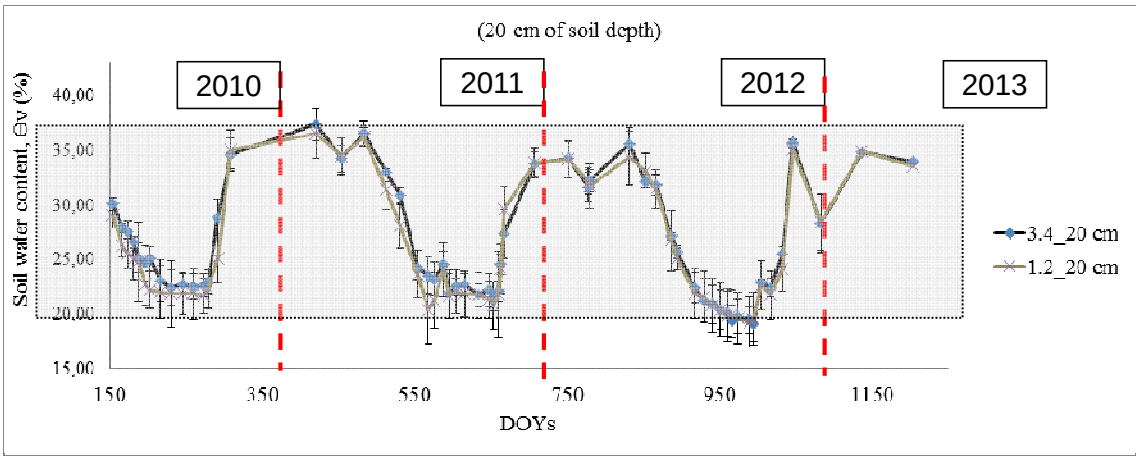

Figure 2. Seasonal evolution (late spring 2010 to early winter 2013) of average (n=4) soil water content (SW) for the layer 20 cm (10 cm to 30 cm) from the soil water profiles 1.2 m and half distance away from the trees, with standard deviation.

Observing vertical soil water profiles during a typical desiccation period (Fig. 3), the higher water availability in intermediate layers can be noticed. It is also clear the fact that desiccation goes far below 1.2 m depth. Our observations are consistent with those of Moreno et al. (1996) for one olive tree that was not irrigated during three months (dry season); from soil water measurements (profile at 0.5 m from the trunk) they observed soil desiccation below 1.4 m depth and between August 31th and September 11th the surface soil exceptionally dry with little or no change in soil water content over these 11 days.

In situ field capacity (FC) and PWP depended on soil layer and were identified layer per layer in order to get the results expressed in available water (AW), as shown in Fig. 4.

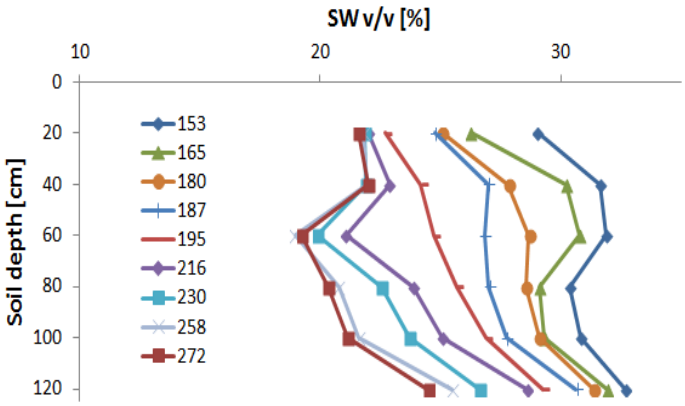

Figure 3. Average (n=4) soil water profiles (10 cm to 130 cm) for the position 1.2 m away from the trees. Desiccation period from 2nd June (DOY 153) until 29th September of 2010.

Either at 20 cm or 120 cm (Fig 4b) in a standard hydrological year, soil water content drops from FC (AW = 100%) in spring to near PWP (AW = 0) in late summer. We conclude that even using AW, no consistent differences between the three horizontal positions (1.2, 2.4 and 3.6 m away from the trees) can be observed. Furthermore, it is clear that the desiccation as well as rehydration occur first in the upper layers. Even in relatively deep soil layers there is an important desiccation, which means that water is taken from even lower layers even in a standard situation (2010), as mentioned above (Fig. 3). It is normally expected that during the long rainy period all soil layers attain FC (www.ipma.pt). It is very unusual the fact that this did not happen after the dry winter of 2012, when soil water content almost did not increase after 1.0 m depth.

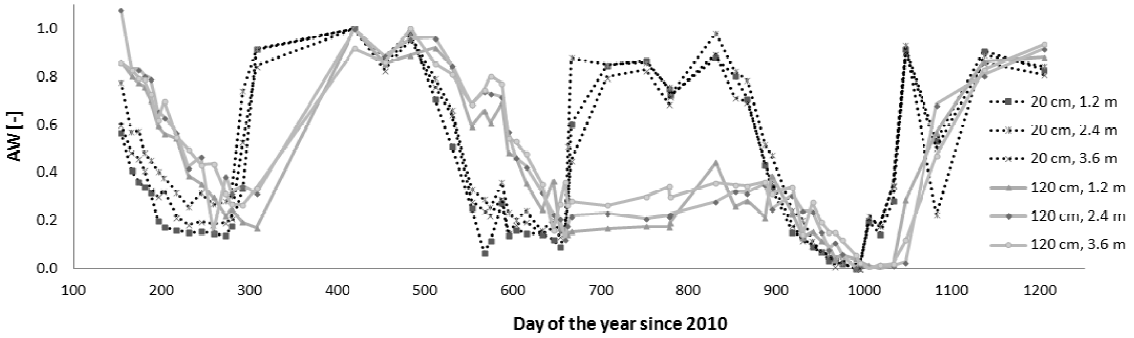

Figure 4. Seasonal evolution (late spring 2010 to early winter 2013) of available soil water (AW) for the layers 20 cm (dark dotted lines) and 120 cm (bright continuous lines) from the soil water profiles 1.2 m, 2.4 m and 3.6 m away from the trees.

Finally, AW for the all profile (average 6 depths) was calculated and the horizontal positions were compared (Fig. 5): half distance between trees versus horizontal positions closer to trees (average of the profile at 1.2 m and 2.4 m from next tree).

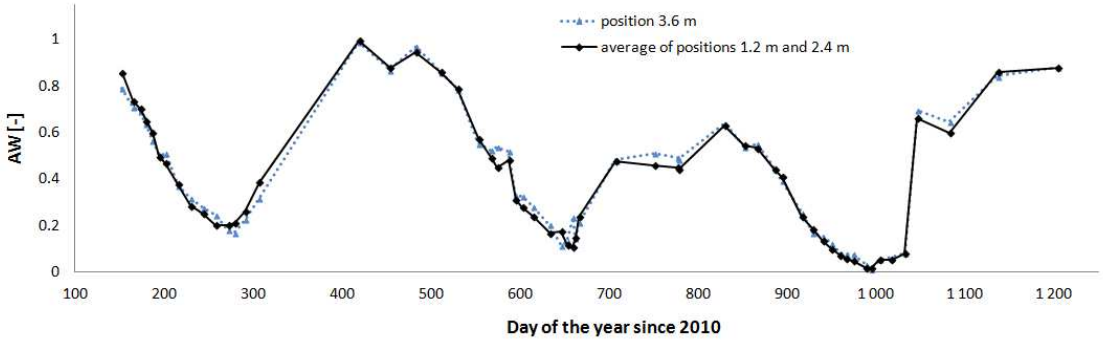

Figure 5. Seasonal evolution (late spring 2010 to early winter 2013) of available soil water (AW) for the profile at half distance from the trees (dotted line) and average profile of the positions 1.2 m and 2.4 m away (continuo lines) from the trees.

Concerning roots direct observation, they were first counted bellow one of the trees analyzed: from the lignotuber 7 extremely large roots (100-20 mm diameter), 20 very large (20-10 mm) and 45 large roots (10-3 mm) and more than 100 medium roots (3-1 mm). Fine (1-0.5 mm) and very fine (<0.5 mm) roots were present down to at least 2.5 m but were not possible to quantify, due to the soil structure (aggregation). The larger roots developed mainly horizontally and after 80 cm depth, only fine and very fine roots were observed. From the lignotuber only a thick root (16 cm diameter in the curvature zone) has vertical direction but changed direction at 0.8 m depth (interface Bt/C1k horizons) to horizontal. Only very few medium and fine to very fine perennial roots reach 2.5 m depth using cracks and other discontinuities in the litological material. The thick roots architecture observed is consistent with the one reported by Natividade (1941). For rainfed conditions (with soil tillage up to 15-20 cm depth, 3 times a year) Fernández et al. (1991) also concluded that the highest root density corresponds to very fine roots (diameter <0.5 mm) even in drip-irrigated conditions. Nevertheless, in drip irrigated conditions, the horizontal and vertical density distribution of very fine roots was different, namely highest densities in zones wetted (irrigation bulbs). These researchers also observed that the volume of soil explored by the finest absorbing roots extends to areas distant from the tree truck and to depths below 1.6 m. Nevertheless for our conditions it was not expected that the maximum density of very fine roots exist below 0.7-0.9 m (*solum*) as the soil conditions only allow a random colonization of fine and very fine roots. In the conditions studied by Fernández et al. (1991), total root and very fine root density was somewhat higher at depths greater than 1 m. For the horizontal root development there it is a good agreement that the roots can go far beyond the diameter of the canopy and the same was observed in our experiment.

CONCLUSIONS

For these adult (well-installed) rainfed trees and this climate (Mediterranean type) and soil (ApBtCk), the similarity between soil water content in all horizontal positions suggests that (1) it is correct to use the average of the data from the different horizontal positions to follow the temporal dynamics of soil water, (2) the observed hydraulic redistribution (HR) previously reported (Ferreira et al. 2013, Nadezhdina et al. 2014) occurred between soil horizons. In other words, in the conditions of this study: (1) roots colonize the soil allowing a homogenous horizontal water uptake which means that HR occurred in vertical direction, between fine roots in lower soil and roots in upper soil layers.

From the direct root observations in 2010 and late 2013 it was observed that almost all roots biomass and the highest root concentration for all diameters were observed until 0.6-0.7 m. However, the large roots observed were absent below the *solum* (ApBt horizons, 0-0.7 m), developing mainly horizontally. Only very few medium, fine and very fine perennial roots were observed between 0.7 and 2.5 m, depth, inside the Ck horizons.

These two sources of data reinforce the importance of the so-called "hidden half". In fact, together with sap flow in roots, the dynamics of water status could provide insights on the high importance for plant survival of water uptake from fine and very fine roots, in the deeper soil layers. Furthermore, there are important practical consequences of these results for the estimations of water use from soil water content: it was clear that the observations made until 1.2 m depth were not deep enough to follow root water uptake and therefore estimate soil water balance, even in a standard hydrological year (2010-2011).

ACKNOWLEDGEMENTS

The Foundation for Science and Technology, I.P. (FCT, Portugal) financed through: Doctoral fellowship SFRH/BD/66967/2009. Project WUSSIAAME - Uso da água, estratégias de sobrevivência hídrica e impacto de agroquímicos nos recursos hídricos em ecossistemas agrícolas mediterrânicos (PTDC/AACAMB/100635/2008). The EU co-financed part of the installation of infrastructure (2010 and 2011) project TELERIEG - Uso da teledetección para a recomendaccion e seguimiento de las practicas de riego en el espacio SUDOE" (SOE1/P2/E082). The authors are very thankful to Mr. Manuel Duarte (farm Monte do Outeirinho) for the efforts in making the orchard available for the study.

REFERENCES

Conceição, N., Häusler, M., Lourenço, S., Pacheco, C., Tezza, L., and Ferreira, M.I. (2016). Evapotranspiration measured in a traditional rainfed and an irrigated intensive olive orchard during a year of hydrological drought. Acta Hortic., in press (submitted 2015).

FAO-UNESCO (2006). IUSS Working Group WRB. World reference base for soil resources 2006. World Soil Resources Reports No. 103. FAO, Rome.

Fernández, J.E., Moreno, F., Cabrera, F., Arrue, J.L., and Martín-Aranda, J. (1991). Drip irrigation, soil characteristics and the root distribution and root activity of olive trees. Plant and Soil 133(2), 239-251. DOI: 10.1007/bf000091.

Ferreira, M.I., Conceição, N., David, T.S., and Nadezhdina, N. (2013). Role of lignotuber versus roots in the water supply of rainfed olives. Acta Hortic. 991, 181-188. 10.17660/actahortic.2013.991.22.

Moreno, F., Fernández, J.E., Clothier, B.E., and Green, S.R. (1996). Transpiration and root water uptake by olive trees. Plant Soil, vol. 184, no. 1, pp. 85–96. http://link.springer.com/10.1007/BF00029277

Nadezhdina N., Ferreira, M.I., Conceição, N., Pacheco, C.A., Häusler, M., and David, T.S. (2014). Water uptake and hydraulic redistribution under a seasonal climate: long-term study in a rainfed olive orchard. Ecohydrology, no. 8: 387-397. DOI: 10.1002/eco.1545

Natividade, J.V. (1940). The aerial root-primordia in the olive tree and their relation to vegetative propagation. Separata da Agronomia Lusitana, 1(2), 25-73. In Portuguese. Available from http://diana.isa.utl.pt/ceres/jsp/ with reference F-14526.

Natividade, J.V. (1941). Note in the root system of the olive tree. Agronomia Lusitana, 1(3), 15-24. In Portuguese. Available from http://diana.isa.utl.pt/ceres/jsp/ with reference PP-A01-2.

6.6 Conceição et al. (2017b)

Conceição N., Tezza L., Häusler M., Lourenço S., Pacheco C.A., Ferreira M.I. 2017. Three years of monitoring evapotranspiration components and crop and stress coefficients in a deficit irrigated intensive olive orchard. Agricultural Water Management 191:138—152.

Agricultural Water Management 191 (2017) 138–152

Contents lists available at ScienceDirect

Agricultural Water Management

journal homepage: www.elsevier.com/locate/agwat

Three years of monitoring evapotranspiration components and crop and stress coefficients in a deficit irrigated intensive olive orchard

Nuno Conceição[a,*], Luca Tezza[b], Melanie Häusler[c], Sónia Lourenço[a,e], Carlos A. Pacheco[d], M. Isabel Ferreira[a,e]

[a] Linking Landscape, Environment, Agriculture and Food (LEAF), Instituto Superior de Agronomia (ISA), Universidade de Lisboa (ULisboa), Tapada da Ajuda, 1349-017, Lisboa, Portugal
[b] CIRVE, Interdepartmental Centre for Research in Viticulture and Enology, University of Padova, Padova, Italy
[c] Centro de Estudos Florestais (CEF), Instituto Superior de Agronomia (ISA), Universidade de Lisboa (ULisboa), Portugal
[d] Departamento dos Recursos Naturais, Ambiente e Território (DRAT), Instituto Superior de Agronomia (ISA), Universidade de Lisboa (ULisboa), Portugal
[e] Departamento de Ciências e Engenharia de Biossistemas (DCEB), Instituto Superior de Agronomia (ISA), Universidade de Lisboa (ULisboa), Portugal

ARTICLE INFO

Article history:
Received 30 November 2016
Received in revised form 21 May 2017
Accepted 30 May 2017

Keywords:
Olea europaea
Drought
Eddy covariance
Sap flow
Mediterranean
Portugal

ABSTRACT

A long-term experiment was conducted to study water use of olive trees in a six-year-old, deficit irrigated, intensive olive orchard ('Arbequina') in one of the driest regions of Southern Portugal. Woody agricultural crops are regularly cultivated with some water stress to maintain an equilibrium between the vegetative and reproductive cycles, to improve production quality and, when irrigated, to save water. To achieve a precise irrigation scheduling it is necessary to quantify water use reduction due to water stress. This study reports results from spring 2010 to autumn 2012, and encompasses a hydrological drought occurred in 2012. A long-term seasonal time series of transpiration (Tr), was obtained by combining data on evapotranspiration (ET) measured with the eddy covariance method, soil evaporation measured with microlysimeters and sap flow measured with a heat dissipation method. For the years 2010 and 2011, with normal precipitation, Tr varied between 2 and 4 mm/day, in the summer. In 2012, due to the winter drought, soil water content did not reach field capacity during the wet season and an important reduction in Tr was observed ranging from 1 to 2 mm/day during summer. Predawn leaf water potential (Ψ_{pd}) was selected as plant water status indicator, because these olive trees showed near-isohydric behaviour. A function relating Ψ_{pd} to the correspondent stress coefficient (Ks) was used to decompose Tr/ETo into the basal crop coefficient (Kcb) and the Ks. The first, during the summer period, oscillated around 0.4 for years with precipitation close to average, while Ks estimated from Ψ_{pd} decreased between 1.0 in early June to about 0.83 before first autumn rain. However, these Ks values did not explain the important reduction observed in Tr during the 2012 severe drought. Measured Kcb values were compared to the ones modelled using approaches based on density factor. The derived Kcb values for summer were lower than those observed.

1. Introduction

The increasing demand for crops with low environmental impact, high nutritional value and standard quality calls for improved knowledge on crop water relations. Olive trees are of recognized high nutritional and socio-economic importance and are cultivated in the Mediterranean basin since the antiquity. In Portugal, the consumption of olive oil per capita was 7.8 kg in 2013 which represents an increment of + 5.7% relatively to 2012; in 2014, the area for table olives was 8 800 ha with a production of 17.4 Mkg of olives and, for oil, 343 600 ha, producing 438.0 Mkg of olives (2012/2013 average is 526.1 Mkg) that originated about 66.5 ML of olive oil (INE, 2015). Following a recent trend in production increase, olive tree plantations represent now in Portugal an area of 53% of total woody agricultural crops, with 1.3% and 52% for table olives and oil respectively, being wine grapes the second most representative woody crop with 27% of the area, on the same basis (INE, 2015).

According to Kaniewski et al. (2012) survival mechanisms of the olive tree are not yet enough clarified. An improved knowledge of olive tree water relations is relevant not only for scientific purposes i.e. to better understand and simulate the physical and biological

* Corresponding author.
E-mail address: nuconceicao@isa.ulisboa.pt (N. Conceição).

http://dx.doi.org/10.1016/j.agwat.2017.05.011
0378-3774/

processes involved, namely water use and survival strategies, but also for its immediate applicability to calibrate and validate evapotranspiration (ET) models, for which there is a possibility to obtain, for common uses, all input variables and parameters.

The models, always combining physical and empirical modules, can be single leaf (Monteith, 1965) or based on two or more compartments (e.g. Shuttleworth and Wallace, 1985) with data from ground level. However, these last usually require input data difficult to get outside the scope of research. Models can also use remote sensing data, such as one source energy balance models SEBAL (Bastiaanssen et al., 1998) and METRIC (Allen et al., 2007), two source energy balance models (e.g. Sánchez et al., 2008) and others still being developed and tested. Finally, a common approach includes the concept of crop coefficient (Kc). Doorenbos and Pruitt (1977) and Allen et al. (1998) are well known examples of compilation of Kc data, from a large collection of previous studies that used this approach for decades. The Kc model can be used in the one source form or single Kc approach (Doorenbos and Pruitt, 1977), with estimated maximum (crop) ET, $ET_c = Kc \times ETo$ where ETo is reference crop ET and where a stress coefficient (Ks) can be added (e.g. Ferreira and Valancogne, 1997) to obtain the actual estimated ET (ET_a). Another option is to use a two source form or dual Kc approach (Allen et al., 1998), where $ET_c = (Kcb \times Ks + Ke) \times ETo$, with Kcb basal crop coefficient, and Ke soil evaporation coefficient (= Es/ETo), being estimated actual transpiration (Tr_a) obtained as $Tr_a = Kcb \times Ks \times ETo$. This separation between the two components transpiration (Tr) and soil evaporation (Es) followed earlier works (e.g. Kanemasu et al., 1979; Wright, 1982).

Measurements of ET and its components are essential to obtain locally adjusted Kc, but measurements for woody crops are more difficult to obtain than for low crops (Ferreira et al., 2008; Allen and Pereira, 2009) and therefore they are scarce, especially for Mediterranean woody crops. These woody crops are usually cultivated with some level of water stress, therefore estimations must separate Kcb and Ks effects. Currently, another way to obtain Kc for large areas is using vegetation indexes (such as the normalized difference vegetation index) from remote sensing data, but this approach also needs measured Kc to validate a function relating measured Kc and vegetation indexes (Campos et al., 2010).

The difficulty to accurately measure ET and its components, for stands of woody plants (using micro-meteorological and hydrological methods) is well known and recognized (Rana and Katerji 2000; Testi et al., 2004; Williams et al., 2004; Ferreira et al., 2008) despite the advances in instrumentation and data acquisition systems, because of technical and/or methodological limitations of such methods, either physical (e.g. meteorological conditions) or biological (e.g. anatomical geometry and dynamics of stems and roots). Woody sparse canopies present increased difficulties mainly due to the complex architecture of roots and shoots (Ferreira et al., 2008).

The ET components, Tr and Es, have different dynamics on short time and seasonal time course (normally out of phase in woody Mediterranean ecosystems), Tr being usually the main component in ET from woody crops during summer, often estimated from sap flow measurements. Methods that allow measuring sap flow in stems, to infer Tr, can underestimate this component (Smith and Allen, 1996; Steppe et al., 2010; Wullschleger et al., 2011) namely when in use for long time (Moore et al., 2010) or due to other reasons not fully clarified (Wilson et al., 2001; Paço et al., 2004). In fact, there are studies reporting good absolute sap flow data in relation to reference methods (e.g. Berbigier et al., 1996) but many others show evidence that it is difficult to expect that the most common sap flow methods provide good absolute values in all circumstances, and mainly for high flows (Ferreira et al., 2008, 2012).

Sap flow techniques allow to have cheap long term measurements of Tr but have to be compared and corrected using other methods, which are more expensive. Due to uncertainties with data from sap flow techniques and due to the limitations of using long term eddy covariance (EC), Ferreira et al. (2004, 2008) proposed and used a combination of methods to obtain high temporal resolution (daily or lower) and simultaneously long time-series of reliable values for Tr (months, few years), for large fields of woody crops. This was done by using, during short periods, simultaneous measurements of ET by the EC technique, used as a reference (Kustas, 1990) and measured or modelled Es data (local adjusted model from good quality direct measurements), to obtain ET − Es, plus trunk sap flow data (possibly under or overestimated). From all these, it is possible to get a relationship to correct trunk sap flow estimates (in relation to ET − Es), which in turn makes it possible to determine reliable absolute long term Tr data, as described in section 2.11.

Several researchers contributed to study olive water use and water relations. For instance, an early attempt to measure Tr during a vegetative cycle was done by Abdel-Rahman and El-Sharkawi (1974). They measured Tr (rapid weighing method) in order to quantify and understand the effects of irrigation (150 mm) under a desert climate zone with 150 mm annual rainfall (western desert in Egypt). On an orchard (15 years old trees 'Shimlali', spaced 7 × 7 m) plots were subjected to different irrigation methods and irrigation scheduling approaches (rainfed, winter surface irrigation, and summer surface and sub-surface irrigation). From some Tr daily courses they estimated seasonal monthly Tr for 14 months (November to January). However, they did not apply the ETo concept but studied the linear correlation between Tr and meteorological variables, underlining that these olive trees showed strong stomatal control.

Other studies were performed on olive showing that these trees have high water-use efficiency (Bacelar et al., 2007; Fernández, 2014). Using the compensation heat pulse method, Fernández et al. (2008, 2011) studied Tr for olive trees, in relation to many different aspects of water relations. The same team modelled Tr at leaf scale but none of those studies reports values for ET.

Villalobos et al. (2000) used the EC method to access ET and its components on a drip-irrigated olive tree orchard 'Picual' (trees with: 4 m height, 6 × 6; ground cover 40%; leaf area index (LAI) of 1.5 and 1.2 in May of 1996 and 1997, respectively), at Cordoba (Spain). From the 11th to the 30th June 1997, they measured convective heat fluxes (latent heat flux (LE) and sensible heat flux (H)) above the canopy (EC sensors at 5 m height, separation path of 0.3 m) and below the canopy (EC sensors at 0.4 m height, separation path of 0.13 m) that would correspond to ET and Es, respectively. Specific Tr measurements were not performed; Tr was calculated as Tr = ET − Es. For the three days with complete 24 h data (DOY 171, 172 and 173) daily ET, Es and T were on average 3.12 mm, 0.74 mm (24% of ET) and 2.38 mm, respectively.

Another experiment was carried out by the same team (Villalobos et al., 2000) in March-June 1996 (before the drip irrigation campaign started); they also measured ET by EC method which ranged from 2.0 to 5.5 mm/day, for ETo from 2.7 to 8.5 mm/day. Using those values, Kc × Ks would be from 0.65 to 0.74. They hypothesised that Es (for a wetted soil fraction of 0.05–0.1) would be between 0.5 and 1 mm day^{-1} and underline the importance of accurate Es values.

When estimating canopy conductance (inverting the Penman–Monteith model for the transpiration flux) Testi et al. (2006) used Tr data obtained as the difference between measured ET (EC method) and Es estimated from a model, as done in our work. By measuring ET from a young drip irrigated olive orchard of 'Arbequina' (3.5 × 7 m spacing, southern Spain), with EC method and soil water balance (from soil water measurements until 2.7 m depth), Testi et al. (2004) found a good agreement between ET from EC method and ET from soil water balance. From June 29 to

August 28 (dry soil conditions) ET was 2.26 mm day^{-1} on average (LAI = 1, in 2000), being Kc's 0.19 (1998), 0.24 (1999) and 0.34 (2000). Again, it is underlined by these authors that Es component has been proved to be critical in these olive orchards, as the relative importance of Es in concurrence with the Mediterranean climate and the evergreen nature of the species, induces an "inverted" behaviour of Kc with respect to the herbaceous crops, as it can be obtained when modelling the components of the dual Kc.

Martínez-Cob and Faci (2010) also measured ET (EC method) of a hedge pruned olive orchard ('Arbequina', fraction of ground surface covered by vegetation (fc) = 0.34, Zaragosa, Spain) from January 2005 to February 2006 having a data set of ET for a total of 425 days. They realized that the calculated Kc values showed high variability, both within a given month and between years, as expected due to the contribution of several factors such as Es, which is highly dependent on precipitation (P, also with high variability in that situation). They conclude that, as they did not measure the ET components in order to compute Kcb and Ke (and interception) separately, the usefulness of the recorded daily Kc values was limited to their experimental situation.

In conclusion, for evergreen orchards in Mediterranean climate, Villalobos et al. (2000), Testi et al. (2004, 2006) and Martínez-Cob and Faci (2010) stress the importance of Es in quantitative and qualitative terms i.e. Es can be a large proportion of ET and, if Es and ET are out of phase, ET can't be used as a surrogate of Tr or vice-versa (for engineering applications). Nevertheless, in some of the studies mentioned above there were no attempts to quantify Tr independently, neither differentiating Kc from Ks.

For a super-intensive olive orchard ('Arbequina', planted in 2006, spaced 1.35 × 3.75 m, ground cover of 0.35, LAI of 1.3 m^2 m^{-2} in final 2011), Paço et al. (2014) measured ET and Tr to calibrate and validate a dual Kc approach model to obtain annual time series of Kcb, Ke and Ks. Usually, commercial olive orchards are deficit irrigated but in 2011 this orchard did not suffer any quantifiable water stress until the middle of summer (August). In 2012, despite the slightly lower LAI, water stress began early (May) and was probably very intense (modelled Ks = 0.3).

Santos et al. (2007) and Fernandes-Silva et al. (2010) used soil water balance down to 0.65 m and 1 m depth, respectively, most likely not deep enough to reach the whole explored soil volume. Again, neither it was possible to separate the two coefficients, nor the interpretation of possible Ks values is made in relation to the water status of the trees or soil. However, as stressed by Fernández et al. (1997), plant water status is necessary to plan deficit irrigation.

The general objective of this research project was to characterize the water use of an olive orchard, in a region with high natural water scarcity during summer (Alentejo, Portugal), by quantifying water status, ET and its components (T and Es) and root sap flow dynamics, while water stress was regularly quantified. This study also deals with the components of the energy balance, the latent heat flux being obtained by EC technique, and with the quantification of ET components, separating the effects of Kcb and Ks in Tr/ETo, therefore contributing to the knowledge of tools for simple modelling. We measured water use during a period of three vegetative cycles (May 2010 to November 2012), including the extreme water scarcity conditions found during a particular drought (by lack of rain not only in summer, as usually, but also in winter, hydrological year 2011/12).

In brief, the specific aims of the study reported here are (1) to characterize the water use dynamics of olive trees during a long period, separating all components, in the deficit irrigated (DI) conditions used in a representative commercial intensive irrigated orchard, (2) to analyse the relationship between Ks and a selected water stress indicator, (3) to discriminate Kcb from Ks and, finally (4) we also considered useful to compare results for Kcb to the ones obtained by the general procedure described in Allen and Pereira (2009).

Table 1
Biometric data for the deficit irrigated olive orchard obtained in summer 2010 and 2012 (n = 21). Trees height and trunk perimeter (about 0.4 m above soil surface); stem height (from soil surface until first branches); ground cover (canopy vertical projection area).

Year	Height [m]	Perimeter [m]	Stem height [m]	Ground cover [m^2]
2010	3.2	0.32	0.68	5.7
2012	3.5	0.40	0.71	8.4

2. Materials and methods

2.1. Location and climate

The experimental work took place at a commercial irrigated olive orchard (henceforward designated as orchard) with about 10 ha (38° 1.34′ N, 8° 10.84′ W, 97 m above sea level, a.s.l.) included in a farm (Monte do Pardieiro) with about 434 ha of contiguous olive orchards. The farm is located in the Alentejo region of Portugal, close to the town of Ferreira do Alentejo (160 km southeast of Lisbon) and 30 km west of the city of Beja. The farm landscape is roughly flat (at the orchard maximum slope is about 1.3%). The climate is Csa (Köppen-Geiger classification, Köppen, 1936), temperate of Mediterranean type, with very hot and dry summers and mild and wet winters (IPMA, 2016). In Beja where the nearest station with historical meteorological records can be found, the annual rainfall is 572 mm (1971–2000, IPMA, 2016).

2.2. Canopy and soil cover

The trees (*Olea europaea* 'Arbequina') were planted in 2004. The trunk height and perimeter were 68 cm and 32 cm respectively (10 cm diameter), in 2010. Tree rows were 7.0 m apart over ridges (2.0 m width and 0.2 – 0.3 m height on centre) whose direction is 330° with north (clockwise). In the rows the distance is about 4.8 m (about the density of an intensive orchard, 300 tree/ha). The training system is in vase. Between the rows there was a continuous 2.0 m width band of permanent soil grassing (spontaneous vegetation), mowed mechanically twice per vegetative cycle, usually in early and late spring/early summer. In the tree rows the soil was bare and weeds were controlled chemically. There was no tillage. In late winter 2012 the trees were pruned to adequate the canopy to the harvesting machinery. The harvest was mechanical in 2010 and 2011 (continuous harvesters) and afterwards semi-mechanical (shaker and nets as olive interceptor). Biometric data (Table 1) and the methods used to get leaf area and ground cover are described in Häusler et al. (2014). The fractions of soil surface covered by the canopy were 0.17 and 0.25 in summers of 2010 and 2012, respectively. Information provided by linear variable displacement transducers (LVDT, Df 2.5 g series, Solartron Metrology, UK) in a few trees (n = 12) were used to obtain trunk growth and compare with the occasional direct measurements of trunk diameter in a large sample (250 trees). Trunk growth data were also used for interpretation of sap flow measurements (Section 2.11).

2.3. Soil description

The soil was classified as Luvisol (FAO-UNESCO, 2006) with a very deep profile, higher than 2.3 m depth, type ApBtC derived from sedimentary sandy rock material. The Ap (0 – 0.5 m) horizon has a loam texture with abundant gravel, Bt (0.5 – 1.3 m) a clay texture with a few gravel and C (1.3 – 2.3 m) has a sandy-loam texture with some gravel. The nature of gravel is quartz and feldspars. From the

C2 horizon (1.7 – 2.3 m) we could not observe any type of roots, being this layer very compact (bulk density of 1.8-1.9 Mg m^{-3}).

2.4. Irrigation system

Each tree row had a line of drippers spaced 0.75 m with nominal flow of 1.6 L h^{-1} being irrigation flux density 0.31 mm h^{-1}. The orchard was irrigated simultaneously (one single irrigation sector) and the farmer irrigated it on almost a daily basis, from late spring to late summer. The irrigation events and amounts were measured by tipping-bucket rain gauges (ARG100, Environmental Measurements Ltd., Sunderland, UK) in the main plot and in each sub-plot.

2.5. Plant water status

To assess plant water status, leaf water potential was measured at pre-dawn (Ψ_{pd}) due to the possible isohydric plant behaviour, as shown later. To measure Ψ_{pd} a portable Dixon-Scholander type pressure chamber (PMS 600, PMS Instrument Company, USA, 0.02 MPa resolution, pressure range 0–4 MPa, Dixon, 1914; Scholander and Hammel, 1965) was used on a variable number of healthy and fully expanded leaves (ca. 20), collected randomly at 1.2-1.8 m height.

2.6. Soil water status

Volumetric soil water content (SWC) was quantified using the neutron scattering method (Gardner and Kirkham,1952) considered the most precise and reliable and, according Evett et al. (2009) exhibiting spatial variation of similar magnitude and pattern as the gravimetric method. The sensor used was a portable neutron probe (model 4301, Troxler Electronic Laboratories, USA). During the measurements, the probe was lowered from soil surface to a depth of 1.2 m, in steps of 0.2 m, inside an aluminium access tube that is "transparent" to high-energy (fast) neutrons, which are scattered by the soil within 0.3–0.5 m of the source. Close to the source, the detector counts only the slow neutrons. The count rate was determined for a 60 s interval. The neutrons counts were normalized as fraction of the counts in water (primary standard) and SWC was calculated by a linear calibration function adjusted for each soil layer. Twelve access tubes were installed in the tree rows at a distance of 1.2 m and 2.4 m away from the trees (six tubes in each position). The drippers were fixed to avoid bleeding around access tubes.

2.7. Turbulent fluxes

To measure ET (or correspondent latent heat flux, LE) the EC micrometeorological method was used, as it is considered to be the most accurate approach for measuring ET in such rough surfaces (Kustas, 1990) and is therefore taken as the reference method to evaluate other measuring approaches. In addition to LE and sensible heat flux (H) by the EC method, the soil heat flux (G) and the net radiation (Rn) were measured (as described in Section 2.8) to verify the closure error of the surface energy balance equation. The closure error (CE = Rn – G – LE – H) should be zero, and is usually graphically represented as the deviation from line 1:1 in the Rn – G versus H + LE relationship when other components are negligible. The fact that ET could be obtained directly from EC direct approach and also from the difference Rn-G-H provides an extra for data validity analysis. Air temperature (Tair) and relative humidity (RH) were measured independently above the canopy, as described below, to perform corrections to the EC data. The sensors were installed at a 6.0 m high metallic tower with a large fetch (about 280 m from the orchard northwest edge, from where dominant wind comes).

The wind velocity vector and sonic temperature were measured by sonic anemometry (Schotland, 1955) and sonic thermometry (Schotanus et al., 1983; Kaimal and Gaynor, 1991) respectively, by a C-Clamp three-dimensional ultrasonic anemometer-thermometer smart sensor (CSAT 3-D, Campbell) and the data received by a data logger (until mid-July 2012, a CR10X and henceforward, a CR1000, both Campbell). The water vapour (absolute humidity) fluctuations in the air were measured by ultraviolet spectrophotometry (water vapour lines absorption at 123.58 nm and 116.49 nm) by a fast response krypton hygrometer (KH20, Campbell) with the output voltage measured by the data logger. The sonic anemometer was mounted (on the metallic tower) pointing into the N/NW direction (prevailing wind) to minimize the amount of data that was contaminated by the anemometer's arms and other supporting structures, and levelled. The hygrometer was mounted close the anemometer (North side) with a 0.1 m path separation.

To keep up with trees vertical growth, the turbulence fluxes (wind vector velocity, sonic temperature and absolute humidity) have been measured at two different heights into two different periods (Table 2). The first period was from June 2010 to mid-July 2012 and the second period henceforward until August 2013, with measurement height of 4.5 m and 5.0 m, respectively. Other changes were made: for the first period the data logger (CR10X, Campbell) was programmed with scan rate of 8 Hz and raw fluxes H and LE were calculated online for 30 min averaging time and stored in memory; the raw data were discarded by lack of memory. The corrections for the air density variation (WPL correction, Webb et al., 1980) and correction of oxygen cross sensitivity for krypton hygrometers (oxygen absorption, Tanner et al., 1993) were performed in post-processing. In the second period, in order to store the raw data the data logger was changed (CR1000, Campbell) to one with higher capacity of non-volatile memory (CFM100 Compact Flash Module, Campbell). The 10 Hz raw data (wind vector velocity, sonic temperature and absolute humidity) were processed using the TK3 software (Mauder and Foken, 2015) that calculates the average fluxes (H and LE) for 30 min intervals and the data corrections/conversions were performed following Foken et al. (2011). ET measurements here reported were obtained only in selected periods (mainly summer time) from mid-June 2010 to August 2012, being this EC system sometimes used in other plots. Those periods were enough to obtain a relationship allowing the use of sap flow data to get Tr, as described in Section 2.11. All automatic measured variables were recorded in UTC +00:00 time, being solar time close to UTC time minus 40 min (i.e., solar noon is at 1:40 p.m. local time, in summer).

2.8. Other energy balance components and meteorological variables at the plots

Air temperature and relative humidity were measured at the 4.5 m height by a band gap sensor and a capacitive sensor (Sensirion SHT75, Sensirion AG, Switzerland), respectively, assembled in a temperature and relative humidity smart sensor (CS215, Campbell). The data were received (SDI-12 protocol) by a data logger (CR3000, Campbell) at 1/5 Hz.

Net radiation was measured at 5.0 m during the all period of measurements by net radiometers (NR2 and NRlite, Kipp & Zonen, Netherlands) and the voltage output measured at 1 Hz by the same data logger as the turbulent fluxes. The soil heat flux (G) was measured by a combination (Liebethal et al., 2005) of the heat flux plate method and estimation of heat stored in the soil control volume, taking into account the sensible heat storage variation in the soil layer above the plates. Heat storage changes were estimated considering the changes in volumetric heat capacity of the soil, obtained from soil water content measurements, according to the procedure described by Snyder and Paw-U (2001). Six flux plates

Table 2
Measurement heights of turbulent fluxes and meteorological variables for the two periods considered. Period 1: from June 2010 to mid-July 2012; Period 2: henceforward until August 2013.

Sensor	Height [m]		Variable	Reference for height
	Period 1	Period 2		
CSAT3	4.5	5.0	Wind velocity vector and virtual sonic temperature	Soil surface on the ridge base
KH20	4.5	5.0	Water vapour fluctuations	Soil surface on the ridge base
CS215	4.5	4.5	Air temperature and RH	Soil surface on the ridge base
NRlite, NR2	5.0	5.0	Net radiation	Soil surface on the ridge base
Type T thermocouples	−0.025	−0.025	Soil temperature	Local soil surface
Soil heat flux plates	−0.050	−0.050	Soil sensible heat flux	Local soil surface

with known thermal conductivity (HFT-3.1, Rebs, Seattle, USA) were placed in a transept, buried at 0.05 m depth, perpendicularly to the heat flow direction. The soil temperature was measured by thermoelectric thermometry using copper-constantan (PR-TI-24, Omega) thermocouple (TC) junctions installed at 0.025 m depth. The TC output voltage was measured by a data logger (CR3000, Campbell). As the orchard is a sparse canopy, there were heterogeneous areas at the ground surface relatively to direct soil radiation and soil water content (irrigation). Therefore, four regions were considered (combination shadow/irrigation) and G was calculated as a weighted average, considering the relative surface in each region.

2.9. Sap flow measurements

To measure sap flow in the trees trunks, the *Granier* heat dissipation method (Granier, 1985) was used due to its simplicity, long term stability and low cost (sensors price, relatively low requirements for data acquisition systems hardware and software). Commercial sap flow sensors (UP GmbH, Germany) with two probes were used. To account for the natural gradients, a third probe with similar construction was added to each commercial sensor. Two holes (0.1 m apart) were drilled in the sapwood of each tree, along the longitudinal axis of the tree trunk and in each one an aluminium tube with 0.002 m external diameter was inserted. The outer 0.02 m of each probe was inserted inside the aluminium tube and the empty space filled with high thermal conductivity grease. Through the upper probe (downstream) resistor, an electric current was maintained with constant intensity, controlled by an electronic circuit (designed and assembled by Mezão, Portugal) based in the LM2575T voltage switching regulator. The power dissipated by Joule effect was 0.24 W, a value selected to get enough sensibility and do not damage the trunk tissues. Details about *Granier* sensors construction can be found in Davis et al. (2012). The sensors were protected from the rodents (and rain) using a plastic bottle applied like a dome. Around the trunk there was a sheet of high reflectance material to avoid the impact of direct solar radiation (in order to minimize natural gradients). The heated probes were installed at 0.4–0.5 m above ground, in a regular part of the trunk, being the lower probe at 0.3–0.4 m above ground. Sensors were inserted in seven apparently representative trees in the main plot and in 12 others, six in each sub-plot (see Section 2.12).

Thermal gradients were especially critical during the day not impacting daily totals unless they affect the maximal temperature difference between the two probes (ΔTmax), a necessary parameter to obtain sap flow (SF) density. Night time flow occurred sometimes; in order to get physically meaningful ΔTmax, those nights were discarded after careful analysis of the records, in relation to meteorological variables. Possible effects of nocturnal thermal gradients were also eliminated due to our installation and algorithm. The SF data were further selected and filtered in relation to non-valid values and irregularities without sense.

2.10. Soil evaporation

Soil evaporation was estimated with a model calibrated on local microlysimeters (ML) measurements (Tezza, 2013), using the same approach as Bonachela et al. (1999), based on the two stage Es theory (Ritchie, 1972). Soil evaporation was measured from mass loss of the undisturbed volume of soil content into the ML, using an electronic scale with 0.1 g resolution. Ten ML were used, in different positions in relation to the shade and drippers: six in the wet soil (split into sunny and shaded areas) and four in the dry soil (split into sunny and shaded areas), operated according to Daamen et al. (1993). To minimize divergence from the surrounding soil, ML's cores were renewed after every irrigation event, for ML in wet soil, and every two days, for ML in dry soil. All data coming from direct Es measurements (18 days during summer time) were used to calibrate the empirical model, allowing to obtain the seasonal time course of soil evaporation (Es_{mod}) for summer time; this methodology and the detailed analysis of the results can be found in Tezza (2013).

2.11. Transpiration estimation from sap flow measurements

The available methods to measure ET and its components (Tr and Es) in natural conditions have technical and methodological limitations especially when used in long term studies to assess the water use. One way to minimize these limitations is to use a combination of sap flow and EC methods as proposed by Ferreira et al. (2008).

Measured Tr was obtained combining the robust, low cost SF measurements with data from the reliable but expensive EC technique (ET_{EC}) and microlysimeters (to get modelled Es), as shortly described in the following: firstly (1), Tr values for the days with all these data were obtained as $Tr_{EC} = ET_{EC} - Es$; secondly (2), a relationship between these Tr_{EC} and the correspondent SF density was used; thirdly (3), this relationship was applied to SF density long term data series, retrieving a Tr long term data series. The reason for these three steps is three-fold: (i) solving the problem of underestimation from SF measurements and uncertainties with determining the xylem functional area, often found (Paço et al., 2004; Silva, 2009; Steppe et al., 2010) or the effect of uneven radial profile (Clearwater et al., 1999), (ii) overcoming the limitations due to discontinuous data set using EC technique (due to limited fetch in some directions, bad weather, technical problems or limited equipment, when being shared between several experiments), and (iii) discriminating between ET and both of its components (Tr and Es).

Besides wounding effects and possible influence of wood parameters and heating power using this SF technique (Ferreira et al., 2009), several other problems have been reported concerning SF up-scaling (Paço, 2003; Silva, 2009; Clearwater et al., 1999), including the lack of appropriate sampling (Köstner et al., 1998). So, as described in Ferreira et al. (2004) the relationship Tr_{EC} ($= ET_{EC} - Es$) versus SF density obtained locally has the potential to accommodate all factors related to the aspects above referred, included the

Table 3
Periods of measurement for the different variables considered.

	2010	2011	2012
Stem sap flow	Since mid June	All year	All year
Sensible heat flux (LE) and latent heat flux (H)	From mid June to mid September	May to October	Mid July to October
Net radiation (Rn)	Since August	All year	All year
Air temperature and relative humidity	Since mid June	All year	All year
Soil temperature and sensible soil heat flux (G)	Since July	All year	All year
Transpiration (Tr)	Since mid June	All year	All year

possible insufficient sampling. One should take into account that such relationships only apply to the particular sample to which they were obtained (with the aim of getting a longer time series than the EC data alone would provide, Table 3). The overall interpretation of the relationships obtained during the three years of this study required the consideration of the trunk growth, either using direct measurements of trunk diameter, or using growth rates derived from the LVDT sensors used in a few trees (Section 2.2).

2.12. Water stress cycles

Water stress cycles are periods during which a well irrigated sub-plot is used as a control while another sub-plot is left to dry out. The aim is to analyse the behaviour of different water status indicators, in different time scales, as the relationships between those can serve different operational purposes, that include (a) obtaining threshold values for the onset of irrigation, and (b) characterizing plants behaviour. Relationships between variables would be used here to derive Ks values from the selected water status indicator.

While ET flux and sap flow measurements took place at the 10 ha main plot, which continued to be irrigated according to regular farmer practices, a short term water stress was imposed in two sub-plots outside the footprint area of the main plot, during a few weeks in 2011 and again in 2012. Therefore, for the duration of each stress cycle there were additionally two small subplots (plot 2 and plot 3, 941 m^2 and 28 trees each) equipped with independent irrigation systems and where six trees, apparently representative (from size and trunk diameter), were equipped with sap flow sensors (and LVDT sensors). Before the beginning of each water stress cycle, both plots were well irrigated to ensure that they reach maximal water status (comfort) and were in a comparable situation. The first stress cycle was induced during those 6 weeks in 2011 between DOY (day of the year) 215 (August 3) and DOY 258 (September 15), meaning that subplot 2 was not irrigated, while subplot 3 was kept well irrigated for reference. A second stress cycle was performed in 2012 from DOY 180(June 28) to DOY 221 (August 8) of 2012. The recorded data used legal summer time: UTC +00:00 time, plus one hour. The full description of the stress indicators analyzed is out of the scope of this paper but some elements about the relationship between relative Tr (RTr = Tr plot2/Tr plot 3) and Ψ_{pd} will be used in this analysis.

2.13. Reference evapotranspiration

The Penman-Monteith equation (Monteith, 1965) was used to compute ETo on a 24-h time step basis, using the grass parameters proposed by Allen et al. (1998). The meteorological data used to compute ETo (daily maximum and minimum air temperature, relative humidity, mean wind velocity and total global solar rradiation) are from the weather station at Herdade do Outeiro (38° 20.7′ N, 08° 15.08′ W, 74 m a.s.l., Datum 73, less than 10 km from the experimental plot) and available as public resource (COTR, 2016).

2.14. Data analysis and statistics

The statistical techniques employed to analyse our data were mainly linear regression and summary statistics. Since our study is not amenable to a block design, our data are not suited to statistical inference and, therefore, we follow a statistical descriptive approach.

2.15. Precipitation and irrigation during the observed period

For the hydrological years 2010/2011 and 2012/2013, total P near the plots was around 764 mm and 582 mm (Fig. 1). For 2011/2012, the total rainfall was only 350 mm (driest winter since 1931), but in spring rainfall was about 150 mm. The total seasonal irrigation volumes and daily averages (Table 4) were respectively 159 mm, 1.3 mm (2010); 141 mm, 1.4 mm (2011) and 226 mm, 1.7 mm (2012).

3. Results and discussion

3.1. Convective fluxes and energy balance

As EC data are used as a reference to correct long term sap flow estimates, as described in 2.11, special care is required with the careful application of the standard data treatment steps and the control of data quality, explained in the following. For the conditions of the convective flux measurements performed, a simplified footprint analysis was applied, according to the methodology described in Schuepp et al. (1990), allowing the quantification of the relative contribution (to the total measured ET) of water vapour coming from different distances from the measurements point (tower). For instance, for a measurement height of 5.0 m (Fig. 2a), more than 85% of the measured heat fluxes were originated from an upwind area less than 140 m away from the tower. As the distance to the border of the plot, for the wind directions W, NW, N and NE, was higher than that value and, for remnant directions, lower, only data from those wind directions were considered. The data were also checked visually for quality assessment.

The closure error of the surface energy balance (Section 2.7) equation was less than 15% being in general within the limits frequently found (10–30%) with the EC method (Wilson et al., 2002). In the example shown (Fig. 2b, for 2011 and 2012), the closure error is only clearly identified with the usual positive values for the higher fluxes at noon, being almost compensated, on a daily basis, by some negative values for the lower fluxes. These results encourage its use as a reference for correcting estimations based on the complementary methods for ET components (as described in Section 2.11).

Besides, as suggested by Foken et al. (2011), no corrections were made for the surface energy balance non-closure; these researchers assume that the unclosed energy balance is not related to errors in the EC technique but to atmospheric phenomena not measurable with this technique. However, some researchers that measured ET in olive tree orchards (Martínez-Cob and Faci, 2010; López-Olivari et al., 2016), and wine vine (Campos et al., 2010) performed the closure error correction, as they hypothesize that this error is due

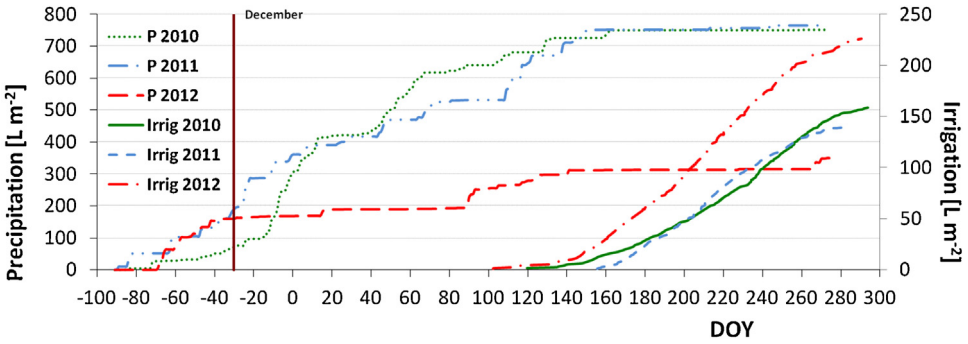

Fig. 1. - Seasonal time course of cumulated irrigation and of precipitation for the three hydrological years (October to September) 2009/2010, 2010/2011 and 2011/2012 (Herdade do Outeiro meteorological data).

Table 4
Total irrigation depths and duration, duration of irrigation season, average irrigation depth and duration (2010–2012). Total precipitation for hydrological year (October to September).The start and end of the irrigation season were considered when respectively 5% and 95% of total irrigation volume was achieved, others before or after where for maintenance and cleaning.

Year	Total irrigation [mm]	Total time irrigation [h]	Start	Stop	No. days	Irrigation avg. [mm/day]	Irrigation time avg. [h/day]	P[mm]
2010	159	518	01-Jun	05-Out	126	1.3	4.1	750
2011	141	461	15-Jun	26-Set	103	1.4	4.5	764
2012	226	736	23-Mai	04-Out	132	1.7	5.6	350

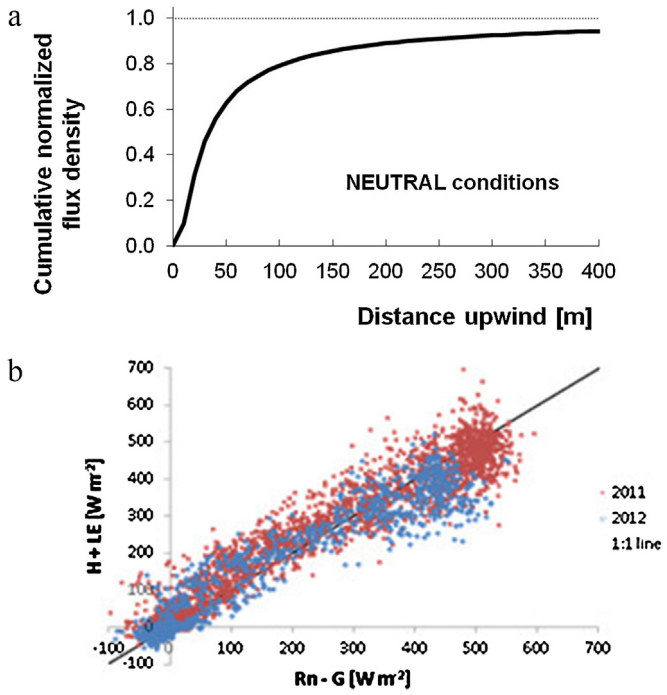

Fig. 2. - Eddy covariance measurements (a) footprint analysis, according to Schuepp et al. (1990) for the period 2 (the most unfavourable condition, see Section 2.7) and surface energy balance closure (b) for 2011 and 2012, 30 min data.

the EC measurement method and that Bowen ratio (H/LE, Bowen, 1926) was accurately measured by the EC system (both H and LE affected by the same error proportion). Paço et al. (2006) for ET data (peach orchard) found a closure error of 10% and stated that the lack of energy balance closure is often associated with measurement errors in Rn and G even if not completely explained by this uncertainty. Another source of uncertainty in the energy balance are the changes in the energy storage within the control volume (olive tree biomass and air) that are not included in this simple analysis and can account for as much as 10% of the available energy in such ecosystems, as stated by Williams et al. (2004). However, considering the relationship shown in Fig. 2b, these are not major concerns in our case; these EC data were considered reliable.

3.2. Energy balance components

This section aims to summarize some relevant data about the energy balance of the orchard, especially at a seasonal scale, which may be of interest for data interpretation and for practical uses, for instance the values of Rn and G in estimating ET with direct ET models (e.g. Rana and Katerji, 2008). Furthermore, it is interesting to compare different experimental situations based on energy balance indicators such as the Bowen ratio.

For cloudless days, during the diurnal period convective flux densities (LE and H) follow the sinusoidal shape of the net radiation flux density. During the night, Rn fluxes were negative reaching 50 W m^{-2}, with small fluctuations. For the diurnal period, not only for Rn but also for LE and H the maximums occurred around the solar noon, H and LE reaching values higher than 250 W m^{-2} (equivalent to 0.37 mm h^{-1}) and Rn, reaching values higher than 650 W m^{-2} (0.95 mm/h). During the diurnal period, G was positive (flux from the control volume to the soil below) and reached 150 W m^{-2} while, during night, G was negative reaching values close to Rn. Bowen ratio changed along the season as a result of increasing dryness in exposed soil and eventually some plant water stress, reducing LE. For instance, and considering dates representative of general trends, for July 7 and 8 (2011) LE and H were similar, being daily Bowen ratio close to 1, while for July 26 and 27 (2012), LE was lower than H, being the Bowen ratio 1.9 and 1.5, respectively. For this last period, the soil surface is dry with the exception of soil moisten by the irrigation drippers (that ranged from 4% to 8% of the soil surface, depending on the irrigation volumes).

Villalobos et al. (2000) for an olive orchard ('Picual', 6 × 6 m, LAI of 1.2) with no expectable tree water stress, used EC method (DOY's 171, 172 and 173) to measure ET (as LE above the canopy) and Es (as LE below the canopy). For those three days, hourly average LE fluxes reached maximum values of 222 W m^{-2} and 54 W m^{-2} above and below the canopy, respectively, two hours after the solar

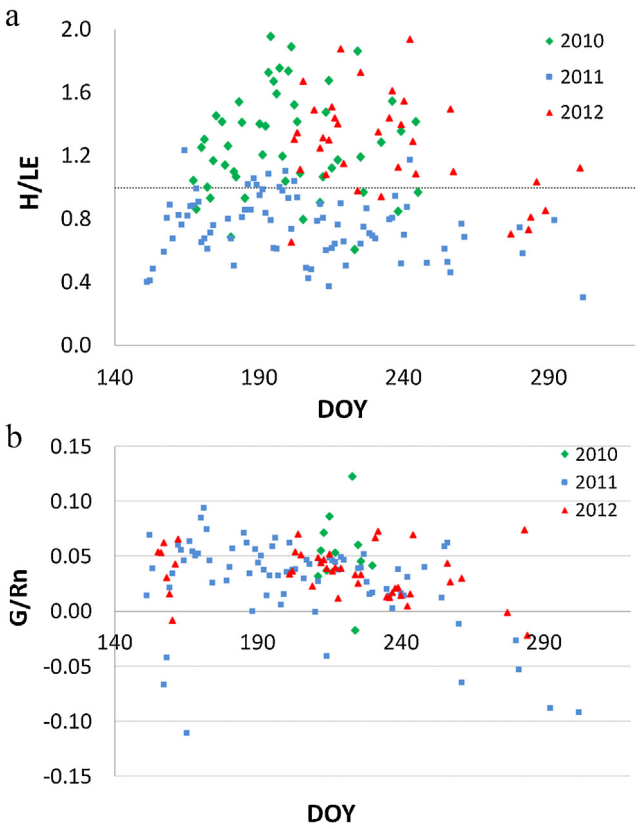

Fig. 3. - Seasonal time course of daily averages for 2010, 2011 and 2012 (summer) (a) Bowen ratio, (b) daily total sensible heat flux to the soil (G) divided by daily total net radiation (Rn).

noon. Although for 2011, LAI was comparable, for 2012 LAI of our orchard was higher. Probably there were also differences in plant and soil water status, with more intense stress in 2012 in our case, as discussed below. Our ET values measured for 2011 were in the same range as those measured by Villalobos et al. (2000) of around 3.12 mm day^{-1}, but our data for 2012 were substantially lower.

For cloudless days, the diurnal course of Bowen ratio has a descending trend in 2011, from the morning to afternoon, indicating that for these days proportionally more energy is used by evaporation during the afternoon, than in the morning. For July 26 (2012), a strong decrease was observed between the morning and the afternoon, Bowen ratio decreasing from about 4–1, with 2 as average, except for the July 27 (2012) and similar days when a diurnal time course reversed relatively to the cloudless days was observed, most likely due the low solar energy during the cloudy morning. We can conclude that Bowen ratio has a marked variation along the diurnal period ranging (in 2011) between 0.8 and 1.5, on average 1.2. The cloudless days pattern of the Bowen ratio is consistent with the one reported by López-Olivari et al. (2016) for a drip irrigated super-intensive olive orchard ('Arbequina', 1333 trees ha^{-1}) with LAI 1.32 m^2 m^{-2}, in Chile. These researchers concluded that H was higher than LE from 09:00 to 14:00 h, while LE was similar or higher than H from 14:00 to 20:00 h. These hourly trends are quite different than those found for some forest and orchard stands, when the stomata tend to close during the afternoon (Zhang et al., 2013).

Observing the seasonal time course of daily average Bowen ratio (Fig. 3a), it is possible to define two groups of data; for 2011 (higher P, lower ETo), Bowen ratio ranged between 0.5 and 1 while for 2010 and 2012, Bowen ratio varied between 1 and 2. Testi et al. (2004) when measuring convective fluxes in a young olive orchard (no water stress) with LAI = 1, found Bowen ratio close to 1 for summer days, independently of the soil surface conditions (soil wetted by irrigation or not). López-Olivari et al. (2016) reported monthly average Bowen ratio from December to March (summer, southern hemisphere) ranging from 0.8 to 2.2 and from 1.2 to 2.4 in 2010 and 2011 respectively. For our situation assuming that Es was similar in the three years considered (2010–2012) and taking in account Testi et al. (2004) we can conclude that, from oscillations in H/LE, water stress was more intense in 2012 and 2010 than in 2011. This is in agreement with the observations of Paço et al. (2014) that reported, for the same region, shorter periods of trees water stress (quantified by Ks from modelling) in 2011 (DOY's 217–241 and DOY's 262–296) than in 2012 (DOY's 131–242, hydrological drought year), for an orchard in comparable climatic conditions but with slightly lower LAI but higher ground cover. They also report trees water stress in 2011 less intense, as modelled Ks reached 0.55 in 2011 and 0.3 in 2012.

The hourly values of the relationship G/Rn (Fig. 3b) were around 20% at noon by the solstice period. As for the daily totals, for the summer periods of 2010–2011 the total daily sensible heat to the soil ranges between zero and a maximum of 8% of the total net radiation, being similar to the values in López-Olivari et al. (2016) that report a range from 0.6 to 0.2 from December to March. Consequently, the simplification of taking as approximately zero the total daily G is not appropriate in this case (summer), as the average G was clearly distinct from zero, a fact that needs consideration when using direct modelling approaches.

3.3. Evapotranspiration components and relation to ETo

The values obtained for ET are separated into Tr and Es. Both will be compared to ETo, corresponding Tr/ETo to the product of Kcb and Ks. Es was estimated with a model (Tezza, 2013) calibrated on local lysimeter measurements (taking into account the combination of sunny – dry and wet – and shaded – dry and wet – areas) using the same approach as Bonachela et al. (1999). During summer time Es in our orchard (Fig. 4 and Fig. 5a), varied generically between 0.2 mm day^{-1} and 1.5 mm day^{-1} being 0.7 mm day^{-1} on average. During the warmer period (August), the ratio Es/ETo was between 0.10 and 0.17 for 2011 and 2012, with exception of 2010, where Es/ETo was between 0.11 and 0.28. Data analysis shows that an area larger than the exposed wet area contributed significantly to direct evaporation (Tezza, 2013). Our data fit to the ranges observed by Bonachela et al. (1999), at a weed-free olive orchard, who obtained an average seasonal Es of 286 mm, which represented around one third of the estimated olive ET and about 50% of the average seasonal rainfall of the area (Córdoba, Spain).

Sap flux density measured with *Granier* method were regressed against $ET_{EC} - Es = Tr_{EC}$, following the approach described in Ferreira et al. (2004), as described in Section 2.11. Due to the fact that these relationships were established directly between sap flow densities and fluxes, they obviously accommodate not only any shift due to uneven radial profile and other aspects that interfere in the proposed calibration relationship (Granier et al., 1985) but also any changes in sapwood area, dependant on trunk cross section area. Slightly different relationships were obtained for the three years, which were found to be due to the irregular trunk growth observed. These could be converted into the same relationship (Fig. 5b) when normalising taking into account the irregular trunk growth, during that period. These locally adjusted relationships were used to calculate seasonal time series of Tr, from the measured sap flow density data.

The seasonal time course of daily Tr at the main plot from mid-June 2010 to early November 2012 is displayed for comparison with the incomplete time series (i.e. with missing data) of the values used as reference (ET_{EC}-Es), showing for Tr a sinusoidal pattern similar to ETo with its maximal in summer, as is typical for an irrigated

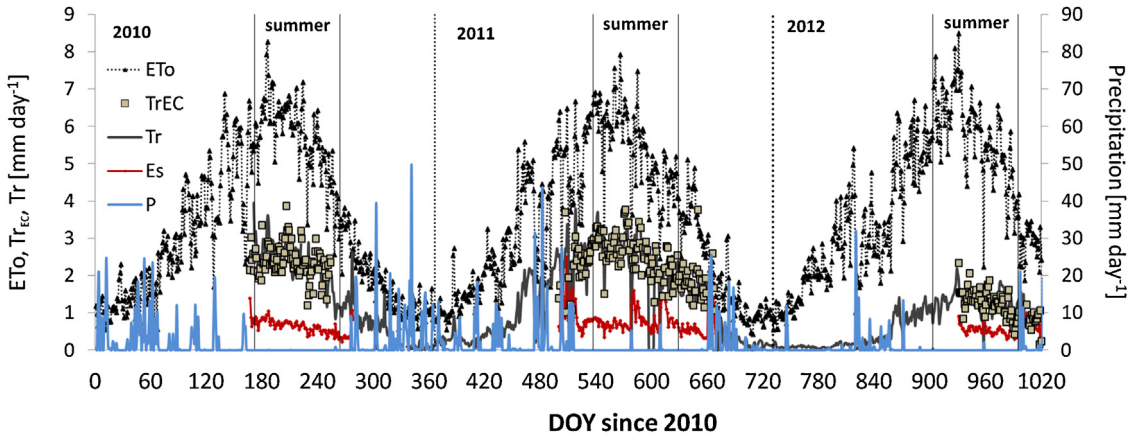

Fig. 4. – Seasonal time course of transpiration (Tr) calculated from sap flow measurements using the local adjusted function (line), Tr as ET_{EC}-Es (small squares) and Es, together with P (bars), and ETo, for interpretation.

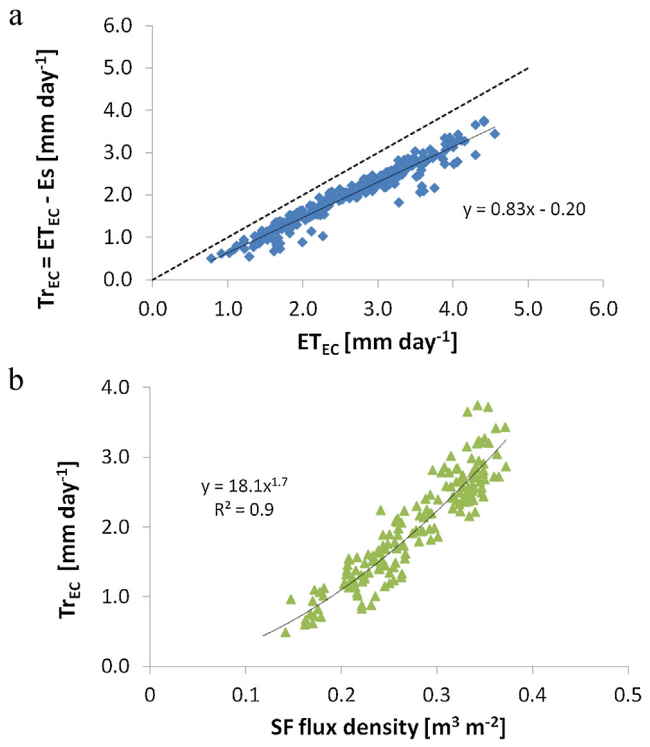

Fig. 5. – Transpiration (Tr_{EC}), obtained as the difference between measured ET (EC method, ET_{EC}) and Es, versus: (a) ET_{EC} and (b) sap flow density data, for 2010, 2011 and 2012. In the following, Tr_{EC} will be designated simply as Tr. The distance of the regression line shown in (a) to the line 1:1 provides approximately the range of Es.

crop. This pattern is also different than what is generally found in these conditions for rainfed crops, where an asymmetrical trend in relation to maximum ETo is generally observed due to increasing water stress (Ferreira et al., 2012a, 2012b; Conceição et al., 2017). Average monthly Tr values (mm day^{-1}) were 2.7, 2.8, 1.1 (June); 2.7, 2.8, 1.5 (July); 2.4, 2.7, 1.2 (August) for 2010, 2011 and 2012 respectively.

Observing the overlay of the Tr/ETo seasonal time series (3 years, Fig. 6), the influence of the special winter drought 2012, when soil water content did not reach field capacity (Fig. 7), as discussed below, is clearly visible, in spite of much higher irrigation volumes then in other years (Fig. 1). The limitations of the water delivery system, either external or at plot level, or other reasons may have limited the possibility to apply more water. In general, Tr/ETo is unstable. This instability is most likely partly due to inter-daily variations in ETo, because usually a tendency for lower values of Tr/ETo is observed when ETo is higher (e.g. Ferreira et al., 2017). On average, during 2011, Tr/ETo generally ranged between 0.1–0.3 during mid/late winter, when approaching the so-called mid-summer or solstice (DOY 172), increased to a platform between 0.4 and 0.6, but with irregular values and a slight decreasing slope. Then Tr/ETo started to decrease to winter values, after the end of October (DOY 304) but a slight temporary increase can be observed after the first autumn rains (late October), suggesting that water stress was limiting Tr. For 2010, after the start of the measurements (DOY 171), the values were similar. The year 2012 was an exception till first autumn rains, with Tr/ETo clearly bellow the values observed for the two other hydrological years, for which P was closer to the average 30-years. Even after a few rainy periods in late spring 2012, Tr/ETo was roughly one half of the normal expected range. A reduction in Tr for 2012, comparatively to 2011 was also observed by Paço et al. (2014). In summary, measured Tr/ETo (from June to August) was roughly around 0.4 but close to 0.2 in 2012.

These values (Fig. 6) correspond to Kcb × Ks (dual Kc approach model terminology, as Ks is applied only to Tr component), but in order to separate these two coefficients, an analysis of plant water status is necessary in order to quantify Ks values.

3.4. Soil and plant water status

We aim at discriminating the two coefficients Kcb and Ks that correspond to different mechanisms and should always be considered separately for modelling and for interpretation of ET or Tr. This is achieved after a first step of analysing soil and plant water status (this section), then using one variable for a relationship with Ks, which is used to derive Ks seasonal course (Section 3.5) in order to extract Kcb values (Section 3.6).

In all the observed soil depths, soil water content was systematically lower closer to the trees (Fig. 7), being this expected during the irrigation season but less expected during the rainy seasons (autumn to spring). However, the interpretation of these values has to take into account the different properties of the soil in both locations, due to the presence of roots. Again it is clear that during the dry year 2012, mainly for the winter, the soil could not reach field capacity while, in a regular year, P is largely enough to bring the soil to field water capacity, as observed by Conceição et al. (2017). We can assume that in between the rows the soil was extremely dry during summer (2012), which could have had an impact in plants behaviour during that year, as discussed later.

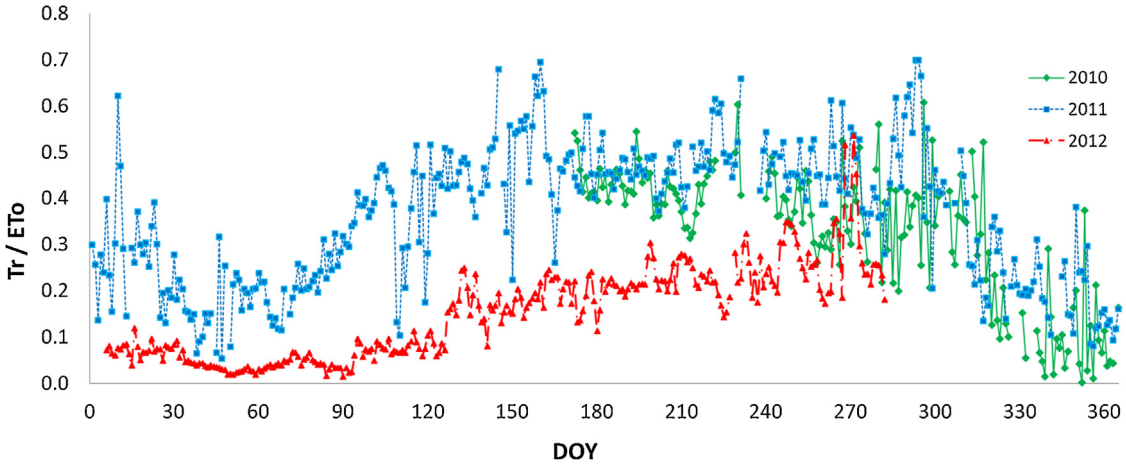

Fig. 6. – Seasonal time course of the ratio Tr/ETo = Kcb × Ks for 2010, 2011 and 2012.

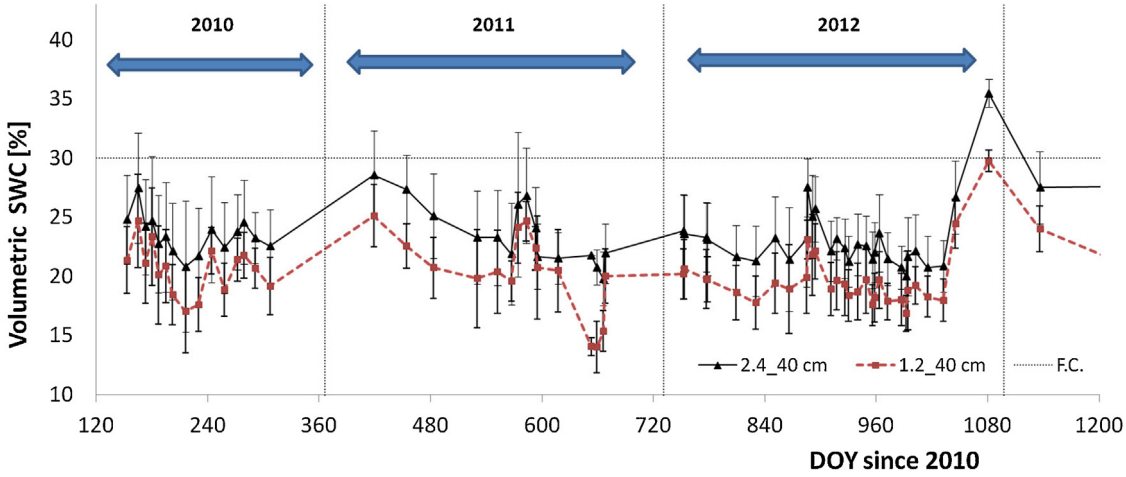

Fig. 7. – Volumetric soil water content (SWC) measured with neutron probe at a depth of 40 cm, near the trees (1.2 m) and in between (2.4 m), both positions in the trees and drippers line (6 access tubes each), from May 2010 to January 2013. The years are indicated by the arrows. During the winter 2012 (January to March 2012), SWC never arrived near field capacity, indicated by the horizontal line (at 0.295 m^3 m^{-3}).

Some daily courses of leaf water potential were performed together with noon stem water potential, in order to select a water stress variable and relate it to relative transpiration, defined in Section 3.5. During the stress cycles performed, comparing the values measured in both very well irrigated and stressed plots, at predawn and respective leaf and stem minimums usually observed about one hour after solar noon, we conclude that differences between treatments were sharper at predawn. For instance, Fernandes-Silva et al. (2016) concluded that 'Cobrançosa' olive trees have near-isohydric behaviour. Férnandez et al. (2011) studied the water relations of 39 year old olive trees ('Manzanilla') during all dry season and they observed a near-isohydric behaviour as deficit drip irrigated trees showed much lower stomatal conductance than full irrigated trees. For those reasons and for practical convenience, the variable selected in this study, for this specific purpose of the plant water status follow-up, was Ψ_{pd}.

The seasonal course of Ψ_{pd} (early spring, DOY 78, to early autumn, DOY 303) was different for the three years considered (Fig. 8a) and showed some fluctuations mainly as a consequence of variations in irrigation volumes (Fig. 1), contrasting with the steady decreasing pattern, when no rainfall occurs, observed in rainfed conditions (Conceição et al., 2017). Generally Ψ_{pd} values were above – 0.5 MPa in late winter to early spring (DOY 166, 2012 was an exception, as in January and February there was no rainfall) and decreased during the summer (June to early September) with a variable pattern defined by the available water in soil and the climatic demand of previous day. In general, the lowest Ψ_{pd} values were observed just before the first autumn rains (September/October). During 2010, Ψ_{pd} ranged between about – 0.5 MPa in late June (DOY 177) to – 0.8 MPa in early August (DOY 217). During 2011, Ψ_{pd} was also – 0.5 MPa in late-June (DOY 176) and reached the minimum by the end of October (- 1 MPa, DOY 294) but during 2012, as a consequence of the winter drought, Ψ_{pd} was – 0.5 MPa in mid-March (DOY 78), finally increasing after first Spring rains (DOY 92) and then between early June (DOY 161) and mid-September (DOY 250), Ψ_{pd} ranged between – 0.5 MPa and – 1 MPa.

These values are similar to the ones observed and reported (including literature review) by Fernandes-Silva et al. (2016): mid-summer Ψ_{pd} ranging from – 0.4 MPa to – 0.7 MPa for well irrigated trees, and from –1.2 MPa to – 6.0 MPa in rainfed conditions. Férnandez et al. (1993) measured Ψ_{pd} between May and middle September (1988) in two plots (olive orchard 7 × 7 m spacing with 20-year-old trees 'Manzanillo'; sandy loam soil with 2 m depth), one dry-farmed (rain prevented to infiltrate during the experimental observations) and another drip irrigated (pan coefficient of 0.4). They measured Ψ_{pd} of –0.15 MPa and – 0.36 MPa in early May; from July until September increasing differences between plots were observed for Ψ_{pd}, in September reaching –0.26 MPa and –

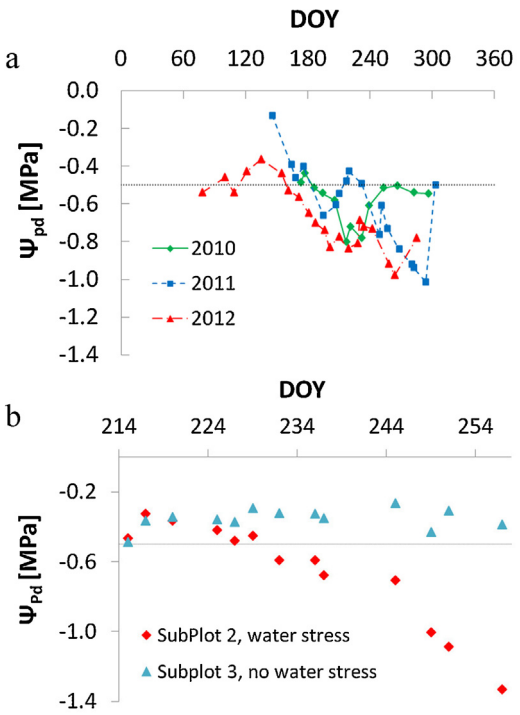

Fig. 8. – Predawn leaf water potential (Ψ_{pd}) (a) seasonal time course in the main plot (10 ha) and (b) for the well irrigated subplot (squares) and not irrigated subplot progressively water stressed (triangles) during a stress cycle (see section 2.12).

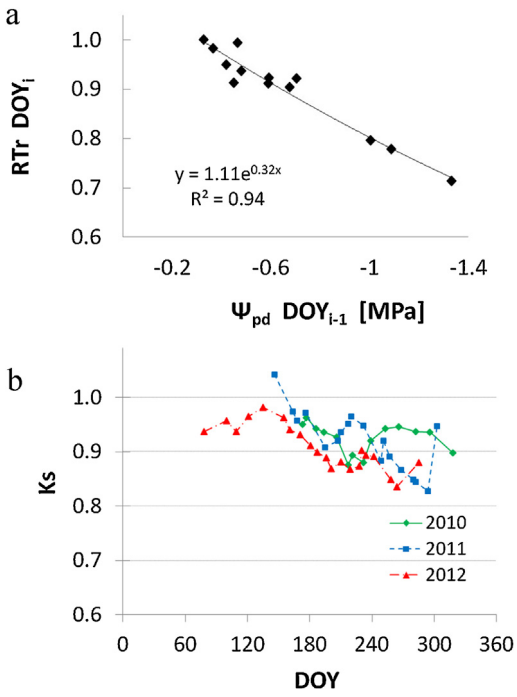

Fig. 9. – Relative transpiration (a) versus Ψ_{pd} during the all stress cycle (2011); and (b) stress coefficients (Ks) estimated using the mathematical function Ks versus Ψ_{pd} derived from the stress cycle, considering only the days with Ψ_{pd} measurements on the main plot (2010–2012).

0.53 MPa in irrigated and rainfed, respectively. For our situation Ψ_{pd} was similar in May, but during the summer even our trees under (deficit) irrigation reached lower values than those observed by Fernández et al. (1993) in the rainfed plot, which let us suppose that irrigation in that case was not as limited as here.

Dichio et al. (2003), for two-year-old own-rooted olive trees ('Coratina') grown outdoors in 18 L pots used Ψ_{pd} to separate plant water status in categories as follows: thresholds of – 0.45 MPa, – 1.6 MPa, – 3.3 MPa, and – 5.2 MPa for no-stress, low-stress, medium-stress, high-stress, respectively. They found that high-stressed trees (Ψ_{pd} = – 6.0 MPa) can use soil water until matric potential as low as – 2.5 MPa and midday leaf water potential could achieve values as lower as – 6.5 MPa. According to those and Fernandes-Silva (2008) thresholds for classifying the water stress, these deficit irrigated trees were in low, approaching medium stress, by the end of summer.

As a consequence, it was not surprising that the values of Tr/ETo (Fig. 6) apart from some correspondence with the general trends observed for Ψ_{pd} after first autumn rains, in general did not exhibit any clear decrease, along the season. These results suggest that any slight decrease of Ψ_{pd} along the period shown (after DOY 150) did not reduce much Tr. This discussion will be developed when analysing Ks values obtained from Ψ_{pd} in the following.

3.5. Relationship between predawn leaf water potential and relative transpiration

The full description of the stress indicators analyzed during stress cycles is out of the scope of this paper but some elements about the relationship between relative transpiration ($RTr = Tr_{plot2}/Tr_{plot3}$) and Ψ_{pd} will be explained, as this relationship is used to discriminate Kcb from Ks in Tr/ETo. For the first stress cycle (from August 3, DOY 215 to September 15, DOY 258), Ψ_{pd} decreased to about –1.3 MPa in plot 2, while remaining relatively stable, at high values in plot 3 (Fig. 8b). After using the method described in Section 2.11 for correcting Tr values, a normalization was performed to take into account any possible shift due to the small sampling. We mean that Tr stressed plot (plot 2)/Tr well irrigated plot (plot 3) should be forced to one at the start of the stress cycle. In fact this would be true, even without forcing, if the sampling was large enough but six trees is a small sample concerning the usual variability in between trees and in between azimuths within a tree (Nadezhdina et al., 2007; López-Bernal et al., 2010). The values of normalized Tr from both plots were related, allowing to calculate RTr. Due to daily and abundant irrigation provided to plot 3, where Ψ_{pd} was at all times above – 0.5 MPa (Fig. 8b), one could assume these RTr values equal Ks. The values obtained were related to Ψ_{pd} for plot 2 (details in Ferreira et al., 2012a, 2012b), and a relationship was derived to estimate Ks from Ψ_{pd} showing that, for RTr close to 0.75, Ψ_{pd} was – 1.3 MPa (Fig. 9a).

Hence, this relationship was used, trying to estimate any possible Ks below unity, in the long term (Fig. 9b), from Ψ_{pd} in the main plot (Fig. 8a). The fact that a relationship obtained during a stress cycle, relatively short in relation to the whole summer, is used for such a long period, when plants had time to adapt to progressive stress can be questionable. Notwithstanding, that risk is reduced as the duration necessary to observe some clear decrease in Ψ_{pd} was as long as six weeks, about one half the summer period.

According to this approach, for 2010 Ks decreased slightly from 1 till 0.9, while for 2011 and 2012 it decreased till 0.83 (Fig. 9b). During 2012, Ks started to decrease below unity already in Spring, earlier then in the other years, due to winter drought. All together, these are small reductions, associated with a very moderate stress, according to literature and to plant water status. As stated by Tognetti et al. (2004) olive trees are sparing users of soil water, maintaining significant gas exchange and Tr levels, even during drought stress.

Finally, about the irrigation practices by the farmer, these results show that the farmer used always DI saving significant amounts of water, mainly as the summer progresses, as in many other

cases reported, with interesting profitability (Egeaa et al., 2017; Fernandez et al., 2016). The relationship between water applied and water used is out of the scope of this discussion and will be the aim of another contribution. However, in the particular situation of 2012, even if the farmer applied more water than in other years (230 mm versus 150 mm), Kcb × Ks was severely reduced. Either the limitations in water availability or of the conveyance system may had limited an application of even higher irrigation volumes, to compensate for the 2012 winter drought. The water scarcity observed in 2012 can be seen as an example where conflicts may arise in water limited regions between different anthropogenic water demanding activities where, as discussed by David et al. (2016), decision-making should always be based on a good scientific perception about involved possible conflicts and trade-offs but also on the underlying physical mechanisms.

3.6. Basal crop coefficients

Using the Ks values in Fig. 9b, ETo and Tr time series, the values for Kcb were estimated as Tr/(ETo × Ks), where Ks was obtained from the values of main plot Ψ_{pd} displayed in Fig. 8a. The results were slightly different from year to year. The following Kcb values were obtained, for the days with Ψ_{pd} measurements (shown in Fig. 8a), before autumn rain started: 0.37 ± 0.07 (n = 11), 0.42 ± 0.09 (n = 16) and 0.28 ± 0.08 (n = 12) for 2010, 2011 and 2012, respectively. We need to consider that water stress affecting significantly only the last part of summer, implicates that the difference between Tr observed and maximal Tr (for comfort) is almost diluted by the scattering observed in Kcb variations, when looking at the evolution of all the data series.

The fact that Kcb is lower for 2012 can eventually be related to the special drought which occurred but the causes of such impact in Tr are not clear, even if water stress was more intense and consequently Kcb × Ks measured was lower than for 2010 and 2011. The fact that, from autumn 2011 to autumn 2012, there was a reduction in trunk growth (in relation to other years) raises the hypothesis of a possible reduction in trunk and stems hydraulic conductivity (Fernández et al., 2001).

Another possibility (Kcb lower for 2012, in spite of trees growth) could be related to the fact that in between the rows the soil was extremely dry in the whole profile, during the summer 2012. If considering that the roots have access to water from irrigation but that some of them were in very dry soil, a stomatal closure could have been induced by the known mechanisms related to the abscisic acid (ABA), that are put at the profit of the farmer, when deficit irrigation is made using a partial root drying system (Fernández et al., 2003). Zhang et al. (2011) discuss the importance of this mechanism in olive trees. One could argue that, every summer, part of the soil in between the trees row is dry, which is true but especially for the upper soil layers. There are two indications that this is not true for other layers, even in between lines: on one side, the discrete hydraulic redistribution observed in this irrigated orchard between the roots in the direction of the lines and those going to the space in-between (Nadezhdina et al., 2012), that allows to keep alive the roots exploring this area and, on the other side, the fact that some soil evaporation occurs in summer in-between the lines, even with the soil surface apparently very dry. For such a severe drought, those roots in-between lines were in a much drier soil than usually during a summer of a regular hydrological year. They could have induced such an important stomatal closure reducing Tr (as is commonly expected in PRD) independently from the values of Ψ_{pd} being not so low.

In such conditions, the relationship used between Ψ_{pd} and Ks is not appropriate as it does not reflect that very particular situation. Ks estimated from Ψ_{pd} can indeed be questionable in case this indicator, used as a surrogate of soil water status, does not fully represent the observed reduction in Tr. A limitation to its use, when part of the root system is in drier soil than they used to, was described by many authors since first studies on ABA impact on stomatal closure, in the 80's. However, the lack of good alternatives in this case and the fact that water redistribution was observed in these irrigated plants (Nadezhdina et al., 2012) justifies the use of Ψ_{pd}.

3.7. Dual source crop coefficient model

Following Allen and Pereira (2009) Kcb adjusted (Kcb_{adj}) was calculated for this orchard, for June, July and August (2010 and 2012), roughly corresponding to the mid-season period (Table 5). Density reduction factor (Kd) was calculated using the multiplier factor (ML) equal to 1.5. In the calculations of basal Kc during peak plant growth, for conditions having LAI equal or greater than 3 (Kcb_{full}), a reduction factor was used to take into account a higher stomatal control than annual crops (Fr), equal to 0.48 as stated in Allen and Pereira (2009) for olives with no vegetation below canopies. The minimum basal Kc for bare soil (Kc_{min}) considered was 0.15 (Allen and Pereira, 2009; Fandiño et al., 2012). The other variables used are listed, as well as the resulting Kcb_{adj} values. Calculated Kcb_{adj} values ranged between 0.26 and 0.34 as a function of the trees height, ground cover, time of the year (effect of mean solar angle on effective fraction of ground cover or area shaded by vegetation near solar noon, fc_{eff}), monthly mean wind velocity and monthly mean minimum RH. Average (June to August) calculated Kcb_{adj} are 0.27 and 0.33 for 2010 and 2012, respectively, when ground cover was measured. These values are consistent with the Kcb value for the mid-season tabled by Allen and Pereira (2009) for olive tree orchards without understorey vegetation, with fc_{eff} of 0.25, which is 0.35 (RH = 45%, U = 2 m/s, h = 3 m, ML = 1.5, Fr = 0.48).

Assuming the function shown in Fig. 9a as valid for 2010, estimated values from the model (0.3) here described (using fc) were lower than measured (0.4) for 2010. Paço et al. (2014) for a super-intensive orchard with fc of 0.35 ('Arbequina') found ML = 1.7. We hypothesize that in our conditions for 2010, the parameter ML that is a multiplier on fc_{eff} attempting to translate the physical limits imposed on water flux through the plant root, stems and leaf systems, expected to range from 1.5 to 2.0 (Allen and Pereira, 2009) was higher than 1.5 for 2010.

4. Conclusions

This 3-year experiment (spring 2010 and autumn 2012) on the water use of an irrigated intensive olive orchard in southern Portugal allowed the quantification and a comparative analysis of ET, Tr, plant and soil water status. It included a severe drought by lack of rainfall in winter 2012, during which the observed soil profile (until 1.2 m depth) did not reach field capacity, a very unusual situation. As far as we know, this is the first study obtaining such long term data on Tr and Es and also discriminating Kcb from Ks, in olive trees, using the heat dissipation method (or any other sap flow method) combined with eddy covariance and microlysimeters, in deficit irrigation conditions.

Plant water status was quantified by Ψ_{pd}, as this cultivar showed near-isohydric behaviour; it fluctuated mainly as a result of variations in irrigation depths relative to soil water storage, due to highly variable winter precipitation, being the minimum observed values of − 0.8 MPa in 2010 (august) and −1 MPa in 2011 and 2012, before the first autumn rains. From this water status indicator, the trees water status can be classified in general in the range low to medium stress.

A relationship was derived to estimate Ks from Ψ_{pd} data. From this equation, for −1.3 MPa (low to medium water stress) Tr reduc-

Table 5
Data for basal crop coefficient (Kcb) estimation according to Allen and Pereira (2009). fc_{eff}, fraction of ground surface covered or shaded by vegetation near solar noon.; U, mean wind velocity at 2 m height; RH, relative humidity; fc, fraction of ground surface covered or shaded by vegetation (canopy vertical projection); h, height of the trees; ML, multiplier factor on fc_{eff}; Kc_{min}, minimum basal crop coefficient for bare soil; Fr, reduction factor; Kd, density factor; Kcb_{full}, Kcb for LAI greater or equal 3; Kcb_{adj}, adjusted Kcb.

Date	U [m/s]	RH [%]	fc	h [m]	ML	Kc_{min}	Fr	fc_{eff}	Kd	Kcb_{full}	Kcb_{adj}
June, 2010	1.5	35.0	0.17	3.2	1.5	0.15	0.48	0.18	0.26	0.59	0.26
July, 2010	1.7	26.2	0.17	3.2	1.5	0.15	0.48	0.18	0.27	0.61	0.27
August, 2010	1.4	25.6	0.17	3.2	1.5	0.15	0.48	0.19	0.28	0.60	0.28
June, 2012	1.8	34.2	0.25	3.5	1.5	0.15	0.48	0.26	0.39	0.59	0.32
July, 2012	1.9	27.6	0.25	3.5	1.5	0.15	0.48	0.26	0.39	0.61	0.33
August, 2012	1.6	30.3	0.25	3.5	1.5	0.15	0.48	0.26	0.42	0.60	0.34

tion (1-relative Tr) was about 15%. Assuming such relationship, and relative Tr as a surrogate of Ks, seasonal values were derived: estimated Ks reached 0.9 in 2010, and 0.83 in 2011 and 2012, corresponding to a reduction in Tr between 10% and 15% relative to the reference plot in comfort. These values allowed the quantification of Kcb, which were compared with literature and a simple model.

For the mid-season period (nearly to June to August) ETo varied between 4 and 8 mm/day. Evaporation coefficient (Ke = Es/ETo) for 2010–2011 (summer period) was on average 0.11. For 2010 and 2011 (June to August) Tr ranged from 2 to 4 mm/day, being on average 2.7 mm/day and calculated Kcb (=Tr/ETo) were respectively 0.37 and 0.42. For the same period of 2012, Tr ranged from 1 to 2 mm/day, being on average 1.3 mm/day and the calculated Kcb was 0.28, lower than the values observed for 2010 and 2011.

This reduction on Tr during the special year of 2012 cannot be explained only by tree water status as quantified by Ψ_{pd}; we hypothesize that plants reacted to the extremely dry conditions of air and of the large area of soil not wetted by irrigation or precipitation during that special year closing stomata, this contributing to explain such a reduction in Tr, independently of its leaf water status at predawn.

Estimated Kcb from the dual source model according to Allen and Pereira (2009), using ground cover as input variable, were (June to August) 0.3 for 2010, lower than Kcb observed (0.4). For 2012 modelled Kcb was comparable to the observed value.

Results achieved within this study provide relevant information on the water relations of olive tree orchards, useful for precision irrigation management and planning, namely under deficit irrigation and when recurrent droughts are observed. They are also necessary to calibrate and validate ground based or remote sensing based, multi-compartment models. Focusing on specific irrigation scheduling issues, Kcb and Ks coefficients are necessary to determine irrigation volumes when using models. Besides, the relationship between a well selected water stress indicator and Ks allows the use of a self-learning process, when combining water status follow-up with ET modelling, a step that is necessary to adjust the model parameters, due to the multiple model uncertainties.

Authors' contributions

The authors' contribution to this research and manuscript were in experimental design: M.I.F., C.A.P., N.C.; instruments installation: N.C., M.I.F., C.A.P.; data collection: N.C., L.T., M.H., S.L., M.I.F.; data processing: N.C., M.I.F., L.T., M.H., C.A.P.; manuscript preparing: N.C., M.I.F., M.H., L.T., S.L.

Acknowledgements

The authors are very thankful to the participating graduates and master students (no automatic measurements) Soroor Amindezfooli, Berta Cumbane, José Miguel Gama, Sonia Surgy and Ondina Miguel; to COTR (www.cotr.pt) for providing meteorological daily data and for collaboration with the soil water content measurements (2010 and 2011); to the owners and to the workers of the farm Monte do Pardieiro (Agricola Alentejo, SA., Mr. Pereira and collaborators).

The experiments were co-financed by European Union through the project TELERIEG (SOE1/P2/E082) and by Fundação para a Ciência e Tecnologia (FCT, Portugal) through the project WUSSIAAME (Water Use, Survival Strategies and Impact of Agrochemicals in Agricultural Mediterranean Ecosystems,PTDC/AACAMB/100635/2008). FCT also financed the fellowships SFRH/BD/66967/2009 and PD/BD/52698/2014.

References

Abdel-Rahman, A.A., El-Sharkawi, H.M., 1974. Response of olive and almond orchards to partial irrigation under dry-Farming practices in semi-Arid regions: II. plant-Soil water relations in olive during the growing season. Plant Soil 31, 13–31.

Allen, R.G., Pereira, L.S., 2009. Estimating crop coefficients from fraction of ground cover and height. Irrig. Sci. 28 (1), 17–34, http://dx.doi.org/10.1007/s00271-009-0182-z.

Allen, R.G., Pereira, L.S., Raes, D., Smith, M., 1998. Crop Evapotranspiration Guidelines for Computing Crop Water Requirements. FAO Irrigation and Drainage Paper 56. FAO, Rome, Italy, http://dx.doi.org/10.1016/j.eja.2010.12.001.

Allen, R.G., Tassumi, M., Trezza, R., 2007. Satellite-Based energy balance for mapping evapotranspiration with internalized calibration (METRIC) — model. J. Irrig. Drain. Eng. 133, 380–394.

Bacelar, E.A., Moutinho-Pereira, J.M., Gonçalves, B.C., Ferreira, H.F., Correia, C.M., 2007. Changes in growth, gas exchange, xylem hydraulic properties and water use efficiency of three olive cultivars under contrasting water availability regimes. Environ. Exp. Bot. 60 (2), 183–192, http://dx.doi.org/10.1016/j.envexpbot.2006.10.003.

Bastiaanssen, W.G.M., Pelgrum, H., Wang, J., Ma, Y., Moreno, J.F., Roerink, G.J., Van der Wal, T., 1998. A remote sensing surface energy balance algorithm for land (SEBAL). 2. validation. J. Hydrol. 3 (6), 511–519, http://dx.doi.org/10.1016/s0022-1694(98)00254-6.

Berbigier, R., Bonnefond, J.M., Loustau, D., Ferreira, M.I., David, J.S., Pereira, J.S., 1996. Transpiration of a 64-year old maritime pine stand in Portugal. 2. Evapotranspiration and stomatal conductance of a maritime pine stand measured by an eddy covariance technique. Oecologia 107, 43–52.

Bonachela, S., Orgaz, F., Villalobos, F.J., Fereres, E., 1999. Measurement and simulation of evaporation from soil in olive orchards. Irrig. Sci. 18 (4), 205–211, http://dx.doi.org/10.1007/s002710050064.

Bowen, I.S., 1926. The ratio of heat losses by conduction and by evaporation from any water surface. The American Physical Society. Phys. Rev. (Series I) 27 (6), 779–787, http://dx.doi.org/10.1103/PhysRev.27.77.

COTR, 2016. SAGRA project, agro-meteorological system for irrigation scheduling in Alentejo (in Portuguese: Sistema Agrometeorológico para a Gestão da Rega no Alentejo). Centro Operativo e de Tecnologia de Regadio. http://www.cotr.pt/cotr/sagra.asp (Accessed 1 November 2016).

Campos, I., Neale, C.M.U., Calera, A., Balbontín, C., González-Piqueras, J., 2010. Assessing satellite-Based basal crop coefficients for irrigated grapes (Vitis vinifera L.). Agric. Water Manage. 98 (1), 45–54, http://dx.doi.org/10.1016/j.agwat.2010.07.011.

Clearwater, M.J., Meinzer, F.C., Andrade, J.L., Goldstein, G., Holbrook, N.M., 1999. Potential errors in measurement of nonuniform sap flow using heat dissipation probes. Tree Physiol. 19, 681–687, http://dx.doi.org/10.1093/treephys/19.10.681.

Conceição, N., Häusler, M., Lourenço, S., Pacheco, C., Ferreira, M.I., Tezza, L., 2017. Evapotranspiration measured in a traditional rainfed and an irrigated intensive olive orchard during a year of hydrological drought. Acta Hortic. 1150, 281–288.

Daamen, C.C., Simmonds, J.S., Wallace, J.S., Laryea, K.B., Sivakumar, M.V.K., 1993. Use of microlysimeters to measure evaporation from sandy soils. Agric. For. Meteorol. 65, 159–173, http://dx.doi.org/10.1016/0168-1923(93)90002-Y.
David, T.S., Pinto, C.A., Nadezhdina, N., David, J.S., 2016. Water and forests in the Mediterranean hot climate zone: a review based on a hydraulic interpretation of tree functioning. For. Syst. 25 (2), eR02 (ISSN 2171-9845).
Davis, T.W., Kuo, C., Liang, X., Yu, P., 2012. Sap flow sensors: construction, quality control and comparison. Sensors 12, 954–971, http://dx.doi.org/10.3390/s120100954.
Dichio, B., Xiloyannis, C., Angelopoulos, K., Nuzzo, V., Bufo, S.A., Celano, G., 2003. Drought-Induced variations of water relations parameters in Olea europaea. Plant Soil 257 (2), 381–389, http://dx.doi.org/10.1023/A:1027392831483.
Dixon, H.H., 1914. Transpiration and the Ascent of Sap in Plants. Macmillon and Co., Ltd, London, https://doi.org/10.5962%2Fbhl.title.44194.
Doorenbos, J., Pruitt, W.O., 1977. Guidelines for Predicting Crop Water Requirements. FAO Irrigation and Drainage Paper 24, 2nd ed. FAO, Rome, Italy.
Egeaa, G., Fernández, J.E., Alconc, F., 2017. Financial assessment of adopting irrigation technology for plant-based regulated deficit irrigation scheduling in super high-density olive orchards. Agric. Water Manage. 187, 47–56.
Evett, S.R., Schwartz, R.C., Tolk, J.A., Howell, T.A., 2009. Soil profile water content determination: spatiotemporal variability of electromagnetic and neutron probe sensors in access tubes. Vadose Zone J. 8 (4), 926, http://dx.doi.org/10.2136/vzj2008.0146 (Soil Science Society of America).
FAO-UNESCO, 2006. IUSS Working Group WRB. World Reference Base for Soil Resources 2006. World Soil Resources Reports No. 103. FAO, Rome, Italy, http://dx.doi.org/10.1017/S0014479706394902.
Fandiño, M., Cancela, J.J., Rey, B.J., Martínez, E.M., Rosa, R.G., Pereira, L.S., 2012. Using the dual-Kc approach to model evapotranspiration of albariño vineyards (Vitis vinifera L. cv albariño) with consideration of active ground cover. Agric. Water Manage. 112, 75–87.
Fernández, J.E., Moreno, F., Martín-Aranda, J., 1993. Water status of olive trees under dry-farming and drip-irrigation. Acta Hortic. 335, 157–164.
Fernández, J.E., Moreno, F., Girón, I.F., Blázquez, O.M., 1997. Stomatal control of water use in olive tree leaves. Plant Soil 190, 179–192.
Fernández, J.E., Palomo, M.J., Díaz-Espejo, A., Clothier, B.E., Green, S.R., Girón, I.F., Moreno, F., 2001. Heat-Pulse measurements of sap flow in olives for automating irrigation: tests, root flow and diagnostics of water stress. Agric. Water Manage. 51 (2), 99–123, http://dx.doi.org/10.1016/S0378-3774(01)00119-6.
Fernández, J.E., Palomo, M.J., Díaz-Espejo, A., Girón, I.F., 2003. Influence of Partial Soil Wetting on Water Relation Parameters of the Olive Tree, 23., pp. 545–552, http://dx.doi.org/10.1051/agro.
Fernández, J.E., Green, S.R., Caspari, H.W., Diaz-Espejo, A., Cuevas, M.V., 2008. The use of sap flow measurements for scheduling irrigation in olive, apple and asian pear trees and in grapevines. Plant Soil 305, 91–104.
Fernández, J.E., Ruiz-Torres, J.M., Martin-Palomo, M.J., 2011. Influence of the soil water content and distribution on both the hydraulic and transpiration of 'Manzanilla' olive trees. Acta Hortic. 889, 323–330.
Fernández, J.E., 2014. Understanding olive adaptation to abiotic stresses as a tool to increase crop performance. Environ. Exp. Bot. 103, 158–179, http://dx.doi.org/10.1016/j.envexpbot.2013.12.003.
Fernandes-Silva, A.A., Ferreira, T.C., Correia, C.M., Malheiro, A.C., Villalobos, F.J., 2010. Influence of different irrigation regimes on crop yield and water use efficiency of olive. Plant Soil 333 (1), 35–47, http://dx.doi.org/10.1007/s11104-010-0294-5.
Fernandes-Silva, A.A., López-Bernal, A., Ferreira, T.C., Villalobos, F.J., 2016. Leaf water relations and gas exchange response to water deficit of Olive (Cv Cobrançosa) in field grown conditions in Portugal. Plant Soil 402 (1-2), 191–209, http://dx.doi.org/10.1007/s11104-015-2786-9.
Fernandes-Silva, A.A.F., 2008. Necessidades Hídricas e Resposta da Oliveira (Olea Europaea L.) ao Deficit Hídrico Na Região da Terra Quente. Universidade de Trás-os-Montes e Alto Douro, Vila Real, Portugal.
Ferreira, M.I., Valancogne, C., 1997. Experimental study of a stress coefficient: application on a simple model for irrigation scheduling and daily evapotranspiration estimation. In: Farkas, I. (Ed.), Proc. 2nd Intern. Symp. on Mathemathical Modelling and Simulation in Agricultural and Bio-Industries. Maio 1997, Budapeste, Hungria.
Ferreira, M.I., Paço, T.A., Silvestre, J., 2004. Combining techniques to study evapotranspiration in woody crops: application to small areas – two case studies. Acta Hortic. 664, 225–232.
Ferreira, M.I., Paço, T.A., Silvestre, J., Silva, R.M., 2008. Evapotranspiration estimates and water stress indicators for irrigation scheduling in woody plants. In: Sorensen, Magnus L. (Ed.), Agricultural Water Management Research Trends. Nova Science Publishers, Inc, New York, USA, pp. 129–170.
Ferreira, M.I., Silva, A.L., Thomsen, A., 2009. Numerical evaluation of sap flow method. Acta Hortic. 846, 61–68.
Ferreira, M.I., Conceição, N., Pacheco, C.A., Häusler, M., 2012a. Análise de indicadores de desconforto hídrico durante ciclos de stress num olival intensivo no Alentejo. In: Bento, A., Pereira, J.A. (Eds.), VI Simpósio Nacional de Olivicultura. Mirandela, Portugal, pp. 207–216.
Ferreira, M.I., Silvestre, J., Conceição, N., Malheiro, A.C., 2012b. Crop and stress coefficients in rainfed and deficit irrigation vineyards using sap flow techniques. Irrig. Sci. 30 (5), 433–447.
Ferreira, M.I., Conceição, N., Malheiro, A.C., Silvestre, J., Silva, R.M., 2017. Water stress indicators and stress functions to calculate soil water depletion in deficit irrigated grapevine and kiwi. Acta Hortic. 1150, 119–126.
Foken, T., Leuning, R., Oncley, S.P., Mauder, M., Aubinet, M., 2011. Corrections and data quality. In: Aubinet, M., Vesala, T., Papale, D. (Eds.), Eddy Covariance: a Practical Guide to Measurement and Data Analysis. Springer, Berlin, Heidelberg.
Gardner, W., Kirkham, D., 1952. Determination of soil moisture by neutron scattering. Soil Sci. 73 (5), 391–402, http://dx.doi.org/10.1097/00010694-195205000-00007.
Granier, A., 1985. Une nouvelle méthode pour la mesure du flux de sève brute dans le tronc des arbres. Annales des Sciences Forestières 42, 193–200.
Häusler, M., Ferreira, M.I., Conceição, N., 2014. Assessment of vegetation parameters in olive trees in the region of Alentejo: a comparison of direct and indirect methods. Acta Hortic. 1038, 407–414.
INE, I.P., 2015. Agriculture Statistics –2014. Statistics Portugal. Instituto Nacional de Estatística, Lisbon, Portugal (Accessed 1 November 2016) www.ine.pt.
IPMA, 2016. Climate normals 1971-2000 for Beja. Synoptic station number 562, Lat, 38(01(N; Lon. 07 (52 (W, 246 m a.s.l. Instituto Português do Mar e da Atmosfera. http://www.ipma.pt/en/oclima/normais.clima/1971-2000/002/(Accessed 1 November 2016).
Köppen, W., 1936. In: Köppen, W., Geiger, R. (Eds.), Das Geographische System Der Klimate. Handbuch Der Klimatologie, vol. 1. Verlag von Gebrüder Borntraeger, Berlin, pp. 1–44 (Part C) https://www.climond.org/Public/Data/Publications/Koeppen_1936_GeogSysKlim.pdf.
Köstner, B., Granier, A., Cermák, J., 1998. Sap flow measurements in forest stands: methods and uncertainties. Ann. For. Sci. 55 (1–2), 13–27.
Kaimal, J.C., Gaynor, J.E., 1991. Another look at sonic thermometry. Bound-Lay. Meteorol. 56 (4), 401–410, http://dx.doi.org/10.1007/BF00119215.
Kanemasu, E.T., Steiner, J.L., Rasmussen, V.P., Bagley, J., 1979. Estimating Water Requirements for Corn with a Programmable Calculator. Bull 15 (Revised October 1979). Agricult. Experim. Station, Kansas State University, Manhattan, U.S.A.
Kaniewski, D., Campo, E.V., Boiy, T., Terral, J.F., Khadari, B., Besnard, G., 2012. Primary domestication and early uses of the emblematic olive tree: palaeobotanical, historical and molecular evidence from the middle east. Biol. Rev. 87 (4), 885–899, http://dx.doi.org/10.1111/j.1469-185X.2012.00229.x.
Kustas, W.P., 1990. Estimates of evapotranspiration with a one- and two-Layer model of heat transfer over partial canopy cover. J. Appl. Meteorol. 29, 704–715.
López-Bernal, A., Alcántara, E., Testi, L., Villalobos, F.J., 2010. 2010. Spatial sap flow and xylem anatomical characteristics in olive trees under different irrigation regimes. Tree Physiol. 30 (12), 536–1544.
López-Olivari, R., Ortega-Farías, S., Poblete-Echeverría, C., 2016. Partitioning of net radiation and evapotranspiration over a superintensive drip – irrigated olive orchard. Irrig. Sci. 34 (1), 17–31, http://dx.doi.org/10.1007/s00271-015-0484-2.
Liebethal, C., Huwe, B., Foken, T., 2005. Sensitivity analysis for two ground heat flux calculation approaches. Agric. For. Meteorol. 132 (3–4), 253–262, http://dx.doi.org/10.1016/j.agrformet.2005.08.001.
Martínez-Cob, A., Faci, J.M., 2010. Evapotranspiration of an hedge-Pruned olive orchard in a semiarid area of NE Spain. Agric. Water Manage. 97 (3), 410–418, http://dx.doi.org/10.1016/j.agwat.2009.10.013.
Mauder, M., Foken, T., 2015. Eddy-Covariance Software TK3. Bayreuth University https://zenodo.org/record/20349#.Vo-G6FlZa2y.
Monteith, J.L., 1965. Evaporation and environment. the state and movement of water in living organisms. Symposium of the Society of Experimental Biologists 19, 205–235.
Moore, G.W., Bond, B.J., Jones, J.A., Meinzer, F.C., 2010. Thermal-Dissipation sap flow sensors may not yield consistent sap-Flux estimates over multiple years. Trees–Struct. Funct. 24 (1), 165–174, http://dx.doi.org/10.1007/s00468-009-0390-4.
Nadezhdina, N., Nadezhdin, V., Ferreira, M.I., Pitacco, A., 2007. Variability with xylem depth in sap flow in trunks and branches of mature olive trees. Tree Physiol. 27, 105–113.
Nadezhdina, N., David, T.S., David, J.S., Nadezhdina, N., Ferreira, M.I., Conceição, N., Dohnal, M., Tesar, M., Gartner, K., Celemans, R., 2012. Chap. 14 in measuring roots. an updated approach. In: Mancuso, S. (Ed.), Root Function: In Situ Studies Through Sap Flow Research. Springer, pp. 267–290.
Paço, T.A., Conceição, N., Ferreira, M.I., 2004. Measurements and estimates of peach orchard evapotranspiration in mediterranean conditions. Acta Hortic. 664, 505–512.
Paço, T.A., Ferreira, M.I., Conceição, N., 2006. Peach orchard evapotranspiration in a Sandy soil: comparison between eddy covariance measurements and estimates by the FAO 56 approach. Agric. Water Manage. 85 (3), 305–313, http://dx.doi.org/10.1016/j.agwat.2006.05.014.
Paço, T.A., Pôças, I., Cunha, M., Silvestre, J.C., Santos, F.L., Paredes, P., Pereira, L.S., 2014. Evapotranspiration and crop coefficients for a super intensive olive orchard. an application of SIMDualKc and METRIC models using ground and satellite observations. J. Hydrol. 519, 2067–2080, http://dx.doi.org/10.1016/j.jhydrol.2014.09.075.
Paço, T.A., 2003. Modelação Da Evapotranspiração Em Cobertos Descontínuos Programação da Rega em Pomar de Pessegueiro Tese de Doutoramento. Universidade Técnica de Lisboa.
Rana, G., Katerji, N., 2000. Measurement and estimation of actual evapotranspiration in the field under mediterranean climate: a review. Eur. J. Agron. 13, 125–153.

Rana, G., Katerji, N., 2008. Operational model for direct determination of evapotranspiration for well-watered crops in Mediterranean region. Theor Appl. Climatol. 97 (3), 243–253, http://dx.doi.org/10.1007/s00704-008-0062-0.
Ritchie, J.T., 1972. Model for predicting evaporation from a row crop with incomplete cover. Water Resour. Res. 8 (5), 1204–1213, http://dx.doi.org/10.1029/WR008i005p01204.
Sánchez, J.M., Scavone, G., Caselles, V., Valor, E., Copertino, V.A., Telesca, V., 2008. Monitoring daily evapotranspiration at a regional scale from landsat-TM and ETM+ data: application to the basilicata region. J. Hydrol. 351 (1-2), 58–70, http://dx.doi.org/10.1016/j.jhydrol.2007.11.041.
Santos, F.L., Valverde, P.C., Ramos, A.F., Reis, J.L., Castanheira, Nádia L., 2007. Water use and response of a dry-Farmed olive orchard recently converted to irrigation. Biosyst. Eng. 98 (1), 102–114, http://dx.doi.org/10.1016/j.biosystemseng.2007.03.027.
Scholander, P.F., Hammel, H.T., 1965. Sap pressure in vascular plants. Science 148 (1), 339–346, http://dx.doi.org/10.1126/science.148.3668.339.
Schotanus, P., Nieuwstadt, F.T.M., Bruin, H.A.R., 1983. Temperature measurement with a sonic anemometer and its application to heat and moisture fluxes. Bound-Lay. Meteorol. 26, 81–93, http://dx.doi.org/10.1007/bf00164332.
Schotland, R.M., 1955. The measurement of wind velocity by sonic means. Journal of Meteorology 12 (4), 386–390, http://dx.doi.org/10.1175/1520-0469(1955)012<0386:TMOWVB>2.0 (CO;2).
Schuepp, P.H., Leclerc, M.Y., Macpherson, J.I., Desjardins, R.L., 1990. Footprint prediction of scalar fluxes from analytical solutions of the diffusion equation. Bound-Lay. Meteorol. 50, 355–373.
Shuttleworth, W.J., Wallace, J.S., 1985. Evaporation from sparse crops an energy combination theory. Q.J.R. Meteorol. Soc. 111, 839–855, http://dx.doi.org/10.1002/qj.49711146910.
Silva, R.M., 2009. Desenvolvimento de um Sistema Inteligente de Determinação das Necessidades Hídricas para Culturas Lenhosas Anisotrópicas Instituto Superior de Agronomia. Universidade Técnica de Lisboa.
Smith, D.M., Allen, S.J., 1996. Measurement of sap flow in plant stems. J. Exp. Bot. 47 (305), 1833–1844, http://dx.doi.org/10.1093/jxb/47.12.1833.
Snyder, R.L., Paw-U, K.T., 2001. Soil Heat Flow and Temperature (Accessed 1 November 2016) http://biomet.ucdavis.edu/biomet/SoilHeatFlow/SoilHF.htm.
Steppe, K., De Pauw, D.J., Doody, T.M., Teskey, R.O., 2010. A comparison of sap flux density using thermal dissipation, heat pulse velocity and heat field deformation methods. Agric. For. Meteorol. 150 (7), 1046–1056.
Tanner, B.D., Swiatek, E., Greene, J.P., 1993. Density fluctuations and use of the krypton hygrometer in surface flux measurements. In: Proceeding of the 1993 National Conference on Irrigation and Drainage Engineering, Park City, Utah 21–23 July 1993. Irrigation and Drainage Division, American Society of Civil Engineers.
Testi, L., Villalobos, F.J., Orgaz, F., 2004. Evapotranspiration of a young irrigated olive orchard in southern Spain. Agr. For. Meteorol. 121, 1–18, http://dx.doi.org/10.1016/j.agrformet.2003.08.005.
Testi, L., Orgaz, F., Villalobos, F.J., 2006. Variations in bulk canopy conductance of an irrigated olive (Olea europaea L.) orchard. Environ. Exp. Bot. 55 (1–2), 15–28, http://dx.doi.org/10.1016/j.envexpbot.2004.09.008.
Tezza, L., 2013. Misura e stima dell'evaporazione dal suolo in oliveto nella regione dell'Alentejo Portogallo. Università Degli Studi di Padova, Padova, Italy.
Tognetti, R., Andria, R., Morelli, G., Calandrelli, D., Fragnito, F., 2004. Irrigation Effects on Daily and Seasonal Variations of Trunk Sap Flow and Leaf Water Relations in Olive Trees., pp. 249–264.
Villalobos, F.J., Orgaz, F., Testi, L., Fereres, E., 2000. Measurement and modeling of evapotranspiration of olive (*Olea europaea L.*) orchards. Eur. J. Agron. 13 (2–3), 155–163, http://dx.doi.org/10.1016/S1161-0301(00)00071-X.
Webb, E.K., Pearman, G.I., Leuning, R., 1980. Correction of flux measurements for density effects due to heat and water vapour transfer. Q. J. Royal Met. Soc. 106 (447), 85–100, http://dx.doi.org/10.1002/qj.49710644707 (Wiley-Blackwell).
Williams, D.G., Cable, W., Hultine, K., Hoedjes, J.C.B., Yepez, E.A., Simonneaux, V., Er-Raki, S., Boulet, G., Bruin, H.A.R., Chehbouni, A., Hartogensis, O.K., Timouk, F., 2004. Evapotranspiration components determined by stable isotope, sap flow and eddy covariance techniques. Agric. For. Meteorol. 125 (3-4), 241–258, http://dx.doi.org/10.1016/j.agrformet.2004.04.008.
Wilson, K.B., Hanson, P.J., Mulholland, P.J., Baldocchi, D.D., Wullschleger, S.D., 2001. A comparison of methods for determining forest evapotranspiration and its components: sap-Flow, soil water budget, eddy covariance and catchment water balance. Agric. For. Meteorol. 106, 153–168.
Wilson, K., Goldstein, A., Falge, E., Aubinet, M., Baldocchi, D., Berbigier, P., Bernhofer, C., Ceulemans, R., Dolman, H., Field, C., et al., 2002. Energy balance closure at FLUXNET sites. Agric. For. Meteorol. 113, 223–243.
Wright, J.L., 1982. New evapotranspiration crop coefficients. J. Irrig. Drain. Div. 108 (1), 57–74.
Wullschleger, S.D., Childs, K.W., King, A.W., Hanson, P.J., 2011. A model of heat transfer in sapwood and implications for sap flux density measurements using thermal dissipation probes. Tree Physiol. 31 (6), 669–679, http://dx.doi.org/10.1093/treephys/tpr051.
Zhang, Y.J., Meinzer, F.C., Qi, J.H., Goldstein, G., Cao, K.F., 2013. Midday stomatal conductance is more related to stem rather than leaf water status in subtropical deciduous and evergreen broadleaf trees. Plant Cell Environ. 36 (1), 49–58, http://dx.doi.org/10.1111/j. 1365-3040.2012.02563. x.
Zhang, C., Gomes-Laranjo, J., Correia, C.M., Moutinho-Pereira, J.M., Carvalho Gonçalves, B.M., Bacelar, E.L.V.A., Peixoto, F.P., Galhano, V., 2011. Response, tolerance and adaptation to abiotic stress of olive, grapevine and chestnut the mediterranean region: role of abscisic nitric acid oxide and MicroRNAs. In: Vasanthaiah, Hemanth (Ed.), Plants and Environment. InTech, http://dx.doi.org/10.5772/24719.

6.7 Häusler et al. (2018)

Häusler M., Conceição N., Tezza L., Sánchez J.M., Campagnolo M., Häusler A.J., Silva J.M.N., Warneke T., Heygster G., Ferreira M.I. 2018. Estimation and partitioning of actual daily evapotranspiration at an intensive olive grove using the STSEB model based on remote sensing. Agricultural Water Management 201:188–198.

Agricultural Water Management 201 (2018) 188–198

Contents lists available at ScienceDirect

Agricultural Water Management

journal homepage: www.elsevier.com/locate/agwat

Estimation and partitioning of actual daily evapotranspiration at an intensive olive grove using the STSEB model based on remote sensing

Melanie Häusler[a,*], Nuno Conceição[c], Luca Tezza[d], Juan M. Sánchez[e], Manuel L. Campagnolo[a,b], Andreas J. Häusler[f], João M.N. Silva[a], Thorsten Warneke[g], Georg Heygster[g], M. Isabel Ferreira[b,c]

[a] Forest Research Centre, School of Agriculture, University of Lisbon, Tapada da Ajuda, 1349-017 Lisbon, Portugal
[b] DCEB, Departamento de Ciências e Engenharia de Biossistemas, Instituto Superior de Agronomia, Universidade de Lisboa, Tapada da Ajuda, 1349-017 Lisboa, Portugal
[c] LEAF, Linking Landscape, Environment, Agriculture and Food, Instituto Superior de Agronomia, Universidade de Lisboa, Tapada da Ajuda, 1349-017 Lisboa, Portugal
[d] CIRVE, Interdepartmental Centre for Research in Viticulture and Enology, University of Padova, 31015 Conegliano, TV, Italy
[e] IDR, Regional Development Institute, Applied Physics Department, University of Castilla-La Mancha, 02071 Albacete, Spain
[f] Salt and Pepper Technology GmbH & Co. KG, Bremen, Germany
[g] Institute of Environmental Physics, University of Bremen, 28359 Bremen, Germany

ARTICLE INFO

Keywords:
Landsat
Evaporation
Transpiration
Evaporative fraction method

ABSTRACT

This study is based on the application of an existing simplified two-source energy balance (STSEB) model, using medium-resolution satellite imagery (Landsat) to estimate instantaneous (at the satellite overpass time) and daily actual crop evapotranspiration (ET_a) over an intensive olive grove. Daily values were obtained by the use of the evaporative fraction method and corrected for latent heat, available energy, and evaporative fraction biases (beta-factor correction). Model estimates were compared to ground-based measurements. Heat flux densities (eddy covariance method) were recorded, and five Landsat images at approximately monthly intervals were used, covering our study site in 2011. Comparison with ground measurements showed a maximum difference of -0.6 mm day^{-1} before, and 0.2 mm day^{-1} after beta-factor correction for the main plot.

The experimental site consisted of a main plot exposed to deficit irrigation, and two small subplots where—during a limited period of time (six weeks)—one was temporarily not irrigated, and the other well-irrigated for reference. One Landsat image was available for this limited period of time.

Additionally, the STSEB algorithm was tested for partitioning evapotranspiration into its evaporation and transpiration components. Evaporation estimated from the STSEB model was compared with evaporation estimated from a model adjusted from local lysimeter measurements. Transpiration data obtained from calibrated sap flow measurements were, after local calibration, also compared to model estimates. Model results agreed with the measured data, showing) under- and overestimation for transpiration and evaporation, respectively.

1. Introduction

Over the last decade, more and more traditional olive orchards (< 100 trees ha^{-1}) have been replaced by intensive to super-intensive ones (> 2000 trees ha^{-1}), especially in the South of Portugal with Mediterranean climate conditions. This development demands improved water management and optimised irrigation practices in terms of quantifying olive water requirements. This study aims to estimate actual evapotranspiration (ET_a) and its contributing parts of canopy transpiration (LE_v) and soil water evaporation (LE_s), as the latter is often seen as water loss for irrigated crops. An existing simplified two-source energy balance model (STSEB) based on Norman et al. (1995) and further simplified by Sánchez et al. (2008b) has been, in combination with satellite imagery, tested for separately estimating LE_s and LE_v on a daily basis.

To estimate the amount of water transferred to the atmosphere from different crops, various estimation approaches have been developed, in general using implicitly (or explicitly) the leaf surface conductance (bulk stomatal and leaf boundary layer). Due to the difficulty in obtaining this variable for every crop in any water status condition, simple semi-empirical models have been used to calculate ET_a for decades. The principle is based on the reference evapotranspiration (ET_0) estimated from on-site collected meteorological data, which then is multiplied by a crop coefficient, obtaining ET_m ($k_c = ET_m/ET_0$) and finally by a stress coefficient ($k_s = ET_a/ET_m$). In a well-known group of guidelines (FAO Irrigation and Drainage Paper 56), Allen et al. (1998) proposed

* Corresponding author.
E-mail address: aa18795@isa.utl.pt (M. Häusler).

https://doi.org/10.1016/j.agwat.2018.01.027
Received 24 March 2017; Received in revised form 24 January 2018; Accepted 29 January 2018

estimating ET_0 based on the Penman-Montheith equation, which incorporates aerodynamic and physiological parameters of a previously defined reference grass to retrieve k_c and k_s coefficients.

An alternative approach to obtain ET_a and its contributing parts, LE_v and LE_s, was adopted from the energy balance equation (Eq. (A.1)). A distinction is drawn between one- and two-source models, to account for the different heat transfers from the soil surface and the plant canopy. One-source models assume one surface temperature and aerodynamic resistance for the zone of soil and vegetation cover while the two-source models identify soil and vegetation layers as separate sources of heat flux.

To date, many studies have been carried out over annual crops or uniform land covers (Tasumi et al., 2005; Agam et al., 2010; Hoffmann et al., 2016; Timmermans et al., 2007), and many studies have dealt with heterogeneous ground cover (Bastiaanssen et al., 1998; Colaizzi et al., 2016; Roerink et al., 2000), and only recently with tree crops (e.g. olive orchards; Cammalleri et al., 2012; Pôças et al., 2014; Ortega-Farías and López-Olivari, 2012).

Due to the accessibility of satellite data, remote sensing based estimations of ET_a (Sun et al., 2012; Peng et al., 2012; Minacapilli et al., 2016), combined with energy balance models (Du et al., 2013; Ruhoff et al., 2013), became more and more attractive, especially because only a few additional meteorological variables (e.g., air temperature, wind speed, global solar radiation) are needed, being regularly measured at meteorological stations. Yang et al. (2015a) made a comparison between three two-source remote sensing evapotranspiration models, where two of them were two-source energy balance models (TSEB) and the third was the MOD16 ET_a algorithm (algorithm according to Norman et al., 1995 and Nishida et al., 2003b,a). Results showed that MOD16 failed to reproduce spatial ET_a patterns over particularly dry environments, while the TSEB model was in agreement with the ET_a measurements.

Generally, TSEB models give reasonable results for ET_a, and are used for separately estimating LE_v and LE_s, which, based on remote sensing has not been tested yet, to its full extent. One reason might be that TSEB models tend to overestimate LE_s and underestimate LE_v (Colaizzi et al., 2014, 2016). Here, the STSEB model gives the opportunity to operate on a larger scale (e.g. field-scale), due to relatively few input variables, the use of standard meteorological data, and satellite imagery. Daily values of ET_a, LE_v, and LE_s were estimated using the Evaporative Fraction (EF) constant method. Correction factors (beta-factors), according to Van Niel et al. (2011), were tested to improve model estimations.

On this background, the objectives of this study were to:

i estimate instantaneous ET_a in discontinuous vegetation e.g., for an olive grove;
ii detect significant reductions in evapotranspiration due to the water status of the trees;
iii test the performance of the model for partitioning evapotranspiration into its contributing parts (transpiration and evaporation); and
iv evaluate the overall ground cover dynamics (effect of canopies and inter-row soil cover) affecting the use of satellite imagery.

On-site measurements of total ET_a, obtained with the eddy covariance (EC) method, and its contributing parts (LE_s and LE_v) were compared to the model estimates. Consequently, the sections highlighting the results of the research at hand, as well as the discussion of these results, are split in accordance with the aforementioned objectives.

2. Materials and methods

A detailed description of the experimental set-up, instrumentation and their specifications are given in Conceição et al. (2017).

2.1. Study site

This work is based on data obtained in an intensive olive grove in the southeast of Portugal, located in the region of Alentejo in 2011 (latitude: 38°1′15.90″ N, longitude: 8°10′44.50″ W, Datum WGS84, 97 m above sea level). In September 2004, a 10-ha olive grove (*cv. Arbequina*) with a tree spacing of 4.8 m, and a row spacing of 7 m was installed, where a continuous area of 434-ha was selected for taking measurements.

In 2010, the average height of the trees was 3.2 m, the average canopy projected area was 5.7 m^2, and the average leaf area index on a total area basis was 1.01 m^2 m^{-2}. Further biometric measurements were taken and are described in Häusler et al. (2014).

The climate in the region of Alentejo is temperate and is one of the Mediterranean types, Csa, characterized by mild and wet winters and very hot and dry summers (Köppen Geiger Classification Rubel and Kottek, 2010). The average annual rainfall is about 580 mm, with around 5% falling during summer time (http://www.ipma.pt/). The soil was classified as *Luvisol* (Food and Agriculture Organization of the United Nations (FAO), 2006) with a ApBtC profile.

The total olive orchard, with the exception of two subplots, during a limited stress period, was deficit-irrigated. Each tree row had a line of drippers spaced 0.75 m apart. The nominal flow for the deficit irrigation was 1.6 L h^{-1}, which corresponds to an irrigation flux density of 0.31 mm h^{-1}. During 2011 the deficit irrigation operated from 15 June to 26 September (103 days) with an average irrigation depth of 1.4 mm day^{-1}.

During six weeks, two subplots received different treatments. One received no water at all (Subplot 2) and the other was well-irrigated (Subplot 3; see also Section 2.2.3 and Conceição et al., 2017). Pre-dawn leaf water potential served to monitor and define the plant water status. According to Fernandes-Silva (2008) plants are in comfort between −0.4 MPa and −0.7 MPa. The observed values for the well-irrigated Subplot 3 were never below −0.5 MPa (Conceição et al., 2017). Trees with a pre-dawn leaf water potential of down to −0.5 MPa were therefore defined as being in comfort. Values below this point indicated water-stressed olive trees.

2.2. On-site measurements

2.2.1. Measurement of energy heat fluxes at the main plot

The installation of EC sensors allowed the measurement of the flux densities of latent heat flux density *LE* and sensible heat flux density *H* with a three-dimensional sonic anemometer and a krypton hygrometer (CSAT3-D and KH20, respectively, Campbell Scientific, USA), which were mounted on a metallic tower at the height of 4.5 m above ground and oriented into the dominant wind direction (Fig. 1). Raw fluxes (*H* and *LE*) were recorded by a data logger (CR10X, Campbell Scientific, USA), and 30 min averages were stored. Corrections for air density variations (WPL-correction, Webb et al., 1980), and oxygen cross sensitivity for krypton hygrometers (because of oxygen absorption, Tanner et al., 1993) were performed.

The net radiation R_n was measured with net radiometers (NR2 and NRlite, Kipp & Zonen, Netherlands) and the soil heat flux density *G* was recorded, using six heat flux plates (heat flux sensors HFP01 and HFT-3.1 manufactured by Hukseflux and Radiation and Energy Balance Systems, respectively) with known thermal conductivity. The heat flux plates were buried in the ground at a depth of 0.05 m, perpendicular to the flow direction. To quantify the heat stored in the soil layer between 0 and 0.05 m, copper-constantan thermocouples were used at 0.025 m soil depth (1/30 Hz, 10 min average). Further information about equipment and data processing, are described in Conceição et al. (2017).

A simplified footprint analysis (Schuepp et al., 1990) allowed the evaluation of the relative contribution of fluxes coming from different areas within the plot to the total measured flux. More than 85% of the

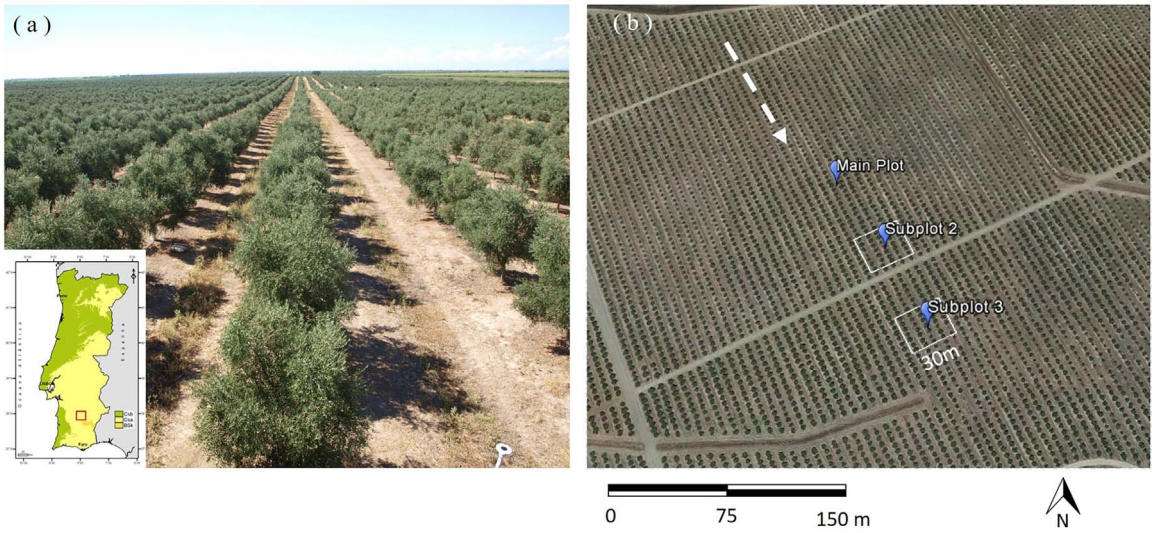

Fig. 1. Image (a) shows a seven-year old intensive olive grove (cv. *Arbequina*) with a tree spacing of 7 × 4.8 m. The location of the experimental site is marked by a red square in the map of Portugal (left corner, Köppen-Geiger Classification) Web references [1]. Image (b) gives an overview of the total test site with its numbered subplots (extracted pixels, 30 m, white squares) and the location of the eddy covariance tower (main plot). The main wind direction is illustrated by white dashed arrows. Web references [2]. (For interpretation of the references to color in this figure legend, the reader is referred to the web version of this article.)

measured *LE* came from an upwind area less than 140 m away from the measurements' point. *LE* and *H* fluxes were selected according to the wind direction, taking into consideration the outputs from the footprint analysis (Conceição et al., 2017) in relation to the fetch for each direction.

2.2.2. Transpiration and soil evaporation at the main plot

Using the thermal dissipation method (Granier, 1985), the sap flow was recorded for seven trees in the main plot. Measurements were taken every 60 s and averaged every 30 min by a data logger (CR3000, Campbell Scientific, USA; for details see also Conceição et al., 2017).

Measurements of LE_s with micro-lysimeters were taken. In total, ten lysimeters were installed. Here, six of them were along the tree line with a spacing of 0.75 m and another four near the line, where two of which were in the shade of the crown and two exposed to the sun (Tezza, 2014). The lysimeter measurements were used to model LE_s for the days were no measurements were taken, using locally adjusted model parameters, as described in Tezza (2014) and Conceição et al. (2017). By subtracting LE_s (micro-lysimeters or model) from ET_a, measured at the EC tower, LE_v was obtained. Subsequently, LE_v was compared with average sap flow data in order to correct it, obtaining a time-series for LE_v of the main plot under deficit irrigation where also total *LE* was measured. Afterwards, it was possible to infer LE_v for the small Subplots 2 and 3, in the way explained in the following section.

2.2.3. Transpiration of the two subplots

For the duration of a stress period (3 August to 15 September, 2011) the experimental site had additionally two small subplots outside the footprint area of the main plot (Fig. 1). In each of the two subplots, sap flow measurements for six trees were taken, also using the thermal dissipation method as described by Granier (1985). Subplots 2 (38°1′13.99″ N, 8°10′42.68″ W) and 3 (38°1′11.81″ N, 8°10′41.12″ W) were equipped with independent irrigation systems, and a stress period was temporarily induced from 3 August (Day of the Year = DoY, 215) until 15 September (258), 2011 in Subplot 2.

Only during the stress period of six weeks, Subplot 2 remained non-irrigated, while Subplot 3 was kept well-irrigated for reference, (pre-dawn leaf water potential above −0.5 MPa). This experimental lay-out was used to analyse the impact of water shortage on water stress indicators and water fluxes (Ferreira et al., 2012a). Before the beginning of the stress period, all plots had reached maximum water status (comfort, > −0.5 MPa of pre-dawn leaf water potential). The main plot (1) continued to be deficit-irrigated (approximately 1.4 mm day^{-1}).

The value of LE_v for the well-irrigated Subplot 3 was obtained by dividing LE_v of the main plot by the stress coefficient of the main plot ($LE_{v,3} = LE_{v,1} \div k_{s,1}$), which takes into account the LE_v reduction in the main plot, being deficit-irrigated. This factor ($k_s = 0.88$) was retrieved from the relationship between pre-dawn leaf water potential and k_s or relative LE_v obtained during the stress period, (Ferreira et al., 2012b; Conceição et al., 2017), by using the values measured in all subplots for the day of satellite overpass during this stress cycle. The same principle was applied to LE_v for the highly stressed Subplot 2 (day of satellite of overpass on DoY 255, 2011) by using the measured relative LE_v of this plot (i.e., $k_s = 0.77$, being LE_v of stressed Subplot 2 = LE_v of the well irrigated Subplot 3 multiplied by 0.77, because $LE_{v,2} = LE_{v,3} \times k_{s,2}$).

Five cloud-free Landsat 5 Thematic Mapper (L5-TM) images were selected in approximately monthly intervals from May until October 2011, including one image during the stress period. The sensor aboard Landsat 5 has a medium spatial resolution (30 m in visible and near-infrared bands, and 120 m in the thermal band), and offers a detailed observation of the Earth's surface. The Level 1 product of surface reflectance data (Level 1 product, Bands 1-5 and 7, atmospherically corrected by Landsat Ecosystem Disturbance Adaptive Processing System, LEDAPS), and the brightness temperature (Band 6), provided by the U.S. Geological Survey Earth Resources Observation and Science (EROS) Data Center (http://earthexplorer.usgs.gov/) were downloaded, and further processed.

For the estimates of the main plot a square of 3 × 3 pixels within the footprint area was extracted and averaged, while for the Subplots 2 and 3 central coordinates were used to extract the corresponding pixels in the images to compare with ground observations. The subplots themselves covered only around 941 m^2 (28 trees), corresponding to the 30 × 30 m pixel size of the visible band of Landsat. We have tested two approaches – averaging over the overlapping pixels or using just the closest pixel to the center of each subplot – and since the latter lead to better estimates we have used it in our calculations, knowing that the tree-lines were rather uniform.

Landsat-derived albedo (α), land surface temperature (T_{rad}) and Normalized Difference Vegetation Index (*NDVI*, see Section 3.4) were plotted against ET_a for 15 observation days along the year 2011. The time pattern of those variables was compared to verify that the input data for the STSEB model were in line with the annual distribution of

remote sensing data. Furthermore, simple and multiple regression models, using as predictors α, T_{rad} or *NDVI*, were fitted to evaluate how the STSEB model improved the ET_a estimation over simple statistical models.

The global solar radiation (S) was provided by the Copernicus Atmosphere Monitoring Service (CAMS) and downloaded from SoDa (Solar Energy Services for Professionals, http://www.soda-pro.com/). Air temperature (T_a) and wind speed (u) were measured on-site at the EC tower, and the instantaneous values used for modeling are given in Table 2.

The incident long-wave radiation (L_{sky}) was provided by the Spinning Enhanced Visible and Infrared Imager (SEVIRI) aboard Meteosat and retrieved with 3 km pixel size from the EUMETSAT Satellite Application Facility on Land Surface Analysis (LSA SAF; https://landsaf.ipma.pt/). Due to uniformity over a large area (Humes et al., 2004), the L_{sky} value of the pixel that included the test site was further processed.

Atmospheric transmissivity (τ), hemispheric down-welling sky irradiance ($L_{atm}^{\downarrow}$) and hemispheric up-welling sky irradiance ($L_{atm}^{\uparrow}$) were obtained by introducing radio-sounding data into the MODTRAN 4.0 code (Berk, 1999). The atmospheric parameters (τ, $L_{atm}^{\downarrow}$, and $L_{atm}^{\uparrow}$) served for atmospheric corrections in order to obtain T_{rad} from brightness temperature and were calculated by the Atmospheric Correction Parameter Calculator (http://atmcorr.gsfc.nasa.gov/, Barsi et al., 2003).

2.3. Model description

The STSEB model (Sánchez et al., 2008a) is based on the energy balance equation (Eq. (A.1)), and estimates instantaneous values for R_n, H and G (W m^{-2}) from meteorological data and satellite imagery, in order to obtain *LE*. To retrieve daily values from the instantaneous ones, the *EF* method (described at the end of this section) was applied, i.e. the ratio of *LE* and the available energy during satellite overpass. G was estimated as a portion of R_n (Eq. (A.11), Choudhury et al., 1987), and considered for retrieving daily ET_a, using the *EF* method.

2.3.1. Instantaneous values

One of the key processes in the STSEB model is the successful partitioning into the contributing parts of the vegetation (v) and the soil (s) (Timmermans et al., 2007; Kustas et al., 2012; Sánchez et al., 2015b) in order to obtain P_v (Eq. (1), Valor and Caselles, 1996). This means that P_v is calculated from the *NDVI* (Eq. (A.5)) and the coefficient K (Eq. (A.6)):

$$P_v = \frac{\left(1 - \frac{NDVI}{NDVI_s}\right)}{\left(1 - \frac{NDVI}{NDVI_s}\right) - K \times \left(1 - \frac{NDVI}{NDVI_v}\right)} \quad (1)$$

Both (*NDVI* and K), were calculated from the red- and near-infrared bands (B_3 and B_4). Band designations (B_i) for Landsat satellites are provided by the official site of U.S. Geological Survey (USGS, http://www.usgs.gov/). The fully vegetated and bare soil areas were manually selected by the use of the *NDVI*, and averaged. They are referred to by the subscripts of v and s, respectively (Region of Interest = ROI; Table 1). The ROIs obtained for the $NDVI_v$ and $NDVI_s$ classification were also used to obtain the average values of the bands for vegetated and bare soil regions for K. The classification of the *NDVI* into vegetated and bare soil regions are found in Sobrino et al. (2004).

Table 1
Changing soil (s) and vegetation (v) characteristics for different Landsat 5 images, where B_3 and B_4 denote the red and near-infrared bands, respectively.

Image (L5-TM)	B_{4v}	B_{4s}	B_{3v}	B_{3s}	*NDVI*	$NDVI_v$	$NDVI_s$
23 May 2011	0.341	0.210	0.041	0.131	0.40	0.782	0.237
24 Jun 2011	0.399	0.281	0.040	0.197	0.43	0.814	0.187
26 Jul 2011	0.378	0.294	0.049	0.206	0.38	0.768	0.175
12 Sep 2011	0.375	0.285	0.039	0.201	0.39	0.810	0.173
30 Oct 2011	0.408	0.177	0.044	0.125	0.40	0.803	0.175

Table 2
Average records of model variables for the main plot (3 × 3 pixels) at the time of satellite overpass. T_a represents the air temperature and u the wind speed recorded at the eddy covariance tower. T_v and T_s were extracted by plotting P_v (partial vegetation) against land surface temperature T_{rad}, and were fixed to certain values for modeling (see Section 2.3 for details).

Date (DoY)	T_a (°C)	T_v (°C)	T_s (°C)	u (m s^{-1})	P_v
23 May (143)	28.7	34.9	37.8	1.4	0.27
24 Jun (175)	27.9	28.5	45.3	1.6	0.39
26 Jul (207)	29.2	29.7	46.9	1.5	0.37
12 Sep (255)	27.5	29.6	41.9	1.2	0.37
30 Oct (303)	20.7	22.3	34.9	0.8	0.28

Separating T_s and T_v when only T_{rad} is available is probably the most intricate issue in the STSEB models. Hereby, for each day, T_{rad} retrieved from the thermal band (Eq. (A.7)) was plotted against P_v (main plot, 3 × 3 pixels), where isolines with an almost linear relationship were obtained (Carlson, 2007; Yang et al., 2015b; Kasim and Usman, 2016). First estimates for the components soil T_s and canopy T_v temperature of T_{rad} were retrieved. Here, higher temperatures related to low values of P_v (bare soil pixels), represented the estimate of T_s, while lower temperatures related to high values of P_v (vegetated pixels) gave the estimate for T_v during satellite overpass (Table 2).

The partitioning of the different fluxes into soil ($1 - P_v$) and canopy (P_v) components was used to estimate H_s (Eq. (A.10)) and H_v (Eq. (A.9)), separately. To be consistent, this approach was also applied to estimating the contributing parts of soil and vegetation cover for R_n, adapting Eq. (A.2), by using the soil and canopy specific emissivities and α. Following this methodology, the component fluxes of LE_s and LE_v, as well as total *LE* were retrieved, applying:

$$LE_s = R_{ns} - H_s - \frac{G}{(1 - P_v)} \quad (2)$$

$$LE_v = R_{nv} - H_v \quad (3)$$

$$LE = P_v LE_v + (1 - P_v) LE_s \quad (4)$$

2.3.2. Daily values

Finally, daily values were retrieved by applying the *EF* constant method as described in Ruan et al. (2014). This algorithm assumes that *EF* is constant during the daytime hours, and is defined for the total scene, and the individual portions of canopy and soil, respectively as:

$$EF_{t,i} = \frac{LE_i}{R_{ni} - G_i} \quad (5)$$

$$EF_{v,i} = \frac{LE_{v,i}}{R_{nv,i}} \quad (6)$$

$$EF_{s,i} = \frac{LE_{s,i}}{R_{ns,i} - G_i} \quad (7)$$

where i denotes the instantaneous values measured (or estimated) at the time of satellite overpass for the total (t) scene, the canopy (v) or soil (s) contribution (Gentine et al., 2007).

However, Van Niel et al. (2011) address three major surface energy balance interactions with *EF* that result in a bias. Those interactions are called beta-factors and represent the systematic errors in *LE*, in the available energy ($R_n - G$), and in the evaporative fraction (assuming daytime self-preservation). The combined influence of the beta-factors was determined and multiplied as explained in Van Niel et al. (2011). The daily values of ET_a were then multiplied by the combined beta-factors as listed in Table 4. Physical background and application of the

beta-factors must be retrieved from the given reference as this is beyond of the scope of this paper.

Daily ET_a (mm day^{-1}) were retrieved from instantaneous observations using (Ruan et al., 2014):

$$ET_{a,daily} = 8.64 \times 10^7 \times EF_i \frac{R_{nd} - G_d}{L \times \rho_w} \quad (8)$$

where L is the latent heat of vaporization given in MJ kg^{-1}, ρ_w is the water density (1000 kg m^{-3}), and EF_i is the evaporative fraction for the total scene, the soil, or the vegetation contribution (Eqs. (5)–(7)).

2.4. Time series analysis of remote sensing data

The STSEB model relies on the surface reflectance and the thermal band of L5-TM. However, for the time series, Landsat 7 Enhanced Thematic Mapper Plus (L7-ETM+) data were also available. A total of 15 observations, from May 15, 2011 until October 30, 2011, were evaluated, testing the representativeness of the five observations used for the STSEB model. Since the STSEB model was not used to estimate ET_a for the additional ten dates, we limited ourselves to looking at the relation between Landsat-derived variables used in the STSEB model, and in-situ measured ET_a. The combination of TM and ETM+ data for the STSEB model, would have further complicated our analysis and add additional variability (different sensors and orbits), and was therefore not considered.

To investigate whether ET_a could be modeled by simple linear regression on the predictor variables α, *NDVI* and T_{rad}, (which were extracted from a time series of Landsat data), multiple linear regression techniques were used. The linear model assumes that the response variable can be written as a linear function of the predictors, plus a Gaussian random error ϵ. Formally,

$$Y_i = \beta_0 + \beta_1 x_{1(i)} + \cdots + \beta_p x_{p(i)} + \epsilon_i, \quad i = 1, \ldots, n \quad (9)$$

for the n observations and p predictors, where ϵ_i has a Gaussian distribution with mean 0 and fixed but unknown variance σ^2. The goodness-of-fit is evaluated with the coefficient of determination R^2, which measures the proportion of the variability of the response that is explained by the regression model. Nested models (*i.e.* where only a subset of predictors is considered) were compared using a *F*-test to understand if the inclusion of additional variables lead to a significant increase in the coefficient of determination (Dytham, 2011).

3. Results

3.1. Instantaneous ET_a

The satellite-derived R_n was underestimated by at most 26 W m^{-2}, compared to that measured. On average, the estimated values mismatched the ground measurements by only −3% (Mean Absolute Deviation = MAD of 17 W m^{-2}). The absolute maximum difference for H was 27 W m^{-2}, resulting in a relative deviation of 4% (MAD of 16 W m^{-2}). For G, a maximum absolute difference of −3 W m^{-2} was observed, and on average the values differed from the measured soil heat flux densities by −1% (MAD of 1.3 W m^{-2}) for the main plot. For *LE*, the maximum deviation of 28 W m^{-2}, resulting in an error of 18% (MAD of 36 W m^{-2}), on average, for the days analysed (see also Table 3).

3.2. Daily ET_a

Comparing the daily estimated values of R_n, *LE*, and H with the ones observed at the main plot, differences of −3% (MAD of 5 W m^{-2}), 14% (MAD of 15 W m^{-2}), and 3% (MAD of 5 W m^{-2}) were observed on average, respectively. Instantaneous values of G were estimated (Eq. (A.11)) and considered for modeling in order to retrieve daily values of *LE* by using the *EF* constant method. In Fig. 2, the daily measured G is given which was between −0.6, and 17 W m^{-2} for the five days used for this study.

Table 3
Comparison of ground-based measurements with instantaneous model estimates of the energy balance surface fluxes (Meas. = Measured and Estim. = Estimated), where R_n is the net radiation, H the sensible heat flux density, *LE* the latent heat flux density and G the soil heat flux density.

Date (DoY)	H (W m^{-2})		*LE* (W m^{-2})		R_n (W m^{-2})		G (W m^{-2})	
	Meas.	Estim.	Meas.	Estim.	Meas.	Estim.	Meas.	Estim.
23 May (143)	154	181	193	247	625	613	189	186
24 Jun (175)	183	182	258	299	621	595	114	115
26 Jul (207)	148	175	242	267	570	550	108	107
12 Sep (255)	166	141	234	256	513	517	123	120
30 Oct (303)	119	120	157	196	371	347	31	30

Generally, the daily estimated ET_a of the subplots were lower than the ones from the main plot with the exception of DoY 255, which was the observation day during the stress period. On that day, ET_a either measured or estimated from the model, was higher in Subplot 3 being well-irrigated. Therefore, Subplot 3 evapotranspirated more than the main plot, which was kept deficit-irrigated. The model was able to detect a clear difference to Subplot 2 receiving no irrigation water at that time (Table 4).

Even though the differences between observed and estimated values were rather small (with exception of DoY 207) for the main plot, ET_a for Subplots 2 and 3 were underestimated, assuming the same conditions in comparison with the main plot, except for DoY 255 (e.g. tree height and tree distribution, water application and irrigation scheduling). Thus, the beta-factor correction as described by Van Niel et al. (2011) was used to account for systematic errors made in *LE*, available energy ($R_n - G$) and the evaporative fraction (assuming daytime self-preservation). The estimations, especially for DoY 207, could be improved (Table 4). In the main plot a difference of only 0.1 mm day^{-1} (before 0.6 mm day^{-1}) between measured and estimated ET_a was achieved after applying the beta-factor of 1.19. Subplots 2 and 3 were also corrected by this factor, reducing the underestimation from 1.0 mm day^{-1} to 0.3 mm day^{-1}.

3.3. Evaporation/transpiration partitioning

The possibility of separating evapotranspiration into its contributing portions of LE_v and LE_s by means of the STSEB algorithm was explored. Again, the *EF* constant method (Eqs. (2)–(8)) was used to estimate daily values from the records during the satellite overpass, and the beta-factor correction was applied as describe in Section 2.3.2.

A clear difference in LE_v was recorded during the stress period, which lasted from DoY 215 to 258 (3 August until 15 September, 2011). During this time, the main plot was kept deficit-irrigated while Subplot 2 was not irrigated at all (stressed), and Subplot 3 was kept near field capacity (control). Accordingly, Subplot 3 transpired the most during the stress period, while in relative terms Subplot 2 transpired the least.

The daily measurements of LE_v at the main plot and the subplots with the corresponding estimates are given in Fig. 3. For DoY 255 the graph displays extra data due to the fact that this was during the stress period applied to Subplot 2, when LE_v for Subplots 2 and 3 were also measured. For the main plot the greatest differences were observed for DoYs 175, and 207, with an underestimation of 1.4 mm day^{-1}, followed by DoY 255, with an underestimation of 1.0 mm day^{-1}.

For the Subplots 2 and 3 the greatest differences between observed and estimated LE_v were recorded at DoY 175 when the overestimation was 1.9 and 1.6 mm day^{-1}, respectively (Fig. 3).

In summary, the estimated daily LE_v values for the main plot and the subplots were underestimated. For the stress period (DoY 255), the

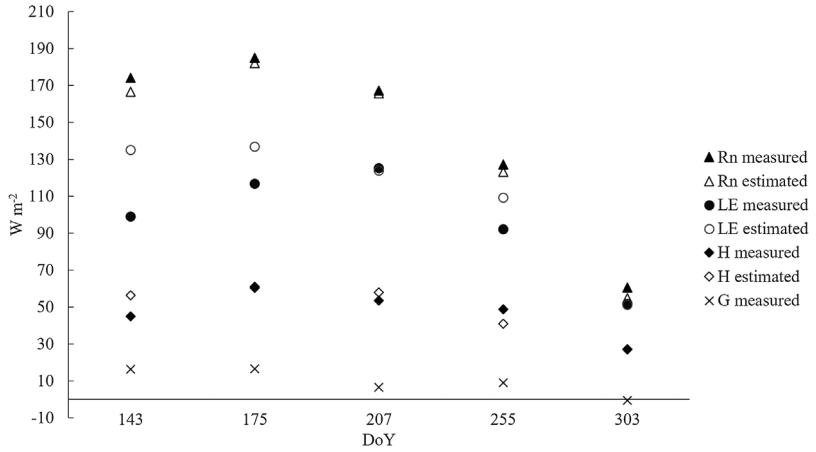

Fig. 2. Comparison of daily model estimates with ground-based measurements (R_n, H, LE, and G).

STSEB algorithm was able to detect differences in LE_v for the different water applications (Fig. 3, where Subplot 3 was highest (control), followed by the main plot (deficit-irrigated) and the Subplot 2 (stressed).

The fraction of LE_s (after application of EF method and systematic error correction) was compared with the model estimates, showing relatively large differences (overestimation) for the DoYs 175, 207, and 255, of at most 1.1 mm day^{-1}, but good agreement for the DoYs 143 and 303 ± 0.2 mm day^{-1}, Table 5.

3.4. Time series analysis of remote sensing data

As discussed, the Landsat data were used to derive α (Eq. (A.3)), *NDVI* (Eqs. (A.5), (1) and (A.6)), and to estimate T_{rad} (Eq. (A.7), see also Fig. 4b). Fig. 4a depicts the relations between the Landsat 5-7 derived variables (α, *NDVI*, and T_{rad}), and ET_a in-situ observations. One can notice that the five observations used in earlier sections were well distributed among the available data, which is an indication of their representativeness.

Fig. 4a shows that α had the best correlation with ET_a and that they were positively correlated. This resulted from the combined effect of both canopy and inter-row components of the Landsat signal: as summer progresses, the herbaceous component of ground cover dries out, and therefore the soil's reflectance increases. Simultaneously and independently, LE_v rates also increase due to irrigation in combination with a higher atmospheric demand.

NDVI (Fig. 4a), on the other hand, showed a very weak correlation with ET_a. As expected, it showed lower values in summer, since the soil surface was almost bare, and increased when the natural conditions were favourable for the development of the ground cover. Therefore, *NDVI* variation reflected mostly the ground cover dynamics, which was mostly driven by the inter-rows, since the leaf area of olive tree canopies was relatively stable over the course of the year (Häusler et al., 2016). In the STSEB model, *NDVI* was in fact used essentially to distinguish the soil from the canopy. It is worth noting that Landsat-derived α and *NDVI* happen to have an almost opposite time pattern, although α correlates more with ET_a.

Multiple linear regression analysis of the data in Fig. 4a was performed to understand if a combination of variables could describe the ET_a values. The most important individual variable was α, followed by T_{rad}, leading to a small increase of the goodness-of-fit from $R^2 = 0.49$ to $R^2 = 0.54$. The inclusion, however, of *NDVI* did not improve the model significantly ($p = 0.5205$). This is further evidence that the STSEB model made better use of Landsat-derived data than a multiple regression model.

4. Discussion

4.1. Instantaneous ET_a

At the olive orchard LE fluxes showed the largest error in relation to the other energy heat fluxes (18%) and were overestimated, on average. However, the errors for R_n (−3%), H (4%) and G (−1%) were rather small. Sánchez et al. (2015a) reported relative errors of 4%, 40%, 14%, and 40% for R_n, G, H, and LE, respectively, at a burnt forest area during the satellite overpass. With the exception of G, this tendency agrees with our results, applying a similar version of the STSEB model and comparing its estimates to EC measurements. In another study the energy heat fluxes were estimated from a two-layer model and compared to instantaneous values from EC measurements at an olive orchard (Ortega-Farías et al., 2016). They reported a rather small error of G (2%), which agrees with our findings. R_n and H were generally both underestimated by around 5%, while our observations resulted in an underestimation of R_n, and an overestimation of H. The largest error was determined for LE (7%), a constant overestimation, which is in agreement with our results. Nevertheless, in our case study LE had a larger deviation mainly due to the first observation date (23 May, DoY

Table 4
Estimations of total ET_a before and after the application of the beta-factor correction. Absolute values and difference between ET_a (mm day^{-1}) from EC method and the estimates from the STSEB model are listed. RMSE is the root mean square error. The linear regression (slope of 0.95, $R^2 = 0.90$) between ground measurements and estimated ET_a, indicated a good correlation even before the beta-factor correction. The beta-factor is the combined factor of systematic error correction in satellite-derived LE, which was applied according to Van Niel et al. (2011). On DoY 255 (stress period from 3 August to 15 September, 2011) the measured ET_a (main plot 1) does not apply to Subplots 2 and 3.

Date (DoY)	Measured (EC)	Estimated (Model)			Subplot 2		Subplot 3		beta-factor
		Before	RMSE	After	Before	After	Before	After	
23 May(143)	3.5	3.6	0.08	3.7	3.4	3.5	3.3	3.3	1.02
24 Jun (175)	4.1	4.0	0.18	4.2	3.6	3.8	3.7	3.9	1.05
26 Jul (207)	4.4	3.8	0.20	4.5	3.4	4.1	3.4	4.1	1.19
12 Sep (255)	3.3	3.2	0.10	3.2	2.9	2.9	3.4	3.4	1.00
30 Oct (303)	1.8	1.7	0.05	1.9	1.3	1.4	1.4	1.5	1.06

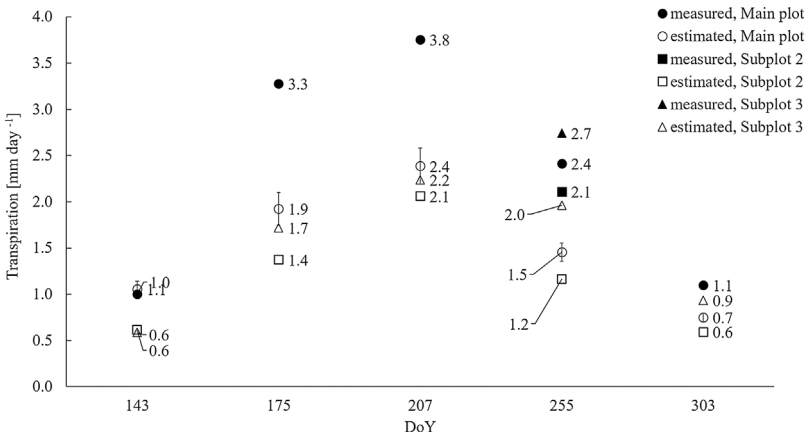

Fig. 3. Comparison between measured and estimated transpiration of the main plot and the subplots. The standard deviation of the 3 × 3 pixels extracted at the main plot (model estimates) is indicated by error bars.

Table 5
Comparison between daily measured and modeled LE_s (Tezza, 2014) with the estimated data from the STSEB model.

Date (DoY)	Measured and modeled LE_s (mm day^{-1})	Estimated (STSEB) LE_s (mm day^{-1})	Absolute Difference (mm day^{-1})
23 May(143)	2.5	2.3	−0.2
24 Jun (175)	0.8	1.9	1.1
26 Jul (207)	0.7	1.5	0.8
12 Sep (255)	0.8	1.3	0.5
30 Oct (303)	0.7	0.8	0.1

143), when *LE* was overestimated by 54 W m^{-2} due to the underestimation of P_v. In order to estimate T_v and T_s, the radiometric surface temperature T_{rad} was plotted against the partial vegetation cover P_v (described in Section 2.3). This relationship depends on soil moisture and surface emissivity (Carlson, 2007; Yang et al., 2015b; Kasim and Usman, 2016). Between 16 and 23 of May there were several rain events with a total of 42.7 mm, moistening and darkening the soil, and thus influencing the reflectance on DoY 143. On this day, $NDVI_s$ was significantly higher compared to the other days (Table 1), and consequently decreased the estimate of P_v. This variable is calculated from the vegetation index *NDVI* (Eq. (A.5)) and the coefficient *K* (A.6), both retrieved from the bands B_4 and B_3. Thus, T_v was higher, leading to an overestimation of *LE*.

4.2. Daily ET_a

In our case study, the model estimates for daily ET_a had the tendency to be underestimated (maximum underestimation of −0.6 mm day^{-1}) before and to be slightly overestimated (maximum overestimation of 0.2 mm day^{-1}) after the beta-factor correction (Table 4). A tendency of underestimating ET_a in TSEB models was also reported by Sánchez et al. (2015b) and Kustas et al. (2013), while Ortega-Farías and López-Olivari (2012) stated an overestimation of ET_a, depending on the phenological stage of the crop, plant moisture, and temperature stress (Zhuang and Wu, 2015). Pôças et al. (2014) stated a maximum overestimation of 0.8 mm day^{-1}. The study by Pôças et al. (2014) was conducted at a super-intensive olive grove not far from our site (75 km), applying the *EF* method to obtain daily values for (partly) the same dates and Landsat imagery, in 2011. In their study, ET_a was estimated using a one-source energy balance model (Mapping Evapotranspiration at high Resolution using Internalised Calibration, METRIC) and the surface energy balance fluxes were compared to ground measurements (EC method). They reported a mean bias of 12.6% between measured and estimated daily ET_a. This is much higher than in our study where the mean bias was < 5%, thus, indicating better results for heterogeneous vegetation surfaces when a two-source energy balance model is used.

4.3. Evaporation/transpiration partitioning

As stated in Section 3.3 for Subplots 2 and 3, differences of more than 1.4 mm day^{-1} were reported. Colaizzi et al. (2014) reported much smaller discrepancies of 0.79 mm day^{-1} for LE_s and 0.76 mm day^{-1} of LE_v in a fully irrigated cotton field, at Bushland, Texas, using a TSEB model to estimate the components of ET_a for different time intervals. One reason could be the difference in P_v: Subplots 2 and 3 had much lower P_v values than the main plot (P_v differences of 0.2, data not shown), which implies reduced canopy fraction. Ortega-Farías et al. (2016) and Ortega-Farías and López-Olivari (2012) stated that canopy training systems and their associated canopy geometry may significantly affect the partitioning into the energy heat flux densities. Another possible explanation would be that the thermal band has a lower spatial resolution of 120 m as compared to the other bands with a spatial resolution of 30 m. Therefore, the T_{rad} for a pixel of a higher resolution than 120 m might not yield the actual surface temperature, and result in errors calculating ET_a. Uncertainties in temperature of 1 K (T_a, T_v, and T_s) have the greatest impact on STSEB flux estimates, and result in errors of up to 30% in *LE* (Sánchez et al., 2008b).

The systematic underestimation of LE_v and overestimation of LE_s might not only be related to the STSEB model itself, but also to the retrieval of the daily values by the use of the *EF* constant method. This method assumes diurnal self-preservation of ET_a, which is often not the case, as shown by Lhomme and Elguero (1999) among other authors. Gentine et al. (2007) have investigated the *EF* principle for ET_a, LE_s and LE_v separately. That study showed that the soil component of *EF* can be assumed to be constant. Here, we have applied the beta-factor correction also to EF_s, which might have partly contributed to the overestimation of LE_s, as the multiplication factors were larger than one (Table 4).

4.4. Time series analysis of remote sensing data

So far, our analysis has focused on each date at a time, which we now extend by a brief description of the temporal pattern of our variables. To that end, we have analysed a denser time series of the major Landsat-derived variables (*NDVI*, *α*, T_{rad}) of the STSEB model. Fig. 4b depicts those Landsat 5–7 responses and relates them to ET_a. It suggests that the overall ground cover dynamics of the study area is driven by the heterogeneity of the olive grove at the Landsat spatial resolution scale, with both, canopies and inter-rows land cover, affecting the

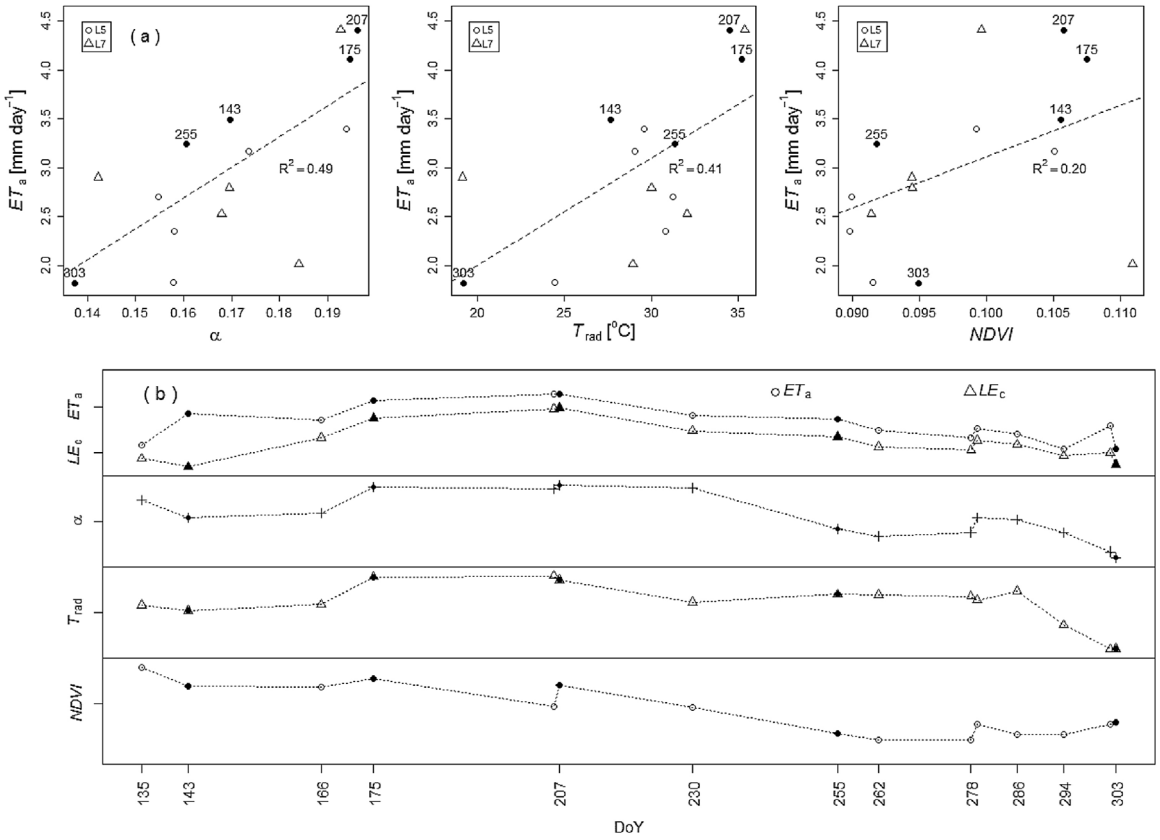

Fig. 4. Relation between Landsat-derived α, T_{rad}, and *NDVI* and in-situ measurements of evapotranspiration for 15 observations in 2011. The top figures indicate the relation between each Landsat variable – L5-TM and L7-ETM + – and crop evapotranspiration (ET_a). The top center figure depicts TOA brightness temperature, available from Landsat Climate Data Record. The lower figure depicts the same observations along time, and includes also measured transpiration values. The five observations discussed in the previous sections are depicted in solid, with the respective date.

signal. This explains the positive correlation found between α and ET_a, which is contrary to Eq. (A.2) (if ET_a was proportional to R_n), but is a result of the combined effect of the dry and hot summer conditions over both components of the system (irrigated plants and increasing drier soil in between plant rows). Moreover, Fig. 4b confirms that the dates that were used as inputs of the STSEB model are in fact representative of the observations along the year.

5. Conclusions

Instantaneous and daily energy heat flux densities, and subsequently ET_a, were estimated for an intensive and deficit-irrigated olive grove in the region of Alentejo, Portugal. The performance of a STSEB model was tested, and the possibility of partitioning evapotranspiration into its components (LE_v and LE_s) was investigated by comparing its estimates with on-site measurements.

i The results show good agreement between measured and estimated R_n, G, H, and LE for instantaneous values on crop trees which have a relatively stable phenology over the course of the year.
ii The maximum difference recorded between modeled and measured daily ET_a was -0.6 mm day^{-1} (with a RMSE of 0.2) before, and 0.2 mm day^{-1} after applying a correction factor, which is in agreement with other studies.
iii After beta-factorcorrection the partitioning of evapotranspiration into its contributing parts showed a maximum underestimation of 1.4 mm day^{-1} for LE_v and a maximum overestimation of 1.1 mm day^{-1} for LE_s at the main plot.
iv Although satellite data with resolution of 30 m (reflectance) and 120 m (temperature) was poorly correlated with measured ET_a and LE_v (R^2 approximately 0.5), which is not surprising due to the heterogeneity of the land cover in one pixel, the STSEB model was able to obtain refined estimates for stress conditions that fit the estimates from ground measurements.

In conclusion, these results add to those previously reported in the literature, resulting in an under- and overestimation of daily values of LE_v and LE_s, respectively, which were retrieved by applying the *EF* method and the beta-factor correction. Nevertheless, the remote sensing based application of the STSEB model showed a good performance in the estimation of instantaneous and daily ET_a from medium-resolution satellite images, and is therefore useful for irrigation management to optimize crop production in relation to agricultural water use.

Funding

This work was supported within the framework of the PhD research grants attributed by FCT (Fundação para a Ciência e a Tecnologia I.P.) to Melanie Häusler (PD/BD/52698/2014) and Nuno Conceição (SFRH/BD /66967/2009). The field work was financed by the project WUSS-IAAME – Water Use, Survival Strategies and Impact of Agrochemicals in Agricultural Mediterranean Ecosystems (PTDC/AAC-AMB/100635/2008, FCT Portugal), and a small part co-financed by the project TELERIEG – Uso de la teledetección para a recomendación y seguimiento de las prácticas de riego en el espacio SUDOE (SOE1/P2/E082) in the framework of the research activities of the research unit LEAF and the Department of Biosystems Eng., at the Instituto Superior de Agronomia, Universidade de Lisboa. CEF is a research unit funded by FCT, Portugal (UID/AGR/00239/2013).

Acknowledgments

The authors are grateful to the engineers and students who contributed to this project, especially to Soroor Amindezfooli, and Sónia Lourenço, who partly contributed to the on-site data collection on plant water status. We are thankful to landowners and workers at Monte do Pardieiro. For their technical support, and fruitful discussions, we would like to thank Prof. José M. C. Pereira, Dr. João P. Nunes, Dr. Yufang Ye, Akli Benali, and Dr. Johannes Michaelsen.

Appendix A. Summary of STSEB approach

The energy balance equation is:

$$R_n = H + LE + G \quad (A.1)$$

where R_n is the net radiation (W m^{-2}), H the sensible heat flux (W m^{-2}), LE the latent heat flux (W m^{-2}) and G the soil heat flux (W m^{-2}).

The R_n was estimated from the albedo α, the global solar radiation S (W m^{-2}), the incident long-wave radiation L_{sky} (W m^{-2}), the total emissivity ε, the Stefan-Boltzmann constant σ (5.67×10^{-8}, W m^{-2} K^{-4}), and the radiometric land surface temperature T_{rad}:

$$R_n = (1 - \alpha)S + \varepsilon L_{sky} - \varepsilon\sigma T_{rad}^4 \quad (A.2)$$

The value of α is given by the equation of Dubayah (1992), using Landsat imagery, where the visible, near-, and short-wave infrared bands (B_1 – B_7) contribute to the total α by weighing the bands with a corresponding factor (assuming Lambertian surface):

$$\alpha = 0.221B_1 + 0.162B_2 + 0.102B_3 + 0.354B_4 + 0.059B_5 + 0.0195B_7 \quad (A.3)$$

The emissivity components for canopy ε_c and soil ε_s were established on the basis of vegetation characterizations and their emissivities using the equation suggested by Rubio et al. (1997). Values of $\varepsilon_c = 0.987$, and $\varepsilon_s = 0.965$ were adopted for this research. The surface emissivity was estimated using the equation proposed by Valor and Caselles (2005), taking into account the partial vegetation cover P_v and the emissivity components ε_c and ε_s:

$$\varepsilon = \varepsilon_c P_v + \varepsilon_s(1 - P_v)(1 - 1.74P_v) + 1.7372P_v(1 - P_v) \quad (A.4)$$

The estimation of P_v is based on the Normalized Difference Vegetation Index *NDVI* and the coefficient K both retrieved from the Landsat surface reflectance bands B_4 and B_3:

$$\mathrm{NDVI} = \frac{B_4 - B_3}{B_4 + B_3} \quad (A.5)$$

$$K = \frac{B_{4v} - B_{3v}}{B_{4s} + B_{3s}} \quad (A.6)$$

To obtain T_{rad} from a single thermal band, different approaches such as the mono-channel algorithm (Qin et al., 2001) or the single-channel algorithm (Jiménez-Muñoz, 2003), based on the radiative-transfer equation, were developed. Here, in-situ radio-sounding data estimated by 4.0 MODTRAN code (Berk, 1999; Barsi et al., 2003) were used and introduced in the following equation:

$$L_{sen} = [\varepsilon B(T_{rad}) + (1 - \varepsilon)L_{atm}^{\downarrow}]\tau + L_{atm}^{\uparrow} \quad (A.7)$$

where L_{sen} is the Top of Atmosphere (TOA) radiance, i.e. the radiance measured by the sensor, ε is the emissivity of the land surface, $B(T_{rad})$ is the radiance of a black body given by Planck's Law, τ is the total atmospheric transmissivity, $L_{atm}^{\downarrow}$ is the atmospheric down-welling, and $L_{atm}^{\uparrow}$ the atmospheric up-welling spectral irradiance (Table A.1). After correcting the radiance for atmospheric and emissivity effects, T_{rad} was obtained.

In the STSEB approach, proposed by Sánchez et al. (2008b), the total sensible heat flux H is obtained by dividing the surface into canopy and soil contributions, H_v and H_s, respectively:

$$H = P_v H_v + (1 - P_v)H_s \quad (A.8)$$

$$H_v = \rho C_p \frac{T_v - T_a}{r_a^h} \quad (A.9)$$

$$H_s = \rho C_p \frac{T_s - T_a}{r_a^a + r_a^s} \quad (A.10)$$

where ρC_p is the volumetric heat capacity of air at constant pressure (J K^{-1} m^{-3}). The estimation of the aerodynamic resistances r_a for stable and unstable conditions used for this work are based on the general framework described in Norman et al. (1995), and Li et al. (2005) and adapted according to Brutsaert (1999). A summary of the expressions to estimate these resistances is given by Sánchez et al. (2008b).

Table A.1
Atmospheric parameters (transmissivity, up- and down-welling sky irradiance) estimated from 4.0 MODTRAN (Berk, 1999), as well as incident-longwave radiation L_{atm} and global solar radiation S at the time of satellite overpass.

Image (L5-TM)	τ	$L_{atm}^{\uparrow}$ (W m^{-2} sr^{-1} μm^{-1})	$L_{atm}^{\downarrow}$ (W m^{-2} sr^{-1} μm^{-1})	L_{sky} (W m^{-2})	S (W m^{-2})
23 May 2011	0.71	2.22	3.60	371	910
24 Jun 2011	0.85	1.18	1.99	339	934
26 Jul 2011	0.76	2.05	3.35	375	884
12 Sep 2011	0.80	1.68	2.73	347	796
30 Oct 2011	0.73	2.01	3.19	328	574

The instantaneous soil heat flux G is given by:

$$G = C_G(1 - P_v)R_n \quad (A.11)$$

where C_G is the ratio of G/R_n when field measurements were around 0.3 for the period of time considered in 2011 (Conceição et al., 2017), and P_v is the partial vegetation cover.

References

Agam, N., Kustas, W.P., Anderson, M.C., Norman, J.M., Colaizzi, P.D., Howell, T.A., Prueger, J.H., Meyers, T.P., Wilson, T.B., 2010. Application of the Priestley-Taylor approach in a two-source surface energy balance model. J. Hydrometeorol. 11 (1), 185–198.

Allen, R.G., Pereira, L.S., Raes, D., Smith, M., 1998. FAO Irrigation and Drainage Paper No. 56, Crop Evapotranspiration (Guidelines for Computing Crop Water Requirements). Rome, Italy.

Barsi, J., Barker, J., Schott, J., 2003. An atmospheric correction parameter calculator for a single thermal band earth-sensing instrument. IGARSS 2003. 2003 IEEE Int. Geosci. and Rem. Sen. Symp. Proceedings (IEEE Cat. No.03CH37477), vol. 5. IEEE, Toulouse, pp. 3014–3016.

Bastiaanssen, W., Pelgrum, H., Wang, J., Ma, Y., Moreno, J., Roerink, G., van der Wal, T., 1998. A remote sensing surface energy balance algorithm for land (SEBAL). J. Hydrol. 212–213, 213–229.

Berk, A., 1999. MODTRAN4 radiative transfer modeling for atmospheric correction. Proc. SPIE 3756 (1993), 348–353.

Brutsaert, W., 1999. Aspects of bulk atmospheric boundary layer similarity under free-convective conditions. Rev. Geophys. 37 (4), 439–451.

Cammalleri, C., Anderson, M., Ciraolo, G., D'Urso, G., Kustas, W., La Loggia, G., Minacapilli, M., 2012. Applications of a remote sensing-based two-source energy balance algorithm for mapping surface fluxes without in situ air temperature observations. Remote Sens. Environ. 124, 502–515.

Carlson, T., 2007. An overview of the "triangle method" for estimating surface evapotranspiration and soil moisture from satellite imagery. Sensors 7 (8), 1612–1629.

Choudhury, B.J., Idso, S.B., Reginato, R.J., 1987. Analysis of an empirical model for soil heat flux under a growing wheat crop for estimating evaporation by an infrared-temperature based energy balance equation. Agric. For. Meteorol. 39 (April (4)), 283–297.

Colaizzi, P.D., Agam, N., Tolk, J.A., Evett, S.R., Howell, T.A., Gowda, P.H., O'Shaughnessy, S.A., Kustas, W.P., Anderson, M.C., 2014. Two-source energy balance model to calculate ET, and ET: comparison of Priestley-Taylor and Penman-Monteith formulations and two time scaling methods. Trans. ASABE 57 (2), 479–498.

Colaizzi, P.D., Agam, N., Tolk, J.A., Evett, S.R., Howell, T.A., O'Shaughnessy, S.A., Gowda, P.H., Kustas, W.P., Anderson, M.C., 2016. Advances in a two-source energy balance model: partitioning of evaporation and transpiration for cotton. Trans. ASABE 59 (1), 181–197.

Conceição, N., Tezza, L., Häusler, M., Lourenço, S., Pacheco, C.A., Ferreira, M.I., 2017. Three years of monitoring evapotranspiration components and crop and stress coefficients in a deficit irrigated intensive olive orchard. Agric. Water Manage. 191, 138–152.

Du, J., Song, K., Wang, Z., Zhang, B., Liu, D., 2013. Evapotranspiration estimation based on MODIS products and surface energy balance algorithms for land (SEBAL) model in Sanjiang Plain, Northeast China. Chin. Geogr. Sci. 23 (1), 73–91.

Dubayah, R., 1992. Estimating net solar radiation using Landsat Thematic Mapper and digital elevation data. Water Resour. Res. 28 (9), 2469–2484.

Dytham, C., 2011. Choosing and Using Statistics: A Biologist's Guide, 3rd ed. Wiley-Blackwell.

Fernandes-Silva, A.F.F., 2008. Nessesidades Hídricas e Resposta da Oliveira (*Olea europea* L.) ao Deficit Hídrico na Região da Terra Quente. Universidade Trás-os-Montes e Alto Douro, Vila Real, Portugal (Ph.D. thesis).

Ferreira, M.I., Conceição, N., Pacheco, C.A., Häusler, M., 2012a. Análise de indicadores de desconforto hídrico durante ciclos de stress num olival intensivo no Alentejo. In: VI Actas do Simpósio Nacional de Olivicultura. Mirandela. pp. 207–2015.

Ferreira, M.I., Silvestre, J., Conceição, N., Malheiro, A.C., 2012b. Crop and stress coefficients in rainfed and deficit irrigation vineyards using sap flow techniques. Irrig. Sci. 30 (5), 433–447.

Food and Agriculture Organization of the United Nations (FAO), 2006. AQUASTAT online database. http://www.fao.org/nr/aboutnr/nrl/en/.

Gentine, P., Entekhabi, D., Chehbouni, A., Boulet, G., Duchemin, B., 2007. Analysis of evaporative fraction diurnal behaviour. Agric. For. Manage. 143 (1–2), 13–29.

Granier, A., 1985. Une nouvelle méthode pour la mesure du flux de sève brute dans le tronc des arbres. Annales des Sciences Forestières 42 (2), 193–200.

Häusler, M., Ferreira, M.I., Conceição, N., 2014. Assessment of vegetation parameters in olive trees in the region of Alentejo: a comparison of direct and indirect methods. Acta Hortic. 1038, 407–414.

Häusler, M., Silva, J.M.N., Cerasoli, S., López-Saldaña, G., Pereira, J.M.C., 2016. Modelling spectral reflectance of open cork oak woodland: a simulation analysis of the effects of vegetation structure and background. Int. J. Remote Sens. 37 (3), 492–515.

Hoffmann, H., Nieto, H., Jensen, R., Guzinski, R., Zarco-Tejada, P., Friborg, T., 2016. Estimating evaporation with thermal UAV data and two-source energy balance models. Hydrol. Earth Syst. Sci. 20 (2), 697–713.

Humes, K., Hardy, R., Kustas, W., Prueger, J., Starks, P., 2004, April. High spatial resolution mapping of surface energy balance components with remotely sensed data. Thermal Remote Sensing in Land Surface Processing. CRC Press, New York, pp. 110–132 (Chapter 3).

Jiménez-Muñoz, J.C., 2003. A generalized single-channel method for retrieving land surface temperature from remote sensing data. J. Geophys. Res. 108 (D22), 4688.

Kasim, A.A., Usman, A.A., 2016. Triangle method for estimating soil surface wetness from satellite imagery in Allahabad District, Uttar Pradesh, India. J. Geosci. Environ. Prot. 4 (January), 84–92.

Kustas, W.P., Alfieri, J.G., Anderson, M.C., Colaizzi, P.D., Prueger, J.H., Evett, S.R., Neale, C.M., French, A.N., Hipps, L.E., Chávez, J.L., Copeland, K.S., Howell, T.A., 2012. Evaluating the two-source energy balance model using local thermal and surface flux observations in a strongly advective irrigated agricultural area. Adv. Water Res. 50, 120–133.

Kustas, W.P., Anderson, M.C., Cammalleri, C., Alfieri, J.G., 2013. Utility of a thermal-based two-source energy balance model for estimating surface fluxes over complex landscapes. Proc. Environ. Sci. 19, 224–230.

Lhomme, J.P., Elguero, E., 1999. Examination of evaporative fraction diurnal behaviour using a soil-vegetation model coupled with a mixed-layer model. Hydrol. Earth Syst. Sci. 3 (2), 259–270.

Li, F., Kustas, W.P., Prueger, J.H., Neale, C.M.U., Jackson, T.J., 2005. Utility of remote sensing based two-source energy balance model under low and high vegetation cover conditions. J. Hydrometeorol. 6, 878–891.

Minacapilli, M., Consoli, S., Vanella, D., Ciraolo, G., Motisi, A., 2016. A time domain triangle method approach to estimate actual evapotranspiration: application in a Mediterranean region using MODIS and MSG-SEVIRI products. Remote Sens. Environ. 174, 10–23.

Nishida, K., Nemani, R.R., Glassy, J.M., Running, S.W., 2003a. Development of an evapotranspiration index from Aqua/MODIS for monitoring surface moisture status. IEEE Trans. Geosci. Remote Sens. 41 (2 Pt 1), 493–500.

Nishida, K., Nemani, R.R., Running, S.W., Glassy, J.M., 2003b. An operational remote sensing algorithm of land surface evaporation. J. Geophys. Res. 108 (D9), 4270.

Norman, J.M., Kustas, W., Humes, K., 1995. A two-source approach for estimating soil and vegetation energy fluxes from observations of directional radiometric surface temperature. Agric. For. Meteorol. 77, 263–293.

Ortega-Farías, S., López-Olivari, R., 2012. Validation of a two-layer model to estimate latent heat flux and evapotranspiration in a drip-irrigated Olive Orchard. Trans. ASABE 55 (4), 1169–1178.

Ortega-Farías, S., Ortega-Salazar, S., Poblete, T., Kilic, A., Allen, R., Poblete-Echeverría, C., Ahumada-Orellana, L., Zuñiga, M., Sepúlveda, D., 2016. Estimation of energy balance components over a drip-irrigated olive orchard using thermal and multispectral cameras placed on a helicopter-based unmanned aerial vehicle (UAV). Remote Sens. 8 (8), 638.

Peng, J., Liu, Y., Zhao, X., Loew, A., 2012. Estimation of evapotranspiration from TOA radiances in the Poyang Lake Basin, China. Hydrol. Earth Syst. Sci. Discuss. 9 (9), 10963–11003.

Pôças, I., Paço, T.A., Cunha, M., Andrade, J.A., Silvestre, J., Sousa, A., Santos, F.L., Pereira, L.S., Allen, R.G., 2014. Satellite-based evapotranspiration of a super-intensive olive orchard: application of METRIC algorithms. Biosyst. Eng. 128, 1–13.

Qin, Z., Karnieli, A., Berliner, P., 2001. A mono-window algorithm for retrieving land surface temperature from Landsat TM data and its application to the Israel-Egypt border region. Int. J. Remote Sens. 22 (18), 3719–3746.

Roerink, G.J., Su, Z., Menenti, M., 2000. S-SEBI: a simple remote sensing algorithm to estimate the surface energy balance. Phys. Chem. Earth B: Hydrol. Oceans Atmos. 25 (2), 147–157.

Ruan, Z., Jia, L., Menenti, M., 2014. Evaluation of algorithms to estimate daily evapotranspiration from instantaneous measurements under all-sky conditions. IOP Conference Series: Earth and Env. Sci. 17 012133.

Rubel, F., Kottek, M., 2010. Observed and projected climate shifts 1901–2100 depicted by world maps of the Köppen-Geiger climate classification. Meteorologische Zeitschrift 19 (April (2)), 135–141.

Rubio, E., Caselles, V., Badenas, C., 1997. Emissivity measurements of several soils and vegetation types in the 8–4 μm wave band: analysis of two field methods. Remote Sens. Environ. 59, 490–521.

Ruhoff, L., Paz, R., Aragao, L.E.O.C., Mu, Q., Malhi, Y., Collischonn, W., Rocha, H.R., Running, S.W., 2013. Assessment of the MODIS global evapotranspiration algorithm using eddy covariance measurements and hydrological modelling in the Rio Grande basin. Hydrol. Sci. J. 58 (8), 1658–1676.

Sánchez, J., Scavone, G., Caselles, V., Valor, E., Copertino, V., Telesca, V., 2008a. Monitoring daily evapotranspiration at a regional scale from Landsat-TM and ETM+ data: application to the Basilicata region. J. Hydrol. 351 (March (1–2)), 58–70.

Sánchez, J.M., Bisquert, M., Rubio, E., Caselles, V., 2015a. Impact of land cover change induced by a fire event on the surface energy fluxes derived from remote sensing. Remote Sens. 7 (11), 14899–14915.

Sánchez, J.M., Kustas, W.P., Caselles, V., Anderson, M.C., 2008b. Modelling surface energy fluxes over maize using a two-source patch model and radiometric soil and canopy temperature observations. Remote Sens. Environ. 112 (3), 1130–1143.

Sánchez, J.M., López-Urrea, R., Doña, C., Caselles, V., González-Piqueras, J., Niclòs, R., 2015b. Modeling evapotranspiration in a spring wheat from thermal radiometry: crop

coefficients and E/T partitioning. Irrig. Sci. 33 (6), 399–410.
Schuepp, P.H., Leclerc, M.Y., MacPherson, J.I., Desjardins, R.L., 1990. Footprint prediction of scalar fluxes from analytical solutions of the diffusion equation. Boundary-Layer Meteorol. 50 (1–4), 355–373.
Sobrino, J.A., Jiménez-Muñoz, J.C., Paolini, L., 2004. Land surface temperature retrieval from LANDSAT TM 5. Remote Sens. Environ. 90 (4), 434–440.
Sun, Z., Gebremichael, M., Ardö, J., Nickless, A., Caquet, B., Merboldh, L., Kutschi, W., 2012. Estimation of daily evapotranspiration over Africa using MODIS/Terra and SEVIRI/MSG data. Atmos. Res. 112 (August), 35–44.
Tanner, B.D., Swiatek, E., Greene, J.P., 1993. Density fluctuations and use of the krypton hygrometer in surface flux measurements. In: Engineers A. S. o. C (Ed.), Proceeding of the 1993 National Conference on Irrigation and Drainage Engineering Irrigation and Drainage Division. Park City.
Tasumi, M., Trezza, R., Allen, R.G., Wright, J.L., 2005. Operational aspects of satellite-based energy balance models for irrigated crops in the semi-arid U.S. Irrig. Drain. Syst. 19 (3–4), 355–376.
Tezza, L., 2014. Misura e stima dell'evaporazione dal suolo in oliveto nella regione dell'Alentejo, Portogallo. Università degli studi di Padova (Ph.D. thesis).
Timmermans, W.J., Kustas, W.P., Anderson, M.C., French, A.N., 2007. An intercomparison of the Surface Energy Balance Algorithm for Land (SEBAL) and the Two-Source Energy Balance (TSEB) modeling schemes. Remote Sens. Environ. 108 (4), 369–384.
Valor, E., Caselles, V., 1996. Mapping land surface emissivity from NDVI. Application to European, African and South-American areas. Remote Sens. Environ. 57, 167–184.
Valor, E., Caselles, V., 2005. Validation of the Vegetation Cover Method for Land Surface Emissivity Estimation. Research Signpost, Kerala.
Van Niel, T.G., McVicar, T.R., Roderick, M.L., van Dijk, A.I.J.M., Renzullo, L.J., van Gorsel, E., 2011. Correcting for systematic error in satellite-derived latent heat flux due to assumptions in temporal scaling: assessment from flux tower observations. J. Hydrol. 409 (1–2), 140–148.
Webb, E.K., Pearman, G.I., Leuning, R., 1980. Correction of flux measurements for density effects due to heat and water vapour transfer. Q. J. R. Meteorol. Soc. 106 (447), 85–100.
Yang, Y., Long, D., Guan, H., Liang, W., Simmons, C., Batelaan, O., 2015a. Comparison of three dual-source remote sensing evapotranspiration models during the MUSOEXE-12 campaign: revisit of model physics. Water Resour. Res. 51 (5), 3145–3165.
Yang, Y., Su, H., Zhang, R., Tian, J., Li, L., 2015b. An enhanced two-source evapotranspiration model for land (ETEML): algorithm and evaluation. Remote Sens. Environ. 168, 54–65.
Zhuang, Q., Wu, B., 2015. Estimating evapotranspiration from an improved two-source energy balance model using ASTER satellite imagery. Water 7 (12), 6673–6688.

Web references

[1] Wikimedia Commons (January 6, 2007). Map of the climatic regions of Portugal according to the Köppen-Geiger climate classification system. IPMA. https://commons.wikimedia.org/wiki/File:Map_of_the_climatic_regions_of_Portugal.jpg [November 16, 2016].
[2] Google earth V 7.1.7.2606. (May 26, 2013). Alentejo, Portugal. 38° 1.34′ N, 8° 10.84′ W, Eye alt 788 m. SIO, NOAA, U.S. Navy, NGA, GEBCO. Image Landsat, DigitalGlobe 2016. http://www.earth.google.com [November 14, 2016].

Conclusões

7.1 Vinha

A cultivar estudada ('Aragonez') apresentou, nas condições edafoclimáticas do estudo, um comportamento isohídrico pelo que se considera adequado o uso do potencial hídrico foliar de base (Ψ_{base}) como indicador do estado hídrico em detrimento do potencial hídrico foliar ou do ramo mínimo, como se refere em Ferreira et al. (2012b) e foi posteriormente discutido num artigo recente que inclui estes resultados (Blanco-Cipollone et al., 2017). Embora não fazendo parte da discussão em nenhum dos artigos incluídos na tese, resultou deste trabalho a evidência experimental de que os tratamentos de rega deficitária em vinha tiveram clara expressão no Ψ_{base} e na densidade de fluxo de transpiração (Tr), não acontecendo o mesmo nas observações de temperatura foliar (dados não publicados) e na variação de diâmetro do tronco (Silvestre et al., 2013).

A transpiração da vinha (Ferreira et al., 2012b, Beja) atingiu no ano em estudo (2009) valores máximos no final de Maio (entre $3\,\text{mm}\,\text{dia}^{-1}$ e $4\,\text{mm}\,\text{dia}^{-1}$) mas a partir do princípio de Junho, decresceu regularmente para valores de $0.5\,\text{mm}^{-1}$ no final do Verão, devido à redução em paralelo do coeficiente cultural basal (Kcb), em consequência dos efeitos de longo prazo da intensidade da carência hídrica na área foliar e do coeficiente de *stress* (Ks) que exprime o efeito do *stress* hídrico de curto termo (imediatamente recuperável caso as plantas fossem bem regadas). Para esta vinha o valor de Kcb máximo calculado foi de 0.7 no início de Maio, quando Ks se considerou igual ao seu valor máximo (*i.e.* $= 1$) e o produto $Kcb \times Ks$ decresceu de 0.7 a 0.1 no final do Verão como documentado em Ferreira et al. (2012b, investigação que englobou outras quatro vinhas).

Tanto a relação de Kcb com o índice de área foliar como com a fracção de solo sombreada pela projecção vertical da copa mostraram-se de interesse prático, embora a preferência por uma ou outra variável (indicador de vegetação) possa depender da geometria do coberto, designadamente entre a altura das plantas e a distância entre linhas de plantação (Häusler et al., 2014).

Obteve-se uma função relacionando Ψ_{base} e Ks, válida para Ψ_{base} entre $-0.2\,\text{MPa}$ e $-1.0\,\text{MPa}$ (Ferreira et al., 2012b, equação 7.1), que permite estimar um valor de Ks de 0.2 no final do Verão, para Ψ_{base} de $-0.8\,\text{MPa}$.

$$Ks = 0.839 \exp^{1.642\Psi_{base}} \tag{7.1}$$

Foi a estimativa de Ks que permitiu obter os valores de Kcb acima referidos, e que se verificou estarem bem relacionados com o índice de área foliar e com a fracção de solo sombreada pela projecção vertical da copa (*ground cover*) e de acordo com os resultados obtidos por outros autores como referido em Ferreira et al. (2012b).

Ao analisar a sensibilidade do índice de vegetação NDVI (*Normalized Difference Vegetation Index*) para traduzir os efeitos do *stress* hídrico no curto prazo, usando dados

de detecção remota (com 30 m de resolução espacial do sensor *Thematic Mapper* a bordo do satélite Landsat-5), concluiu-se que os valores de NDVI não traduziam os efeitos da carência hídrica de curto prazo (Conceição et al., 2011), restringindo-se assim o uso do índice NDVI a estimar Kcb.

Assim, conhecendo uma função que relacione Ks com um indicador do estado hídrico (*e.g.* Ψ_{base}), por medição deste último calcula-se Ks, permitindo estimar Tr conhecendo ET_o, sendo Kcb estimado a partir de NDVI. Desta forma com apenas um tipo de medição no campo quantifica-se o estado hídrico e Tr, que são duas variáveis fundamentais para determinar respectivamente, a oportunidade e a dotação de rega. No trabalho apresentado em Conceição et al. (2011) foi obtida outra função relacionando Kcb com Ks (equação 7.2) e que é consistente com a função apresentada em Ferreira et al. (2012b, equação 7.1).

$$Ks = 1.3 \exp^{3.1\Psi_{base}} \tag{7.2}$$

7.2 Olival de sequeiro

Em 2012 (ano de seca hidrológica, precipitação total 350 mm) foi quantificada a ETr, no olival de sequeiro, entre meados de Maio e meados de Julho tendo $\text{ETr}/\text{ET}_\text{o}$ decrescido de 0.5 para 0.2, respectivamente. Neste mesmo período, ETr decresceu de $3.0\,\text{mm}\,\text{dia}^{-1}$ para $1.5\,\text{mm}\,\text{dia}^{-1}$ e Ψ_{base} decresceu de -0.4 MPa para -1.1 MPa . O decréscimo de ETr foi mais acentuado até meados de Junho, altura em que se observou a total senescência da vegetação em sobcoberto (Conceição et al., 2017a).

A quase totalidade de biomassa e a grande concentração de raízes de todos os diâmetros foi observada até 0.6 m–0.7 m. As raízes grossas seguiam trajectórias quase horizontais (figura 7.1), partindo da toiça (figura 7.2), e só foram observadas no *solum* (horizontes Ap e Bt, 0 m–0.7 m, figura 7.3). Entre 0.7 m e 2.5 m só foram observadas raízes finas (Conceição et al., 2017c).

Os valores mínimos observados de Ψ_{base} (antes das primeiras chuvas de Outono) foram -1.4 MPa (início de Outubro), -2 MPa (finais de Outubro) e -3 MPa (meados de Setembro) para 2010, 2011 e 2012, respectivamente. O valor mais baixo de Ψ_{base} em 2012 reflecte a dificuldade acrescida por parte das árvores para usar a água do solo.

Considerando o ano de 2012, concluiu-se que a precipitação até ao final da Primavera não foi suficiente para levar todo o perfil de solo observado (0 m–1.3 m) até à capacidade de campo, como sucedeu em 2011 e 2013 e como se espera que suceda num ano hidrológico padrão. Só a camada 0 m–0.5 m atingiu a capacidade de campo. O decréscimo do armazenamento de água do solo (0 m–1.3 m) foi muito acentuado até meados de Julho em todas as camadas até 1.3 m, continuando a decrescer progressivamente de forma pouco acentuada até à quase depleção em meados de Setembro (antes das primeiras chuvas de Outono). Embora só tenham sido feitas medições do teor de água no solo até 1.3 m pode concluir-se que o sistema radicular explorou as camadas de solo abaixo desta profundidade (Conceição et al., 2017a).

Embora em 2012, as árvores tenham esgotado a reserva utilizável na camada de solo observada (0 m–1.3 m), após as primeiras chuvas de Outono (35 mm) houve um rápido aumento de Ψ_{base}, certamente favorecido pela infiltração preferencial ao longo das fendas

Figura 7.1: Olival de sequeiro, vista da disposição de raízes grossas da oliveira estudada (*vide* Conceição et al., 2017c). A estaca de madeira na vertical, visível na fotografia, indica o centro do tronco da oliveira arrancada. À frente na fotografia é visível a parede da trincheira para observação do perfil de solo (figura 7.3). Monte do Outeirinho, Ferreira do Alentejo, Portugal, Outono de 2013.

existentes nos horizontes superficiais (Ap e Bt, ricos em argilas expansíveis) e onde as árvores têm uma elevada concentração de raízes (0.1 m–0.6 m) (Conceição et al., 2017c).

Concluiu-se que as raízes finas foram essenciais para a sobrevivência das árvores (Conceição et al., 2017c) e que a forma de colonização do solo pelas raízes lhes permitiu usar a água do solo de forma homogénea nos planos horizontais.

7.3 Olival de regadio

No olival de regadio (Conceição et al., 2017b) durante o Verão de 2010 e 2011 a transpiração variou entre 2 mm dia^{-1} e 4 mm dia^{-1}, sendo que $\mathrm{ET_o}$ variou entre 4 mm dia^{-1} e 8 mm dia^{-1}; a razão Tr/ET_o oscilou entre 0.4 e 0.6. No ano de seca (2011/2012), para idênticos valores de $\mathrm{ET_o}$, a razão Tr/ET_o foi de cerca de 0.2 sendo que Tr variou entre 1 mm dia^{-1} e 2 mm dia^{-1}. Para manter o estado hídrico observado, no olival, foi usado um volume de rega total de 226 mm. Este volume foi aplicado num período de 132 dias (mais 29 dias do que em 2011) o que corresponde a 1.7 mdia, sendo este valor inferior à ETr média diária observada (Conceição et al., 2017a).

A discriminação das componentes Kcb e Ks, de acordo com a abordagem já antes usada em Ferreira et al. (2012b), permitiu quantificar Kcb como sendo cerca de 0.4 no início do Verão (*i.e.* $Ks = 1$) em 2010 e 2011. No ano de 2011/2012 em que, devido à quase ausência de precipitação no Inverno, nas camadas de solo abaixo de 0.5 m não se atingiu a capacidade de campo, o valor de Kcb foi de 0.3.

A cultivar ('Arbequina') também apresentou um comportamento isohídrico no intervalo de Ψ_{base} observado (*i.e.* até −1.4 MPa), pelo que se considera adequado o uso de Ψ_{base} como indicador do estado hídrico. Em 2012, o valor observado de Ψ_{base} em meados de Maio foi de −0.4 MPa, tendo o mínimo (−1 MPa) sido observado em meados de Setembro (antes das primeiras chuvas de Inverno). A função encontrada relacionando

Figura 7.2: Olival de sequeiro, toiça da oliveira arrancada para estudo do sistema radicular (*vide* Conceição et al., 2017c). Monte do Outeirinho, Ferreira do Alentejo, Portugal, Outono de 2013.

Ψ_{base} e Ks, válida entre $-0.2\,\text{MPa}$ e $-1.4\,\text{MPa}$ (equação 7.3) permite estimar para este intervalo de Ψ_{base} valores de Ks entre 1 e 0.7. Os valores estimados de Ks decresceram desde a unidade (fim da Primavera) até cerca de 0.8 o que mostra que houve uma variação relativamente pequena de Ks associada a um *stress* hídrico moderado. De salientar que no ano de seca (2012) Ks começou a decrescer logo no início da Primavera.

$$Ks = 1.11 \exp^{0.32\Psi_{base}} \tag{7.3}$$

A evolução sazonal do índice de vegetação NDVI, no olival de regadio, traduz essencialmente a dinâmica do sobcoberto, tendo-se concluído que apesar de a resolução espacial de 30 m (sensores TM e ETM+) ser grosseira, o modelo de dois compartimentos (Sánchez et al., 2008) utilizado (Häusler et al., 2018) permitiu estimar ETr total diária com precisão aceitável. Já para os valores diários estimados de Tr e Es houve subestimativa e sobrestimativa, respectivamente. Do conjunto de dados disponível (considerando os sensores TM e ETM$^+$) foram consideradas cinco datas compreendidas entre meados de Maio e final de Outubro de 2011 e concluiu-se que eram representativas desse conjunto.

Figura 7.3: Olival de sequeiro, trincheira para acesso ao perfil do solo (*vide* Conceição et al., 2017c). Na trincheira está o Prof. Carlos Arruda Pacheco a analisar o perfil de solo. Monte do Outeirinho, Ferreira do Alentejo, Portugal, Outono de 2013.

7.4 Conclusões gerais

Em ambos os olivais houve evidências de redistribuição hidráulica, de forma muito discreta no olival de regadio, no plano horizontal entre zonas de solo humedecidas pela rega e de solo seco. No olival de sequeiro a redistribuição hidráulica ocorreu na direcção vertical (*hidraulic lift,* Ferreira et al., 2013; Nadezhdina et al., 2014) sendo a extracção radicular relativamente homogénea nas direcções horizontais (Conceição et al., 2017c). Durante o período estival foi observada extracção radicular abaixo de 1.2 m de profundidade, em ambos os olivais, apesar de abaixo de 0.8 m de profundidade só terem sido observadas raízes finas (visíveis até 2.5 m e 1.7 m no olival de sequeiro e de regadio, respectivamente).

Estes dois conjuntos de informação permitem evidenciar e explicar o contraste entre as condições de superfície do solo e as condições hídricas das plantas que aparecem muito dissociadas, graças ao papel dos sistemas radiculares profundantes e da expressiva redistribuição hidráulica vertical identificada, aspecto que tem pertinência na aplicabilidade das técnicas de detecção remota.

A complexidade das interacções entre solo e a vegetação têm obviamente implicações na utilização de técnicas de detecção remota por satélite. O sinal obtido pelos sensores a bordo de satélites resulta da integração de múltiplas contribuições do sistema solo/vegetação/atmosfera que são analisadas em pormenor nesta dissertação, não sendo simples decompor esse sinal nas componentes relevantes para cada um dos compartimentos considerados nos modelos de estimação da evapotranspiração e a sua partição em transpiração e evaporação do solo. Os resultados da investigação realizada no contexto desta tese sugerem de facto que os modelos com base em dados DR necessitam de calibração com medidas obtidas por técnicas clássicas.

Vários autores têm avaliado a possibilidade de automatizar a rega com base na utilização de sensores de fluxo de seiva (*vide* por exemplo Fernández et al., 2001; Fernández, 2017). Na nossa perspectiva, no curto médio prazo, esta solução é difícil de implementar nas empresas agrícolas por dois motivos principais. Primeiro os métodos de fluxo de seiva que recorrem a sensores colocados directamente no xilema não permitem acompanhar o crescimento da planta uma vez que se destrói o câmbio vascular, tendo pois o sensor uma vida útil reduzida. Em segundo lugar a sua utilização não conduz a uma boa relação qualidade/preço porque o preço dos sensores é elevado, necessitam de manutenção cuidada e a correcta análise de dados exige operadores treinados.

Para as cultivares estudadas de vinha ('Aragonez') e oliveira ('Arbequina'), Ψ_{base} pode ser usado como indicador do estado hídrico da planta. Contudo, para a oliveira, surgiram evidências de que a função que relaciona Ks e Ψ_{base} não permite uma correspondência biunívoca. Para a vinha, o potencial hídrico do ramo ou da folha mínimo mostrou não ser um bom indicador do estado hídrico da planta.

Os índices derivados de medições da variação do diâmetro do tronco mostraram-se de difícil utilização como indicadores do estado hídrico da planta, tanto na vinha como no olival. Na vinha não foi possível encontrar correlação com indicador do estado hídrico (Silvestre et al., 2013). No olival foi necessário construir um índice que integra também medições de diâmetro do tronco de plantas em conforto hídrico (Ferreira et al., 2012a), o que é de difícil aplicabilidade em termos práticos.

Embora a vinha e a oliveira sejam culturas características das zonas com clima Mediterrânico e como tal terem a possibilidade de produzir e/ou sobreviver em condições de elevadas intensidades de radiação, temperatura e secura atmosférica e edáfica, as cultivares de vinha e oliveira estudadas, embora ambas com comportamento isohídrico, apresentaram estratégias contrastantes relativamente ao uso da água e à sensibilidade ao *stress* hídrico. Enquanto a vinha mostrou um decréscimo de Tr muito acentuado para Ψ_{base} da ordem de $-1\,\text{MPa}$ (redução da transpiração de cerca de 80 % relativamente à transpiração máxima, Ks de 0.2), para este mesmo valor de Ψ_{base} na oliveira, foi observada uma redução da transpiração inferior a 20 %.

A análise do povoamento do solo pelas raízes mostrou ser difícil determinar qual o volume de solo efectivamente usado pelas raízes mesmo em situações em que se fazem medições do teor de água no solo. Assim os algoritmos que se baseiam no balanço hídrico do solo para estimar a reserva utilizável e posterior estimativa de Ks são de difícil aplicabilidade na prática corrente dada a incerteza que existe na estimativa do volume efectivamente usado pelas raízes. Adicionalmente o volume efectivamente explorado pode variar em função da reserva utilizável de cada uma das camadas de solo.

Do trabalho de investigação aqui desenvolvido em campos experimentais instalados em parcelas agrícolas comerciais resultou um considerável volume de informação quantitativa sobre o uso da água e respectivo estado hídrico, bem como informação qualitativa que permite elucidar sobre o funcionamento do *continuum* solo-planta-atmosfera. Esta informação tem aplicabilidade directa na condução e gestão da rega, bem como no apoio à decisão nas empresas agrícolas. Esta aplicabilidade é ainda mais acentuada no sentido em que são escassos os estudos nestas culturas lenhosas na região do Alentejo e dadas as situações de seca recorrentes já observadas nesta década.

Perspectivas

A investigação descrita nesta tese conduz a novas questões que se apresentam seguidamente de forma resumida.

Caso se confirme que o estado hídrico do solo e o armazenamento das várias camadas, como observado no olival de regadio no ano de seca (2012), tenha papel preponderante na redução de Kcb (logo menor uso da água para idênticas condições de ETr e LAI) será de investigar quais os efeitos na produção líquida de fotoassimilados (com consequências, nomeadamente, ao nível das reservas, produção actual e indução/diferenciação floral) e na produtividade da água.

Com a entrada em funcionamento dos satélites Europeus da constelação Sentinel-2 (programa Copernicus) está minimizado o problema da insuficiente resolução temporal associada à utilização apenas dos dados provenientes do programa Norte Americano Landsat. O facto de os dados serem do domínio público facilita a exploração e teste de forma sistemática dos modelos de estimativa de Kcb a partir do índice de vegetação NDVI[1] ou outros índices de vegetação que têm vindo a revelar bons resultados para este propósito. Os dados provenientes dos sensores a bordo dos satélites Sentinel-2 podem permitir estimar outras variáveis importantes como a concentração de azoto nas folhas e o teor de clorofila (Clevers et al., 2017). Este conjunto de informação poderá ser usado na construção de ferramentas para apoio à decisão na condução da rega e da adubação azotada nomeadamente, no estabelecimento de programas de fertirrega. Uma melhor gestão da rega e da adubação azotada certamente poderá contribuir para minimizar as perdas de azoto e poluição por lixiviação, evitando a degradação dos recursos em zonas vulneráveis como o Alentejo (Paralta e Francés, 2000; Paralta e Ribeiro, 2001). Como a resolução espacial dos dados Sentinel-2 não permite individualizar os compartimentos solo e planta certamente a aplicação será ainda mais difícil quando a vinha e olival são cultivados com a técnica de conservação do solo e da água do enrelvamento em sobcoberto (que só não estará activo durante o Verão e até às primeiras chuvas de Outono). Assim será necessário continuar a desenvolver tecnologia (sensores e aplicações informáticas) que permita obter uma resolução espacial adequada (*e.g.* sensores aerotransportados por máquinas não tripuladas) e com relação qualidade/preço que torne viável a sua utilização sistemática pelas empresas agrícolas.

Não é expectável que a utilização directa do índice de vegetação NDVI para estimar Ks $\times$Kcb conduza a uma boa estimativa de Tr, necessária a uma gestão e condução da rega precisa em condições de rega deficitária, uma vez que o NDVI não mostrou sensibilidade ao stress hídrico de curto prazo. Contudo, o NDVI pode ser usado para estimar Kcb

[1] A resolução espacial do sensor a bordo dos satélites Sentinel-2 é de 10 m para as bandas 4 e 8.

e por estimativa independente de Ks, obter-se Tr. Em consequência é indispensável obter funções que permitam estimar Ks em função de indicadores do estado hídrico adequados à cultura e que podem ser obtidos usando as técnicas clássicas (*e.g.* potencial hídrico). Contudo as técnicas clássicas têm várias limitações nomeadamente por serem normalmente invasivas e/ou não permitirem resolução espacial e temporal adequadas às exigências de uma agricultura de precisão. Neste aspecto as técnicas de detecção remota devem assumir um papel relevante no âmbito da investigação dada a sua natureza não invasiva e possivelmente permitindo medições com resolução espacial adequada para a construção de mapas, neste caso, caracterizando (idealmente de forma quantitativa) o estado hídrico de uma dada cultura.

Anexo I

Anexo I

Diagrama de fluxo simplificado do algoritmo relativo, a uma das abordagens, para a combinação de métodos com o objectivo de medir a ET_r e suas componentes (transpiração e evaporação do solo). Mais detalhes podem ser consultados em Paço, 2003; Ferreira et al., 2008; Silvestre, 2003; Conceição, 2007 e Silva, 2009.

$T\,[K]$, temperatura do ar medida à altura **z**, frequência de 8 a 10 Hz;

$u_x\,[m\,s^{-1}]$, componente segundo o eixo do x da velocidade do vento, medida à altura z, frequência de 8 a 10 Hz;

$u_y\,[m\,s^{-1}]$, componente segundo o eixo do y da velocidade do vento, medida à altura z, frequência de 8 a 10 Hz;

$u_z\,[m\,s^{-1}]$, componente segundo o eixo do z da velocidade do vento, medida à altura z, frequência de 8 a 10 Hz;

$U_{Abs}\,[kg\,m^{-3}]$, humidade absoluta da atmosfera, medida à altura z, frequência de 8 a 10 Hz;

$T_{Ar}\,[K]$, temperatura média do ar, à altura z, intervalo de integração 1800 s;

$RH\,[-]$, humidade relativa média do ar, à altura z, intervalo de integração 1800 s;

$\text{Direcção vento}\,[rad]$, distribuição de frequência da direcção da velocidade horizontal do vento, intervalo de observação 1800 s;

$R_n\,[W\,m^{-2}]$, densidade de fluxo de radiação liquida (balanço de radiação);

$T_{solo}\,[K]$, temperatura do solo (normalmente medida a 0.025 m de profundidade;

$G_{raw}\,[W\,m^{-2}]$, densidade de fluxo de calor por condução de ou para o solo medida à profundidade p (normalmente 0.05 m) com placas de fluxo de calor;

$G\,[W\,m^{-2}]$, densidade de fluxo de calor por condução para o solo à superfície do solo, resulta da adição a G_{raw} do balanço de energia armazenada na camada de solo entre a superfície e a profundidade p de medição de G_{raw};

$HU_{solo}\,[kg\,kg^{-1}]$, humidade do solo;

$E_{s_{raw}}\,[kg]$, evaporação do solo medida com microlisímetros expressa em variação da massa;

$H\,[W\,m^{-2}]$, densidade de fluxo média de calor sensível, intervalo de integração 1800 s;

$LE_{raw}\,[W\,m^{-2}]$, densidade de fluxo média de calor latente ou evapotranspiração real sem correcções para a absorção pelo O_2 e WPL, intervalo de integração 1800 s;

$LE\,[W\,m^{-2}]$, densidade de fluxo média de calor latente ou evapotranspiração real com correcções para a absorção pelo O_2 (Tanner et al., 1993) e WPL (Webb et al., 1980), intervalo de integração 1800 s;

$E_s\,[W\,m^{-2}]$, densidade de fluxo média de evaporação do solo, intervalo de integração 1800 s;

$K\,[-]$, índice de fluxo (método de *Granier*);

$T_G\,[W\,m^{-2}]$, densidade de fluxo de transpiração média para a parcela, intervalo de integração 1800 s;

$T_{G\ \text{Diária}}\,[W\,m^{-2}]$ ou $T_{G\ \text{Diária}}\,[mm\,dia^{-1}]$, densidade de fluxo de transpiração média para a parcela, intervalo de integração 86400 s (24 h);

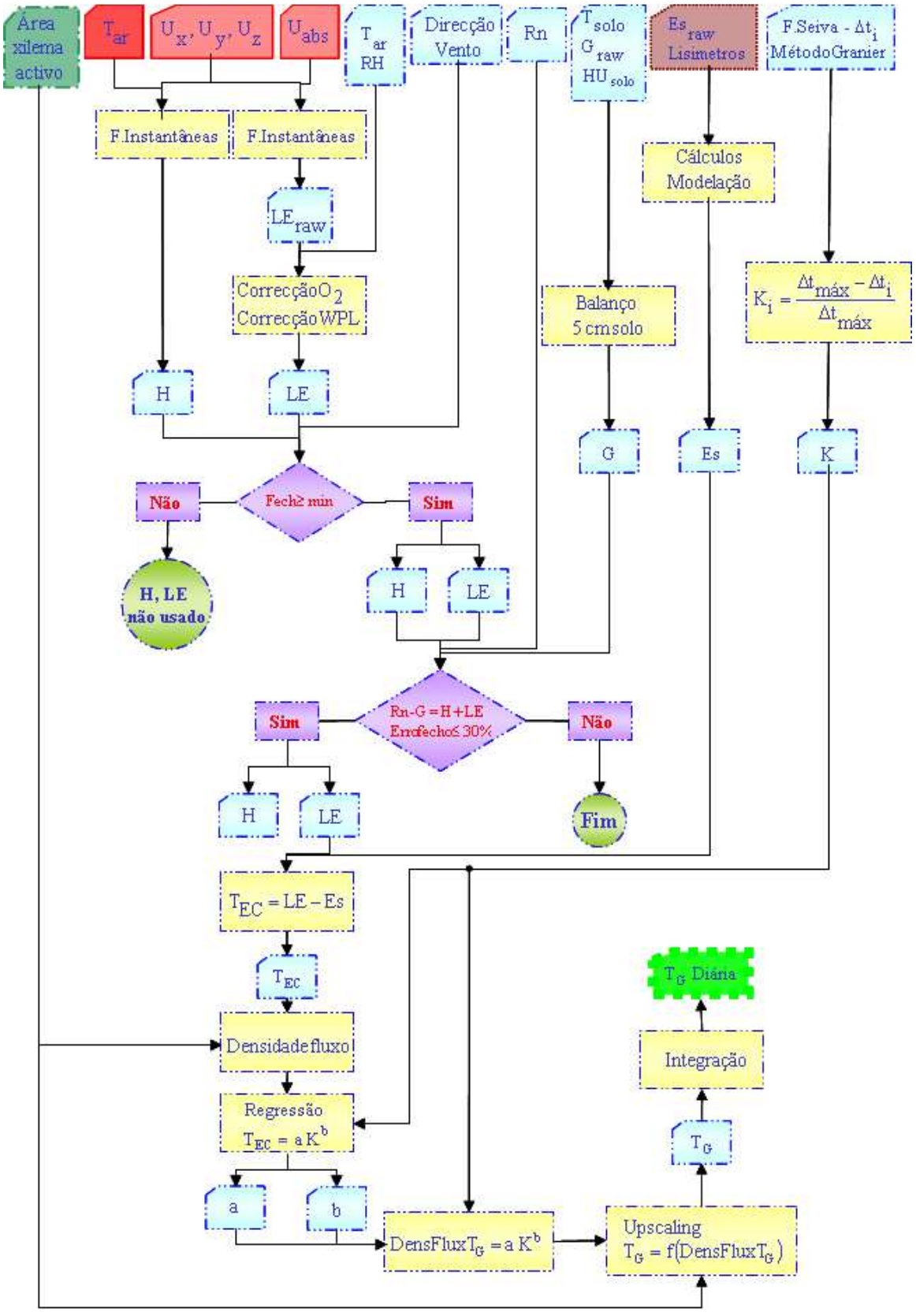
Área xilema activo
T_{ar}
U_x, U_y, U_z
U_{abs}
T_{ar} RH
Direcção Vento
Rn
T_{solo} G_{raw} HU_{solo}
Es_{raw} Lisimetros
F.Seiva - Δt_i MétodoGranier
F.Instantâneas
F.Instantâneas
Cálculos Modelação
LE_{raw}
CorrecçãoO_2 CorrecçãoWPL
Balanço 5 cmsolo
$K_i = \frac{\Delta t_{máx} - \Delta t_i}{\Delta t_{máx}}$
H
LE
G
Es
K
Não
Fech≥ min
Sim
H, LE não usado
H
LE
Sim
Rn-G = H+LE Erro fecho≤ 30%
Não
H
LE
Fim
$T_{EC} = LE - Es$
T_{EC}
T_G Diária
Densidade fluxo
Integração
Regressão $T_{EC} = a K^b$
T_G
a
b
$DensFlux T_G = a K^b$
Upscaling $T_G = f(DensFlux T_G)$

Lista de referências

Allen, R. G., Tasumi, M. e Trezza, R. 2007. Satellite-Based Energy Balance for Mapping Evapotranspiration with Internalized Calibration (METRIC-Model. *Journal of Irrigation and Drainage Engineering* 133 (4): 380–394. http://dx.doi.org/10.1061/(asce)0733-9437(2007)133:4(380). (Ver p. 11).

Allen, R., Pereira, L., Raes, D. e Smith, M. 1998. *Crop Evapotranspiration Guidelines for Computing Crop Water Requirements: FAO Irrigation and Drainage Paper 56*. Ed. por Food and Agriculture Organization of the United Nations. Vol. FAO Irrigation and Drainage. Rome, Italy. http://www.fao.org/docrep/x0490e/x0490e00.htm. (Ver p. 11).

Alvino, A. e Marino, S. 2017. Remote Sensing for Irrigation of Horticultural Crops. *Horticulturae* 3 (2): 40. https://doi.org/10.3390%2Fhorticulturae3020040. (Ver p. 11).

Anderson, M. C. e Kustas, W. P. 2008. Mapping Evapotranspiration and Drought at local to Continental Scales using Thermal Remote Sensing. Em *IGARSS 2008 - 2008 IEEE International Geoscience and Remote Sensing Symposium*. IEEE. https://doi.org/10.1109%2Figarss.2008.4779671. (Ver p. 2).

Aubinet, M., Vesala, T. e Papale, D. 2012. *Eddy Covariance. A Practical Guide to Measurement and Data Analysis*. Springer, Dordrecht. https://link.springer.com/book/10.1007%2F978-94-007-2351-1#about. (Ver p. 8).

Baldocchi, D. 2003. Assessing the eddy covariance technique for evaluating carbon dioxide exchange rates of ecosystems: past, present and future. *Global Change Biology* 9 (4). http://gen.lib.rus.ec/scimag/index.php?s=10.1046/j.1365-2486.2003.00629.x. (Ver p. 8).

Baldocchi, D. 2014a. «ESPM 228, Advanced Topics in Biometeorology and Micrometeorology: Lecture on Micrometeorological Flux Measurement Methods». Ecosystems Science Division. Department of Environmental Science, Policy e Management. 345 Hilgard. http://www2.icnf.pt/portal/pn/biodiversidade/ei/unccd-PT/pancd/o-pancd-de-1999-2014-1/object-pancd. (Ver p. 8).

— . 2014b. Measuring fluxes of trace gases and energy between ecosystems and the atmosphere - the state and future of the eddy covariance method. *Global Change Biology* 20 (12): 3600–3609. https://doi.org/10.1111%2Fgcb.12649. (Ver p. 7).

Baldocchi, D., Falge, E., Gu, L., Olson, R., Hollinger, D., Running, S., Anthoni, P., Bernhofer, C., Davis, K., Evans, R., Fuentes, J., Goldstein, A., Katul, G., Law, B., Lee, X., Malhi, Y., Meyers, T., Munger, W., Oechel, W., U, K. T. P., Pilegaard, K., Schmid, H. P., Valentini, R., Verma, S., Vesala, T., Wilson, K. e Wofsy, S. 2001. FLUXNET: A New Tool to Study the Temporal and Spatial Variability of Ecosystem-Scale Carbon Dioxide, Water Vapor, and Energy Flux Densities. *Bulletin of the American Meteorological Society* 82 (11): 2415–2434. https://doi.org/10.1175/1520-0477(2001)082%3C2415:FANTTS%3E2.3.CO;2. (Ver p. 7).

Bastiaanssen, W. G. M., Noordman, E. J. M., Pelgrum, H., Davids, G., Thoreson, B. P. e Allen, R. G. 2005. SEBAL Model with Remotely Sensed Data to Improve Water-Resources Management under Actual Field Conditions. *Journal of Irrigation and Drainage Engineering* 131 (1): 85–93. https://doi.org/10.1061%2F%28asce%290733-9437%282005%29131%3A1%2885%29. (Ver p. 14).

Bastiaanssen, W., Menenti, M., Feddes, R. e Holtslag, A. 1998a. A remote sensing surface energy balance algorithm for land (SEBAL). 1. Formulation. *Journal of Hydrology* 212—213:198–212. http://www.sciencedirect.com/science/article/pii/S0022169498002534. (Ver pp. 11, 14).

Bastiaanssen, W., Pelgrum, H., Wang, J., Ma, Y., Moreno, J., Roerink, G. e Wal, T. van der. 1998b. A remote sensing surface energy balance algorithm for land (SEBAL): Part 2: Validation. *Journal of Hydrology* 212-–213. http://www.sciencedirect.com/science/article/pii/S0022169498002546. (Ver p. 14).

Bellvert, J., Zarco-Tejada, P. J., Girona, J. e Fereres, E. 2013. Mapping crop water stress index in a 'Pinot-noir' vineyard: comparing ground measurements with thermal remote sensing imagery from na unmanned aerial vehicle. *Precision Agriculture* 15 (4): 361–376. https://doi.org/10.1007%2Fs11119-013-9334-5. (Ver p. 2).

Blanco-Cipollone, F., Lourenço, S., Silvestre, J., Conceição, N., Moñino, M., Vivas, A. e Ferreira, M. I. 2017. Plant Water Status Indicators for Irrigation Scheduling Associated with Iso- and Anisohydric Behavior: Vine and Plum Trees. *Horticulturae* 3 (3): 47–64. https://doi.org/10.3390%2Fhorticulturae3030047. (Ver p. 107).

Brunsell, N. A., Ham, J. M. e Arnold, K. A. 2011. Validating remotely sensed land surface fluxes in heterogeneous terrain with large aperture scintillometry. *International Journal of Remote Sensing* 32 (21): 6295–6314. https://doi.org/10.1080%2F01431161.2010.508058. (Ver p. 6).

Büntgen, U., Tegel, W., Nicolussi, K., McCormick, M., Frank, D., Trouet, V., Kaplan, J. O., Herzig, F., Heussner, K.-U., Wanner, H., Luterbacher, J. e Esper, J. 2011. 2500 Years of European Climate Variability and Human Susceptibility. *Science* 331 (6017): 578–582. https://doi.org/10.1126%2Fscience.1197175. (Ver p. 1).

Büntgen, U., Krusic, P. J., Verstege, A., Sangüesa-Barreda, G., Wagner, S., Camarero, J. J., Ljungqvist, F. C., Zorita, E., Oppenheimer, C., Konter, O., Tegel, W., Gärtner, H., Cherubini, P., Reinig, F. e Esper, J. 2017. New Tree-Ring Evidence from the Pyrenees Reveals Western Mediterranean Climate Variability since Medieval Times. *Journal of Climate* 30 (14): 5295–5318. https://doi.org/10.1175%2Fjcli-d-16-0526.1. (Ver p. 1).

Burba, G. 2013. *Eddy Covariance Method for Scientific, Industrial, Agricultural, and Regulatory Applications: A Field Book on Measuring Ecosystem Gas Exchange and Areal Emission Rates*. Lincoln, NE, USA: LI-COR Biosciences. www.licor.com. (Ver p. 8).

Calera, A., Campos, I., Osann, A., D'Urso, G. e Menenti, M. 2017. Remote Sensing for Crop Water Management: From ET Modelling to Services for the End Users. *Sensors* 17 (5): 1104. https://doi.org/10.3390%2Fs17051104. (Ver p. 11).

Campos, I., Neale, C. M., Calera, A., Balbontín, C. e González-Piqueras, J. 2010. Assessing satellite-based basal crop coefficients for irrigated grapes (Vitis vinifera L.) *Agricultural Water Management* 98 (1): 45–54. https://doi.org/10.1016%2Fj.agwat.2010.07.011. (Ver pp. 12, 13).

Campoy, J., Ruiz, D. e Egea, J. 2011. Dormancy in temperate fruit trees in a global warming context: A review. *Scientia Horticulturae* 130 (2): 357–372. https://doi.org/10.1016%2Fj.scienta.2011.07.011. (Ver p. 1).

Chaves, M. M., Maroco, J. P. e Pereira, J. S. 2003. Understanding plant responses to drought – from genes to the whole plant. *Functional Plant Biology* 30 (3): 239–264. (Ver p. 9).

Chehbouni, A., Lo Seen, D., Njoku, E. e Monteny, B. 1996. Examination of the difference between radiative and aerodynamic surface temperatures over sparsely vegetated surfaces. *Remote Sensing of Environment* 58 (2): 177–186. http://www.sciencedirect.com/science/article/pii/S0034425796000375. (Ver p. 13).

Chehbouni, A., Seen, D. L., Njoku, E., Lhomme, J.-P., Monteny, B. e Kerr, Y. 1997. Estimation of sensible heat flux over sparsely vegetated surfaces. *Journal of Hydrology* 188-189:855–868. https://doi.org/10.1016%2Fs0022-1694%2896%2903174-5. (Ver p. 13).

Clevers, J., Kooistra, L. e van den Brande, M. 2017. Using Sentinel-2 Data for Retrieving LAI and Leaf and Canopy Chlorophyll Content of a Potato Crop. *Remote Sensing* 9 (5): 405. https://doi.org/10.3390%2Frs9050405. (Ver p. 113).

Conceição, N. 2007. Balanço energético e coeficientes culturais em *Pyrus communis* L . cv. Rocha. Tese de mestrado, Universidade Técnica de Lisboa. Instituto Superior de Agronomia. https://www.repository.utl.pt/handle/10400.5/596.

Conceição, N., Ferreira, M. I., Pacheco, C. A., Fabião, M., Boteta, L. e Silvestre, J. C. 2011. Transpiration from a vineyard in South Portugal - stress coefficients, NDVI and leaf water potential. *Acta Horticulturae*, n.º 922: 277–284. https://doi.org/10.17660%2Factahortic.2011.922.36. (Ver p. 15).

Conceição, N., Häusler, M., Lourenço, S., Pacheco, C. A., Tezza, L. e Ferreira, M. I. 2017a. Evapotranspiration measured in a traditional rainfed and an irrigated intensive olive orchard during a year of hydrological drought. *Acta Horticulturae*, n.º 1150: 281–288. https://doi.org/10.17660%2Factahortic.2017.1150.39.

Conceição, N., Tezza, L., Häusler, M., Lourenço, S., Pacheco, C. A. e Ferreira, M. I. 2017b. Three years of monitoring evapotranspiration components and crop and stress coefficients in a deficit irrigated intensive olive orchard. *Agricultural Water Management*, n.º 191: 138–152. https://doi.org/10.1016%2Fj.agwat.2017.05.011.

Conceição, N., Tezza, L., Lourenço, A., Häusler, M., Boteta, L., Pacheco, C. e Ferreira, M. I. 2017c. Importance of very fine roots in deep soil layers for the survival of rainfed olive trees. In press, *Acta Horticulturae*. (Ver pp. 21, 109–111).

Cook, B. I., Anchukaitis, K. J., Touchan, R., Meko, D. M. e Cook, E. R. 2016. Spatiotemporal drought variability in the Mediterranean over the last 900 years. *Journal of Geophysical Research Atmospheres* 121 (5). http://gen.lib.rus.ec/scimag/index.php?s=10.1002/2015JD023929. (Ver p. 1).

Courault, D., Seguin, B. e Olioso, A. 2005. Review on estimation of evapotranspiration from remote sensing data: From empirical to numerical modeling approaches. *Irrigation and Drainage Systems* 19 (3-4): 223–249. https://doi.org/10.1007%2Fs10795-005-5186-0. (Ver p. 11).

Daamen, C. C., Simmonds, L., Wallace, J., Laryea, K. e Sivakumar, M. 1993. Use of microlysimeters to measure evaporation from sandy soils. *Agricultural and Forest Meteorology* 65 (3—4): 159–173. http://www.sciencedirect.com/science/article/pii/016819239390002Y. (Ver p. 6).

De Leonardis, A. M., Petrarulo, M., De Vita, P. e Mastrangelo, A. M. 2012. Genetic and Molecular Aspects of Plant Response to Drought in Annual Crop Species. Em *Advances in Selected Plant Physiology Aspects*. InTech. https://doi.org/10.5772%2F31352. (Ver p. 9).

Denmead, O. 1984. Plant physiological methods for studying evapotranspiration: Problems of telling the forest from the trees. *Agricultural Water Management* 8 (1—3): 167–189. http://www.sciencedirect.com/science/article/pii/0378377484900520. (Ver p. 7).

Dicionário-Priberam. 2017. «Dicionário Priberam da Língua Portuguesa». https://www.priberam.pt. (Ver p. ix).

Doorenbos, J. e Pruitt, W. O. 1977. *Guidelines for predicting crop water requirements: FAO Irrigation and Drainage Paper 24*. Ed. por Food e A. O. of the United Nations. Vol. FAO Irrigation and Drainage. Rome, Italy. http://www.fao.org/3/a-f2430e.pdf. (Ver p. 11).

Fernández, J. E. e Moreno, F. 1999. Water Use by the Olive Tree. *Journal of Crop Production* 2, n.º 2 (). http://gen.lib.rus.ec/scimag/index.php?s=10.1300/J144v02n02_05. (Ver p. 5).

Fernández, J. E., Palomo, M. J., Díaz-Espejo, A., Clothier, B. E., Green, S. R., Girón, I. F. e Moreno, F. 2001. Heat-pulse measurements of sap flow in olives for automating irrigation: tests, root flow and diagnostics of water stress. *Agricultural Water Management* 51 (2): 99–123. https://doi.org/10.1016%2Fs0378-3774%2801%2900119-6. (Ver p. 112).

Fernández, J. 2017. Plant-Based Methods for Irrigation Scheduling of Woody Crops. *Horticulturae* 3 (2): 35. https://doi.org/10.3390%2Fhorticulturae3020035. (Ver p. 112).

Ferreira, M. I. 1996. Evapotranspiração e stress hídrico em cobertos arbóreo-arbustivos numa perspectiva de gestão da água em região mediterrânica. *Anais do Instituto Superior de Agronomia*, n.º 45: 343–385. (Ver pp. 5–7).

Ferreira, M. I., Conceição, N., David, T. S. e Nadezhdina, N. 2013. Role of lignotuber versus roots in the water supply of rainfed olives. *Acta Horticulturae*, n.º 991: 181–188. http://www.actahort.org/books/991/991_22.htm. (Ver pp. 24, 111).

Ferreira, M. I., Conceição, N., Pacheco, C. A. e Häusler, M. 2012a. Análise de indicadores de desconforto hídrico durante ciclos de stress num olival intensivo no Alentejo. Em *VI Simpósio Nacional de Olivicultura*, ed. por A. Bento e J. A. Pereira, 207–216. 21. Mirandela: Associação Portuguesa de Horticultura (APH). http://www.aphorticultura.pt/. (Ver p. 112).

Ferreira, M. I., Paço, T. A. e Silvestre, J. 2004. Combining techniques to study evapotranspiration in woody crops: application to small areas – two case studies. *Acta Horticulturae*, n.º 664: 225–232. https://doi.org/10.17660%2Factahortic.2004.664.26. (Ver p. 8).

Ferreira, M. I., Paço, T. A., Silvestre, J. e Silva, R. M. 2008. Evapotranspiration estimates and water stress indicators for irrigation scheduling in woody plants. Cap. 3 em *Agricultural Water Management Research Trends*, 129–170. New York, USA. https://www.novapublishers.com/catalog/product_info.php?products_id=6658. (Ver pp. 5, 7, 8, 10).

Ferreira, M. I., Silvestre, J., Conceição, N. e Malheiro, A. C. 2012b. Crop and stress coefficients in rainfed and deficit irrigation vineyards using sap flow techniques. *Irrigation Science* 30 (5): 433–447. http://link.springer.com/article/10.1007%2Fs00271-012-0352-2. (Ver pp. 8, 107, 108).

Ferreira, M. I., Green, S., Conceição, N. e Fernández, J.-E. 2018. Assessing hydraulic redistribution with the compensated average gradient heat-pulse method on rain-fed olive trees. *Plant and Soil*. https://doi.org/10.1007%2Fs11104-018-3585-x. (Ver p. 24).

Ferreira-Gama, M. I. F. R. 1987. Evapotranspiração real. Estudo realizado na cultura do tomate em região de clima mediterrânico. PhD thesis, Technical University of Lisbon. Instituto Superior de Agronomia. (Ver p. 10).

Fiorentino, G., Caracuta, V., Calcagnile, L., D'Elia, M., Matthiae, P., Mavelli, F. e Quarta, G. 2008. Third millennium B.C. climate change in Syria highlighted by Carbon stable isotope analysis of 14C-AMS dated plant remains from Ebla. *Palaeogeography, Palaeoclimatology, Palaeoecology* 266 (1-2). http://gen.lib.rus.ec/scimag/index.php?s=10.1016/j.palaeo.2008.03.034. (Ver p. 1).

Foken, T. 2006. 50 Years of the Monin–Obukhov Similarity Theory. *Boundary-Layer Meteorology* 119 (3). http://gen.lib.rus.ec/scimag/index.php?s=10.1007/s10546-006-9048-6. (Ver p. 8).

Fuchs, M. 1990. Infrared measurement of canopy temperature and detection of plant water stress. *Theoretical and Applied Climatology* 42 (4): 253–261. http://dx.doi.org/10.1007/BF00865986. (Ver p. 10).

Gentine, P., Entekhabi, D., Chehbouni, A., Boulet, G. e Duchemin, B. 2007. Analysis of evaporative fraction diurnal behaviour. *Agricultural and Forest Meteorology* 143 (1-2): 13–29. https://doi.org/10.1016%2Fj.agrformet.2006.11.002. (Ver p. 11).

Gentine, P., Entekhabi, D. e Polcher, J. 2011. The Diurnal Behavior of Evaporative Fraction in the Soil–Vegetation–Atmospheric Boundary Layer Continuum. *Journal of Hydrometeorology* 12 (6): 1530–1546. https://doi.org/10.1175%2F2011jhm1261.1. (Ver p. 14).

Geological-Survey, U. S. 2015. *Landsat 4-7 Climate Data Record (CDR) Surface Reflectance: Product Guide*. USGS. http://landsat.usgs.gov/documents/cdr_sr_product_guide.pdf. (Ver pp. 3, 18).

Girona, J., Mata, M., Fereres, E., Goldhamer, D. A. e Cohen, M. 2002. Evapotranspiration and soil water dynamics of peach trees under water deficits. *Agricultural Water Management*, n.º 54: 107–122. http://www.irnase.csic.es/users/jefer/Articulos%20en%20papel%20JE/MODELOS/Girona2002.pdf. (Ver pp. 1, 7).

Gonzalez-Dugo, M. P., Neale, C. M. U., Mateos, L., Kustas, W. P., Prueger, J. H., Anderson, M. C. e Li, F. 2009. A comparison of operational remote sensing-based models for estimating crop evapotranspiration. *Agricultural and Forest Meteorology* 149 (11): 1843–1853. http://dx.doi.org/10.1016/j.agrformet.2009.06.012. (Ver p. 15).

Gonzalez-Dugo, V., Zarco-Tejada, P., Berni, J., Suárez, L., Goldhamer, D. e Fereres, E. 2012. Almond tree canopy temperature reveals intra-crown variability that is water stress-dependent. *Agricultural and Forest Meteorology* 154-155:156–165. http://www.sciencedirect.com/science/article/pii/S0168192311003224. (Ver p. 10).

Granier, A. 1985. Une nouvelle méthode pour la mesure du flux de sève brute dans le tronc des arbres. *Ann. For. Sci.* 42 (2): 193–200. http://dx.doi.org/10.1051/forest:19850204. (Ver pp. 3, 8, 20).

Granier, A. e Gross, P. 1987. Mesure du flux de sève brute dans le tronc du Douglas par une nouvelle méthode thermique. *Annales des Sciences Forestières* 44 (1): 1–14. https://doi.org/10.1051%2Fforest%3A19870101. (Ver p. 8).

Green, S., Clothier, B. e Perie, E. 2009. A Re-analysis of heat pulse theory across a wide range of sap flows. *Acta Horticulturae*, n.º 846: 95–104. https://doi.org/10.17660%2Factahortic.2009.846.8. (Ver pp. 9, 24).

Häusler, M., Conceição, N., Tezza, L., Sánchez, J. M., Campagnolo, M. L., Häusler, A. J., Silva, J. M., Warneke, T., Heygster, G. e Ferreira, M. 2018. Estimation and partitioning of actual daily evapotranspiration at an intensive olive grove using the STSEB model based on remote sensing. *Agricultural Water Management* 201:188–198. https://www.sciencedirect.com/science/article/pii/S0378377418300775.

Häusler, M., Ferreira, M. I. e Conceição, N. 2014. Assessement of vegetation parameters in olive trees in the region of Alentejo: a comparison of direct and indirect methods. *Acta Horticulturae*, n.º 1038: 407–414. http://www.actahort.org/books/1038/1038_49.htm. (Ver p. 107).

Hinckley, T. e Ceulemans, R. 1989. Current focuses in woody plant water relations and drought resistance. *Annales des sciences forestières* 46 (Suppl): 317–324. https://hal.archives-ouvertes.fr/hal-00882562. (Ver p. 9).

Hsiao, T. C., Acevedo, E., Fereres, E. e Henderson, D. W. 1976. Water Stress, Growth, and Osmotic Adjustment. *Philosophical Transactions of the Royal Society of London.*

B, Biological Sciences 273 (927): 479–500. http://rstb.royalsocietypublishing.org/content/273/927/479.abstract. (Ver p. 9).

Hsiao, T. C. 1973. Plant Responses to Water Stress. *Annual Review of Plant Physiology* 24 (1): 519–570. https://doi.org/10.1146%2Fannurev.pp.24.060173.002511. (Ver p. 9).

Huete, A. 1988. A soil-adjusted vegetation index (SAVI). *Remote Sensing of Environment* 25 (3). http://gen.lib.rus.ec/scimag/index.php?s=10.1016/0034-4257(88)90106-x. (Ver p. 13).

ICNF. 2014a. «O PANCD de 1999-2014.Objetivos: Convenção de Combate à Desertificação. Programa de Ação Nacional de Combate à Desertificação». Instituto da Conservação da Natureza e das Florestas. http://www2.icnf.pt/portal/pn/biodiversidade/ei/unccd-PT/pancd/o-pancd-de-1999-2014-1/object-pancd. (Ver p. 1).

— . 2014b. «Programa de Ação Nacional de Combate à Desertificação». Instituto da Conservação da Natureza e das Florestas. http://www2.icnf.pt/portal/pn/biodiversidade/ei/unccd-PT/pancd. (Ver p. 1).

Idso, S. B. 1982. Non-water-stressed baselines: A key to measuring and interpreting plant water stress. *Agricultural Meteorology* 27 (1—2): 59–70. http://www.sciencedirect.com/science/article/pii/0002157182900206. (Ver p. 10).

IPCC. 2013. *Climate Change 2013: The Physical Science Basis: Contribution of Working Group I to the Fifth Assessment Report of the Intergovernmental Panel on Climate Change*. http://www.ipcc.ch/report/ar5/wg1/. (Ver p. 1).

— . 2014. *Climate Change 2014: Synthesis Report: Contribution of Working Groups I, II and III to the Fifth Assessment Report of the Intergovernmental Panel on Climate Change*. IPCC. http://www.ipcc.ch/report/ar5/syr/. (Ver p. 1).

— . 2015. *Climate Change 2014: Mitigation of Climate Change: Working Group III Contribution to the IPCC Fifth Assessment Report*. Ed. por W. G. I. T. S. Unit. Cambridge University Press. (Ver p. 1).

IPMA. 2014. «Serviços de Clima - Cenários Climáticos para Portugal Continental no Século XXI». Instituto Português do Mar e da Atmosfera. https://www.ipma.pt/pt/oclima/servicos.clima/index.jsp?page=cenarios21.clima.xml&print=true. (Ver p. 1).

Jackson, R. D., Idso, S. B., Reginato, R. J. e Pinter, P. J. 1981. Canopy temperature as a crop water stress indicator. *Water Resources Research* 17 (4): 1133–1138. http://dx.doi.org/10.1029/WR017i004p01133. (Ver p. 10).

Jarvis, P. G. e McNaughton, K. G. 1986. Stomatal Control of Transpiration: Scaling Up from Leaf to Region. Em *Advances in Ecological Research*, 1–49. Elsevier. https://doi.org/10.1016%2Fs0065-2504%2808%2960119-1. (Ver pp. 2, 6).

Jarvis, P. 1985. Transpiration and assimilation of tree and agricultural crops: 'the omega factor'. Em *Trees as crop plants*, ed. por M. Cannel e J. Jackson, 460–480. Scotland: Institute of Terrestrial Ecology. (Ver p. 10).

Jensen, M. E. 1968. Water consumption by agricultural plants. Em *Water deficits and plant growth*, 1–22. Academic Press. http://eprints.nwisrl.ars.usda.gov/742/1/92.pdf. (Ver p. 11).

Jones, H. G. e Vaughan, R. A. 2010. *Remote sensing of vegetation: principles, techniques, and applications*. Oxford, NY (US): Oxford, University Press Inc. (Ver pp. 10, 11).

Jones, H. G. 1999. Use of infrared thermometry for estimation of stomatal conductance as a possible aid to irrigation scheduling. *Agricultural and Forest Meteorology* 95 (3): 139–

149. http://www.sciencedirect.com/science/article/pii/S0168192399000301. (Ver p. 10).

Jones, H. G., Stoll, M., Santos, T., Sousa, C., Chaves, M. M. e Grant, O. M. 2002. Use of infrared thermography for monitoring stomatal closure in the field: application to grapevine. *Journal of Experimental Botany* 53 (378): 2249–2260. http://jxb.oxfordjournals.org/content/53/378/2249.abstract. (Ver p. 10).

Kramer, P. J. 1963. Water Stress and Plant Growth1. *Agronomy Journal* 55 (1). http://gen.lib.rus.ec/scimag/index.php?s=10.2134/agronj1963.00021962005500010013x. (Ver p. 9).

Kustas, W. P. 1990. Estimates of Evapotranspiration with a One- and Two-Layer Model of Heat Transfer over Partial Canopy Cover. *Journal of Applied Meteorology* 29:704–715. http://dx.doi.org/10.1175/1520-0450(1990)029%3C0704:EOEWAO%3E2.0.CO;2. (Ver p. 7).

Launder, B. E. 2015. First steps in modelling turbulence and its origins: a commentary on Reynolds (1895) 'On the dynamical theory of incompressible viscous fluids and the determination of the criterion'. *Philosophical Transactions Mathematical Physical & Engineering Sciences* 373 (2039). http://gen.lib.rus.ec/scimag/index.php?s=10.1098/rsta.2014.0231. (Ver p. 8).

Lichtenthaler, H. K. 1996. Vegetation Stress: an Introduction to the Stress Concept in Plants. *Journal of Plant Physiology* 148 (1—2): 4–14. http://www.sciencedirect.com/science/article/pii/S0176161796802872. (Ver p. 9).

Loizidou, M., Giannakopoulos, C., Bindi, M. e Moustakas, K. 2016. Climate change impacts and adaptation options in the Mediterranean basin. *Regional Environmental Change* 16 (7): 1859–1861. https://doi.org/10.1007/s10113-016-1037-9. (Ver p. 1).

Malheiro, A. C., Ferreira, M. I., Conceição, N. e Green, S. 2016. Root and stem water dynamics of rainfed grapvines in the Douro region. *Acta Horticulturae*, n.º 1136: 221–228. https://doi.org/10.17660%2Factahortic.2016.1136.30. (Ver p. 24).

Masek, J., Vermote, E., Saleous, N., Wolfe, R., Hall, F., Huemmrich, K., Gao, F., Kutler, J. e Lim, T.-K. 2006. A Landsat Surface Reflectance Dataset for North America, 1990–2000. *IEEE Geoscience and Remote Sensing Letters* 3 (1): 68–72. https://doi.org/10.1109%2Flgrs.2005.857030. (Ver pp. 3, 17).

Melo-Abreu, J. P. D., Barranco, D., Cordeiro, A. M., Tous, J., Rogado, B. M. e Villalobos, F. J. 2004. Modelling olive flowering date using chilling for dormancy release and thermal time. *Agricultural and Forest Meteorology* 125 (1-2): 117–127. https://doi.org/10.1016%2Fj.agrformet.2004.02.009. (Ver p. 1).

Min-Agricultura. 2013. *Estratégia de adaptação da agricultura e das florestas às alterações climáticas: Portugal Continental*. Ministério da Agricultura, do Mar, do Ambiente e do Ordenamento do Território. https://www.apambiente.pt/_zdata/Politicas/AlteracoesClimaticas/Adaptacao/ENAAC/RelatDetalhados/Relat_Setor_ENAAC_Agricultura.pdf. (Ver p. 1).

Monteith, J. L. 1965. Evaporation and Environment. Em *19th Symposia of the Society for Experimental Biology*, ed. por editor, 19:205–234. Cambridge: University Press. http://www.unc.edu/courses/2010spring/geog/595/001/www/Monteith65.pdf. (Ver p. 10).

Monteith, J. e Unsworth, M. 1990. *Principles of Environmental Physics*. Second. London: Edward Arnold. https://www.elsevier.com/books/principles-of-environmental-physics/monteith/978-0-12-386910-4. (Ver pp. 6, 7).

Myers, B. J. 1988. Water stress integral–a link between short-term stress and long-term growth. *Tree Physiology* 4 (4): 315–323. https://doi.org/10.1093%2Ftreephys%2F4.4.315. (Ver p. 23).

Nadezhdina, N., Cermák, J. e Nadezhdin, V. 1998. Heat field deformation method for sap flow measurements. Em *Measuring Sap Flow in Intact Plants*, ed. por J. Cermák e N. Nadezhdina. IUFRO Publications, Publishing House of Mendel University. (Ver pp. 9, 24).

Nadezhdina, N., David, T. S., David, J. S., Nadezhdina, N., Ferreira, M. I., Conceição, N., Dohnal, M., Tesar, M., Gartner, K. e Celemans, R. 2012. Root Function: In Situ Studies Through Sap Flow Research. Cap. 14 em *Measuring Roots. Un updated approach*, ed. por S. Mancuso, 267–290. Springer. http://link.springer.com/chapter/10.1007/978-3-642-22067-8_14#. (Ver p. 24).

Nadezhdina, N., Ferreira, M. I., Conceição, N., Pacheco, C. A., Häusler, M. e David, T. S. 2014. Water uptake and hydraulic redistribution under a seasonal climate: long-term study in a rainfed olive orchard. *Ecohydrology*, n.º 8: 387–397. http://onlinelibrary.wiley.com/doi/10.1002/eco.1545/abstract. (Ver p. 111).

Norman, J. M. e Becker, F. 1995. Terminology in thermal infrared remote sensing of natural surfaces. *Agricultural and Forest Meteorology* 77 (3-4): 153–166. https://doi.org/10.1016%2F0168-1923%2895%2902259-z. (Ver pp. ix, 13).

Norman, J., Kustas, W. e Humes, K. 1995. Source approach for estimating soil and vegetation energy fluxes in observations of directional radiometric surface temperature. *Agricultural and Forest Meteorology* 77 (3–4): 263–293. http://www.sciencedirect.com/science/article/pii/016819239502265Y. (Ver p. 13).

Paço, T. A., Pôças, I., Cunha, M., Silvestre, J. C., Santos, F. L., Paredes, P. e Pereira, L. S. 2014. Evapotranspiration and crop coefficients for a super intensive olive orchard. An application of SIMDualKc and METRIC models using ground and satellite observations. *Journal of Hydrology* 519:2067–2080. https://doi.org/10.1016%2Fj.jhydrol.2014.09.075. (Ver p. 8).

Paço, T. 2003. Modelação da evapotranspiração em cobertos descontínuos. Programação da rega em pomar de pessegueiro. PhD thesis, Technical University of Lisbon, Instituto Superior de Agronomia. http://www.isa.utl.pt/wateruse/PUBLICATIONS/tese%20final%20definitivo%20pdf.pdf. (Ver pp. 7, 8).

Paralta, E. A. e Francés, A. P. 2000. Caracterização hidrogeológica e avaliação da vulnerabilidade à poluição do complexo gabro-diorítico de Serpa-Brinches (sector oriental do sistema aquífero dos Gabros de Beja). *Geonovas*, n.º 14: 27–35. http://lneg.pt/download/3854/20.pdf. (Ver p. 113).

Paralta, E. e Ribeiro, L. 2001. Stochastic modelling and probability risk maps of nitrate pollution in the vicinities of Beja (Alentejo, south Portugal). 3rd International Conference on FUTURE GROUNDWATER RESOURCES AT RISK, 25-27 June, Lisbon, Portugal. http://www.lneg.pt/download/3849/06.pdf. (Ver p. 113).

Pôças, I., Paço, T. A., Cunha, M., Andrade, J. A., Silvestre, J., Sousa, A., Santos, F. L., Pereira, L. S. e Allen, R. G. 2014. Satellite-based evapotranspiration of a super-intensive olive orchard: Application of METRIC algorithms. *Biosystems Engineering* 128:69–81. http://dx.doi.org/10.1016/j.biosystemseng.2014.06.019. (Ver p. 15).

Ponti, L., Gutierrez, A. P., Ruti, P. M. e Dell'Aquila, A. 2014. Fine-scale ecological and economic assessment of climate change on olive in the Mediterranean Basin reveals winners and losers. *Proceedings of the National Academy of Sciences* 111 (15): 5598–5603. https://doi.org/10.1073%2Fpnas.1314437111. (Ver p. 1).

Programa Copernicus. 2017. «copernicus». http://www.copernicus.eu/. (Ver p. 12).

Rana, G. e Katerji, N. 2000. Measurement and estimation of actual evapotranspiration in the field under Mediterranean climate: a review. *European Journal of Agronomy* 13 (2–3): 125–153. http://www.sciencedirect.com/science/article/pii/S1161030100000708. (Ver pp. 6, 7).

Raz-Yaseef, N., Rotenberg, E. e Yakir, D. 2010. Effects of spatial variations in soil evaporation caused by tree shading on water flux partitioning in a semi-arid pine forest. *Agricultural and Forest Meteorology* 150 (3): 454–462. http://www.sciencedirect.com/science/article/pii/S016819231000033X. (Ver p. 6).

R-Core-Team. 2017. *R: A Language and Environment for Statistical Computing*. Vienna, Austria: R Foundation for Statistical Computing. https://www.R-project.org/. (Ver p. 18).

Reynolds, O. 1895. On the Dynamical Theory of Incompressible Viscous Fluids and the Determination of the Criterion. *Philosophical Transactions of the Royal Society of London A (1887-1895)* 186. http://gen.lib.rus.ec/scimag/index.php?s=10.2307/90643. (Ver p. 8).

Riera, P., Peñuelas, J., Farreras, V. e Estiarte, M. 2007. VALUATION OF CLIMATE-CHANGE EFFECTS ON MEDITERRANEAN SHRUBLANDS. *Ecological Applications* 17 (1): 91–100. http://dx.doi.org/10.1890/1051-0761(2007)017[0091:VOCEOM]2.0.CO;2. (Ver p. 1).

Rose, C. e Sharma, M. 1984. Summary and recommendations of the Workshop on "Evapotranspiration from plant communities". *Agricultural Water Management* 8 (1–3): 325–342. http://www.sciencedirect.com/science/article/pii/0378377484900611. (Ver p. 6).

Rouse, J., Haas, R., Shell, J., Deering, D. e Harlan, J. 1973. *Monitoring the vernal advancement and retrogradation of natural vegetation: Final Report*. Greenbelt, USA. http://citeseerx.ist.psu.edu/viewdoc/download?doi=10.1.1.464.7884&rep=rep1&type=pdf. (Ver p. 13).

Rstudio-Team. 2016. *Rstudio: Integrated Development Environment for R*. Boston, MA: Rstudio, Inc. http://www.rstudio.com/. (Ver p. 18).

Sánchez, J. M., Kustas, W. P., Caselles, V. e Anderson, M. C. 2008. Modelling surface energy fluxes over maize using a two-source patch model and radiometric soil and canopy temperature observations. *Remote Sensing of Environment* 112 (3): 1130–1143. https://doi.org/10.1016%2Fj.rse.2007.07.018. (Ver pp. 11, 23, 24, 110).

Schmidt, G., Jenkerson, C., Masek, J., Vermote, E. e Gao, F. 2013. *Landsat Ecosystem Disturbance Adaptive Processing System (LEDAPS) Algorithm Description: Open–File Report 2013–1057*. U.S. Geological Survey. http://pubs.er.usgs.gov/publication/ofr20131057. (Ver pp. 3, 17).

Scrase, F. J. 1930. Some Characteristics of Eddy Motion in the Atmosphere. *Geophysical Memoirs* 52. http://gen.lib.rus.ec/scimag/index.php?s=10.1046/j.1365-2486.2003.00629.x. (Ver p. 8).

Shuttleworth, W. J. e Wallace, J. S. 1985. Evaporation from sparse crops an energy combination theory. *Quarterly Journal of the Royal Meteorological Society* 111 (469): 839–855. https://doi.org/10.1002%2Fqj.49711146910. (Ver p. 10).

Silva, R. 2009. Desenvolvimento de um Sistema Inteligente de Determinação das Necessidades Hídricas para Culturas Lenhosas Anisotrópicas. PhD thesis, Technical University of Lisbon. Instituto Superior de Agronomia. (Ver pp. 7, 8).

Silvestre, J., Ferreira, M. I., Conceição, N. e Malheiro, A. C. 2013. Can continuous records with plant-based methods be used to estimate water stress intensity in deficit irrigated vineyards? *Ciência e Técnica Vitivinícola*, n.º 28: 140–146. (Ver pp. 107, 112).

Silvestre, J. 2003. Evapotranspiração e funcionamento hídrico em *Vitis vinifera* L. PhD thesis, Technical University of Lisbon.Instituto Superior de Agronomia. (Ver pp. 1, 5, 7).

Swinbank, W. C. 1951. The measurement of vertical transfer of heat and water vapor by eddies in the lower atmosphere. *Journal of Meteorology* 8 (3): 135–145. https://doi.org/10.1175/1520-0469(1951)008%3C0135:TMOVTO%3E2.0.CO;2. (Ver p. 8).

Tanner, B., Swiatek, E. e Greene, J. 1993. Density fluctuations and use of the krypton hygrometer in surface flux measurements. Em *Proceeding of the 1993 National Conference on Irrigation and Drainage Engineering Irrigation and Drainage Division*. American Society of Civil Engineers.

Teixeira, J. L. e Rolim, J. 2014. *Impacte das alterações climáticas nos sistemas de regadio no Alentejo*. ISA Press. https://dspace.uevora.pt/rdpc/bitstream/10174/13246/1/Livro_Impacte_alteracoes_climaticas.pdf. (Ver p. 1).

Testi, L. e Villalobos, F. J. 2009. New approach for measuring low sap velocities in trees. *Agricultural and Forest Meteorology* 149 (3-4): 730–734. https://doi.org/10.1016%2Fj.agrformet.2008.10.015. (Ver pp. 9, 24).

United-Nations. 1994. *United Nations Convention to Combat Desertification in Those Countries Experiencing Drought and/or Desertification, particularly in Africa: Final text of the Convention*. http://www2.icnf.pt/portal/pn/biodiversidade/ei/unccd-PT/resource/doc/convencao/conv-eng.pdf. (Ver p. 1).

van-Wijk, W. R. e de-Vries, D. A. 1954. Evapotranspiration. *Nub. J. Agr. Sci.* 2 (105). (Ver p. 11).

Vermote, E. e Saleous, N. 2007. «LEDAPS surface-reflectance product description (ver. 2.0)». https://dwrgis.water.ca.gov/documents/269784/4654504/LEDAPS+Surface+Reflectance+Product+Description.pdf. (Ver pp. 3, 17).

Ward, H. C., Evans, J. G., Hartogensis, O. K., Moene, A. F., Bruin, H. A. R. D. e Grimmond, C. S. B. 2013. A critical revision of the estimation of the latent heat flux from two-wavelength scintillometry. *Quarterly Journal of the Royal Meteorological Society* 139 (676): 1912–1922. https://doi.org/10.1002%2Fqj.2076. (Ver p. 6).

Ward, H. C. 2017. Scintillometry in urban and complex environments: a review. *Measurement Science and Technology* 28 (6). http://gen.lib.rus.ec/scimag/index.php?s=10.1088/1361-6501/aa5e85. (Ver p. 6).

Webb, E. K., Pearman, G. I. e Leuning, R. 1980. Correction of flux measurements for density effects due to heat and water vapour transfer. *Quarterly Journal of the Royal Meteorological Society* 106 (447): 85–100. https://doi.org/10.1002%2Fqj.49710644707.

Weiss, E. 2015. Beginnings of Fruit Growing in the Old World – two generations later. *Israel Journal of Plant Sciences* 62 (1-2): 75–85. https://doi.org/10.1080%2F07929978.2015.1007718. (Ver p. 5).

Wright, J. L. 1982. New evapotranspiration crop coefficients. *Journal of the Irrigation and Drainage Division* 108 (1): 57–74. (Ver p. 11).

Zohary, D. e Spiegel-Roy, P. 1975. Beginnings of Fruit Growing in the Old World. *Science* 187 (4174): 319–327. http://gen.lib.rus.ec/scimag/index.php?s=10.1126/science.187.4174.319. (Ver p. 5).